

VOLUME XLII

GEMS & GEMOLOGY

SUMMER 2006



*LA-ICP-MS in Gemology
The Cullinan Diamonds
Zircon in Heated Sapphire
Faceting Rhodonite*

THE QUARTERLY JOURNAL OF THE GEMOLOGICAL INSTITUTE OF AMERICA



pg. 116



pg. 121

EDITORIAL

- 95 **GIA Celebrates 75 Years . . .**

Alice S. Keller

- 97 **LETTERS**

FEATURE ARTICLES

- 98 **Applications of Laser Ablation–Inductively Coupled Plasma–Mass Spectrometry (LA-ICP-MS) to Gemology**



Ahmadjan Abduriyim and Hiroshi Kitawaki

Summarizes the principles of this powerful technique and examines its usefulness for detecting Be-diffusion treatment and determining locality of origin.

- 120 **The Cullinan Diamond Centennial: A History and Gemological Analysis of Cullinans I and II**

Kenneth Scarratt and Russell Shor

Offers previously undocumented details about the largest gem diamond ever found, as well as two of the famous diamonds that were cut from it.

- 134 **The Effects of Heat Treatment on Zircon Inclusions in Madagascar Sapphires**

Wuyi Wang, Kenneth Scarratt, John L. Emmett, Christopher M. Breeding, and Troy R. Douthit

Documents the alteration of zircon inclusions during heat treatment of sapphires at different temperatures.

NOTES & NEW TECHNIQUES

- 151 **Faceting Transparent Rhodonite from Broken Hill, New South Wales, Australia**

Paul W. Millstead

Presents a technique for faceting transparent rhodonite.

REGULAR FEATURES

- 159 **Thank You, Donors**

- 160 **Lab Notes**

• Bone pendant • Diamonds with circular radiation stains • Diamond with intense graining • Coated pink diamonds • Diamond with unusual etch channel • Diamond with sapphire inclusions • Imitation Melo “pearls” • Moonstone imitations

- 169 **Gem News International**

• Alaskan amber • Iridescent andradite from Mexico • Star emeralds • Euclase from Colombia • Color-change fluorite • Herderite from Pakistan • Jeremejevite from Myanmar and Sri Lanka • Pink opal from Peru • Prehnite from Australia and Mali • Unusual sapphire inclusions • Sillimanite resembling moonstone • Sphene from Afghanistan • Uvite-dravite tourmaline from Tanzania • Triplodite from China • Väyrynenite from Afghanistan • Diffusion-treated synthetic sapphire • Lead glass-filled ruby bead necklace

- 189 **Book Reviews**

- 192 **Gemological Abstracts**

- 204 **The Last Page: A Colored Diamonds Chronology**



pg. 163



pg. 170

EDITORIAL STAFF

Editor-in-Chief

Alice S. Keller
akeller@gia.edu

Managing Editor

Thomas W. Overton
tom.overton@gia.edu

Technical Editor

Sally Magaña
sally.magaña@gia.edu

Consulting Editor

Carol M. Stockton

Contributing Editor

James E. Shigley

Editor

Brendan M. Laurs
The Robert Mouawad Campus
5345 Armada Drive
Carlsbad, CA 92008
(760) 603-4503
blaurs@gia.edu

Associate Editor

Stuart Overlin
soverlin@gia.edu

Circulation Coordinator

Debbie Ortiz
(760) 603-4000, ext. 7142
dortiz@gia.edu

Editors, Lab Notes

Thomas M. Moses
Shane F. McClure

Editor, Gem News International

Brendan M. Laurs

Editors, Book Reviews

Susan B. Johnson
Jana E. Miyahira-Smith
Stuart Overlin

Editors, Gemological Abstracts

Brendan M. Laurs
Thomas W. Overton

PRODUCTION STAFF

Art Director

Karen Myers

Production Assistant

Allison DeLong

Website:

www.gia.edu

EDITORIAL REVIEW BOARD

Shigeru Akamatsu
Tokyo, Japan

Alan T. Collins
London, United Kingdom

G. Robert Crowningshield
New York, New York

John Emmett
Brush Prairie, Washington

Emmanuel Fritsch
Nantes, France

Henry A. Hänni
Basel, Switzerland

A. J. A. (Bram) Janse
Perth, Australia

Alan Jobbins
Caterham, United Kingdom

Mary L. Johnson
San Diego, California

Anthony R. Kampf
Los Angeles, California

Robert E. Kane
Helena, Montana

Thomas M. Moses
New York, New York

George Rossman
Pasadena, California

Kenneth Scarratt
Bangkok, Thailand

James E. Shigley
Carlsbad, California

Christopher P. Smith
New York, New York

Christopher M. Welbourn
Reading, United Kingdom

SUBSCRIPTIONS

Subscriptions to addresses in the U.S. are priced as follows: **\$74.95** for one year (4 issues), **\$194.95** for three years (12 issues). Subscriptions sent elsewhere are **\$85.00** for one year, **\$225.00** for three years. Canadian subscribers should add GST.

Special rates are available for GIA alumni and current GIA students. One year: **\$64.95** to addresses in the U.S., **\$75.00** elsewhere; three years: **\$179.95** to addresses in the U.S., **\$210.00** elsewhere. Please have your student or Alumni number ready when ordering. Go to www.gia.edu or contact the Circulation Coordinator.

Single copies of this issue may be purchased for **\$19.00** in the U.S., **\$22.00** elsewhere. Discounts are given for bulk orders of 10 or more of any one issue. A limited number of back issues are also available for purchase. Please address all inquiries regarding subscriptions and single copy or back issue purchases to the Circulation Coordinator (see above) or visit www.gia.edu.

To obtain a Japanese translation of *Gems & Gemology*, contact GIA Japan, Okachimachi Cy Bldg., 5-15-14 Ueno, Taikoku, Tokyo 110, Japan. Our Canadian goods and service registration number is 126142892RT.

MANUSCRIPT SUBMISSIONS

Gems & Gemology welcomes the submission of articles on all aspects of the field. Please see the Guidelines for Authors on our Website, or contact the Managing Editor. Letters on articles published in *Gems & Gemology* are also welcome.

Abstracting is permitted with credit to the source. Libraries are permitted to photocopy beyond the limits of U.S. copyright law for private use of patrons. Instructors are permitted to photocopy isolated articles for noncommercial classroom use without fee. Copying of the photographs by any means other than traditional photocopying techniques (Xerox, etc.) is prohibited without the express permission of the photographer (where listed) or author of the article in which the photo appears (where no photographer is listed). For other copying, reprint, or republication permission, please contact the Managing Editor.

Gems & Gemology is published quarterly by the Gemological Institute of America, a nonprofit educational organization for the gem and jewelry industry, The Robert Mouawad Campus, 5345 Armada Drive, Carlsbad, CA 92008.

Postmaster: Return undeliverable copies of *Gems & Gemology* to The Robert Mouawad Campus, 5345 Armada Drive, Carlsbad, CA 92008.

Any opinions expressed in signed articles are understood to be the opinions of the authors and not of the publisher.

ABOUT THE COVER

Locality of origin has long been a major element of colored stone valuation in some markets, but as the number of gem localities expands, determining origin requires ever-more-advanced gemological expertise. The lead article in this issue reviews the applications of laser ablation-inductively coupled plasma-mass spectrometry to gemology, among them locality determination for emeralds.

Shown here is a magnificent Colombian emerald and diamond necklace with matching earrings, designed by Jean Schlumberger for Tiffany & Co. in the 1950s. The three large emeralds in the necklace are 6.65–7.41 ct; the emeralds in the earrings are 3.27 and 4.03 ct. Jewelry courtesy of a private collector; photo © Harold & Erica Van Pelt.

Color separations for Gems & Gemology are by Pacific PreMedia, Carlsbad, California. Printing is by Allen Press, Lawrence, Kansas.

© 2006 Gemological Institute of America All rights reserved. ISSN 0016-626X

The logo features a large, stylized number '75' in a blue, metallic font. To the right of the '5', the words 'SINCE' and '1931' are stacked vertically in a smaller, white, sans-serif font.

GIA Celebrates 75 Years...

This year marks GIA's 75th anniversary, an appropriate occasion to celebrate the Institute's many accomplishments over the decades. The more than 300,000 students who have completed its educational programs. The creation in 1953 of the International Diamond Grading System™, the industry standard for analyzing polished diamonds. The gemological instruments and research discoveries it has fostered.

Yet GIA's diamond anniversary is also an appropriate time to take stock of its service mission and consider the age-old question, "What have you done for me lately?"

- Diamond cut, the most complex of the 4 Cs, has been the subject of extensive research at the Institute. January 1 saw the introduction of the GIA Diamond Cut Grading system for standard round brilliant cut diamonds in the D-to-Z color range. To familiarize the industry with the techniques and terminology of the new system, free seminars have been conducted in cities worldwide. The entire "GIA on Diamond Cut" series of research articles is available at www.gia.edu/research, and all three *G&G* diamond cut articles can be downloaded free at www.gia.edu/gemsandgemology.
- Several other research efforts continue, such as identifying the latest generation of synthetic diamonds and detecting beryllium diffusion in a range of corundum colors. These studies are aimed at protecting public confidence in the industry, and the Institute's researchers routinely present their results in journals and at conferences throughout the world.
- In February, the GIA Laboratory expanded its identification services so that rubies, sapphires, and alexandrites—in addition to emeralds—now receive their own gem-specific reports. In response to increasingly sophisticated techniques for enhancing colored stones, the updated reports contain detailed information on any treatments that have been applied.
- GIA Education is constantly updating its core diamond, colored stones, and jewelry manufacturing arts programs—most recently, a major revision of its Gem Identification course. This October, the GIA School of Business will launch a college-level degree program, culminating in a Bachelor of Business Administration (BBA) diploma, which will further raise the academic profile of gemology and the jewelry industry.
- On the international front, the Institute now has campuses in nine countries, with the Dubai campus scheduled to open in 2007.
- The Institute provides complimentary access to many informative resources, including: *The Loupe*, the news magazine for the industry; the *GIA Insider*, the Institute's biweekly electronic newsletter; and the online tutorials "How to Buy a Diamond" and "How to Buy a Gemstone." The *G&G* section of the website (www.gia.edu) includes a data depository,



several free article downloads, and the entire set of back issues from 1934 through 1980.

- The Richard T. Liddicoat Gemological Library and Information Center, located at GIA's Carlsbad headquarters, serves as the repository of gemological knowledge for the public and members of the trade. The Library's growing collection of some 38,000 books, 300 periodicals, and 1,000 videos are available for on-site research. Just e-mail library@gia.edu for assistance from the Library's helpful staff.
- The constantly expanding GIA Museum in Carlsbad houses an extensive collection of gems and jewelry, making it a valuable educational resource for the Institute's students and the public. Some samples may be loaned for nondestructive research. Scheduled tours of the museum's galleries are available on weekdays, and admission is free (to schedule a tour, call 760-603-4116).
- The Institute's career services department supports jobseekers and employers by maintaining a free

database of jobs available in the gem and jewelry industry. In addition, GIA students and graduates are eligible to receive free career preparation assistance. Two annual GIA Jewelry Career Fairs—in New York in July and Carlsbad in October—match jobseekers with companies and offer one-on-one career coaching, at no cost to attendees (e-mail careerservices@gia.edu).

- Over the years, through the generous support of the industry, GIA has awarded hundreds of scholarships to deserving students. In 2004 and 2005 alone, 54 scholarships were awarded for a total of over \$196,000.
- With more than 30 chapters worldwide, the GIA Alumni Association provides an important vehicle for continuing education as well as communication.
- And, of course, *Gems & Gemology*, which now goes to subscribers in more than 100 countries worldwide, continues to receive most of its funding directly from GIA, as part of the Institute's mission to serve the industry and the gem-buying public.

I do not normally use this forum to talk about GIA, as *G&G* is a technical journal for and about the entire gemological community. But without GIA, there would be no *Gems & Gemology*, just as there would be no International Diamond Grading System, no Graduate Gemologist diploma, and no Richard T. Liddicoat Gemological Library. That's an important message to share as the Institute celebrates 75 years of service.

So, what have you done for us lately, GIA? More than we can say.

Alice S. Keller
Editor-in-Chief

LETTERS

MORE ABOUT “MEDUSA QUARTZ”

Shortly after the publication of the Gem News International entry on gilalite-bearing quartz (Fall 2005, pp. 271–272), I received a reprint request from a marine biologist who specializes in medusa systematics, Dr. Francesc Pagès of the University of Barcelona. He was surprised by the striking similarity between the gilalite clusters we described and the medusa stage of *Rhizostoma pulmo*, an attractive but venomous jellyfish he commonly observes in the Mediterranean. Hence, he felt that the name chosen for this new variety of quartz was quite appropriate.

He was also kind enough to send a photograph of a specimen he encountered recently. Placed beside the photomicrograph of a gilalite cluster in “medusa quartz,” the resemblance is striking (figure 1). This provides a surprising and aesthetic link between gemology and marine biology.

Benjamin Rondeau
Muséum National d’Histoire Naturelle, Paris

CHELSEA FILTERS AND SYNTHETIC EMERALDS

The excellent article on the characterization of Malossi hydrothermal synthetic emerald will be of great value when gemologists start issuing “Country of Origin” certificates for synthetic materials. Unfortunately, today it is of little practical use for the working gemologist.

The authors confirmed what Basel Anderson, the developer of the Chelsea Filter, wrote almost 65 years ago (see *Gem Testing for Jewellers*, Heywood & Co., London, 1942, p. 56), that is, it can differentiate natural emeralds from green glass, but it cannot separate natural from synthetic emeralds.

On the other hand, the Hanneman-Hodgkinson Synthetic Emerald Filters have been successfully performing this function for almost a decade. I believe the time



Figure 1. The medusa form of this jellyfish (*Rhizostoma pulmo*) on the left bears a striking resemblance to the gilalite inclusion in quartz on the right. Photos by Francesc Pagès and B. Rondeau (right, magnified 16×).

has come for *G&G* to acknowledge their existence and in future articles of this nature require the notation of a gem’s appearance through these filters.

W. Wm. Hanneman, Ph.D.
Granbury, Texas

Editors’ Reply

We thank Dr. Hanneman for his comments. Unfortunately, there are some practical limits to the testing we can require from authors, especially if it involves equipment they may not have access to. Note that *Gems & Gemology* has recognized the utility of the Hanneman-Hodgkinson filters in the past (see E. Boehm, “Portable instruments and tips on practical gemology in the field,” Spring 2002 *Gems & Gemology*, pp. 14–27), and readers are referred to page 24 of that article for a discussion of their use.

APPLICATIONS OF LASER ABLATION–INDUCTIVELY COUPLED PLASMA–MASS SPECTROMETRY (LA-ICP-MS) TO GEMOLOGY

Ahmadjan Abduriyim and Hiroshi Kitawaki

Laser ablation–inductively coupled plasma–mass spectrometry (LA-ICP-MS) is an important technique for quantitative chemical analysis. The authors have applied this minimally destructive technique to gemology to take advantage of its high spatial resolution, rapid and direct analysis of gemstones (whether loose or mounted), and precise measurement of a wide range of elements—even in ultra-trace amounts. This article summarizes LA-ICP-MS principles and describes the successful application of this technique to detecting beryllium diffusion treatment in corundum and identifying the geographic origin of emeralds. LA-ICP-MS is significantly less expensive than SIMS and more sensitive than LIBS, which is the least costly of the three instruments.

In recent years, gemologists worldwide have faced a variety of new treatments, synthetics and simulants, and gem sources that have caused confusion in the trade. Several techniques—including UV-visible, infrared, and Raman spectral analysis—have been employed to solve some of these problems. However, each of these techniques has limitations, and even in combination they have not been entirely successful in addressing all of these challenges. Now, chemical analysis by laser ablation–inductively coupled plasma–mass spectrometry (LA-ICP-MS) has emerged as a powerful tool for gemologists.

ICP-MS has been used for decades to chemically characterize materials, but historically this technique has required dissolving solid samples in strong acids prior to analysis. The use of laser ablation with ICP-MS was developed by Gray (1985) and became commercially available in the early- to mid-1990s. Combined with the development of extremely sensitive mass spectrometers, laser ablation allowed ICP-MS to be used on gemstones with minimal damage, since the laser vaporizes only a microscop-

ic amount of the sample for analysis. Additional advantages include a high spatial resolution (just a few micrometers), low detection limits, and high precision and accuracy. This technique is also particularly attractive to scientists who want to study micro-spatial distributions of trace elements and isotopic compositions, from light (helium) to heavy (uranium). In addition, the analysis is rapid and no sample preparation is required. As a result, LA-ICP-MS has become one of the most exciting instruments in gemology, geology, and materials science.

LA-ICP-MS analyses provide quantitative data for major, minor, and trace elements in the analyzed samples, from which variation diagrams and “chemical element fingerprints” can be established. Such fingerprinting can reveal differences between samples that may be attributed to the geographic origin of

See end of article for About the Authors and Acknowledgments.
GEMS & GEMOLOGY, Vol. 42, No. 2, pp. 98–118.
© 2006 Gemological Institute of America



Figure 1. In late 2001, substantial numbers of beryllium diffusion-treated sapphires entered the gem trade, spurring a need for proper identification. Shown here are a collection of loose and mounted beryllium-diffused sapphires (the mounted stones include some untreated sapphires). The bracelet and earrings are courtesy of Michael Couch © Assocs.; the loose sapphires are courtesy of Deepam Inc. and Robert E. Kane. Photo by Harold © Erica Van Pelt.

the sample or subsequent treatment. An introduction to the potential use of this method in gemology was reported by Günther and Kane (1999a,b). Due to the high cost of the instrumentation and the micro-destructive nature of the method, gemologists were slow to explore its full range of applications. At this time, however, the Gemmological Association of All Japan (GAAJ, in Tokyo), Gemological Institute of America (GIA, in Carlsbad), Central Gem Laboratory (CGL, in Tokyo), and Tiffany & Co.'s Merchandise and Testing Laboratory (in New Jersey) all have LA-ICP-MS systems for gemstone analysis (as well as other applications, such as metals testing). Other gemological labs use LA-ICP-MS systems at nearby universities. For example, the Gübelin Gem Lab (Lucerne, Switzerland), the GRS Gemresearch Swisslab (Lucerne), and the SSEF Swiss Gemmological Institute (Basel) have access to the LA-ICP-MS facilities at the Swiss Federal Institute of Technology (ETH) Laboratory in Zurich.

LA-ICP-MS has been applied to a variety of topics in earth sciences (see, e.g., Hirata and Nesbitt, 1995; Jeffries et al., 1995; Jackson et al., 2001; Norman, 2001) and archeology (e.g., Pollard and Heron, 1996; Devos et al., 2000; Tykot, 2002). However, publications on the application of LA-ICP-MS to gem materials were uncommon until relatively recently (Watling et al., 1995; Günther and Kane, 1999a,b; Guillon and Günther, 2001; Rankin et al., 2003; Saminpanya et al., 2003; Wang et al., 2003; Abduriyim and Kitawaki, 2006).

In this article, we will examine two areas in which LA-ICP-MS can be particularly useful: detecting new treatments and determining the geographic origin of gemstones (using the specific example of emeralds).

Detection of New Treatments. Toward the end of 2001, unprecedented amounts of saturated orange-pink to pinkish orange sapphires (the so-called padparadscha colors), as well as yellow sapphires, became widely available on the worldwide jewelry market (Scarratt, 2002; Shida et al., 2002; see figure 1). Many studies subsequently revealed that beryllium (Be) had been diffused into the sapphires at high temperatures, with the Be originating from chrysoberyl (see, e.g., Emmett et al., 2003, and references cited therein). Because beryllium is a "light" (i.e., low atomic weight) element, trace levels of Be cannot be detected by most analytical techniques, including energy-dispersive X-ray fluorescence (EDXRF), energy-dispersive spectroscopy with a scanning electron microscope (SEM-EDS), and, in some cases, electron-microprobe analysis (EMPA). Secondary ion mass spectrometry (SIMS) has proved successful in detecting trace amounts of Be, but analyses are extraordinarily expensive (see, e.g., Emmett et al., 2003; Novak et al., 2004). For this reason, the present authors focused their attention on LA-ICP-MS. Since May 2003, GAAJ has offered an identification service for Be-diffused heat-treated corundum, using LA-ICP-MS. Recently, a less expensive instrument, laser-induced breakdown

spectroscopy (LIBS), has been applied to this problem, but it has some limitations, as discussed below.

Geographic Origin Determination. Geographic origin is an important consideration for many gem materials in some markets. Within Japan in particular, geographic origin may be a critical factor in the sale of major gems such as corundum, emerald, tourmaline, alexandrite, and opal. However, without reliable and detailed analytical data, determination of origin may be difficult, if not impossible. Even the most experienced laboratories regard origin determinations as opinions based largely on the experience, literature, and/or data collected by that laboratory. Thus, there is a need for origin determinations based on a more rigorous scientific foundation.

BACKGROUND

Chemical Analysis of Gem Materials. EDXRF and SEM-EDS are the standard methods used in gemological laboratories for the nondestructive qualitative (and possibly quantitative) chemical analysis of gem materials (see, e.g., Stockton and Manson, 1981; Stern and Hänni, 1982; Muhlmeister et al., 1998). EDXRF is capable of measuring the chemical composition of a gemstone in a matter of minutes, by detecting the energy of emitted X-rays that are produced when the sample is exposed to an X-ray beam. With SEM-EDS, an electron beam scans across the specimen's surface, producing signals from secondary or backscattered electrons that can be used to produce a high-resolution image. In addition, X-rays emitted from the sample can reveal its chemical composition. Using an attachment for energy-dispersive spectroscopy, a more precise chemical composition can be obtained with the SEM at high spatial resolution. Although both EDXRF and SEM-EDS are limited in their detection and measurement of light elements, when combined with other analytical methods such as UV-Vis spectroscopy, they can identify some trace elements that provide useful information on the geologic occurrence, geographic origin, and causes of color in gem materials.

EMPA is another well-established method being used in gemology (Dunn, 1977). This technique uses a high-energy focused beam of electrons to generate X-rays characteristic of the elements within a sample. It can provide quantitative analyses of elements ranging from beryllium (in some cases) to uranium, at levels as low as 100 parts per million (ppm or $\mu\text{g/g}$, which are fractional weights). Thus far, this is the only fully quantitative technique that is nondestructive.

Unfortunately, EMPA is not useful for analyzing beryllium in diffused corundum, since Be is present in amounts that are below the detection limit of the instrument.

SIMS is a powerful micro-destructive technique for chemical analysis of a wide variety of solid materials (Benninghoven et al., 1987). A beam of primary ions such as oxygen or argon is focused on the sample, causing a very small amount of the surface to be sputtered. A portion of the sputtered atoms are ionized and extracted using an electrical field. The ionized atoms are then filtered according to their energy and mass by an electrostatic sector and a magnetic field, at which point they go to a mass spectrometer for isotopic analysis. This technique can provide sensitivities near parts per billion (ppb or ng/g) for all elements from hydrogen to uranium. However, it is only available in some universities and research laboratories due to its high cost and sophisticated operating requirements.

LIBS can detect a full range of major, minor, and trace elements simultaneously (see, e.g., García-Ayuso et al., 2002), and its low cost and easy operation have attracted the interest of several gem laboratories. A single-pulse high-energy Nd:YAG 1064 nm laser is used to vaporize a microscopic area of a sample at high temperature (i.e., $>5000^\circ\text{C}$ – $10,000^\circ\text{C}$), and the sputtered particles are broken down into a mixture of atoms, ions, and electrons. After the laser pulse has ended, excited electrons in the atoms drop down to a low energy level and discharge light. By detecting the wavelength and strength of this emission with a high-resolution fiber-optic spectrometer, optical emission spectra can be generated that may then be converted to qualitative and semiquantitative chemical data. However, precise quantitative analyses cannot be obtained with this technique (Krzemnicki et al., 2004; Themelis, 2004).

LA-ICP-MS Instrumentation. The LA-ICP-MS analysis process can be thought of in two main parts: sampling (i.e., laser ablation and ionization in a plasma) and mass spectrometry. While mass spectrometry has been well developed for many decades, the sampling techniques of laser ablation and inductively coupled plasma were developed more recently.

Mass Spectrometry. Following J. J. Thomson's use of electromagnetic fields to separate ions for analysis (Thomson, 1911), scientists such as Dempster (1918), Aston (1919), and Stephens (1946) developed this technique into what it is today, a highly sensitive

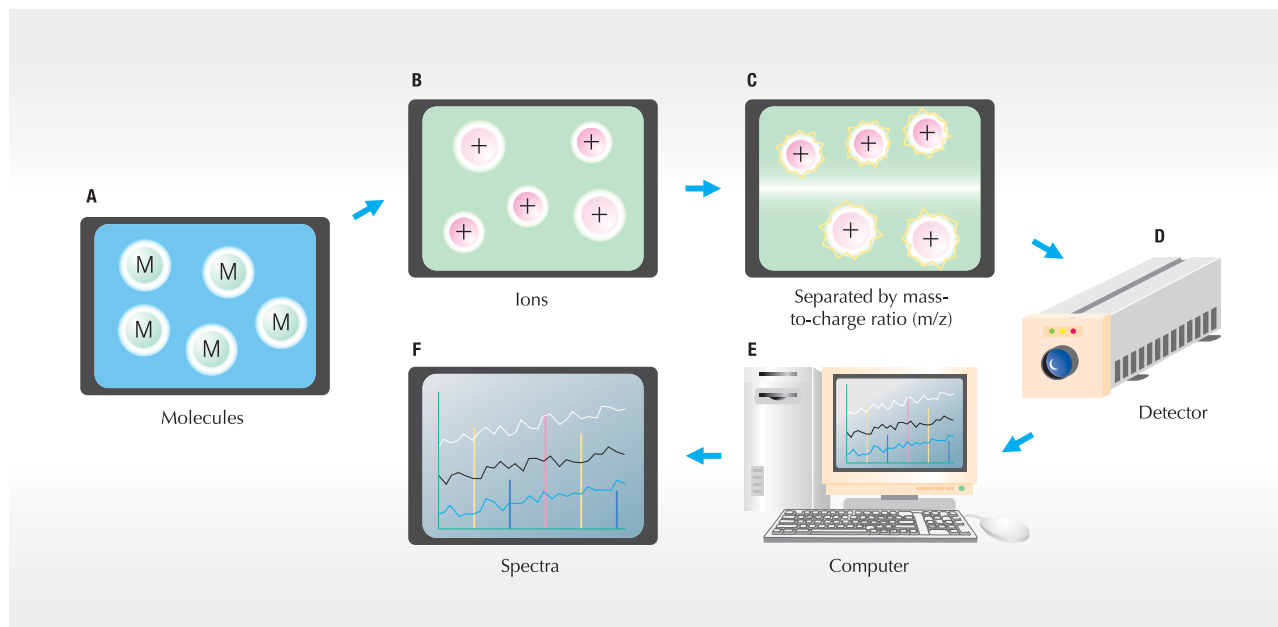


Figure 2. This chart shows how a mass spectrum is obtained from a sample. Gaseous molecules of the sample (A) are ionized to form gaseous ions (B). The ions are separated according to their mass-to-charge ratio when they pass through a mass analyzer (C) to the detector (D). A computer (E) transforms the signal from each element into a spectrum, which is displayed on the screen (F).

method capable of analyzing both chemical elements and small organic molecules. Early mass spectrometers required that the sample be in a gaseous state, but developments over time have expanded the applicability of mass spectrometry to include solutions and solids. A mass spectrometer is an instrument that measures the masses of elements or molecules of chemical compounds by separating charged particles according to their mass-to-charge ratio (m/z ; in most cases, the value of $z = +1$). The sample is ionized and the ions are electrostatically directed into a mass analyzer, where they are separated according to their m/z ratio and then sent to a detector (figure 2). A spectrum is then generated that represents the masses of components of a sample.

The most popular mass spectrometer used in ICP-MS is the quadrupole mass analyzer (figure 3), which consists of four parallel metal rods arranged in a square. Each pair of opposite rods has a combined AC and DC electrical potential. When the DC and AC voltages are set to certain values, only ions with a specific m/z ratio are able to continue on a path between the rods. By sequentially selecting many combinations of voltages, the technician can detect an array of different ions. Semi-quantitative measurements of the mass spectrum or isotope ratios are obtained by measuring the intensities of the ions passing through the quadrupole mass analyzer as the voltages on the rods are varied.

Inductively Coupled Plasma. In the 1980s, inductively coupled plasma at atmospheric pressure was developed as a technique for ionizing samples. The sample (in solution or vaporized using a laser ablation system) is conveyed in a flow of argon gas into a torch that is inductively heated to approximately 10,000°C. At this temperature almost all matter in the sample is atomized and ionized, forming a plasma that provides a rich source of both excited and ionized atoms (Jarvis et al., 1992). With the combination of ICP and MS technologies, rapid quantitative elemental analysis with high accuracy and low detection limits became possible.

Laser Ablation. The combination of laser ablation with ICP-MS has been widely used for multi-elemental determination and *in situ* isotopic analysis of solid materials (Gray, 1985; Arrowsmith, 1987). In the laser ablation process, the sample is placed in the ablation cell (which does not need to be under vacuum), and a minute portion of its surface is vaporized using a pulsed high-energy laser beam that is directed through the objective lens of a modified petrographic microscope. The surface of the sample is viewed with a charge-coupled device (CCD) camera mounted on the microscope, allowing for precise location of the laser spot. The laser pulses cause energetic atoms, ions, molecules, and solid particles to be ejected from the target, and these ablated aerosols are transported in argon or helium gas to the

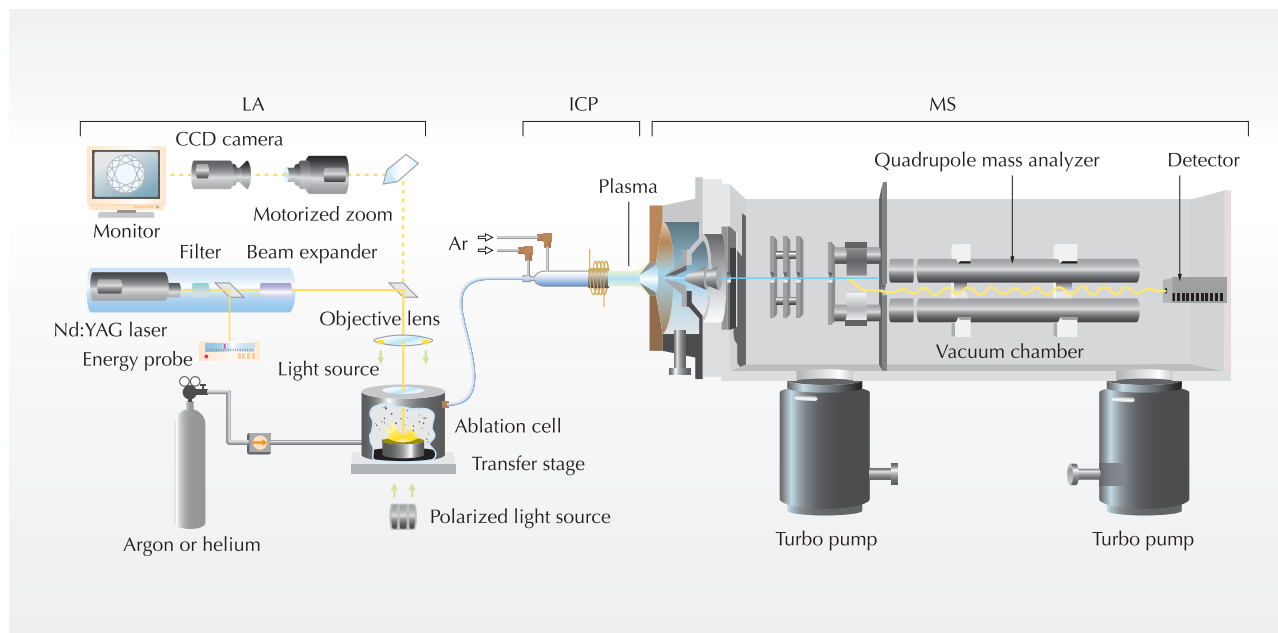


Figure 3. This schematic diagram shows the components of a 213 nm Nd:YAG laser ablation system combined with a quadrupole ICP-MS instrument. The sample is placed in the ablation cell and the laser beam is focused onto the sample with the help of a CCD camera. The ablated material forms an aerosol, which is transported by an argon or helium carrier gas to the plasma of the ICP-MS. At the ICP, laser-ablated particles are vaporized and ionized. The ions are extracted by the vacuum interface and guided into the mass analyzer, where they are separated by their mass-to-charge ratio and finally detected.

plasma of the ICP-MS. Helium is typically used as the carrier gas in the sample cell, and is combined with Ar in the tubing that leads to the ICP. During the ablation process, less material is left around the laser spot crater when using He as compared to Ar, so more of the sample can be transferred to the ICP, leading to a higher-intensity, more stable signal (Günther and Heinrich, 1999). Two types of laser have been widely used for ablating minerals or glassy materials: (1) an argon fluoride (ArF) excimer laser with a wavelength of 193 nm (Loucks et al., 1995; Günther et al., 1997; Horn et al., 2000), and (2) a Nd:YAG 1064 nm (infrared) laser that is frequency-multiplied to UV wavelengths (fourth harmonic at 266 nm and fifth harmonic at 213 nm; Jenner et al., 1993; Jeffries et al., 1998).

Data Quality Considerations. A mass spectrum consists of a series of peaks representing the distribution of components (atoms or molecules) by mass-to-charge ratio. The relative intensities of the various isotopes in the spectrum provide a semi-quantitative chemical analysis (Tye et al., 2004). To produce quantitative data, the analysis of a sample must be calibrated against an external standard of known composition, that is, by measuring the signals for the elements of interest in the sample and

comparing them to the signals from a standard with known concentrations of those elements. Several calibration strategies have been developed for quantification of LA-ICP-MS analyses, including those using solid standards (glass, ceramic, cement, and metals) and those using standard solutions (Kanicky and Mermet, 1999). In general, the use of matrix-matched standards (e.g., a corundum standard for analyzing sapphires) is advantageous, because the ablation behavior will be similar for both the standard and the sample. However, in many cases this approach is limited by a lack of suitable materials. For example, NIST (National Institute of Standards and Technology) glass is widely used as an external standard for successfully analyzing the trace-element contents of silicates and carbonates. However, the matrix of simple oxide minerals (e.g., corundum) is much different from the NIST glass. Variation in these matrices can give rise to inconsistencies in ionization efficiency, which will create differences in the signal of a given element in those materials (even if they contain identical concentrations of the element).

To obtain accurate quantitative chemical data for gem corundum, the external standard should consist of a well-characterized homogenous sample of ultra-pure synthetic corundum that has been

doped with the element(s) of interest. However, if such a standard is not available, an internal element standard may be used to correct the analyzed signals. In this procedure, the concentration of Al in the sample is measured using another quantitative technique, such as EMPA. Calibration for other elements in the sample can then be achieved by comparing the LA-ICP-MS signal for Al obtained from an external NIST glass standard to that obtained from the specimen.

MATERIALS AND METHODS

For our investigations of beryllium diffusion-treated corundum, we used LA-ICP-MS to analyze a total of 121 faceted natural and synthetic rubies and sapphires: 21 were unheated, 19 were subjected to traditional heat treatment, and 81 were treated with Be diffusion and then repolished (table 1). Some of the stones treated by Be diffusion were analyzed before and after treatment to confirm that Be was diffused by the process; these samples included four colorless sapphires and four rubies, as well as eight colorless Verneuil synthetic sapphires and two pink flux-grown synthetic sapphires. At the request of the authors, treaters in Thailand heated the stones in a crucible together with powdered chrysoberyl to over 1800°C in an oxidizing atmosphere (for 22 hours in Bangkok and more than 10 hours in Chanthaburi). Samples SCL001, SCL003, VCS001, and VCS005 were cut in half after Be-diffusion treatment and eight point analyses were performed by LA-ICP-MS on the cut cross-section of each sample. In addition, sample MPd-H1 was used for both LA-ICP-MS and SIMS analyses, with six point analyses across the cut cross-section.

The emeralds analyzed by LA-ICP-MS for geographic origin investigations consisted of 29 faceted Brazilian stones and 82 parallel-polished slabs, cabochons, and faceted samples from Colombia, Nigeria, Zambia, Zimbabwe, Pakistan, and Afghanistan (table 2). Of the latter samples, 50 parallel-polished slabs were supplied by Dr. Dietmar Schwarz; these emeralds were purchased or collected directly from the mine areas. The authors acquired the other samples at the Tokyo and Tucson gem fairs. The samples covered the color range from light green to deep green. FTIR and Raman spectroscopic analyses showed that, with only a few exceptions, the emeralds were not filled with oil or resin. LA-ICP-MS data for 26 elements were obtained from three different areas on each sample. Averaged data were

used for the ranges that are reported in table 2.

The LA-ICP-MS analyses were obtained with a New Wave Research laser ablation system (using a Merchantek UP-213A/F laser) combined with a quadrupole ICP-MS instrument from Agilent (7500a series). The operating conditions of the LA-ICP-MS used for this study are indicated in table 3. Analytical sensitivity improves as the amount of vaporized sample increases, and our research showed that it was advantageous to inscribe our logo "GAAJ" on the girdle of all specimens during the laser ablation process (figure 4). This allowed us to obtain good sensitivity for light elements with the least "damage" to the sample. When testing for Be-diffused corundum, care was taken to avoid analyzing areas that might contain interfering inclusions. This very small inscription proves the analysis has been conducted and does not affect the beauty of a gemstone. As with laser inscriptions that are currently performed on diamonds, the LA-ICP-MS laser logo is barely visible with a 10× loupe.

Calibration was done using NIST SRM 612 multi-element glass (Pearce et al., 1997), with Al as the internal element standard (based on an average Al_2O_3 concentration of 99.00%, determined by EMPA) for corundum analyses; the same NIST standard was used for emerald calibration.

We monitored the signals of selected isotopes in the corundum and emerald samples, and the concentrations of some of these elements in the samples were calculated (see table 3). "Blank" samples of carrier gas were repeatedly analyzed (10 times) at regular intervals to determine the detection limit of each element (table 4). The higher background counts for Na, Si, Ca, and Fe were related to mass interference from the sum of various elements in the air within the instrument— ^{28}Si ($^{12}\text{C}^{16}\text{O}$), ^{29}Si ($^{12}\text{C}^{16}\text{O}^1\text{H}$), ^{44}Ca ($^{12}\text{C}^{16}\text{O}_2$), ^{56}Fe ($^{40}\text{Ar}^{16}\text{O}$), ^{57}Fe ($^{40}\text{Ar}^{16}\text{O}^1\text{H}$)—and/or contamination of the system with debris from the NIST SRM 612 calcium silicate glass where, for example, a silicon ion from the glass might be misidentified as a corundum impurity— ^{23}Na (^{23}Na), ^{28}Si (^{28}Si), ^{43}Ca (^{43}Ca or $^{27}\text{Al}^{16}\text{O}$), ^{44}Ca ($^{28}\text{Si}^{16}\text{O}$), ^{56}Fe ($^{40}\text{Ca}^{16}\text{O}$ or $^{28}\text{Si}^{28}\text{Si}$)—before the measurements were made. Due to these possible interference problems, we monitored two isotopes each of Si, Ca, and Fe. Concentration levels in this article are described as *trace* elements (<10,000 ppm or <1 wt.%), *minor* elements (<10 wt.% or <100,000 ppm), and *major* elements. To facilitate comparison with the literature, some trace-element values have been

TABLE 1. Corundum samples analyzed by LA-ICP-MS for Be-diffusion investigations.^a

Sample nos.	No. of samples	Description	Origin	Weight (ct)	Be (ppm)		
					LA-ICP-MS	LIBS	SIMS
Unheated							
SY001-002	2	Yellow	Sri Lanka	0.23-0.76	bdl	bdl	na
SP001-002	2	Padparadscha	Sri Lanka	0.63-0.85	bdl	na	na
EO001-002	2	Orange	East Africa	0.30-1.32	bdl	na	na
MB001-002	2	Blue	Madagascar	1.23-2.12	bdl	na	na
SCL001-003	3	Colorless	Sri Lanka	0.57-0.68	bdl	na	na
VCS001-010	10	Colorless	Verneuil synthetic	0.85-1.03	bdl	na	na
Traditionally heated							
SY003-004	2	Yellow	Sri Lanka	1.56-3.87	bdl	na	na
EO003-004	2	Orange	East Africa	0.47-2.31	bdl	na	na
MP001-004	4	Pink	Madagascar	0.42-4.01	bdl	na	na
TPL001-002	2	Purple	Tanzania	0.59-2.50	bdl	na	na
MB003-005	3	Blue	Madagascar	1.56-3.52	bdl	na	na
ECC001-002	2	Color change (dark purple)	East Africa	0.40-4.01	bdl	na	na
SCL004-005	2	Colorless	Sri Lanka	0.50-0.71	bdl	na	na
TR001-002	2	Ruby (dark red)	Thailand	0.83-2.59	bdl	na	na
Be-diffusion treated^b							
SY-H1-H8	8	Yellow	Sri Lanka	0.63-2.96	1.8-8.1	Detected (very low) ^c	na
MPd-H1-H12	12	Pinkish orange	Madagascar	0.34-4.36	bdl-8.4 ^d	Detected ^e	bdl-9.54 ^d
EO001-003	3	Saturated orange	East Africa	0.23-1.21	3.6-4.1	na	na
EO004-007	4	Orange	East Africa	0.34-3.90	1.9-2.2	na	na
MP-H1-H4	4	Pink	Madagascar	0.63-3.59	1.9-3.3	Detected ^f	na
TPL-H1-H10	10	Purple	Unknown	0.32-3.81	2.6-7.8	na	na
MB-H1-H10	10	Blue	Madagascar	0.89-3.68	1.4-6.3	na	na
MB-H11-H16	6	Blue	Australia	3.82-4.77	3.4-15	na	na
MB-H17-H20	4	Blue	China	2.65-5.26	2.9-6.7	na	na
ECC001	1	Dark green-purple	East Africa	0.32	2.6	na	na
ECC002	1	Dark purple	East Africa	3.93	1.7	na	na
SCL001-002	2	Light yellow	Sri Lanka	0.48-0.56	1.4-5.4	na	na
SCL003-004	2	Light yellow	Sri Lanka	0.40-0.62	bdl-2.3	na	na
TR001-002	2	Ruby (bright red)	Thailand	0.70-2.50	6.3-16	na	na
TR003-004	2	Ruby (bright red)	Thailand	1.13-2.52	0.43-2.43	na	na
VCS001-004	4	Colorless	Verneuil synthetic	0.72-0.81	1.1-5.0	na	na
VCS005-008	4	Colorless	Verneuil synthetic	0.77-0.94	bdl-1.6	na	na
FPS001	1	Whitish pink	Flux synthetic	0.54	4.7	na	na
FPS002	1	Pink	Flux synthetic	0.66	0.3	na	na

^a All analyses were performed on the girdle of faceted stones (the Be-diffused samples were repolished after treatment). For LA-ICP-MS: External standard = NIST SRM 612, internal standard = 99.00% Al₂O₃. For SIMS: Accuracy of Be is ±10%, detection limit is 0.01 ppm Be, external standard = Be-implanted synthetic corundum. The following samples were analyzed by LA-ICP-MS before and after Be-diffusion treatment: EO001-004, ECC001-002, SCL001-004, TR001-002, and VCS001-008. These data include one point analysis of the re-polished girdle and eight point analyses of the cross-sections of samples SCL001, SCL003, VCS001, and VCS005. Abbreviations: bdl=below detection limit, na=not analyzed.

^b Samples shown in blue were Be-diffused in Bangkok for 22 hours at 1800°C, whereas the samples shown in green were Be-diffused in Chanthaburi for approximately 10 hours. The exact conditions are not known for the Be-diffusion treatment of samples SY-H1-H8, MPd-H1-H12, MP-H1-H4, TPL-H1-H10, MB-H1-H10, MB-H11-H16, and MB-H17-H20.

^c Sample SY-H1 only.

^d Sample MPd-H1 only: six point analyses of the sample's cross-section using both LA-ICP-MS and SIMS.

^e Sample MPd-H10 only.

^f Sample MP-H4 only.

converted to weight percent (wt.%) oxides from their simple elemental concentrations (ppm).

To compare the accuracy of our LA-ICP-MS

analyses to those obtained with SIMS, we analyzed six points on corundum sample MPd-H1 by both techniques. Each point analyzed by LA-ICP-MS

TABLE 2. Range of chemical compositions by LA-ICP-MS of emeralds from eight localities.^a

Property	Kaduna, Nigeria	Kafubu, Zambia	Sandawana, Zimbabwe	Itabira- Nova Era, Brazil	Santa Terezinha, Brazil	Swat, Pakistan	Panjshir, Afghanistan	Cordillera Oriental, Columbia
Sample no.	ENNIO1-10	ENZA01-10, EZ100-110	ENZI01-10	EBI001-014	EBS001-015	ENPAI01-10	EAF001-012	ENCO01-10, 1EC001-010
No. of samples	10	20	10	14	15	10	12	20
Color	Bluish green to light green	Bluish green to green	Pale green to green	Green to deep green	Green to deep green	Green to deep green	Pale green to green	Pale green to green to deep green
Weight	0.59-1.07	0.19-3.29	0.13-0.77	0.32-2.25	0.55-3.01	0.15-0.83	0.20-1.77	0.45-3.67
Type	Rough and parallel pol- ished plates	Mixed cuts and parallel polished plates	Parallel pol- ished plates and cabo- chons	Mixed cuts	Mixed cuts	Parallel pol- ished plates and cabo- chons	Mixed cuts	Parallel pol- ished plates, cabochons, mixed cuts
Minor elements (wt.% oxides)								
Na ₂ O	0.22-0.64	0.93-1.87	1.97-2.30	1.33-2.18	1.61-2.43	1.11-2.01	0.79-1.55	0.33-0.82
MgO	0.04-0.09	1.41-2.36	0.88-3.13	1.78-2.54	2.17-2.82	1.86-2.65	0.75-1.82	0.05-1.33
FeO ^{tot}	0.48-0.96	1.23-2.17	0.34-1.13	1.13-1.42	1.42-2.34	0.30-1.29	0.28-0.76	bdl-0.23
K ₂ O	0.006-0.07	0.03-0.42	0.01-0.12	0.02-0.05	0.04-0.91	0.01-0.05	bdl-0.05	bdl-0.02
CaO	0.03-0.07	bdl-0.06	0.05-0.28	bdl-0.02	0.10-0.26	0.01-0.06	bdl-0.02	bdl-0.001
Sc ₂ O ₃	0.003-0.03	0.006-0.04	0.01-0.09	bdl-0.01	bdl-0.02	0.01-0.49	0.001-0.27	bdl-0.001
V ₂ O ₃	0.01-0.06	0.01-0.04	0.02-0.10	0.03-0.07	0.001-0.10	bdl-0.06	0.16-0.50	0.11-1.21
Cr ₂ O ₃	0.01-0.55	0.10-0.80	0.41-1.41	0.09-1.10	0.25-2.66	0.10-0.84	0.30-0.41	0.01-0.64
Cs ₂ O	0.009-0.01	0.07-0.15	0.01-0.30	bdl-0.01	0.36-0.64	bdl-0.02	bdl-0.009	bdl-0.003
Trace elements (ppm)								
Li	54-200	320-1,260	161-1,370	90.5-305	220-954	163-500	98-229	10-92
B	bdl-2.3	bdl-10	bdl-2.0	bdl	bdl	bdl-2.1	bdl	bdl
Ti	5.0-63	8.2-30	3.1-61	5.2-15	2.6-55	3.5-53	bdl-30	bdl-51
Mn	4.0-43	9.3-156	5.0-180	10-39	9.3-37	bdl-29	9.3-42	bdl-4.4
Co	bdl-1.3	1.9-10	1.2-7.5	bdl-4.9	bdl-3.0	bdl-3.2	bdl-5.4	bdl
Ni	bdl-6.1	6.1-44	3.2-62	17-26	21-105	2.3-26	bdl-27	bdl-5.2
Cu	bdl	bdl-297	bdl-9.7	bdl-1.4	bdl-7.1	bdl-27	bdl-1.6	bdl-4.9
Zn	14-91	21-970	9.1-254	31-117	6.4-32	bdl-6.9	96-135	bdl-3.9
Ga	10-86	8.1-55	6.0-67	12-33	8.7-25	2.3-14	16-57	3.1-70
Rb	6.0-64	24-319	10-570	37-65	46-110	3.1-38	21-44	bdl-5.7
Sr	bdl	bdl	bdl-14	bdl	5.4-39	bdl	bdl-1.1	bdl-1.4
Sn	bdl-3.4	bdl-4.2	bdl-10	bdl-1.5	bdl-5.8	bdl-3.3	bdl-1.3	bdl-5.1
Ba	bdl-2.0	bdl-20	bdl-5.4	bdl-2.0	bdl-3.5	bdl-6.5	bdl-20	bdl
Pb	bdl-7.2	bdl-110	bdl-8.8	bdl	bdl-7.6	bdl-1.1	bdl-1.4	0.1-180
Bi	bdl	bdl-36	bdl-10	bdl-3.5	bdl-17	bdl-3.5	bdl-4.6	bdl-3.7
Pt	bdl	bdl-8.7	bdl-2.1	bdl-1.0	bdl-4.3	bdl	bdl	bdl-3.1
Au	bdl	bdl-4.5	bdl-1.7	bdl-1.4	bdl-5.1	bdl	bdl	bdl-9.6

^a Be, Al, and Si were not calculated, and S, P, F, Cl, and H₂O were not measured in this study. The following elements in table 5 were not detected in this study: As, Br, Y, Zr, Ag, Cd, La, and Ce. Abbreviation: bdl = below detection limit.

consisted of a 30 µm round spot, and 10 seconds of ablation resulted in a crater about 2-3 µm deep. The SIMS data were obtained at the Foundation of Promotion for Materials Science and Technology of Japan in Tokyo using a Cameca IMS-6f instrument. A beam current of 150 nA and accelerating voltage of 14.5 kV was used. The beam was composed of O²⁺. The surface of the sample was analyzed in a minute square pattern measuring 30 × 30 µm, to a depth of about 150 nm. The sputtering rate was approximately 0.15 nm/s, under a vacuum of 3 × 10⁻⁷ Pascal (or about one-quadrillionth of

atmospheric pressure at sea level). For both the SIMS and LA-ICP-MS analyses of sample MPd-H1, beryllium concentrations were determined using a Be-ion-implanted external standard of pure synthetic corundum. (The Be-ion-implanted synthetic corundum was not used for the other LA-ICP-MS analyses of corundum in this article because its Be content was homogeneous to only a shallow level [i.e., within several nanometers to several hundred nanometers of the surface].)

LIBS data were collected with an Ocean Optics 2000+ instrument at the GAAJ Research Laboratory

in Tokyo. This instrument was developed recently for gemological applications by the SSEF Swiss Gemmological Laboratory in cooperation with the manufacturer (Krzemnicki et al., 2004; Hänni et al., 2004). To investigate the detection limit of Be, we selected seven samples of Be diffusion-treated corundum (SY001–002, SY003–004, SY-H1, MPd-H10, and MP-H4) for comparison of the LIBS results with those from LA-ICP-MS. The LIBS spectra were obtained with Ar gas in the sample chamber and a 1064 nm Nd:YAG laser (from Big Sky Quantel). The girdle of each sample was subjected to 20 single laser shots with a laser energy of 30 mJ, resulting in a laser hole measuring 100 μm in diameter. Emission spectra of detectable elements were recorded in the range of 200–980 nm.

TABLE 3. LA-ICP-MS operating conditions.

ICP-MS parameters	
Radio frequency (RF) power	1500 watts
Carrier gas flow rate	Ar ~1.20–1.23 L/minute, He 0.50 L/minute
Distance from the ICP torch to the sampler	7 mm
Sampler and skimmer	Ni; 1 and 0.4 mm diameters
Mass number (m/z)	2–260
Integration time	0.1 seconds per point (corundum) or 0.01 seconds per point (emerald)
Laser ablation parameters	
Wavelength	213 nm Nd:YAG laser
Pulse duration	5–10 nanoseconds
Pulse frequency	10 Hz
Output power	2.5 mJ
Laser line size	16 μm in width, logo size 8 \times 230 μm , 4–7 μm in depth
Laser point size	30 μm diameter, 2–3 μm deep
Pre-ablation time	5 seconds
Ablation time	25 seconds
ICP-MS data acquisition time	40 seconds
Isotope signals selected	
Be-diffused corundum	
Isotopes analyzed	$^9\text{Be}^+$
Signals monitored	$^{27}\text{Al}^+$, $^{47}\text{Ti}^+$, $^{53}\text{Cr}^+$, $^{56}\text{Fe}^+$, $^{57}\text{Fe}^+$, $^{69}\text{Ga}^+$
Emeralds	
Isotopes analyzed	$^7\text{Li}^+$, $^{11}\text{B}^+$, $^{23}\text{Na}^+$, $^{24}\text{Mg}^+$, $^{39}\text{K}^+$, $^{43}\text{Ca}^+$, $^{44}\text{Ca}^+$, $^{45}\text{Sc}^+$, $^{47}\text{Ti}^+$, $^{51}\text{V}^+$, $^{53}\text{Cr}^+$, $^{55}\text{Mn}^+$, $^{56}\text{Fe}^+$, $^{57}\text{Fe}^+$, $^{59}\text{Co}^+$, $^{60}\text{Ni}^+$, $^{63}\text{Cu}^+$, $^{66}\text{Zn}^+$, $^{69}\text{Ga}^+$, $^{85}\text{Rb}^+$, $^{88}\text{Sr}^+$, $^{118}\text{Sn}^+$, $^{133}\text{Cs}^+$, $^{137}\text{Ba}^+$, $^{195}\text{Pt}^+$, $^{197}\text{Au}^+$, $^{208}\text{Pb}^+$, $^{209}\text{Bi}^+$
Signals monitored	$^9\text{Be}^+$, $^{27}\text{Al}^+$, $^{28}\text{Si}^+$, $^{29}\text{Si}^+$



Figure 4. During the laser ablation process, our research showed that inscribing the GAAJ logo on the girdle of a gemstone provided sufficient material for analysis of one area; this inscription also proves that a sample has been analyzed by LA-ICP-MS. The tiny mark measures 80 \times 230 μm and penetrates the stone to a depth of ~5–10 μm . Photomicrograph by A. Abduriyim; magnified 80 \times .

PRACTICAL APPLICATIONS

Be-diffused Corundum. Mass spectra for typical LA-ICP-MS analyses of corundum are shown in figure 5, as obtained by ablating the GAAJ logo using the conditions summarized in table 3. A detectable beryllium signal is shown in figure 5 for a Be-diffused sapphire, whereas the samples that did not undergo Be diffusion treatment have only a background signal for Be. As shown in table 1, Be was below the detection limit (i.e., <0.1 ppm)¹ in all the unheated and traditionally heated corundum samples of various colors (40 pieces in total). However, Be (on the order of several parts per million) was detected in all corundum samples, natural and synthetic, that had been treated by Be diffusion (81 pieces; see, e.g., figure 6). In the 20 samples analyzed before and after Be diffusion, no Be was detected before treatment but significant amounts were measured in all samples after treatment, regardless of whether any color alteration occurred. No significant color alteration was seen in any of the samples

¹ In this article, we use ppm to indicate the concentration of trace elements. The concentration also can be written as ppmw (parts per million by weight), which is a fractional weight. The concentration of ions, as ion/cm³, is typically expressed as ppma (parts per million atomic). The mutual relation between these units is approximated by the following expression:

$$ppma = \left[\frac{(\text{molecular weight of } \text{Al}_2\text{O}_3)}{5 \times (\text{atomic weight of element})} \right] \times ppmw$$

treated for approximately 10 hours (figure 7). With the 22-hour heating process, the synthetic sapphires remained colorless, whereas the natural sapphires became yellow.

The concentration of Be was higher in the stones that were heated for 22 hours at 1800°C than in those that were treated for approximately 10 hours. Figure 8 illustrates the Be concentrations measured across some representative samples. The stones that were treated for 22 hours contained 4.2–4.4 ppm Be at the rim and 1.1–1.4 ppm at the center, and the repolished girdles had 5.0 and 5.4 ppm Be. In contrast, the samples treated for the shorter time period contained only 1.0–1.3 ppm Be at the rim, with no Be detected in the core, and the

repolished girdles contained 1.6 and 2.3 ppm Be.

Comparative analyses of the cross-section of Be-diffused pinkish orange sapphire MPd-H1 using LA-ICP-MS and SIMS techniques are graphed in figure 9. The stone showed no concentrations of Be in the center and high concentrations in the rim. The pattern of Be concentration is very similar for both techniques, with slightly lower values obtained with LA-ICP-MS. For example, at the edge of the sample the Be concentration was measured at about 9.5 ppm with SIMS and 8.0 ppm with LA-ICP-MS. The laser ablation pit was deeper than that vaporized by the SIMS beam, so it is clear that as the depth of ablation increases, the ratio of Be to intrinsic elements decreases. While the exact ablation depth cannot be controlled when using LA-ICP-MS, SIMS has a high spatial resolution that therefore can be used for depth profiling across a sample.

Results from the LIBS study are shown in figure 10, which presents the emission spectra of three corundum samples that underwent Be-diffusion and four that did not. There was no Be emission at 313.068 nm in the spectra of the unheated yellow sapphires (SY001-002). In the spectra of the traditionally heated yellow sapphires (SY003-004), an emission peak at 313.16 nm was detected which overlapped parts of Be spectra, with an intensity of just two counts. However, LA-ICP-MS found no measurable Be in that sample, but did show traces of vanadium. Emission related to V occurs at 313.16 nm in the LIBS spectra, which is close to the wavelength of Be emission.

A small Be emission peak (~2–3 counts) was detected in one Be-diffused yellow sapphire (SY-H1) in which 1.8 ppm Be was measured by LA-ICP-MS. Much higher Be concentrations were measured by LA-ICP-MS in a pink sapphire (MP-H4, 3.3 ppm) and in a pinkish orange sapphire (MPd-H10, 8.4 ppm), and these samples had Be peaks in the LIBS spectra of ~5–6 counts and ~10–11 counts, respectively. For very low intensities of Be emission at 313.068 nm, such as 2–3 counts, it is difficult to determine with LIBS whether or not a sample has been Be-diffusion treated; such stones should be tested on another area of the sample, or by another method such as LA-ICP-MS.

Implications. With the increased use of LA-ICP-MS in gem laboratories and the importance of detecting low ppm levels of Be in corundum, the need for standardization between gemological labs has grown.

TABLE 4. LA-ICP-MS detection limits for this study.^a

Mass	Element	Average counts (10 empty runs)	Detection limits 3σ (ppm)
7	Li	1,067	1.9
9	Be	11	0.1
11	B	152	1.6
23 ^b	Na	4,321	17
24	Mg	57	0.4
27	Al	137	0.8
28 ^b	Si	38,187	540
29 ^b	Si	1,532	410
39	K	761	3.4
43 ^b	Ca	96	230
44 ^b	Ca	1,423	240
45	Sc	85	0.3
47	Ti	11	0.6
51	V	44	0.1
53	Cr	353	14
55	Mn	122	0.4
56 ^b	Fe	2,630	12
57 ^b	Fe	72	7.1
60	Ni	28	0.5
63	Cu	39	0.3
66	Zn	78	2.0
69	Ga	30	0.1
85	Rb	15	0.1
88	Sr	4	0.01
118	Sn	60	0.5
133	Cs	23	0.1
137	Ba	3	0.1
195	Pt	19	0.1
197	Au	24	0.1
208	Pb	34	0.1
209	Bi	28	0.1

^a The average intensity of 10 empty runs was used to determine the detection limit of each element. 3σ = 3 standard deviations.

^b Mass interferences are created by polyatomic ions formed from the combination of species derived from the plasma gas, sample matrix, etc. For example, ¹²C¹⁶O overlaps ²⁸Si, ⁴⁰Ar¹⁶O overlaps ⁵⁶Fe, ²⁸Si¹⁶O overlaps ⁴⁴Ca, ⁴⁰Ca¹⁶O overlaps ⁵⁶Fe, and ²³Na contamination from NIST SRM 612 overlaps ²³Na from the sample. High background counts for Na, Si, Ca, and Fe were caused by mass interference.

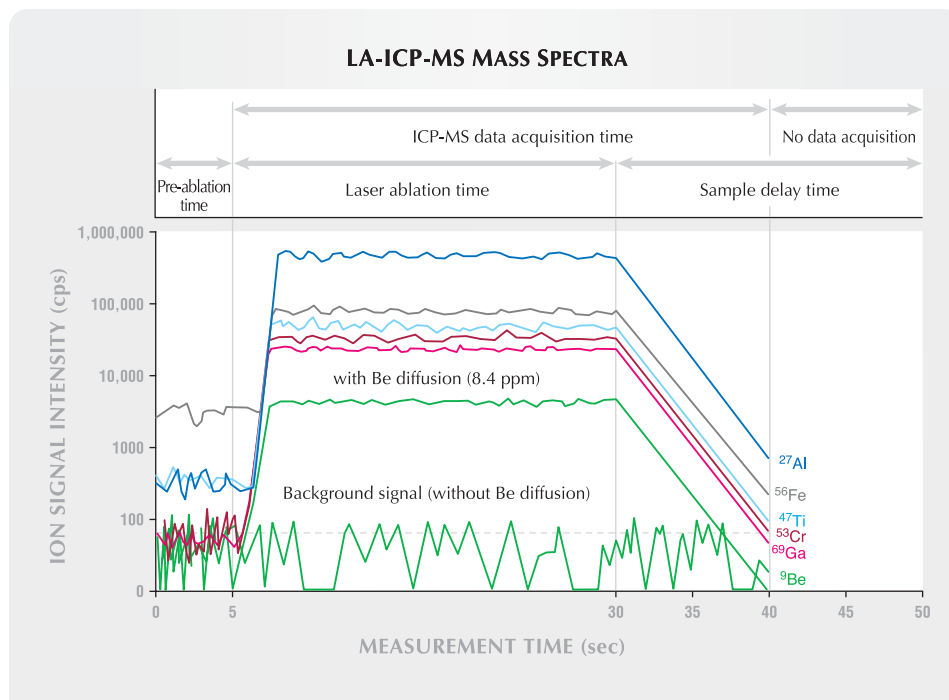


Figure 5. Mass spectra for Be in corundum were generated by laser ablating the GAAJ logo for a 25-second period. The pre-ablation time was 5 seconds, and 35 seconds were used for ICP-MS data acquisition. A detectable Be signal is shown for a Be-diffused sapphire, whereas samples that were either not heated or had been heated by traditional methods do not show a Be signal above the background level. Signals for Al and the common trace elements in corundum (Ti, Cr, Fe, and Ga) were monitored, as shown here, but the concentrations of these elements were not calculated for this study.

Clearly, a high level of confidence is needed in such analyses and a similar level of consistency is desired when comparing results between laboratories. While the results presented here are valid for the conditions of this study, the authors continue to work with other laboratories (particularly members of the Laboratory Manual Harmonization Committee) on an internationally agreed set of analytical parameters and standards.

Under normal geologic conditions, it is difficult for Be atoms to enter the corundum lattice. However, natural corundum contains various types of inclusions (crystals, clouds, silk, etc.) that may host small amounts of Be. Further investigations into the chemical composition of inclusions in natural corundum are under way.

At present and notwithstanding ongoing research, GAAJ believes that when the concentration of Be is



Figure 6. These Be-diffused sapphires and rubies (0.45–3.98 ct) are typical of the material that was analyzed by LA-ICP-MS for this study. Photo by Masaaki Kobayashi.

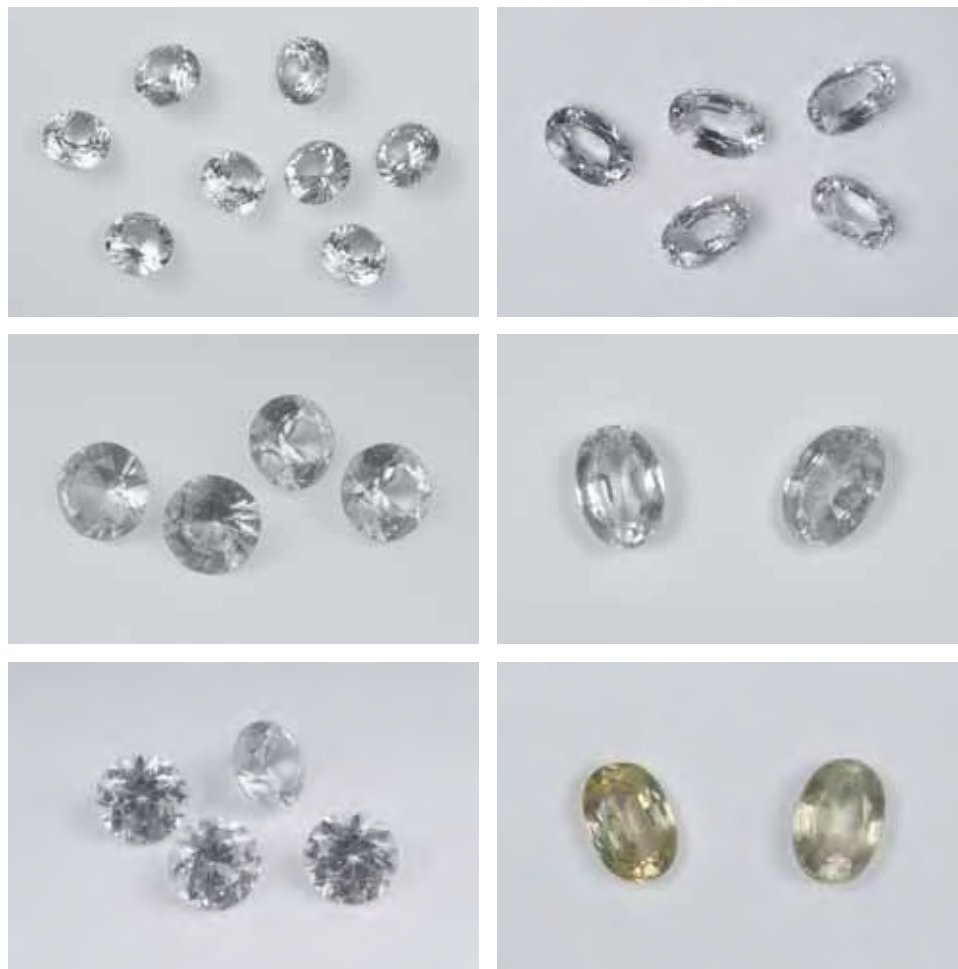


Figure 7. Verneuil colorless synthetic sapphires (top left, samples VCS001–008, 0.86–1.01 ct) and four of the five natural colorless sapphires (top right, samples SCL001–004, 0.50–0.68 ct) were treated by Be diffusion, half for approximately 10 hours (center row) and half for 22 hours (bottom row) at 1800°C in an oxidizing environment. The synthetic sapphires remained colorless even after 22 hours of Be diffusion (bottom left), whereas yellow color was produced in the natural sapphires SCL001–002 after 22 hours of Be diffusion (bottom right). Photos by Masaaki Kobayashi.

lower than the LA-ICP-MS detection limit of about 0.1 ppm (or 0.2 ppma), and internal features indicate that the corundum has been heated (see, e.g., Emmett et al., 2003; Wang et al., 2006), the stone should be identified as having undergone traditional heat treatment (i.e., without beryllium diffusion). The laboratory report may state “indications of heating” only. However, care should be taken to ensure that proper parts of the stone are analyzed (e.g., at least three areas that are free from potentially interfering inclusions).

GAAJ’s present policy also states that when a heat-treated stone contains more than 1 ppm (or 2 ppma) of Be by LA-ICP-MS (using the external NIST glass standards), in areas that are free of inclusions, this stone should be identified as Be diffused. The laboratory report in this case should state that the stone shows “indications of heating, (shallow) color induced by (lattice) diffusion of a chemical element(s) from an external source” (Laboratory Manual Harmonization Committee Information Sheet #2, February 2004; available at www.agta-gtc.org/information_sheets.htm).

Be diffusion-treated corundum commonly has a Be concentration ranging from a few to several hundred ppm. These values are sufficient to indicate Be-diffusion treatment, but the fact that some Be-diffused sapphires contain very low Be concentrations creates challenges for the laboratory gemologist. For example, if a very small amount of Be (e.g., less than 1 ppm) is measured in several analyses of a stone from areas that are *free of inclusions*, this may, until ongoing research is completed, be regarded as falling within an area of uncertainty and this fact should be reflected in the identification report.

Based on our experience using LIBS for routine corundum testing at GAAJ since May 2005, we feel that this technique can detect a minimum of ~1–2 ppm (or 2–5 ppma) Be in corundum. Therefore, LIBS would not be expected to reliably detect the very low concentration of Be mentioned above.

Geographic Origin Determination of Emerald. Emerald crystallizes in complex geologic environments, and the crystals may reflect abrupt changes in

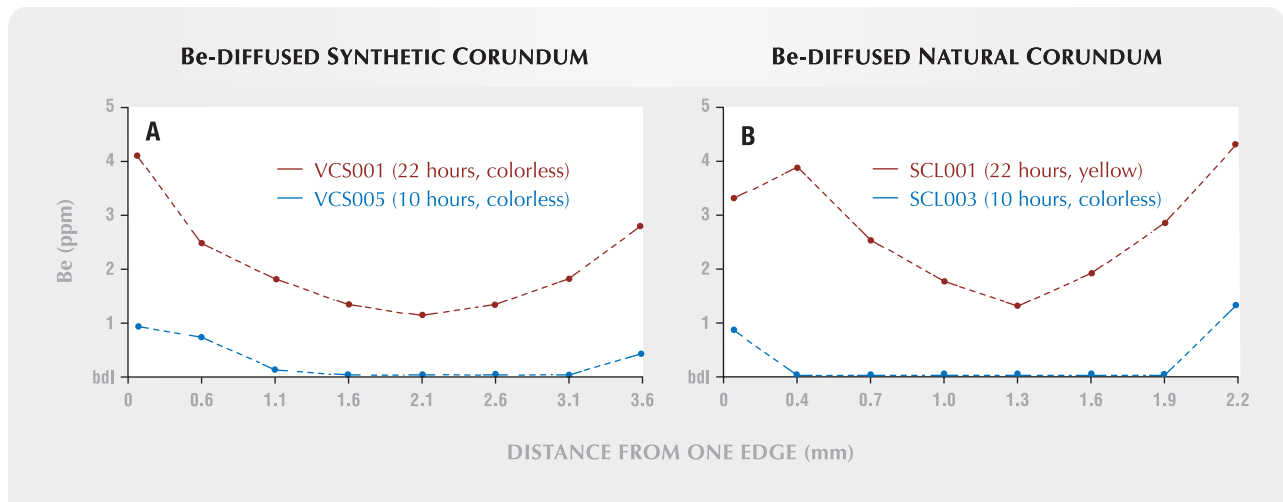


Figure 8. These graphs show the distribution of Be concentrations across cut cross-sections of synthetic sapphires VCS001 and VCS005 (left; 3.5 mm traverse) and natural sapphires SCL001 and SCL003 (right; 2.1 mm traverse) that underwent Be diffusion for different amounts of time. Considerably more Be was recorded in the samples that were diffused longer; both pairs showed Be enrichments near their edges. (The relative error in the analyses is estimated to be ± 0.5 ppm Be.) No color modifications were seen in the synthetic sapphires, whereas the natural sapphires changed from colorless to yellow, but only after the longer period of Be diffusion (see figure 7).

the geologic environment and/or mechanical stress. In contrast, other gem beryls, such as aquamarine, develop in relatively stable environments (e.g., within cavities in granitic pegmatites). Emeralds have been mined from the five major continents, with famous localities in South America (Colombia and Brazil), Asia (Russia, Pakistan, and Afghanistan), and Africa

(Zambia and Zimbabwe), as well as Madagascar. The geologic characteristics of emerald deposits have been classified into two groups (Schwarz and Giuliani, 2000; Schwarz, 2004) as follows:

- Group 1**—Crystallization associated with pegmatites
- *Category A*: Pegmatite without schist-related

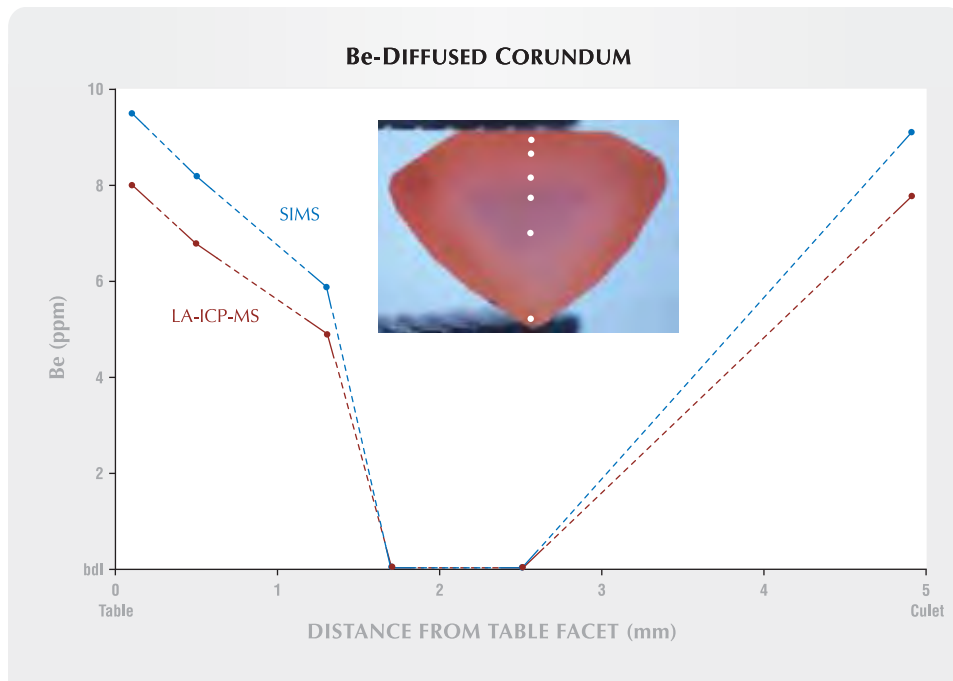
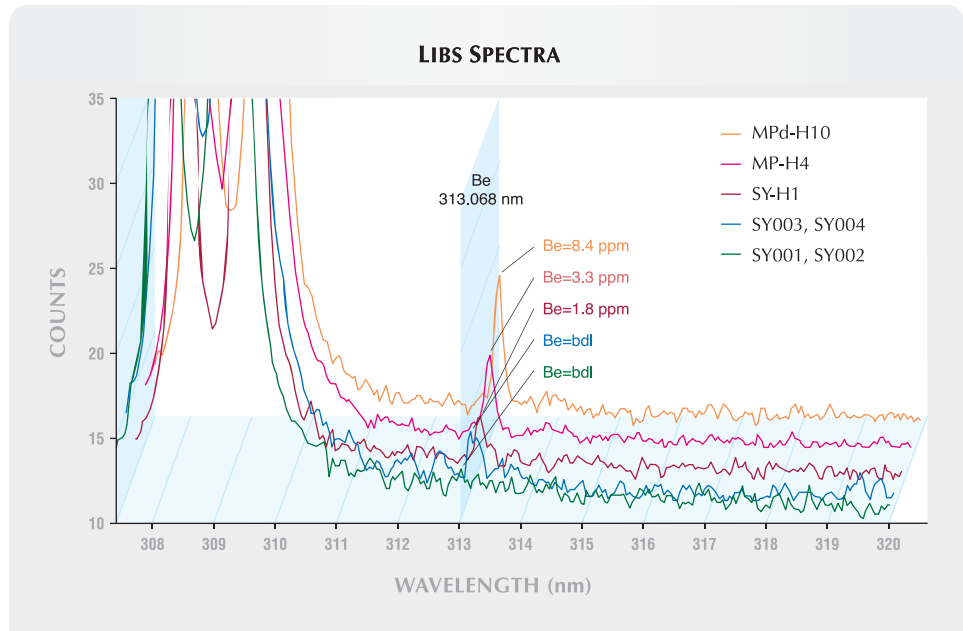


Figure 9. The cut cross-section of a Be-diffused pinkish orange sapphire (sample MPd-H1) was analyzed for Be with both LA-ICP-MS and SIMS, using an external standard of Be-implanted synthetic corundum. The (natural) pink core of the sapphire is surrounded by orange and orangy pink outer zones that resulted from Be diffusion. Slightly higher Be concentrations were consistently measured in the SIMS analyses, except in the pink core, which did not contain any detectable Be by either technique.

Figure 10. LIBS spectra are shown in the range of 307–320 nm for non-heated sapphires (SY001 and SY002), traditional heat-treated sapphires (SY003 and SY004), and Be diffusion-treated sapphires (SY-H1, MP-H4, and MPd-H10). The Be emission peak is located at 313.068 nm. The large peaks around 308 and 309 nm are due to Al. Be was only detected in the samples that underwent Be diffusion treatment.



emerald (Kaduna, Nigeria)

- *Category B:* Pegmatite and greisen with schist-related emerald (Kafubu, Zambia; Sandawana, Zimbabwe; and Itabira–Nova Era, Brazil)

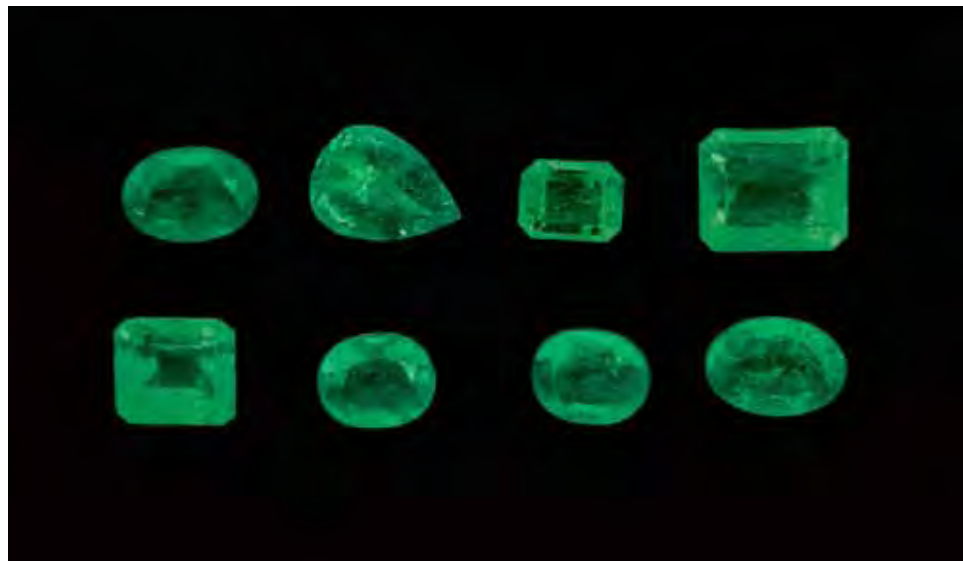
Group 2—Crystallization without the involvement of pegmatites

- *Category C:* Metamorphic phlogopite schist-related emerald (Santa Terezinha, Brazil)
- *Category D:* Talc-carbonate schist-related emerald (Swat, Pakistan)
- *Category E:* Muscovite schist-related emerald (Panjshir, Afghanistan)

- *Category F:* Black shale with vein- and breccia-related emerald (Cordillera Oriental, Colombia)

Representative emeralds from each of these geologic deposit types were selected for this study (see table 2 and figure 11). LA-ICP-MS analyses of 111 gem-quality emeralds from the eight localities are summarized in table 2. The minor elements Na, Mg, and Fe and the trace elements K, Ca, Sc, V, Cr, and Cs were converted to oxide weight percent values for comparison with data reported on emeralds from the literature: Kaduna (Lind et al., 1986; Schwarz, 1996), Kafubu (Milisenda et al., 1999; Zwaan et al., 2005),

Figure 11. These emeralds are from the eight deposits that were analyzed by LA-ICP-MS for this study. From left to right, top row: Santa Terezinha, Brazil (0.72 ct); Swat, Pakistan (0.83 ct); Panjshir, Afghanistan (0.48 ct); and Cordillera Oriental, Colombia (1.73 ct). Bottom row: Kaduna, Nigeria (1.07 ct); Kafubu, Zambia (0.57 ct); Sandawana, Zimbabwe (0.68 ct); and Itabira–Nova Era, Brazil (0.78 ct). Photo by Kohei Yamashita.



Sandawana (Zwaan et al., 1997), Itabira–Nova Era (Schrader, 1987; Schwarz, 1990b; Kanis, 2001; Zwaan, 2001), Santa Terezinha (Hänni and Kerez, 1983; Schwarz, 1990a; Moroz et al., 1998; Pulz et al., 1998), Swat (Henn, 1988; Hammarstrom, 1989), Panjshir (Hammarstrom, 1989; Moroz et al., 1998) and Cordillera Oriental (Moroz et al., 1998). In addition, the trace elements Li, Ti, Zn, Ga, and Rb were all present in detectable quantities. However, B, Mn, Co, Ni, Cu, Sr, Sn, Ba, Pb, Bi, Pt, and Au were near or below the detection limits of our instrument.

Average data for each of the 111 emeralds from the eight localities are plotted in two different chemical fingerprint diagrams (separate plots for minor and trace elements). The oxide weight percent ratios of the minor elements Cs_2O+K_2O versus $FeO+MgO$ are plotted in figure 12. Based on Cs_2O+K_2O content, the Santa Terezinha, Kafubu, and Sandawana emeralds could be separated from the Kaduna, Panjshir, Itabira–Nova Era, and Colombian emeralds. The Cs_2O+K_2O concentrations were particularly high in the Santa Terezinha emeralds. Moreover, the $FeO+MgO$ contents were useful for separating the Kaduna emeralds from the other localities, although there was considerable overlap with Colombian samples. However, a ternary diagram of Zn–Li–Ga

(figure 13) was quite effective at separating the Colombian emeralds from the Kaduna specimens, and also the Swat emeralds from the Itabira–Nova Era and Panjshir specimens (which overlap in figure 12). The Swat specimens occupied the Li-dominant field, while emeralds from Sandawana, Kafubu, Itabira–Nova Era, Panjshir, and Santa Terezinha overlapped to various degrees in the Zn–Li region.

The alkali granite–related Kaduna emeralds of Category A were characterized by relatively low Na, Mg, Cs, and K contents. Generally, the elements that are not intrinsic to beryl (i.e., Na, Mg, Fe, V, Cr, Cs, K, and Ca) were lower than 1.5 wt.% oxide, and the concentration of Fe was greater than the sum of the other nonintrinsic elements. The trace elements Li, Ti, Mn, Zn, Ga, and Rb were usually present in concentrations significantly above background.

The emeralds belonging to Category B (Kafubu, Sandawana, and Itabira–Nova Era) are associated with various metamorphic schist rocks containing phlogopite, biotite, talc, carbonate, and actinolite-tremolite (Schwarz et al., 1996). Their contents of Cr, as well as subordinate Na, Mg, and Fe, showed a wide variation. The Mg concentrations (generally between 1.41 and 3.13 wt.% MgO) were higher than those of Na and Fe. Nevertheless, emeralds originating from these three

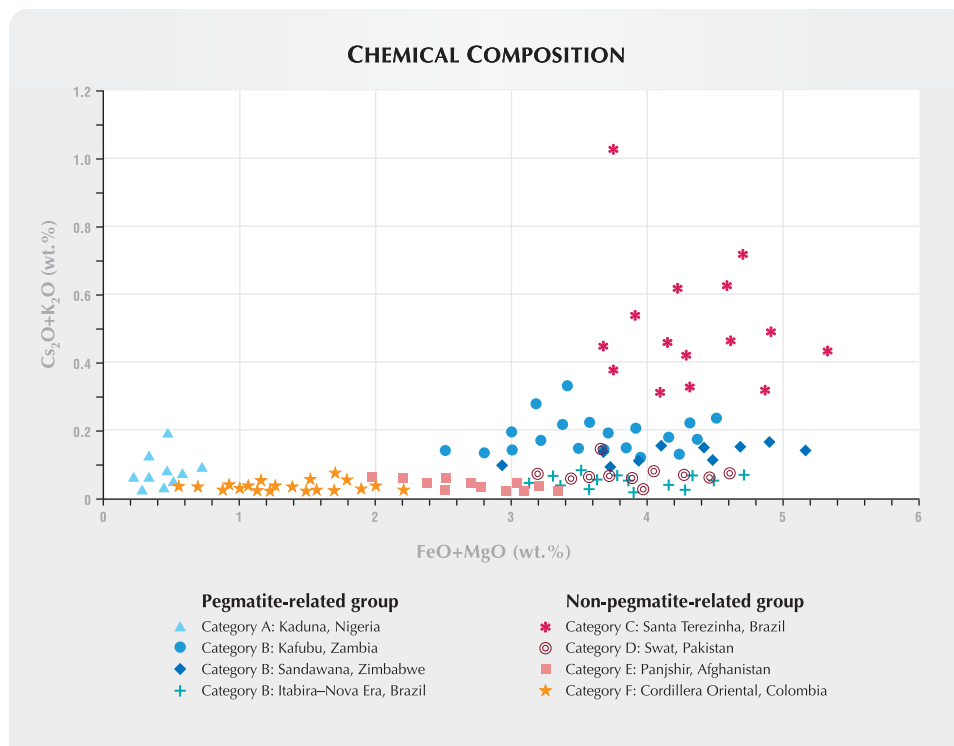


Figure 12. This plot of minor-element concentrations (Cs_2O+K_2O vs. $FeO+MgO$, in wt.%) of emeralds from the eight localities shows various amounts of overlap. Samples from Santa Terezinha are notable for their high Cs_2O+K_2O contents, whereas those from Kaduna contain the lowest concentrations of all these minor elements.

deposits showed similar ranges of FeO+MgO, and the Zambian samples had the highest sum of Cs₂O+K₂O and relatively enriched trace elements Li, Zn, Rb, and Pb. The Itabira–Nova Era emeralds showed the lowest concentration of Cs₂O+K₂O and overlapped with samples from Category D (Swat). Although the Swat emeralds showed considerable overlap with other categories in figure 13, the trace elements Li, Sc, Mn, Ni, Zn, Ga, and Rb were particularly helpful in distinguishing them.

Category C emeralds from Santa Terezinha are hosted in carbonate-talc-phlogopite schists that had some metasomatic exchange between the Be-bearing fluid and the ultrabasic host rocks (Pulz et al., 1998). Santa Terezinha emeralds had the highest sum of Na₂O+MgO+FeO+V₂O₃+Cr₂O₃ (up to 10 wt.%), and also had the highest Fe, Cr, and Cs concentration measured in this study. In addition, the Santa Terezinha emeralds contained the most Li (up to 950 ppm), with Na>Cs>Li. They also contained the trace elements Ti, Mn, Zn, Ga, and Rb (with Ba and Pb near the detection limits), as well as high levels of Ni, Sr, and Sn.

Emeralds belonging to Category D (Swat,

Pakistan), originating from talc-carbonate schist, also had high contents of Na₂O+MgO+FeO+V₂O₃+Cr₂O₃, up to 6.85 wt.%. The range of FeO+MgO was distinctly larger than for the Panjshir emeralds of Category E. The different populations of these two deposits are quite evident, especially in the trace elements V, Ga, Rb, and Ba that are enriched in the Afghan emeralds.

Compared to emeralds from the other deposits, the black shale-hosted Colombian emeralds of Category F were rather pure, with only about 4 wt.% of Na₂O+MgO+FeO+V₂O₃+Cr₂O₃. Generally Na, Mg, and Fe were low, but the two chromophores V and Cr were anomalously high, up to about 1.85 wt.% for V₂O₃+Cr₂O₃. The FeO+MgO content of Colombian emeralds was typically sufficient to distinguish them from neighboring populations of Nigerian and Afghan emeralds.

Implications. Many of the minor and trace elements showed a wider range of concentrations in our samples than were reported previously in the literature (table 5). Mg, K, and V were consistent with the analyses of emeralds reported in most localities, but

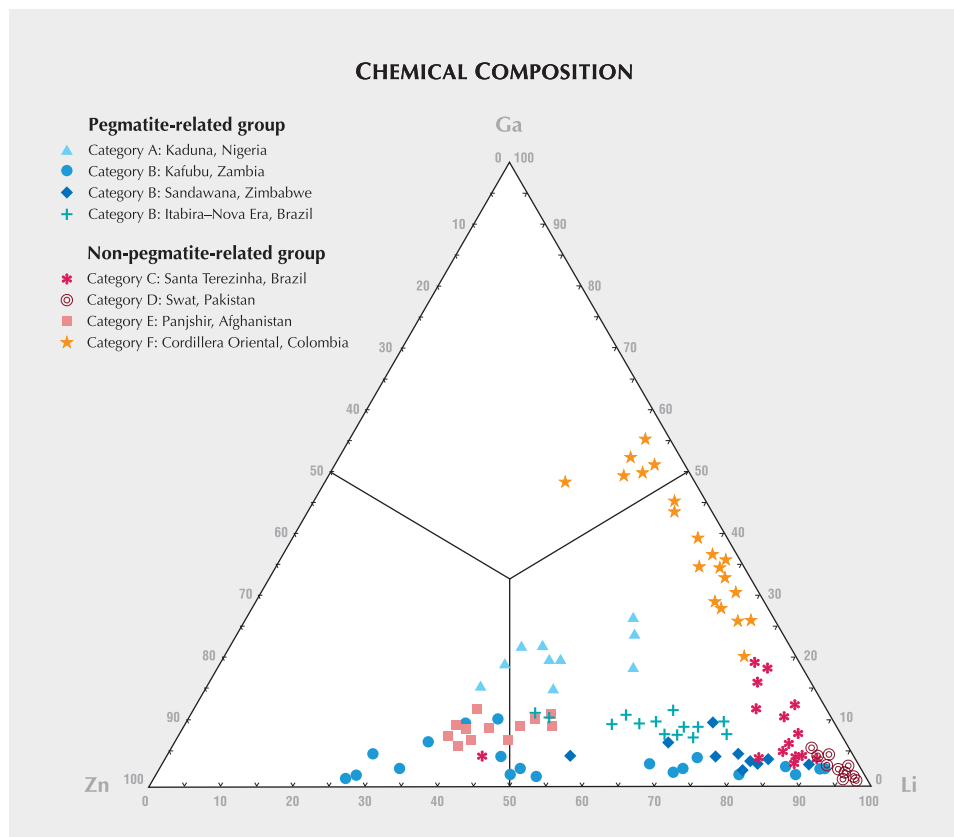


Figure 13. The trace-element concentrations of emeralds from the eight localities are plotted in this Zn-Li-Ga ternary diagram. The Swat and some Santa Terezinha emeralds are Li-dominant, while Colombian stones have intermediate Li-Ga contents. Emeralds from Kafubu, Sandawana, Itabira–Nova Era, and Panjshir are Li-Zn dominant, whereas the Kaduna specimens fall closer to the center of the plot.

our Colombian and Panjshir samples did contain somewhat greater contents of V. In addition, we found more Sc and Cs in emeralds from most of the eight localities; these elements were reported as below or near the detection limits in the literature. The highest amount of Cr found in this study was 2.66 wt.% Cr₂O₃ in emeralds from Santa Terezinha. We measured the highest Fe contents in emeralds from Santa Terezinha and Kafubu, but even greater concentrations of Fe were reported in samples from Swat by Hammarstrom (1989).

Using proton-induced X-ray emission (PIXE), several trace elements that were not measured or detected in our samples (i.e., P, S, Cl, As, Br, Y, Zr, Ag, Cd, La, and Ce) were reported in the literature for emeralds from Kafubu, Sandawana, Santa Terezinha, Swat, and Colombia (again, see table 5). Compared to our LA-ICP-MS data, the PIXE analyses showed relatively high Ti, Mn, Co, Cu, Zn, Ba, Pt, Au, and Bi in emeralds from Kafubu, Sandawana, Santa Terezinha, Swat, and Colombia, but ICP-MS data from Pulz et al. (1998) showed a range similar to that measured in our emeralds from the Santa Terezinha. Using elements such as Li, Zn, Rb, and Pb, it may be possible to differentiate Colombian emeralds (figure 14), arguably the world's most important source, from those of other localities.

Our LA-ICP-MS analyses of emeralds from the eight localities provided no consistent way of clearly distinguishing between pegmatite-related and non-pegmatite-related sources, but the various localities could be separated by a combination of chemical fingerprint diagrams (figures 12 and 13). In figure 12, the Kaduna emeralds correspond to the lowest concentrations of Cs₂O+K₂O and FeO+MgO, although a few data points overlap with the Colombian emeralds. However, there is absolutely no overlap in these localities in figure 13, so Colombian emeralds can easily be separated. Emeralds from Category B (Kafubu, Sandawana, and Itabira–Nova Era) plotted higher in the FeO+MgO field, and can be separated from Santa Terezinha, and Colombian stones on this basis. Swat emeralds completely overlap those from Itabira–Nova Era in figure 12, but figure 13 can be used to make a clear distinction between them. Category B emeralds overlap to some extent in both diagrams, but other trace elements can be used to separate them. Zambian stones showed the greatest sum of Cs₂O+K₂O and high values of Li, Zn, Rb, and Pb. Emeralds from Itabira–Nova Era had the least Cs₂O+K₂O values and low values of Li, Mn, Zn, and Rb. Moderate contents of Cs₂O+K₂O and the highest values of Li, Ti, Mn, and

Rb occurred in Sandawana emeralds. Notably, Santa Terezinha, which is one of the major sources of emerald in the market, had the highest concentrations of Fe, Cr, and Cs, with relatively high contents of Li, Ni, and Sr, enabling them to be separated from Colombian emeralds. Therefore, chemical data obtained by LA-ICP-MS is effective for separating emeralds from each of the eight geographic origins analyzed for this study. However, for added confidence, the chemical data should be supported by optical properties and internal characteristics that would help substantiate the origin determination. Note that the diagrams provided in this article do not take into account all major emerald sources (e.g., samples from Russia and Madagascar were not included).

COMPARISON OF LA-ICP-MS TO SIMS AND LIBS

The advantages and disadvantages of using LA-ICP-MS, SIMS, and LIBS for analyzing gemstones are listed in table 6. LA-ICP-MS is qualitative to fully quantitative, and can analyze a full range of major, minor, and trace elements, which makes it particularly useful for the geographic origin determination of gem materials. With further research, this technique may prove useful (in certain situations) for determining the geographic origin of diamonds (Watling et al., 1995, Resano et al., 2003, Wang et al., 2003). Note, too, that LA-ICP-MS can be used to analyze solid materials with minimal damage; and because chemical dissolution of the sample is not necessary, there is no solvent-induced spectral interference. Both loose and mounted gem materials can be tested, without need for a conductive coating of carbon or gold and/or other charge balancing techniques, as are required for SIMS and EMPA techniques. For trace-element analysis using a well-characterized standard, a larger number of elements can be accurately quantified with LA-ICP-MS than with SIMS or LIBS. Also, LA-ICP-MS can yield low detection limits, close to that of SIMS (Nenoyer et al., 1991). As with SIMS, the ablation area can be controlled from a minimum crater diameter of several micrometers to a maximum of several hundred micrometers (i.e., greater than the beam diameter that is possible for electron or ion microprobes; Reed, 1989). However, a pit diameter of at least 100 μm is required for LIBS analysis, and there is a risk that the stone may be damaged by the laser.

The disadvantages of LA-ICP-MS analysis include mass interference and element fractiona-

TABLE 5. Chemical compositions of emeralds from the literature, for the eight localities in this study.^a

	Kaduna	Kafubu	Sandawana	Itabira-Nova Era	Santa Terezinha	Swat	Panjshir	Cordillera Oriental			
Oxides (wt.%) ^b	Lind et al., 1986 (4); Schwarz et al., 1996 (16)	Milisenda et al., 1999 (5); Zwaan et al., 2005 (27)	Zwaan et al., 1997 (4)	Schrader, 1987 (1); Schwarz, 1990b (48); Kanis, 2001 (4); Zwaan, 2001 (23)	Hänni et al., 1983 (4); Schwarz, 1990a (14); Moroz et al., 1998 (2)	Henn, 1988 (10); Hammarstrom, 1989 (2)	Hammarstrom, 1989 (3); Moroz et al., 1998 (3)	Moroz et al., 1998 (2)			
Na ₂ O	0.04–0.33	0.74–1.99	2.07–2.41	0.79–1.93	1.46–2.18	1.08–2.11	0.01–1.61	≤0.65			
MgO	0.01–0.20	1.26–2.90	2.52–2.75	1.39–2.64	1.27–3.36	2.21–3.10	0.22–1.89	≤0.76			
FeO ^{tot}	0.11–1.13	0.34–1.31	0.45–0.82	0.41–1.30	0.48–1.82	0.20–2.51	0.21–1.16	≤0.25			
K ₂ O	bdl–0.05	bdl–0.26	0.03–0.06	≤0.08	≤0.16	≤0.02	≤0.09	≤0.03			
CaO	bdl–0.01	bdl–0.07	≤0.03	≤0.10	≤0.10	bdl	≤0.07	≤0.23			
Sc ₂ O ₃	bdl–0.03	bdl–0.03	bdl	-	-	≤0.19	-	-			
V ₂ O ₃	bdl–0.09	bdl–0.06	0.04–0.07	≤0.08	≤0.12	0.04–0.07	0.03–0.29	≤0.21			
Cr ₂ O ₃	bdl–0.08	bdl–0.63	0.61–1.33	0.06–1.42	0.06–1.54	0.61–1.33	0.10–0.54	≤0.29			
Cs ₂ O	bdl–0.05	bdl–0.23	0.06–0.10	≤0.01	≤0.20	-	≤0.27	≤0.23			
Trace elements (ppm) ^c	Kaduna	Kafubu	Sandawana	Itabira-Nova Era	Santa Terezinha	Swat	Panjshir	Cordillera Oriental			
		Yu et al., 2000 (25) Calligaro et al., 2000 (11)	Calligaro et al., 2000 (22)		Pulz et al., 1998 (5) Calligaro et al., 2000 (8) Yu et al., 2000 (5)	Yu et al., 2000 (6) Calligaro et al., 2000 (4)		Yu et al., 2000 (20)			
Li	-	-	580	800	-	24–30	580	-	-		
P	-	bdl–433	-	-	-	-	bdl	bdl–302	-	bdl–224	
S	-	bdl–10,707	-	-	-	-	175–916	90–422	-	83–923	
Cl	-	109–1,188	-	-	-	-	351–924	227–758	-	356–1,864	
Ti	-	bdl–89	-	-	-	<118 ^d	bdl–355	bdl–219	-	bdl–115	
Mn	-	bdl–156	-	-	-	<154 ^d	bdl–189	bdl	-	bdl–124	
Co	-	bdl–262	-	-	-	-	bdl	bdl–233	-	bdl–110	
Ni	-	-	-	-	-	37–97	-	-	-	-	
Cu	-	44–329	-	-	-	2	-	bdl–285	bdl–185	-	42–1,070
Zn	-	22–212	-	-	-	2–8	-	50–187	20–93	-	bdl–203
Ga	-	19–273	-	-	-	-	-	53–261	17–35	-	57–243
As	-	bdl	-	-	-	-	-	bdl–44	bdl	-	bdl–32
Br	-	bdl	-	-	-	-	-	bdl–82	bdl–75	-	bdl
Rb	-	bdl–120	140	350	-	<168 ^d	140	bdl–30	bdl–122	6	bdl–61
Sr	-	bdl–29	-	-	-	2–38	-	bdl–91	bdl	-	bdl
Y	-	bdl–100	-	-	-	<2	-	bdl	bdl	-	bdl–145
Zr	-	bdl–98	-	-	-	<4	-	bdl	bdl	-	0
Ag	-	-	-	-	-	<0.4	-	-	-	-	-
Cd	-	-	-	-	-	<0.5	-	-	-	-	-
Sn	-	-	-	-	-	-	-	-	0	-	-
Ba	-	bdl–367	-	-	-	<2	-	bdl–233	282–978	-	bdl–1,265
La	-	bdl–474	-	-	-	-	-	175–805	bdl–546	-	bdl–1,371
Ce	-	bdl–509	-	-	-	-	-	bdl–669	bdl–443	-	bdl–2,335
Pt	-	bdl–392	-	-	-	-	-	bdl–132	bdl–66	-	bdl–154
Au	-	bdl–213	-	-	-	-	-	bdl–123	bdl–96	-	bdl–260
Pb	-	bdl–252	-	-	-	<5	-	bdl	bdl–86	-	bdl
Bi	-	bdl–335	-	-	-	<5	-	bdl–174	bdl–58	-	bdl–90

^a The number of analyzed samples is shown in parentheses after the corresponding reference. Abbreviation: bdl = below detection limit.

^b Analyzed by EMPA.

^c Analyzed by ICP-MS, except for Pulz et al. (1998), which used particle-induced x-ray emission (PIXE).

^d Calculated as ppm by weight.

tion. Element isotope determination with the ICP-MS may suffer a strong spectral interference from air entrainment, from the sample's matrix, and from

polyatomic ions, resulting in mass spectral overlap and a high background. (With SIMS, the high vacuum required in the sample chamber eliminates the

mass interference from air, but matrix interference is still problematic.) The lack of adequate external standards for calibration for a wide variety of samples of interest makes it difficult to obtain reliable quantitative results for some materials by LA-ICP-MS. Even with the use of a well-characterized standard such as Be ion-implanted synthetic sapphire, LA-ICP-MS is not an effective technique for depth profiling due to fluctuations in the laser power density and the rate of ablation.

Assuming an instrument configuration that is equivalent to that used in this study, the cost of an LA-ICP-MS system is more than US\$400,000, whereas a SIMS system exceeds \$1,000,000. The newly introduced LIBS equipment is much less expensive, and can range from \$50,000 to \$90,000, but it is not as effective as LA-ICP-MS and SIMS for providing highly sensitive multi-element quantitative analysis of a small selected area.

CONCLUSIONS

A 213 nm Nd:YAG laser ablation system combined with a quadrupole ICP-MS instrument is a very sensitive and satisfactory method for the analysis of gem materials, as it is capable of ablating the gemstone in a controlled way (e.g., with a laser logo on the girdle of the stone) to obtain a sensitive, stable signal for quantitative chemical analysis. LA-ICP-MS can be used to detect trace levels of Be (i.e., 0.1 ppm) in corundum to detect diffusion treatment, and can also provide data that can be used to create chemical fingerprint diagrams for geographic origin determination.



Figure 14. Emeralds from Colombia have a distinctive chemical composition that is related to their formation in black shale. LA-ICP-MS analysis is therefore useful for separating Colombian emeralds from those of other localities. This 1.77 ct emerald from the Coscuez mine in Colombia was photographed together with the pyrite-bearing black shale host rock. Courtesy of Ronald Ringsrud Co., Saratoga, California; photo © Robert Weldon.

TABLE 6. Comparison of the advantages and disadvantages of LA-ICP-MS, SIMS, and LIBS.

Characteristic	LA-ICP-MS	SIMS	LIBS
Resolution	Highly sensitive	Highly sensitive	Sensitive
Operation	Technical personnel	Technical personnel	Lab staff
Cost of instrument	More than \$400,000	More than \$1,000,000	More than \$50,000
Element detection	Simultaneous multi-element	Simultaneous multi-element	Simultaneous multi-element (based on spectral range of 200–980 nm)
Focusing	CCD auto focus with microscope	CCD auto focus with microscope	Manual
Be detection limit	>0.1 ppm (this study)	>0.01 ppm (this study)	>2 ppm (Krzemnicki, 2004; Themelis 2004)
Spot size	~5–160 μm	~1–300 μm (beam scan)	>100 μm
Crater depth	More than 1 μm , depending on laser ablation used	Several thousandths to tenths of a μm , depending on beam power	More than several μm , depending on laser ablation used
Laser logo mark	Possible	Impossible	Impossible
Calibration reference	External and/or internal standard	External and/or internal standard	External standard
Sample chamber	No vacuum	High vacuum	No vacuum

ABOUT THE AUTHORS

Dr. Abduriyim (ahmadjan@gaii-zenhokyo.co.jp) is manager, and Mr. Kitawaki is director, at the research laboratory of the Gemmological Association of All Japan, Tokyo.

ACKNOWLEDGMENTS

The authors thank Dr. Dietmar Schwarz for supplying

detailed information on worldwide emerald deposits as well as emerald samples for analysis. Katsuo Mizobuchi and Masahiko Endo at Agilent Technologies in Tokyo provided advice and technical discussion regarding this work. Dr. Ichiro Sunagawa (Tokyo, Japan) and Kenneth Scarratt (GIA Research, Bangkok, Thailand) kindly provided a critical reading and helped revise an early draft of this manuscript.

REFERENCES

- Abduriyim A., Kitawaki H. (2006) Determination of the origin of blue sapphire using laser ablation inductively coupled plasma mass spectrometry (LA-ICP-MS). *Journal of Gemmology*, Vol. 30, No. 1–2, pp. 23–36.
- Arrowsmith P. (1987) Laser ablation of solids for elemental analysis by inductively coupled plasma mass spectrometry. *Analytical Chemistry*, Vol. 59, No. 10, pp. 1437–1444.
- Aston F.W. (1919) A positive-ray spectrograph. *Philosophical Magazine*, Vol. 38, pp. 707–715.
- Benninghoven A., Rüdenauer F.G., Werner H.W. (1987) *Secondary Ion Mass Spectrometry: Basic Concepts, Instrumental Aspects, Applications, and Trends*. Wiley, New York, 1227 pp.
- Calligaro T., Dran J.C., Poirot J.P., Querré G., Salomon J., Zwaan J.C. (2000) PIXE/PIGE characterization of emeralds using an external micro-beam. *Nuclear Instruments and Methods in Physics Research B*, Vol. 161–163, pp. 769–774.
- Dempster A.J. (1918) A new method of positive ray analysis. *Physical Review*, Vol. 11, No. 4, pp. 316–324.
- Devos W., Senn-Luder M., Moor C., Salter C. (2000) Laser ablation inductively coupled plasma spectrometry (LA-ICP-MS) for spatially resolved trace analysis of early-Medieval archaeological iron finds. *Fresenius' Journal of Analytical Chemistry*, Vol. 366, No. 8, pp. 873–880.
- Dunn P.J. (1977) The use of the electron microprobe in gemology. *Journal of Gemmology*, Vol. 15, No. 5, pp. 248–258.
- Emmett J.L., Scarratt K., McClure S.F., Moses T., Douthit T.R., Hughes R., Novak S., Shigley J.E., Wang W., Bordelon O., Kane R.E. (2003) Beryllium diffusion of ruby and sapphire. *Gems & Gemology*, Vol. 39, No. 2, pp. 84–135.
- García-Ayuso L.E., Amador-Hernandez J., Fernandez-Romero J.M., Luque de Castro M.D. (2002) Characterization of jewellery products by laser-induced breakdown spectroscopy. *Analytica Chimica Acta*, Vol. 457, No. 2, pp. 247–256.
- Gray A.L. (1985) Solid sample introduction by laser ablation for inductively coupled plasma source mass spectrometry. *Analyst*, Vol. 110, No. 5, pp. 551–556.
- Günther D., Frischknecht R., Heinrich C.A., Kahlert H.J. (1997) Capabilities of an argon fluoride 193 nm excimer laser for laser ablation inductively coupled plasma mass spectrometry microanalysis of geological materials. *Journal of Analytical Atomic Spectrometry*, Vol. 12, No. 9, pp. 939–944.
- Günther D., Heinrich C.A. (1999) Enhanced sensitivity in laser ablation-ICP mass spectrometry using helium-argon mixtures as aerosol carrier. *Journal of Analytical Atomic Spectrometry*, Vol. 14, No. 9, pp. 1363–1368.
- Günther D., Kane R.E. (1999a) Laser ablation-inductively coupled plasma-mass spectrometry: A new way of analyzing gemstones. *Gems & Gemology*, Vol. 35, No. 3, pp. 160–161.
- Günther D., Kane R.E. (1999b) Laser ablation-inductively coupled plasma-mass spectrometry—A new way of analyzing gemstones. In *Gemmologist's Handbook*, XXXVII International Gemmological Conference, India 1999, Forum of Indian Gemmologists for Scientific Studies, Bombay, p. 25.
- Guillong M., Günther D. (2001) Quasi “non-destructive” laser ablation-inductively coupled plasma-mass spectrometry fingerprinting of sapphire. *Spectrochimica Acta B*, Vol. 56, No. 7, pp. 1219–1231.
- Hänni H.A., Kezer C.J. (1983) Neues vom Smaragdorkommen von Santa Terezinha de Goiás, Brasilien. *Gemmologie: Zeitschrift der Deutschen Gemmologischen Gesellschaft*, Vol. 32, No. 1, pp. 50–58.
- Hänni H.A., Krzemnicki M.S., Kiefert L., Chalain, J.P. (2004) Ein neues Instrument für die analytische Gemmologie: LIBS. *Gemmologie: Zeitschrift der Deutschen Gemmologischen Gesellschaft*, Vol. 53, No. 2–3, pp. 79–86.
- Hammarstrom J.M. (1989) Mineral chemistry of emeralds and some associated minerals from Pakistan and Afghanistan: A electron microprobe study. In A.H. Kazmi and L.W. Snee, Eds., *Emeralds of Pakistan: Geology, Gemology and Genesis*, Van Nostrand Reinhold, New York, pp. 125–150.
- Henn U. (1988) Untersuchungen an Smaragden aus dem Swat-Tal, Pakistan. *Zeitschrift der Deutschen Gemmologischen Gesellschaft*, Vol. 37, No. 3/4, pp. 121–127.
- Hirata T., Nesbitt R.W. (1995) U-Pb isotope geochronology of zircon: Evaluation of the laser probe-inductively coupled plasma mass spectrometry technique. *Geochimica et Cosmochimica Acta*, Vol. 59, No. 12, pp. 2491–2500.
- Horn I., Rudnick R.L., McDonough W.F. (2000) Precise elemental and isotope ratio measurement by simultaneous solution nebulization and laser ablation-ICP-MS: Application to U-Pb geochronology. *Chemical Geology*, Vol. 164, No. 3–4, pp. 281–301.
- Jackson S., Pearson N., Griffin W. (2001) In situ isotope ratio determination using laser-ablation (LA)-magnetic sector-ICP-MS. In P. Sylvester, Ed., *Laser-Ablation-ICPMS in the Earth Sciences: Principles and Applications*, Short Course Series, Vol. 29, Mineralogical Association of Canada, St. Johns, Newfoundland, pp. 105–120.
- Jarvis K.E., Gray A.L., Houk R.S. (1992) *Handbook of Inductively Coupled Plasma Mass Spectrometry*. Chapman and Hall, New York.
- Jeffries T.E., Perkins W.T., Pearce N.J.G. (1995) Comparison of infrared and ultraviolet-laser probe microanalysis inductively-coupled plasma-mass spectrometry in mineral analysis. *Analyst*, Vol. 120, No. 5, pp. 1365–1371.
- Jeffries T.E., Jackson, S.E., Longerich H.P. (1998) Application of a frequency quintupled Nd:YAG source ($\lambda = 213$ nm) for laser ablation ICP-MS analysis of minerals. *Journal of Analytical Atomic Spectrometry*, Vol. 13, No. 9, pp. 935–940.
- Jenner G.A., Foley S.F., Jackson S.E., Green T.H., Fryer B.J., Longerich H.P. (1993) Determination of partition coefficients for trace elements in high pressure-temperature experimental run products by laser ablation microprobe-inductively coupled plasma-mass spectrometry (LAM-ICP-MS). *Geochimica et Cosmochimica Acta*, Vol. 57, No. 23–24, pp. 5099–5103.

- Kanicky V., Mermet J.-M. (1999) Use of a single calibration graph for the determination of major elements in geological materials by laser ablation inductively coupled plasma atomic emission spectrometry with added internal standards. *Fresenius' Journal of Analytical Chemistry*, Vol. 363, No. 3, pp. 294–299.
- Kanis J. (2001) The Itabira emerald field, MG, Brazil. *28th International Gemmological Conference*, Madrid, Spain, October 8–11, pp. 49–52.
- Krzemnicki M.S., Hänni H.A., Walters R.A. (2004) A new method for detecting Be diffusion-treated sapphires: Laser-induced breakdown spectroscopy (LIBS). *Gems & Gemology*, Vol. 40, No. 4, pp. 314–322.
- Lind Th., Schmetzer K., Bank H. (1986) Blue and green beryls (aquamarine and emeralds) of gem quality from Nigeria. *Journal of Gemmology*, Vol. 20, No. 1, pp. 40–48.
- Loucks R.R., Eggins S.M., Shegley L.M.G., Kinsley L.P.J., Ware N.G. (1995) Development of the inductively-coupled-plasma mass spectrometry ultraviolet laser trace-element micro-analyzer (ICPMS-ULTEMA). In *Research School of Earth Sciences Annual Report*, Australian National University, Canberra, pp. 138–140.
- Milisenda C.C., Malango V., Taupitz K.C. (1999) Edelsteine aus Sambia-Teil 1: Smaragd. *Gemmologie: Zeitschrift der Deutschen Gemmologischen Gesellschaft*, Vol. 48, No. 1, pp. 9–28.
- Moroz I.I., Eliezri I.Z. (1998) Emerald chemistry from different deposits: An electron microprobe study. *Australian Gemmologist*, Vol. 20, No. 2, pp. 64–69.
- Muhlmeister S., Fritsch F., Shigley J.E., Devouard B., Laurs B.M. (1998) Separating natural and synthetic rubies on the basis of trace-element chemistry. *Gems & Gemology*, Vol. 34, No. 2, pp. 80–101.
- Nenoyer E.R., Fredeen K.J., Hager J.W. (1991) Laser solid sampling for inductively coupled plasma mass spectrometry. *Analytical Chemistry*, Vol. 63, No. 8, pp. 445A–475A.
- Norman M. (2001) Applications of laser-ablation ICPMS to the trace element geochemistry of basaltic magmas and mantle evolution. In P. Sylvester, Ed., *Laser-Ablation-ICP-MS in the Earth Sciences: Principles and Applications*, Short Course Series, Vol. 29, Mineralogical Association of Canada, St. Johns, Newfoundland, pp. 163–184.
- Novak S.W., Magee C.W., Moses T., Wang W. (2004) Using SIMS to diagnose color changes in heated gem sapphires. *Applied Surface Science*, Vol. 231–232, pp. 917–920.
- Pearce N.J.G., Perkins W.T., Westgate J.A., Gorton M.P., Jackson S.E., Neal C.R., Chenery S.P. (1997) Application of new and published major and trace elements data for NIST SRM 610 and NIST SRM 612 glass reference materials. *Geostandards Newsletter*, Vol. 21, No. 1, pp. 115–144.
- Pollard A.M., Heron H. (1996) *Archaeological Chemistry*. The Royal Society of Chemistry, London.
- Pulz G.M., D'el-Rey Silva L.J.H., Barros Neto L.S., Brum T.M.M., Juchem P.L., Santos C.A., Pereira V.P., Silva J.J. (1998) The chemical signature of emeralds from the Campos Verdes-Santa Terezinha mining district, Goiás, Brazil. *Journal of Gemmology*, Vol. 26, No. 4, pp. 252–261.
- Rankin A.H., Greenwood J., Hargreaves D. (2003) Chemical fingerprinting of some east African gem rubies by laser ablation ICP-MS. *Journal of Gemmology*, Vol. 28, No. 8, pp. 473–482.
- Reed S.J.B. (1989) Ion microprobe analysis: A review of geological applications. *Mineralogical Magazine*, Vol. 53, pp. 3–24.
- Resano M., Vanhaecke F., Hutsebaut D., De Corte K., Moens L. (2003) Possibilities of laser ablation-inductively coupled plasma-mass spectrometry for diamond fingerprinting. *Journal of Analytical Atomic Spectrometry*, Vol. 18, No. 10, pp. 1238–1242.
- Saminpanya S., Manning D.A.C., Droop G.T.R., Henderson C.M.B. (2003) Trace elements in Thai gem corundums. *Journal of Gemmology*, Vol. 28, No. 7, pp. 399–415.
- Scarratt K. (2002) Orange-pink sapphire alert. American Gem Trade Association Gemological Testing Center, www.agta-gtc.org/2002-01-08_orangesapphirealert.htm, January 8.
- Schrader H.W. (1987) *Natürliche und synthetische Smaragde. Einbeitrag zur Kristallchemie der Berylle*. Ph.D. dissertation, Fachbereich Geowissenschaften der Johannes Gutenberg Universität Mainz, Germany.
- Schwarz D. (1990a) Die brasilianischen Smaragde und ihre Vorkommen: Santa Terezinha de Goiás/GO. *Zeitschrift der Deutschen Gemmologischen Gesellschaft*, Vol. 39, No. 1, pp. 13–44.
- Schwarz D. (1990b) Die chemische Eigenschaften der Smaragde I. Brasilien. *Zeitschrift der Deutschen Gemmologischen Gesellschaft*, Vol. 39, No. 4, pp. 233–272.
- Schwarz D. (2004) The world of emeralds. *30th Gemmological Conference of All Japan*, Abstracts Volume, Kyoto, Japan, June 12–13.
- Schwarz D., Kanis J., Kinnaird J. (1996) Emerald and green beryl from central Nigeria. *Journal of Gemmology*, Vol. 25, No. 2, pp. 117–141.
- Schwarz D., Giuliani K. (2000) Emerald deposits: A review. In *Brazil 2000: 31st International Geological Congress*, Abstracts Volume, Aug. 6–17, Rio de Janeiro.
- Shida J., Kitawaki H., Abduriyim A. (2002) Investigation of corundum heat-treated by a new technique. *Journal of the Gemmological Society of Japan*, Vol. 24, No. 1–4, pp. 13–23.
- Stephens W.E. (1946) A pulsed mass spectrometer with time dispersion. *Physical Review*, Vol. 69, No. 11–12, pp. 691.
- Stern W.B., Hänni H.A. (1982) Energy-dispersive X-ray spectrometry: A non-destructive tool in gemmology. *Journal of Gemmology*, Vol. 18, No. 4, pp. 285–296.
- Stockton C.M., Manson D.V. (1981) Scanning electron microscopy in gemology. *Gems & Gemology*, Vol. 17, No. 2, pp. 72–79.
- Themelis T. (2004) LIBS: A spark of inspiration in gemological analytical instrumentation. *Australian Gemmologist*, Vol. 22, pp. 138–145.
- Thomson J.J. (1911) Rays of positive electricity. *Philosophical Magazine*, Vol. 6, No. 20, pp. 752–767.
- Tye C., Woods G., McCurdy E., Wilbur S. (2004) Semiquantitative analysis—7500 ORS as a powerful & rapid survey tool. *Agilent ICP-MS Journal*, No. 20, pp. 2–3.
- Tytkot R.H. (2002) Chemical fingerprinting and source tracing of obsidian: The central Mediterranean trade in black gold. *Accounts of Chemical Research*, Vol. 35, pp. 618–627.
- Wang W., Hall M., Smith C.P., Shigley J.E. (2003) Applications to diamond testing: A new analytical technique: LA-ICP-MS. *Rapaport Diamond Report*, Vol. 26, No. 33, pp. 177–181.
- Wang W., Scarratt K., Emmett J.L., Breeding C.M., Douthit T.R. (2006) The effects of heat treatment on zircon inclusions in Madagascar sapphires. *Gems & Gemology*, Vol. 42, No. 2, pp. 134–150.
- Watling R.J., Herbert H.K., Barrow I.S., Thomas A.G. (1995) Analysis of diamond and indicator minerals for diamond exploration by laser ablation-inductively coupled plasma mass spectrometry. *Analyst*, Vol. 120, No. 5, pp. 1357–1364.
- Yu N.K., Tang S.M., Tay T.S. (2000) PIXE studies of emeralds. *X-Ray Spectrometry*, Vol. 29, pp. 267–278.
- Zwaan J.C., Kanis J., Petsch E.J. (1997) Update on emerald from the Sandawana mines, Zimbabwe. *Gems & Gemology*, Vol. 33, No. 2, pp. 80–100.
- Zwaan J.C. (2001) Preliminary study of emeralds from the Piteiras emerald mine, Minas Gerais, Brazil. *XXVIII International Gemmological Conference, Spain 2001, Extended Abstracts*, Oct. 8–11, Madrid, pp. 106–109.
- Zwaan J.C., Seifert A.V., Vrana S., Laurs B.M., Anckar B., Simmons W.B., Falster A.U., Lustenhouwer W.J., Muhlmeister S., Koivuola J.L., Garcia-Guillerminet H. (2005) Emeralds from the Kafubu area, Zambia. *Gems & Gemology*, Vol. 41, No. 2, pp. 116–148.

Last chance to register for the

GIA®

Gemological Research Conference

2006
August 26-27

Manchester Grand Hyatt Hotel
San Diego, California

Sponsored by Charles & Colvard, Ltd.

THE SCIENCE OF GEMOLOGY is expanding in many exciting directions that encompass not only mineralogy and geology, but also fields such as physics, chemistry, and materials science. At the GIA Gemological Research Conference, a multidisciplinary approach will explore the challenges posed by new synthetic and treated gem materials, as well as the characterization of natural gems from traditional and new sources. Invited lectures, submitted oral presentations, and a poster session will explore a diverse range of contemporary topics in gemology and related sciences.



List of Confirmed Presentations Now Available

The titles of confirmed presentations (both oral and poster) for the Gemological Research Conference are now available on the conference website (www.gia.edu/gemsandgemology). The list will be updated as additional presentations are confirmed, and attendees should check periodically for future updates as the conference approaches.

Pala Pegmatite Field Trips—Sold Out

The August 25 and 30 field trips to the Pala pegmatite district have reached full capacity, and there are substantial waiting lists for each trip.

Register Now

The Gemological Research Conference costs only \$295 (\$395 after August 11), including breakfast and lunch both days, a cocktail reception on August 26, and GIA's 75th Anniversary Gala on August 27. To register for the Gemological Research Conference or the International Gemological Symposium, visit www.symposium.gia.edu.



NAVIGATING THE
CHALLENGES AHEAD

The GIA Gemological Research Conference will be held in conjunction with the 4th International Gemological Symposium, which will take place August 27-29, 2006. For further information on attending the GIA Gemological Research Conference, contact the organizing committee at:

E-mail: gemconference@gia.edu
Dr. James E. Shigley, Phone: 760-603-4019
Brendan M. Laurs, Phone: 760-603-4503
Fax: 760-603-4021
Web: www.gia.edu/gemsandgemology
or www.symposium.gia.edu



Keynote Speakers

Geology of Gem Deposits

- **Dr. Jeff Harris**, University of Glasgow, UK
Diamond occurrence and evolution
- **Dr. David London**, University of Oklahoma, Norman
Geochemical cycle of certain elements that form gems

Gem Characterization Techniques

- **Dr. George Rossman**, California Institute of Technology, Pasadena
Characterization of nanofeatures in gem materials
- **Dr. Emmanuel Fritsch**, IMN, University of Nantes, France
Review and forecast of important techniques in gemology

New Gem Localities

- **Dr. Lawrence Snee**, U.S. Geological Survey, Denver
Mapping of gem localities in Afghanistan and Pakistan
- **Dr. Federico Pezzotta**, Museo Civico di Storia Naturale, Milan
Update on gem localities in Madagascar

Gem Synthesis

- **Dr. James Butler**, Naval Research Laboratory, Washington, DC
Growth of CVD synthetic diamond
- **Dr. Ichiro Sunagawa**, Tokyo
Growth, morphology, and perfection of single crystals: Basic concepts in discriminating natural from synthetic gemstones

General Gemology

- **Shane McClure**, GIA Laboratory, Carlsbad
Genetic source type classification of gem corundum
- **Menahem Sevdemish**, Advanced Quality A.C.C. Ltd., Ramat Gan, Israel
Color communication: The analysis of color in gem materials

Diamond and Corundum Treatments

- **Ken Scarratt**, GIA Research, Bangkok
Corundum treatments
- **Dr. Mark Newton**, University of Warwick, Coventry, UK
Diamond treatments

Eight additional speakers for each session will be selected from submitted abstracts.

Register Now!

THE CULLINAN DIAMOND CENTENNIAL: A HISTORY AND GEMOLOGICAL ANALYSIS OF CULLINANS I AND II

Kenneth Scarratt and Russell Shor

The year 2005 marked a century since the discovery of the largest gem diamond ever found: the 3,106 ct Cullinan. Eight decades after it was mined, a team of gemologists conducted the first modern examinations of the two largest diamonds cut from the rough, the 530 ct Cullinan I and the 317 ct Cullinan II, which have been part of the Crown Jewels of England since their presentation to King Edward VII in 1908. This article traces the history of this famous piece of rough and its source, South Africa's Cullinan (formerly Premier) mine, which has yielded more significant diamonds than any other single locality. It also presents the full details of the examination and grading of these two approximately D-color, potentially flawless historic diamonds.

The huge rough diamond known as the Cullinan was found a century ago, when the British Empire was at the apex of its power. Its discovery, telegraphed around the world, also brought fame to the then newly opened Premier mine near Pretoria, South Africa. For many years, the great diamond was a symbol of the world's mightiest empire. At 3,106 ct, today it remains the largest gem diamond ever discovered, and two of the diamonds cut from it lie at the heart of the Crown Jewels of England (figure 1). Although much has been written about the original piece of rough and the diamonds fashioned from it, this article offers previously undocumented details about the famed Cullinan diamond, including the first comprehensive report on the gemological examination of the 530 ct Cullinan I and the 317 ct Cullinan II.

THE PREMIER/CULLINAN MINE

Located on a former farm 25 km east of Pretoria, the Premier mine (figure 2; renamed the Cullinan mine for its centennial in 2003) began full operation in 1903. The Cullinan was discovered less than two years later, the first extremely large diamond from a

mine that, in its 100+ years of operation, has yielded more rough diamonds over 100 ct (300+) than any other single source, including more than 25% of all the 400+ ct diamonds ever discovered (De Beers Group, 2006).

Among the other legendary diamonds that have come from the mine are (all weights are for the rough): the Taylor-Burton (240.8 ct), Premier Rose (353.9 ct), Niarchos (426.5 ct), Centenary (599.1 ct), and Golden Jubilee (755.5 ct). The Fancy Vivid blue Heart of Eternity (27.64 ct polished—rough weight not disclosed) and the other 11 large blue diamonds that formed De Beers's Millennium Collection also came from this mine (L. Hori, pers. comm., 2005).

The Premier mine ceased operations several times during the past century and weathered a critical redevelopment project. It first closed in 1914 at the outbreak of World War I and reopened two years later shortly before De Beers acquired a majority

See end of article for About the Authors and Acknowledgments.
GEMS & GEMOLOGY, Vol. 42, No. 2, pp. 120–132.
© 2006 Gemological Institute of America



stake. The Great Depression, which brought a precipitous drop in world diamond sales, forced it to close again in 1932. The mine did not reopen until after World War II. De Beers acquired full ownership of the Premier mine in 1977 (De Beers Group, 2006). At the time, continued operation seemed doubtful because excavations were nearing a 70-m-thick sill of volcanic rock that protruded through the entire kimberlite pipe at the 550 m mark. Because the mine remained so productive, De Beers ultimately determined that the expense of driving



Figure 1. The Cullinan I and II diamonds are focal points in the Crown Jewels of England. The 530 ct Cullinan I is set in the Sovereign's Sceptre with Cross (left), and the 317 ct Cullinan II is set in the Imperial State Crown (above). Also shown in the crown is the Black Prince's "Ruby" (actually, a red spinel; 170 ct) and St. Edward's Sapphire. Photo of scepter by Alan Jobbins. Top photo, Crown ©/The Royal Collection © Her Majesty Queen Elizabeth II.

an underground shaft through the sill to excavate the pipe from beneath would be economic. When open, the mine has consistently produced well over a million carats yearly. In 2004, the renamed Cullinan mine yielded 1.3 million carats (De Beers Group, 2004).

Current mining is 763 m below the surface, and De Beers is investigating the extension of mining below 1100 m. This would add 20–25 years to the life of the mine (Fernandes, 2005).

BACKGROUND OF THE CULLINAN DIAMOND

On January 26, 1905, the manager of the Premier mine, Captain Frederick Wells, retrieved the large crystal (figure 3) from near the rim of the shallow pit



Figure 2. The Cullinan diamond mine (renamed from the Premier mine in 2003) has yielded more large diamonds than any other source in history. The Cullinan diamond was found on the opposite side of the rim shown here. Photo courtesy of Diamond Trading Co.

("Some facts . . .," 1905). Announcement of this discovery touched off an immediate torrent of press reports that offered estimates of its value ranging from US\$4 million to \$100 million, and caused an 80-fold jump in the share price of the Premier (Transvaal) Diamond Mining Company Ltd. ("The largest diamond," 1905). Local newspapers began referring to the great crystal as the "Cullinan

Diamond" in reference to Sir Thomas Major Cullinan, the chairman of the company and discoverer of the mine (Helme, 1974).

T. M. Cullinan settled in gold-rush Johannesburg in 1887. Within several years, he became one of the town's most prominent builders—a lucrative enterprise during a period when the settlement grew from a collection of gold miners' tents and shanties to a full-fledged city. The great Kimberley Diamond Rush had occurred years earlier, some 500 km to the south. In 1892, however, reports of sporadic diamond finds prompted Cullinan and several associates to form a syndicate to prospect locally for diamonds. The venture, the Driekopies Diamond Mining Company, made several small diamond discoveries but was forced to cease activities when the South African War (also known as the Second Boer War) broke out in October 1899 (Helme, 1974).

During the 1890s, prospectors found scattered alluvial diamonds within the Dutch-ruled Transvaal near Pretoria and traced their origins to springs on a farm called Elandsfontein that was owned by Willem Petrus Prinsloo. Although a number of prospectors made offers, the elderly Prinsloo consistently rebuffed them (Helme, 1974). However, the end of the war in May 1902 left the Transvaal under British rule and the Prinsloo family destitute. The elder Prinsloo had died and the war had devastated the farm.

Cullinan offered the three Prinsloo heirs £150,000 for prospecting rights, to be paid out over an unspecified period of time, or £45,000 in cash for outright purchase. Prinsloo's heirs accepted the latter option, after negotiating the price up to £52,000. Cullinan formed the Premier Diamond Syndicate to buy and develop the property and signed the transaction on November 7, 1902. At this point, the syndicate was renamed the Premier (Transvaal) Diamond Mining Company. Among the company's shareholders was Bernard Oppenheimer, elder brother of Ernest Oppenheimer, who would later become director of De Beers Consolidated Mines (Helme, 1974).

Sampling commenced within days of the signing. By year's end, 187 carats of diamonds had been collected, and reports circulated that the "true pipe of the Pretoria formation has been found" (Helme, 1974, p. 52). In July 1903, as reports of the full scale of the Elandsfontein deposit began filtering out, the Transvaal legislature imposed a tax of 60% on the operation's profits. By the following year, the Premier reported a yearly production of 749,653 carats and profit of £667,738.

Following the Cullinan's discovery, the company displayed the great diamond at the Standard Bank in Johannesburg. An estimated 8,000–9,000 onlookers crowded the building to view it, though the company had issued only 3,000 visitor passes. The local newspaper, the *Transvaal Leader*, referred to the stone as the "Cullinan Diamond" in a February 2, 1905, report on the exhibition. The article also proposed the idea of purchasing the large piece of rough for £500,000 for presentation to King Edward VII of England who, because of the South African War, had extended his imperial rule to the Transvaal.

The discovery also touched off a mystery that has never been solved. An interview with Dr. Molengraaff of the South African Mines, Commerce and Industries Commission shortly after the big diamond was found noted that it was but a portion of a much larger stone, because only a relatively small section of the crystal had its "original natural surface" ("More about . . .," 1905, p. 71). He added that "four pieces of this original stone have been broken off along cleavage planes . . . each of these fragments must have been of considerable size" ("More about . . .," 1905, p. 71). This conclusion was disputed later on, but most of those who disagreed had not examined the rough stone. No identifiable pieces have ever been found (R. Walker, pers. comm., 2006).

In April 1905, the rough gem was dispatched to the Premier (Transvaal) Diamond Mining Company's London sales agent, S. Neumann & Co., where it remained for more than two years while the Transvaal Legislative Assembly debated whether or not to buy it. By this time, Afrikaans leaders General Louis Botha and Jan Smuts had pledged to support British rule and thrown their influence behind the purchase. After the intercession of then-Colonial Under-Secretary Winston Churchill, the Transvaal legislature approved in August 1907 a resolution to purchase the diamond for £150,000 and made the offer formal in October.

The monarch replied through the Secretary of State for the Colonies, Lord Elgin, that he would accept the diamond "as a token of the loyalty and attachment of the people of Transvaal, to his throne and person." King Edward VII also promised that the diamond would be "preserved among the historical jewels which form the heirlooms of the Crown" (Helme, 1974, p. 86). He received the rough diamond on November 9, 1907, the occasion of his 66th birthday.

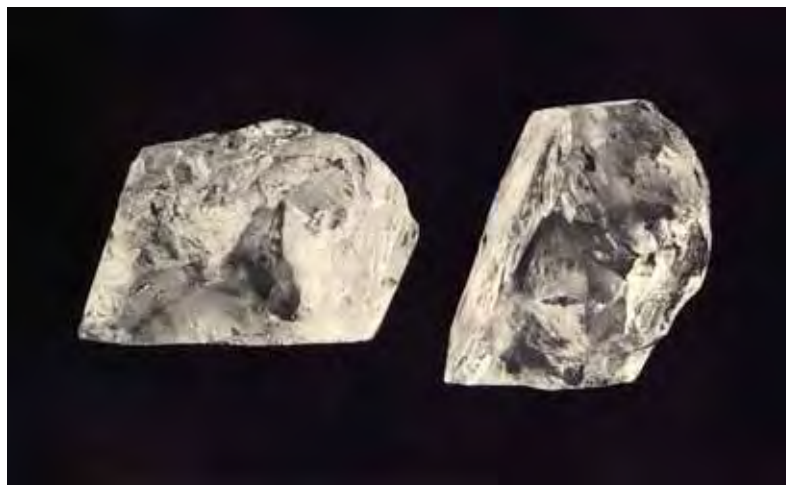


Figure 3. This model illustrates the Cullinan rough from two angles. Some geologists, based on the relatively small surface with naturals, had the opinion that the Cullinan rough was only part of a much larger crystal that had been cleaved by natural forces. Photo courtesy of the Diamond Trading Co.

Following the Discovery, Controversy About the Weight.

Although the Cullinan is perhaps the most documented diamond in history, reports of its actual weight varied because of inaccurate scales and the lack of standardization in carat weights. A "British carat" was equivalent to 0.2053 g while a "Dutch carat" equaled 0.2057 g; both differed from the metric carat, 0.2 g. The now-accepted weight of 3,106 ct was based on the metric carat. The differences prompted demands to create an international carat weight standard (Spencer, 1910).

Initial press reports cited the weighing at the mine as 3,032 ct. The Premier Company's Johannesburg office weighed the diamond at 3,024³/₄ ct, while the London office gave a reading of 3,025³/₄ ct. These differences, all in British carats, were attributed to the fact that the brass weights used to counterbalance the scales were not uniform (some having been worn after a great deal of use) and to the variation in altitude between Johannesburg and London.

The man selected to cut the diamond was Joseph Asscher of Amsterdam. His firm, I. J. Asscher and Company of Amsterdam, had cut the 995 ct Excelsior diamond in 1903. Asscher weighed the diamond at 3,019³/₄ Dutch carats.

The Cutting of the Cullinan. Even before the Transvaal legislature had enacted its resolution, Cullinan had engaged I. J. Asscher to polish the approximately 10 × 6 × 5 cm diamond. Ian Balfour's *Famous Diamonds* (2000) offers a vivid, detailed

account of the cutting process, summarized here.

On February 6, 1908, Asscher commenced examining the diamond, which had two visible inclusions (Helme, 1974). Four days later, he began the cleaving operation (figure 4). The first blow broke the knife and left the diamond intact. The second blow, using a new cleaving knife (figure 5), split the stone into two sections; one weighing 1977.5 Dutch carats and the other weighing 1040.5 Dutch carats (now given as 2029.9 and 1068.8 ct, respectively). On February 14, he cleaved the larger piece into two. The polishing fell to his staff, overseen by Henri Koe, a 20-year veteran. Polishing of the Cullinan I began March 2, 1908. Asscher's staff started work on May 29 on the section that would become the Cullinan II.

The Cullinan yielded a total of nine major stones (see text below and figure 6), 96 smaller gems, and 9.5 carats of unpolished "fragments."

Figure 4. Joseph Asscher reenacts the cleaving of the 3,106 ct Cullinan rough. Photo courtesy of the Diamond Trading Co.



Figure 5. The hammer and knife used to cleave the Cullinan diamond. The knife is seen here spanning two models of the rough Cullinan. Photo by Alan Jobbins.

Work on the Cullinan I was completed September 12, 1908, and with three polishers working 14 hours a day, all of the gems were finished by early November. On November 21, the two largest gems, Cullinan I (530.2 ct) and Cullinan II (317.4 ct), were presented to King Edward VII at Windsor. The king named the large diamond the Great Star of Africa, though the Cullinan appellation has remained (Balfour, 2000).

The Cullinans I and II (figure 7) were retained by the monarch for the Crown Jewels. Most of the other stones (with the exceptions noted below) were given to Asscher for his fee. King Edward purchased the Cullinan VI for his consort, Queen Alexandra. The people of South Africa purchased the other six major diamonds and presented them to Edward's daughter-in-law Queen Mary (consort of George V, and an avid jewelry collector) in 1910, the year her husband acceded to the throne. These now belong to her granddaughter, Queen Elizabeth II.

The major gems are:

- **Cullinan I** (also called the Great Star of Africa)—a 530.20 ct pear shape set in the Sovereign's (or Royal) Sceptre with Cross on display in the Tower of London.
- **Cullinan II** (also known as the Lesser Star of Africa)—a 317.40 ct cushion-shaped brilliant set in the Imperial State Crown on display in the Tower of London.
- **Cullinan III**—a 94.40 ct pear shape that is set with the Cullinan IV (nicknamed "Granny's chips") in a brooch currently in the private collection of Queen Elizabeth II. In 1911, they had

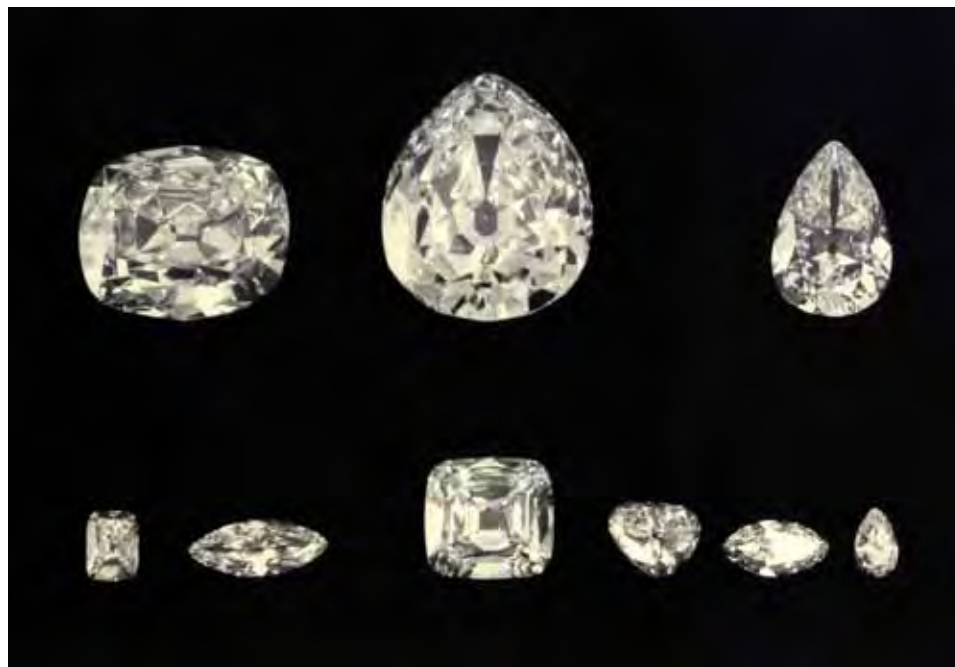


Figure 6. These are replicas of the major polished stones cut from the 3,106 ct Cullinan rough. Top (left to right): II, I, III. Bottom (left to right): VIII, VI, IV, V, VII, IX. Photo courtesy of the Diamond Trading Co.

been set in a detachable setting in Queen Mary's crown, but she removed them and replaced them with replicas (Balfour, 2000).

- **Cullinan IV**—a 63.60 ct square-cut brilliant that is set with the Cullinan III (see above).
- **Cullinan V**—an 18.80 ct heart shape set in a brooch for Queen Mary that is now owned by Queen Elizabeth II.
- **Cullinan VI**—an 11.50 ct marquise that was originally presented to Queen Alexandra by King Edward VII, and is now mounted in an emerald and diamond necklace owned by Queen Elizabeth II.
- **Cullinan VII**—an 8.80 ct marquise set with the Cullinan VIII in a pendant now owned by Queen Elizabeth II.
- **Cullinan VIII**—a 6.80 ct modified cushion shape set with the Cullinan VII (see above).
- **Cullinan IX**—a 4.39 ct pear shape mounted into a ring for Queen Mary that is now owned by Queen Elizabeth II.

The remaining 96 polished diamonds with a total weight of 7.55 ct were sold by Asscher to various clients (Spencer, 1910). Two were purchased by Gen. Louis Botha, then prime minister of South Africa. Several small stones went to Arthur and Alexander Levy, the London diamond merchants chosen to oversee the cutting operation.

GEMOLOGICAL EXAMINATIONS OF THE CULLINANS I AND II

Each February during the 1980s, a team from Garrard & Co., The Crown Jewellers, visited the Jewel House in the Tower of London to clean and, if necessary, repair the many crowns, scepters, and other items in the English Crown Jewels. These annual visits necessitated that the Jewel House, which is normally open for public viewing, be closed for the duration of each visit.

When it was recognized that the descriptions of the Regalia (Holmes, 1937, 1959; Holmes, 1974; Mears, 1986) were outdated and needed to be

Figure 7. The Cullinan II and I diamonds are shown here with a 1 ct round brilliant-cut for scale. Photo by Alan Jobbins.



revised, the annual cleaning periods were also used to conduct a thorough examination of the jewels, including a detailed gemological examination. These took place each February from 1986 to 1989.

This effort originated when Alan Jobbins, curator of minerals and gemstones at the Geological Museum of London from 1950 to 1983, was asked by Claude Blair, formerly keeper of metalwork at the Victoria & Albert Museum, to organize the gemological portion of the Regalia's examination with a view toward the production of a book (catalogue) on the subject. Jobbins then approached the senior author (KS, at the time head of the Gem Testing Laboratory of Great Britain [GTLGB; now the Gem Testing Laboratory of Gem-A]) and Dr. Roger Harding of the Geological Museum of London and asked that they join him in this endeavor. Subsequently, other gemologists were occasionally asked to be present during these examinations, including Nigel Israel (gemologist and appraiser) and Eric Emms (GTLGB), as well as Dr. Chris Welbourn of DTC Research, Maidenhead. The two-book set, *The Crown Jewels: The History of the Coronation Regalia in the Jewel House of the Tower of London*, was eventually published in 1998 (Blair et al., 1998). The work, of which only 650 were printed by the Stationery Office, London, at £1,000 per set, did not include details of the spectra, images of the diamonds in the spectrometers, or the color grading images, which are included in the following report.

With the exception of the George IV diadem, which was examined in 1989 on the premises of the GTLGB, all the gemological examinations of the Crown Jewels took place in the vault below the Waterloo Barracks in the Tower of London. Described here is the examination of the Cullinan I and II diamonds. The smaller Cullinan diamonds, which are in the Queen's personal collection and not part of the Crown Jewels, were not examined.

MATERIALS AND METHODS

The Cullinan I and II diamonds were graded for color and clarity in accordance with the normal CIBJO diamond grading practices in place at the time of the examination. First, both diamonds were thoroughly cleaned (figure 8), which was particularly important since both were still encased in their basket settings. Color grading was carried out within a standard light box, and the diamonds were compared against masterstones belonging to the GTLGB. Clarity grading was conducted using both a 10× loupe and a GIA GemoLite microscope set at 10× magnification. Due



Figure 8. The Cullinan II diamond is cleaned by Alan Jobbins prior to examination. Photo by K. Scarratt.

Figure 9. The Cullinan II diamond, still in its basket setting, is positioned with Blu Tack in the beam of the Nicolet 510 FTIR to measure its infrared spectrum. The inset provides a closer view of Cullinan II in the sample chamber. Photos by K. Scarratt.



to security restrictions, a temporary laboratory had to be set up within the vault housing the Crown Jewels, providing an environment that was less than ideal for diamond grading.

For the other visual examinations, gemological and mineralogical microscopes with magnifications ranging from 10× to 70× were employed. Fluorescence observations were made using a standard desktop long-wave (365 nm)/short-wave (253.7 nm) ultraviolet (UV) lamp in the total darkness of the central core of the display units in the middle of the vault.

At the time of these examinations, UV-visible and Fourier-transform infrared (FTIR) spectrometers were not found in most gem laboratories, so it was common practice when documenting diamond data to take a short-wave UV transparency image of each stone. These images were recorded by immersing photographic paper in a dish of water (emulsion-side up), placing the diamond table-down on the paper so that the water covered the entire stone, and then exposing the film to short-wave UV radiation by holding the same lamp used for the fluorescence observations about 30 cm directly above the paper. Once the paper was developed, if the center of the stone appeared dark (allowing for surface reflections from some facets), there was a good possibility that it was a type II diamond (i.e., transparent to short-wave UV); if the center was white, it was probably a type I diamond (i.e., opaque to short-wave UV). This procedure was performed on the Cullinans I and II using the underside of a workbench, a cardboard box, and a blackout curtain as a makeshift darkroom.

Note that this technique is only rarely practiced in gem laboratories today, as FTIR spectrometers are commonly available and produce definitive data on a diamond's type classification. Although infrared spectroscopy was also carried out on the Cullinans I and II (see below), the decision was made to conduct both tests to accommodate those gemologists who were not familiar with IR spectra.

Both OPL (diffraction grating) and Beck (dispersion) handheld spectrometers were used to examine the visible-range spectra.

UV-visible spectra were recorded between 220 and 900 nm at room temperature using a Pye-Unicam PU8800 spectrometer with a scan rate of 0.5 nm/s and a bandwidth of 0.5 nm. Mid-infrared spectra were recorded between 7800 and 400 cm^{-1} using a Nicolet 510 bench at a resolution of 4 cm^{-1} . The diamonds were too large for any of the standard sample chamber accessories, such as a beam condenser, so none were used. To acquire the spectra, the dia-



Figure 10. This front view of the head of the Sovereign's Sceptre with Cross with Cullinan I removed shows the screws that hold the basket setting in place. The scepter, which dates to 1660–1661, had to be slightly reworked to accommodate the Cullinan I diamond. Photo by Alan Jobbins.

monds were held with the aid of the putty-like adhesive Blu Tack (figure 9), and the stones were aligned so the beams entered the table and exited the culet or vice versa. Note that, with diamonds of this size, such "parallel windows" are likely to be large enough to permit the collection of fairly good spectral data without the use of a beam condenser.

RESULTS

Cullinan I. General Description and Grading. The Cullinan I diamond is mounted in a yellow gold basket setting that is held in the head of the Sovereign's Sceptre with Cross (also known as the Royal Sceptre with Cross) by means of a series of screws (figure 10).



Figure 11. Cullinan I and Cullinan II, both in their basket settings, are being compared with masterstones and other diamonds of known color using a standard viewing environment. The pear-shaped diamond in the foreground had previously been color graded as “D”. Photo by Alan Jobbins

The scepter dates to 1660–1661, but it has had various alterations that culminated with the addition of Cullinan I by Garrard & Co. in 1910 (Blair et al., 1998). The basket setting designed for Cullinan I has a hook attachment at its narrow end that connects to a ring attachment on the basket setting of

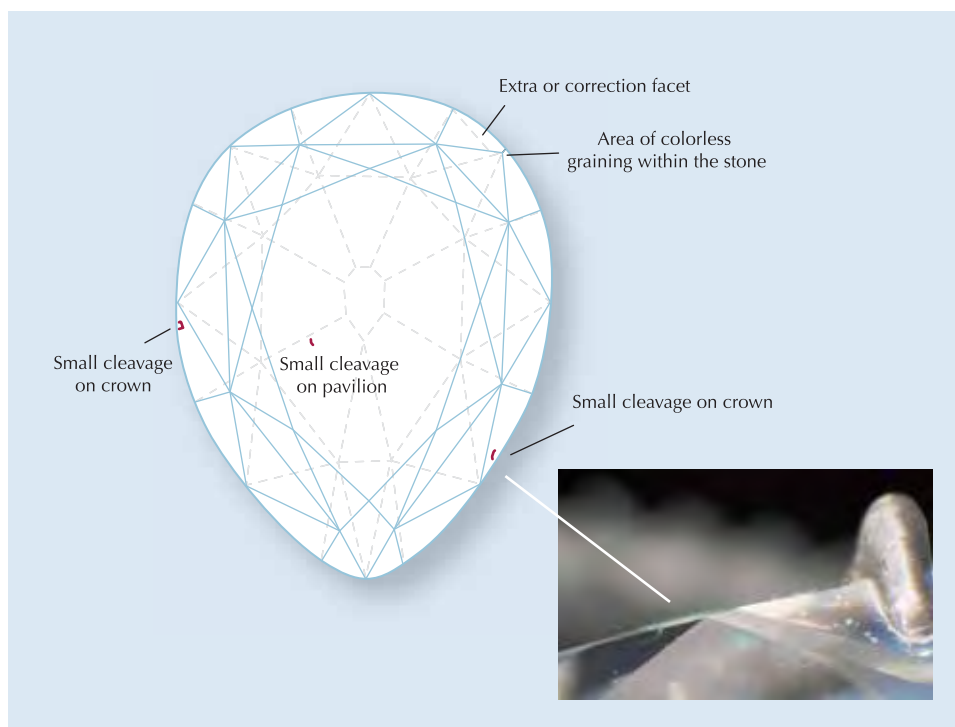
Cullinan II, allowing both to be mounted in a pin fitting and worn as a single brooch (figures 7 and 11).

Cullinan I is cut as a pear-shaped brilliant with 41 crown and 34 pavilion (including one extra) facets; it measures 58.9 × 45.4 × 27.7 mm and weighs 530.20 ct. The girdle is faceted.

While it was possible to remove Cullinan I from the scepter, it was not possible to remove it from its basket setting. Therefore, grading for color and clarity was restricted by the presence of the yellow gold setting. However, when the stone was placed next to diamond color masterstones (in the ±1 ct range), Cullinan I compared well with the one of least color, indicating that it approximated a D on the GIA color scale (again, see figure 11). Despite the reflections from the setting, the overall opinion of those examining the stone was that it is very probably a D color.

Affecting the clarity of Cullinan I were a number of surface imperfections: a small cleavage (“gletz”) on the pavilion and two further cleavages on the crown, an extra facet, and an area of colorless graining (figure 12). Cullinan I appeared to be free of any other clarity features, indicating that it warranted a clarity description of “potentially flawless.” Given the historical significance of this very attractive diamond, though, it will likely never be recut.

Figure 12. In this plotting diagram of Cullinan I, several clarity characteristics are shown, including cleavages on the pavilion and crown (see also inset) and some graining within the stone. Photomicrograph by K. Scarratt.



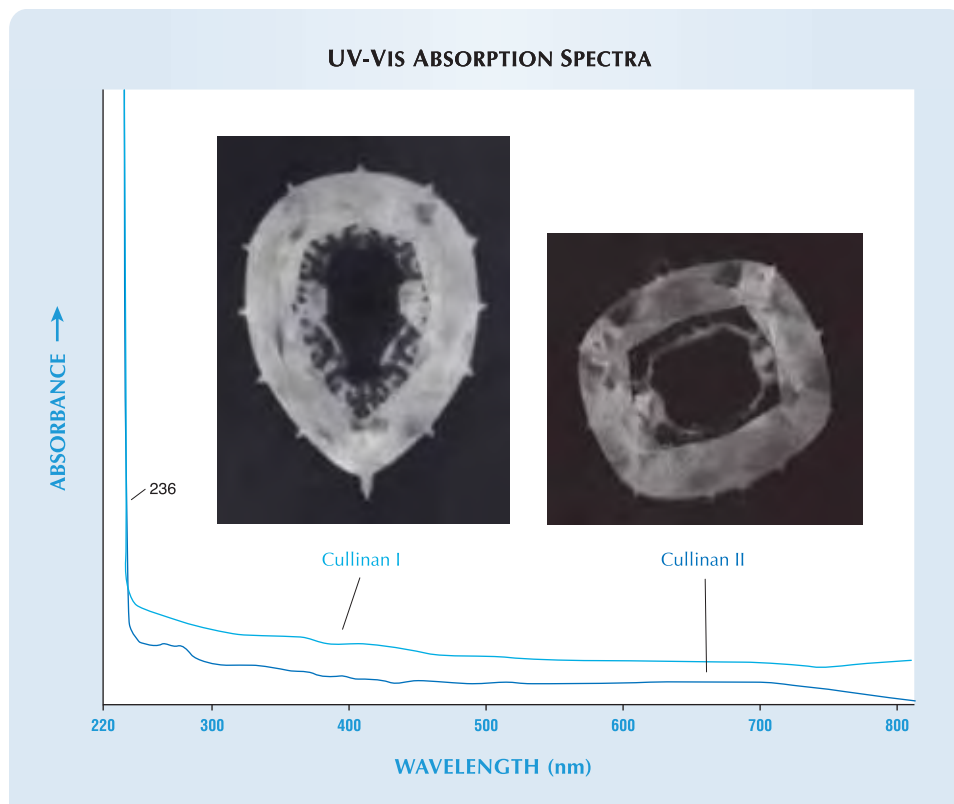


Figure 13. The UV-visible spectra recorded for the Cullinan I and Cullinan II diamonds are consistent with type II diamonds. This was supported by the dark centers in the short-wave UV transparency images also shown here.

Fluorescence. Cullinan I was inert to long-wave UV radiation, but fluoresced a weak greenish gray to short-wave UV. After the short-wave lamp was turned off, the diamond showed a weak green phosphorescence for at least 18 minutes.

UV-visible Spectroscopy. The UV-visible spectrum of Cullinan I (figure 13) revealed a featureless curve that rose slightly toward the shorter wavelengths, with total absorption occurring at 236 nm. This spectrum is consistent with that of type II diamonds (Wilks and Wilks, 1991).

The dark center of the short-wave UV image obtained on Cullinan I also indicated a strong possibility that it was a type II diamond (again, see figure 13).

Infrared Spectroscopy. The infrared spectrum for Cullinan I (figure 14) is normal for a diamond with an extremely low level of impurities and is consistent with that of type IIa diamonds (see, e.g., Fritsch and Scarratt, 1992).

Cullinan II. General Description and Grading. Cullinan II also is set in a yellow gold basket setting (again, see figure 11) that is held in the center front of the Imperial State Crown by screws (figure 15). Much of the content of the Imperial State Crown dates to 1838, with Cullinan II added in 1909, but

Figure 14. The infrared spectrum of Cullinan I is quite similar to the spectra of other diamonds with low quantities of impurities, which are designated type IIa.

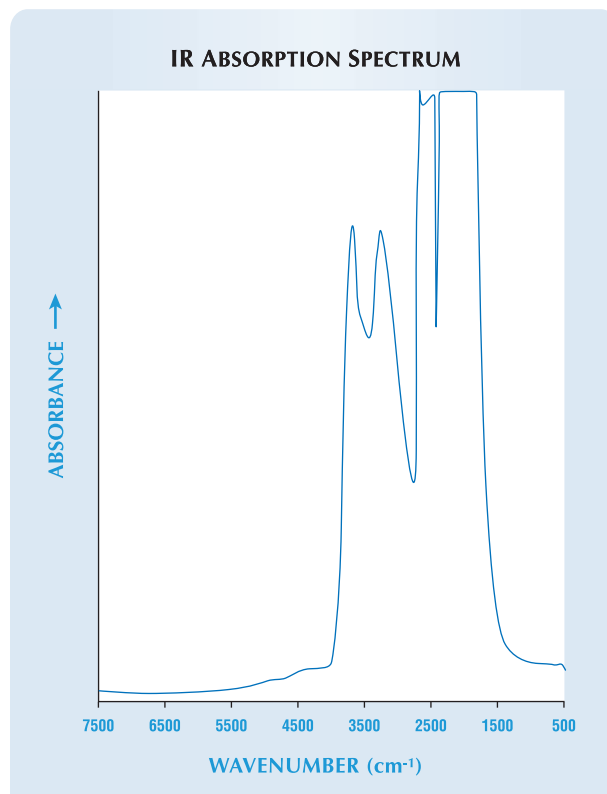




Figure 15. The front of the Imperial State Crown with Cullinan II and the large spinel known historically as the Black Prince's "Ruby" removed for this examination. These settings are flanked by two emeralds and two sapphires. Photo by K. Scarratt.

the crown in its present state (again, see figure 1) was executed by Garrard & Co. for the Coronation of George VI in 1937; the arches were lowered for Queen Elizabeth II in 1953 (Blair et al., 1998). As with the Cullinan I diamond, the basket setting designed for Cullinan II has a ring attachment that allows the two diamonds to be connected and worn as a single brooch (again, see figure 7).

Cullinan II is a cushion-shaped brilliant with 33 crown and 33 pavilion facets (including the table and culet, but excluding one very small extra facet on the pavilion). It measures $45.4 \times 40.8 \times 24.2$ mm and weighs 317.40 ct. The girdle is faceted.

As with Cullinan I, grading for color and clarity was restricted because the diamond could not be removed from its basket setting. However, when the stone was compared to the same diamond color masterstones, Cullinan II compared well with the

one of least color, indicating that it approximated a D on the GIA color scale (again, see figure 11), despite the reflections from the gold-colored setting.

The examination for clarity revealed a number of surface imperfections: a small chip at the girdle, a tiny pit with associated small "feathers" on the table, and a similar feature at the edge of a star facet. There are two small parallel cleavages on a star facet and two more near the girdle on a pavilion facet, as well as a small extra facet. A series of scratches runs diagonally across the table facet (figure 16). Cullinan II appeared to be free of any other imperfections. Like Cullinan I, the diamond is certainly potentially flawless, though, again, its historical significance would likely prohibit recutting.

Fluorescence. Like Cullinan I, Cullinan II was inert to long-wave UV radiation (figure 17), but fluoresced a weak greenish gray to short-wave UV. After the short-wave lamp was turned off, however, Cullinan II displayed only short-lived phosphorescence, in contrast to that of Cullinan I. The reason for this discrepancy in two diamonds from the same piece of rough is still unknown.

UV-Visible Spectroscopy. As might be expected (again, given that the two stones were cut from

Figure 16. This plotting diagram of Cullinan II shows the general locations of some imperfections, including small pits with feathers, small cleavages, faint scratches, and a small chip and natural at the girdle.

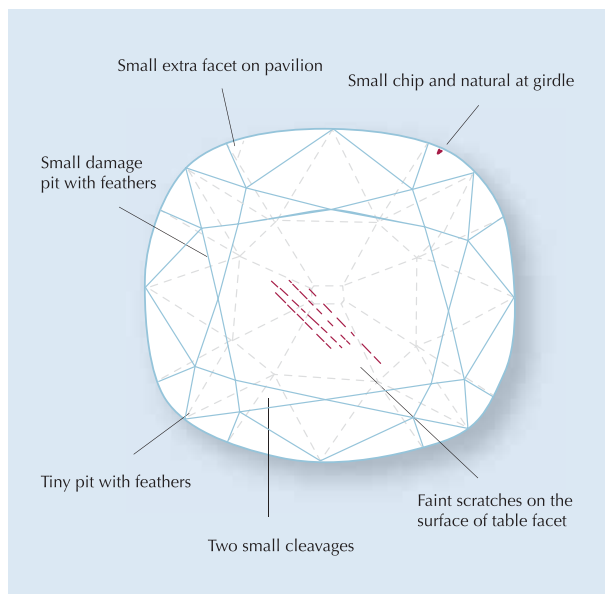




Figure 17. The Imperial State Crown with Cullinan II in place is shown during exposure to long-wave UV radiation. Note that the Cullinan II is inert under these conditions. A ruby inset in the red spinel (the Black Prince's "Ruby," which had been pierced during medieval times to be worn as a pendant) located above the Cullinan II and two rubies set in fleurs-de-lis show red fluorescence; several other diamonds show blue fluorescence. Photo by Alan Jobbins.

the same rough), the spectrum produced was similar to that of Cullinan I (again, see figure 13). It revealed a curve that rose slightly toward the shorter wavelengths, a low absorbance band at 265 nm (not present in the spectrum of Cullinan I), and total absorption occurring at 236 nm. As with Cullinan I, the dark center of the short-wave UV image for Cullinan II indicated that it was UV transparent. These results are consistent with type II diamonds.

Infrared Spectroscopy. The infrared spectrum for Cullinan II was recorded between 7800 and 400 cm^{-1} at room temperature. The spectrum is normal for a diamond with an extremely low level of impurities, consistent with type IIa diamonds, and similar to the infrared spectrum of Cullinan I (figure 14). A slight hump centered near 1100 cm^{-1} present in the spectrum of Cullinan II was the only difference detected in the spectra of the two diamonds (figure 18).

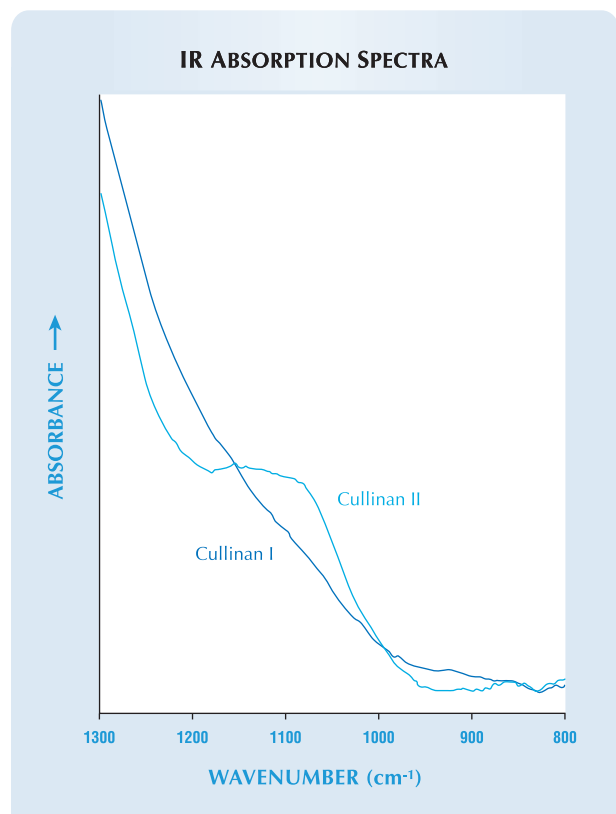
CONCLUSION

To date, the original Cullinan diamond is, at 3,106 ct, the largest rough diamond on record. Last year, 2005, marked the centennial of its discovery, and

2008 marks the centennial of the cutting of this historic piece of rough by Joseph Asscher. Although the 530.20 ct Cullinan I has been surpassed in size by the 545.67 ct Golden Jubilee—a brown diamond cut in 1990 from rough that was also found at South Africa's Premier mine—it remains the largest colorless cut diamond and one of the world's most legendary gemstones, on view to millions of visitors each year in the Tower of London. It is a cornerstone of the Crown Jewels of England and, because of the period and circumstances of its discovery and acquisition, it remains a powerful symbol of the British Empire at its zenith.

Despite its legendary status, a complete published gemological report on the diamond was not available until this article. These gemological examinations, which found the polished diamonds to be D color, potentially flawless in clarity, and type IIa, serve to enhance the Cullinan's legendary stature.

Figure 18. The infrared spectra of Cullinans I and II are expanded here to show the "nitrogen region" at 1300–800 cm^{-1} . The slight hump in the spectrum for Cullinan II occurs at ~1100 cm^{-1} .



ABOUT THE AUTHORS

Mr. Scarratt (ken.scarratt@gia.edu) is director of GIA Research (Thailand), in Bangkok, and Mr. Shor is senior industry analyst at GIA in Carlsbad, California; previously, he served as diamonds editor for Jewelers' Circular Keystone and editor-in-chief of New York Diamonds and Gemkey magazines.

ACKNOWLEDGMENTS

The authors are grateful to the following for providing information: Lynette Hori, Diamond Trading Company, London; Brig. Kenneth Mears, former keeper of the Crown Jewels, London; Robin Walker, former manager of technical information, De Beers, London; and E. Alan Jobbins, president of Gem-A, London.

REFERENCES

- Balfour I. (2000) *Famous Diamonds*. Christie, Manson & Woods Ltd., London.
- Blair C., Bury S., Grimwade A., Harding R., Jobbins E.A., King D., Scarratt K. (1998) *The Crown Jewels: The History of the Coronation Regalia in the Jewel House of the Tower of London*, Stationery Office Books, London.
- De Beers Group (2004) *Annual Review 2004*. http://www.debeersgroup.com/NR/rdonlyres/96870848-824D-495A-B273-135AC9657613/739/DeBeers_AR2004.pdf.
- De Beers Group (2006) History. <http://www.debeersgroup.com/debeersweb/debeersweb/De+Beers+Home/Visit+a+Mine/Cullinan/History.htm>.
- Fernandes C. (2005) Cullinan diamond mine, Gauteng. <http://www.miningweekly.co.za/min/sector/diamonds/?show=19865>.
- Fritsch E., Scarratt K. (1992) Natural-color nonconductive gray-to-blue diamonds. *Gems & Gemology*, Vol. 28, No. 1, pp. 35–42.
- Helme N. (1974) *Thomas Major Cullinan: A Biography*. McGraw-Hill, Johannesburg.
- Holmes M. (1974) *The Crown Jewels at the Tower of London*. Reissued 1981. Dept. of Environment, HM Stationery Office, London.
- Holmes M.R. (1937) The crowns of England. *Archaeologia*, Vol. 86, pp. 73–90.
- Holmes M.R. (1959) New light on St. Edward's crown. *Archaeologia*, Vol. 97, pp. 213–223.
- The largest diamond (1905) *Jewelers' Circular*, Vol. 50, No. 1, pp. 108–109.
- Mears K. (1986) *The Crown Jewels: Tower of London*. Historic Royal Palaces Agency, London.
- More about the great Cullinan diamond found in the Transvaal. (1905) *Jewelers' Circular*, Vol. 50, No. 10, pp. 70–71.
- Some facts about the colossal diamond found at the new Premier mine in the Transvaal (1905) *Jewelers' Circular*, Vol. 50, No. 7, p. 86.
- Spencer L. (1910) Notes on the weight of the Cullinan diamond and the value of the carat-weight. *Mineralogical Magazine*, Vol. 15, No. 71, pp. 318–326.
- Wilks J., Wilks E. (1991) *Properties and Applications of Diamond*. Butterworth-Heinemann, Oxford.

2005 Manuscript Reviewers

GEMS & GEMOLOGY requires that all articles undergo a peer review process in which each manuscript is evaluated by at least three experts in the field. This process is vital to the accuracy and readability of the published article, but it is also time consuming for the reviewer. Because members of our Editorial Review Board cannot have expertise in every area, we sometimes call on others in our community to share their intellect and insight. In addition to the members of our Editorial Review Board, we extend a heartfelt thanks to the following individuals who reviewed manuscripts for *G&G* in 2005:

Mr. William Boyajian
Mr. Charles Carmona
Mr. John Chapman
Mr. Paul Cory
Dr. David Fisher
Dr. Carl Francis
Mr. Mike Gray

Dr. Lee Groat
Mr. Hertz Hasenfeld
Mr. John King
Dr. Paul Martineau
Mr. Roland Naftule
Dr. Mark Newton
Mr. Rory More O'Ferrall

Mr. Carl Pearson
Mr. Benjamin Rondeau
Mr. Charles Schiffman
Dr. Dietmar Schwarz
Mr. George Solario
Dr. Wuyi Wang
Dr. Christopher Welbourn

Spring 1999

The Identification of Zachery-Treated Turquoise
Russian Hydrothermal Synthetic Rubies and Sapphires
The Separation of Natural from Synthetic Colorless Sapphire

Summer 1999

On the Identification of Emerald Filling Substances
Sapphire and Garnet from Kalalani, Tanzania
Russian Synthetic Ametrine

Fall 1999—Special Issue

Special Symposium Proceedings Issue, including:
Observations on GE-Processed Diamonds,
Abstracts of Featured Speakers, Panel
Sessions, War Rooms, and Poster Sessions

Winter 1999

Classifying Emerald Clarity Enhancement at the GIA
Gem Trade Laboratory

Clues to the Process Used by General Electric to Enhance
the GE POL Diamonds

Diopside Needles as Inclusions in Demantoid Garnet from Russia
Garnets from Madagascar with a Color Change of
Blue-Green to Purple

Spring 2000

Burmese Jade
Lapis Lazuli from Chile
Spectroscopic Evidence of GE POL Diamonds
Chromium-Bearing Taaffeites

Summer 2000

Characteristics of Nuclei in Chinese Freshwater Cultured Pearls
Afghan Ruby and Sapphire
Yellow to Green HPHT-Treated Diamonds
New Lasering Technique for Diamond
New Oved Filling Material for Diamonds

Fall 2000

GE POL Diamonds: Before and After
Sapphires from Northern Madagascar
Pre-Columbian Gems from Antigua
Gem-Quality Hatiyne from Germany

Winter 2000—Special Issue

Gem Localities of the 1990s
Enhancement and Detection in the 1990s
Synthetics in the 1990s
Technological Developments in the 1990s
Jewelry of the 1990s

Spring 2001

Ammolite from Southern Alberta, Canada
Discovery and Mining of the Argyle Diamond Deposit, Australia
Hydrothermal Synthetic Red Beryl

Summer 2001

The Current Status of Chinese Freshwater Cultured Pearls
Characteristics of Natural-Color and Heat-Treated
“Golden” South Sea Cultured Pearls
A New Method for Imitating Asterism

Fall 2001

Modeling the Appearance of the Round Brilliant
Cut Diamond: Fire
Pyrope from the Dora Maira Massif, Italy
Jeremejevitte: A Gemological Update

Winter 2001

An Update on “Paraíba” Tourmaline from Brazil
Spessartine Garnet from San Diego County, California
Pink to Pinkish Orange Malaya Garnets from
Bekily, Madagascar
“Voices of the Earth”: Transcending the Traditional in
Lapidary Arts

Spring 2002—Special Issue

The Ultimate Gemologist: Richard T. Liddicoat
Portable Instruments and Tips on Practical Gemology in the Field
Liddicoatite Tourmaline from Madagascar
Star of the South: A Historic 128 ct Diamond

Summer 2002

Characterization and Grading of Natural-Color Pink Diamonds
New Chromium- and Vanadium-Bearing Garnets from
Tranoroa, Madagascar
Update on the Identification of Treated “Golden” South
Sea Cultured Pearls

Fall 2002

Diamonds in Canada
“Diffusion Ruby” Proves to Be Synthetic Ruby Overgrowth
on Natural Corundum

Winter 2002

Chart of Commercially Available Gem Treatments
Gemesis Laboratory-Created Diamonds
Legal Protection for Proprietary Diamond Cuts
Rhodizite-Londonite from the Antsongombato Pegmatite,
Central Madagascar

Spring 2003

Photomicrography for Gemologists
Poudretteite: A Rare Gem from Mogok
Grandidierite from Sri Lanka

Summer 2003

Beryllium Diffusion of Ruby and Sapphire
Seven Rare Gem Diamonds

Fall 2003

G. Robert Crowningshield: A Legendary Gemologist
Cause of Color in Black Diamonds from Siberia
Obtaining U.S. Copyright Registration for the Elara Diamond

Winter 2003

Gem-Quality CVD Synthetic Diamonds
Pezzottaite from Madagascar: A New Gem
Red Beryl from Utah: Review and Update

Spring 2004

Identification of CVD-Grown Synthetic Diamonds
Cultured Pearls from Gulf of California, Mexico
X-Ray Fingerprinting Routine for Cut Diamonds

Summer 2004

Gem Treatment Disclosure and U.S. Law
Lab-Grown Colored Diamonds from Chatham
The 3543 cm⁻¹ Band in Amethyst Identification

Fall 2004

Grading Cut Quality of Round Brilliant Diamonds
Amethyst from Four Peaks, Arizona

Winter 2004

Creation of a Suite of Peridot Jewelry: From the Himalayas
to Fifth Avenue
An Updated Chart on HPHT-Grown Synthetic Diamonds
A New Method for Detecting Beryllium Diffusion—
Treated Sapphires (LIBS)

Spring 2005

Treated-Color Pink-to-Red Diamonds from Lucent Diamonds Inc.
A Gemological Study of a Collection of Chameleon Diamonds
Coated Pink Diamond: A Cautionary Tale

Summer 2005

Characterization and Grading of Natural-Color Yellow Diamonds
Emeralds from the Kafubu Area, Zambia
Mt. Mica: A Renaissance in Maine's Gem
Tourmaline Production

Fall 2005

A Review of the Political and Economic Forces Shaping
Today's Diamond Industry
Experimental CVD Synthetic Diamonds from LIMHP-
CNRS, France
Inclusions in Transparent Gem Rhodonite from
Broken Hill, New South Wales, Australia

Winter 2005

A Gemological Pioneer: Dr. Edward J. Gübelin
Characterization of the New Malossi Hydrothermal
Synthetic Emerald

70 PLUS Years of GEMS & GEMOLOGY The Quarterly Journal That Lasts A Lifetime



Fall 2003



Winter 2003



Fall 2005



Winter 2005



Spring 2003



Summer 2003



Spring 2005



Summer 2005



Fall 2002



Winter 2002



Fall 2004



Winter 2004



Spring 2002/Special Issue



Summer 2002



Spring 2004



Summer 2004

Order Your BACK ISSUES Today!

E-Mail: gandg@gia.edu or visit www.gia.edu

Call Toll Free 800-421-7250 ext. 7142

or 760-603-4000 ext. 7142

Fax: 760-603-4595 or Write: G&G Subscriptions, P.O. Box 9022,

Carlsbad, CA 92018-9022 USA

	U.S.	Canada	International
Single Issues	\$ 12 ea.	\$ 15 ea.	\$ 18 ea.
Complete Volumes*			
1991–2005	\$ 40 ea.	\$ 48 ea.	\$ 60 ea.
Three-year set	\$ 115 ea.	\$ 135 ea.	\$ 170 ea.
Five-year set	\$ 190 ea.	\$ 220 ea.	\$ 280 ea.

*10% discount for GIA Alumni and active GIA students.

Some issues from 1981–1998 are also available. Please call or visit our website for details on these and the 2006 issues as they are published.

Limited Quantities Available.

THE EFFECTS OF HEAT TREATMENT ON ZIRCON INCLUSIONS IN MADAGASCAR SAPPHIRES

Wuyi Wang, Kenneth Scarratt, John L. Emmett, Christopher M. Breeding, and Troy R. Douthit

Zircon inclusions in sapphires from Madagascar were studied to investigate the effects of heat treatment on their gemological and spectroscopic features. Progressive decomposition of zircon and chemical reactions between zircon and the host sapphire occurred at temperatures between 1400°C and 1850°C. In unheated sapphires, transparent zircon inclusions displayed euhedral slightly elongated forms and clear interfaces with their corundum host. Most were confined within the host under relatively high pressures (up to 27 kbar), and showed evidence of natural radiation-related damage (metamictization). Subsolidus reactions (i.e., the decomposition of zircon into its component oxides without melting) of some zircon inclusions started at temperatures as low as 1400°C, as evidenced by the formation of baddeleyite (ZrO_2) and a SiO_2 -rich phase. Differences in the degree of preexisting radiation damage are the most likely cause for the decomposition reactions at such relatively low temperatures. Melting of zircon and dissolution of the surrounding sapphire occurred in all samples at 1600°C and above. This resulted in the formation of both baddeleyite and a quenched glass rich in Al_2O_3 and SiO_2 . From these data and observations, a systematic sequence of both modification and destruction of zircon inclusions with increasing temperature was compiled. This zircon alteration sequence may be used (1) as a gemological aid in determining whether a zircon-bearing ruby/sapphire has been heated, and (2) to provide an estimate of the heating temperature.

Because of the high demand for attractive sapphires and rubies, many different treatments have been applied to mid- and low-grade corundum to enhance color and clarity. On an atomic level, by modifying trace-element concentrations and defect configurations in the corundum crystal structure, selective light absorption in the visible spectrum can be changed to produce pleasant bodycolors and thus more valuable sapphires (see, e.g., Crowningshield, 1966; Beesley, 1982; Emmett and Douthit, 1993). Heating traditionally has been one of the most common treatments and remains so today.

As would be expected, temperature is one of the most critical factors in the heat treatment of sapphire. Modern technology has allowed sapphires to be exposed to higher temperatures, has produced more dramatic color changes in shorter periods of

time, and has expanded the range of material suitable for enhancement. With the recent development of the beryllium-diffusion process, treatment temperatures as high as 1850°C, near the melting point of corundum (2030°C–2050°C), have become common (Emmett et al., 2003).

Zircon ($ZrSiO_4$) is a common inclusion in Madagascar sapphires, which are important because they span the color spectrum (figure 1); stones from this locality may also be sourced for Be diffusion. Zircon is prevalent in corundum from many other geographic sources as well (see, e.g., Schwieger, 1990; Guo et al., 1996; Hughes, 1997; Rankin, 2002;

See end of article for About the Authors and Acknowledgments.
GEMS & GEMOLOGY, Vol. 42, No. 2, pp. 134–150.
© 2006 Gemological Institute of America

Figure 1. Natural sapphires, such as these 45 princess cuts from Madagascar, come in a broad range of colors. Nevertheless, the high demand for fine ruby and sapphire has led to a wide variety of treatments, of which heating to improve color and/or clarity is perhaps the most common. These sapphires have a total weight of 23.08 ct. Courtesy of Pala International, Fallbrook, California; photo © Jeff Scovil.



Rankin and Edwards, 2003). During heat treatment, included mineral crystals are subjected to the same conditions as the corundum host, but since they have different thermodynamic and chemical properties, they may expand, recrystallize, melt, or chemically react with the host corundum in very different ways that are dependent on the heating temperature, time, and other factors. Observation of destroyed or modified mineral inclusions using an optical microscope has long been used to identify heat-treated sapphires (see, e.g., Gübelin, 1973; Scarratt, 1983; Gübelin and Koivula, 1986; Cozar and de Vincente-Mingarro, 1995; Hughes, 1997). However, systematic descriptions of morphological changes in response to heating for specific mineral inclusions such as zircon are not widely available (Cozar and de Vincente-Mingarro, 1995; Rankin and Edwards, 2003).

Of particular concern in recent years, diffusion of a trace amount of beryllium (from several up to tens of parts per million) into corundum can lead to a fundamental change in bodycolor (Emmett et al., 2003). Although the diffusion coefficient of Be in corundum is higher than that of many other elements, diffusion of Be into corundum is still a very slow process. A very high temperature (~1800°C) is often necessary to process the stone in a reasonable amount of time, although Be diffusion may occur at lower temperatures. Using the morphology of zircon inclusions to estimate the heating temperature could minimize the number of samples that would have to be submitted for trace-element analysis.

MATERIALS AND METHODS

A total of 41 rough sapphires from Madagascar, ranging from 0.21 to 4.34 ct, were selected for this study based mainly on the possible occurrence of zircon inclusions. All of the samples were irregular in shape, and over half exhibited the flat morphology that is common for Madagascar sapphires. Most were from GIA's collection of specimens obtained directly from the Ilakaka area of Madagascar; the rest (slightly less than one-third) were purchased from reliable sources in the market. All were known to be natural and untreated by heat or any other method.

Twenty-five samples were heated to various temperatures so we could observe changes in their zircon inclusions; their properties and heating conditions are given in table 1. The remaining 16 were left unheated for comparison. After heating, most were pink or purplish pink of varying saturation, but some were near colorless or had slight blue or yellow hues. While we did note overall color changes, since the focus of this study was the zircon inclusions, we did not track color changes with temperature or attempt to control the atmosphere to achieve optimal coloration.

Heating experiments were carried out using a vertical furnace with an oxidizing atmosphere in the facilities of Crystal Chemistry, Brush Prairie, Washington. Target annealing temperatures varied from 1400°C to 1850°C. For each experimental run, two to three samples were heated at the target temperature in a high-purity alumina crucible for 5 hours; this time was considered adequate to reach

equilibrium conditions. To evaluate the effects of different heating durations, additional experiments at 1600°C and 1730°C were performed for 25 and 12 hours, respectively. During each run, the temperature was raised from room temperature to 1000°C at a rate of 300°C/hour, and then to the target temperature at a rate of 600°C/hour. Temperatures measured in this study are believed to be accurate to about ±1%, and fluctuation in each experimental run was less than ±10°C. After annealing at the tar-

get temperature for 5 hours, in most cases the temperature was then decreased to room temperature over a period of 4 hours. Following the heating experiments, all samples were ground on both sides to at least 0.5 mm depth to remove possible surface contamination, and then polished for observation and analysis.

In two unheated and all the heated sapphires, the surface-reaching zircon inclusions were analyzed using a high-resolution analytical scanning electron microscope (LEO 1550 VP FESEM) equipped with an Oxford INCA Energy 300 energy-dispersive X-ray spectrometer (EDS) at the California Institute of Technology. A thin layer of carbon was coated over a polished surface of each sapphire to improve electrical conductivity. Since most zircon inclusions are very small and the decomposition products are even smaller, the results of quantitative elemental analysis were normalized. This way, a relative accuracy of better than 5% and a detection limit of better than 0.5 wt.% could be obtained. The analyses were performed using an accelerating voltage of 20 kV, a focused electron beam with a spot size of 1–2 μm, and a beam current of 10 nA. Backscattered electron (BSE) images were obtained to provide a means of mapping areas in a sample that contained elements of different atomic weights.

Infrared absorption spectra of the host sapphire were recorded in the mid-infrared region (6000–400 cm⁻¹, 1.0 cm⁻¹ resolution) at room temperature with a Thermo-Nicolet Nexus 670 Fourier-transform infrared (FTIR) spectrometer equipped with a KBr beam splitter and MCT-B detector. Prior to analysis, the samples were cleaned using an ultrasonic bath with pure acetone to remove surface contamination. A 2-mm-diameter center portion of each sample was selected for analysis, and the rest of the sample was shielded using a clean metal mask. A 6× beam condenser focused the incident beam through the sample, and a total of 256 scans (per spectrum) were collected to improve the signal-to-noise ratio.

Raman spectra of the zircon inclusions and their host sapphires were recorded at room temperature using a Renishaw 1000 Raman microspectrometer with a polarized Ar-ion laser at two different laser excitations (488.0 and 514.5 nm). The two lasers were used to help clarify the identity of some emission peaks (Raman scattering vs. luminescence). The instrument was calibrated against the first-order Raman shift of a type IIa diamond at 1332.5 cm⁻¹. Spectra were collected using a confocal

TABLE 1. Heated (with experimental conditions) and unheated Madagascar sapphires studied for this report.

Sample no.	Weight (ct)	Thickness (mm)	Heating experiment		
			Temperature (°C)	Duration (hours)	Environment
75965	0.65	1.07	1400	5	Oxidizing
75966	0.89	1.41		5	
75967	1.29	1.73		5	
65458	1.61	2.58	1450	5	Oxidizing
65459	1.12	2.06		5	
65460	1.05	2.50	1500	5	Oxidizing
65461	1.10	1.62		5	
65462	1.79	2.59	1550	5	Oxidizing
65463	0.96	2.16		5	
56016	1.88	3.76	1600	5	Oxidizing
56017	3.32	4.25		5	
75968	0.83	1.27		25	
75969	1.18	1.80		25	
75970	0.70	1.21		25	
56018	3.25	3.64	1680	5	Oxidizing
56019	2.82	nd ^a		5	
56020	2.03	2.23	1730	5	Oxidizing
56021	2.27	nd		5	
75971	0.35	0.91		12	
75972	0.64	1.14		12	
75973	0.75	2.15		12	
56022	2.94	3.49	1780	5	Oxidizing
56023	1.90	3.32		5	
56024	1.52	2.36	1850	5	Oxidizing
56025	4.34	nd		5	
56536	0.65	nd	Not treated		
75974	0.72	1.08			
75975	0.77	1.99			
75976	1.09	1.81			
76726	0.60	1.41			
76728	0.32	1.15			
76729	0.63	1.29			
76730	0.38	1.30			
76731	0.26	1.07			
76732	0.21	0.62			
76733	0.53	1.56			
76734	0.23	1.07			
76735	0.31	1.42			
76736	0.30	1.07			
76737	0.40	1.09			
76738	0.92	1.99			

^a nd = not determined.



Figure 2. Discrete zircon inclusions were common in the Madagascar sapphires. With magnification, the interfaces between the zircon inclusions and their host sapphire were almost always clear and transparent, showing no frostiness or turbidity. The crystal faces were flat or somewhat rounded and shiny. Photomicrograph by W. Wang; magnified 90 \times .

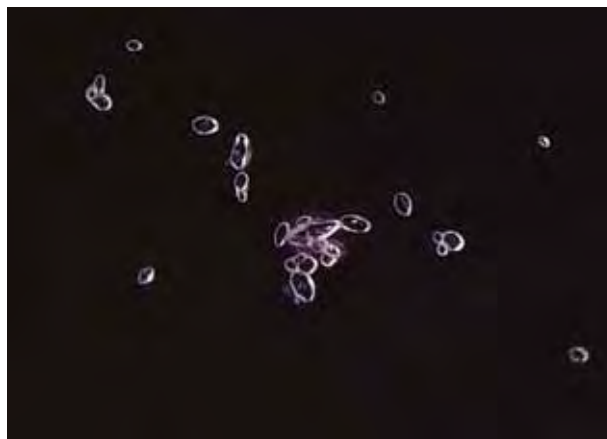


Figure 3. Clusters of zircon inclusions were present in many of the Madagascar sapphires. Aggregations usually consisted of less than 10 crystals, and no other minerals were observed as part of these clusters. In rare cases, up to 100 crystals were seen in a large cluster. Photomicrograph by W. Wang; magnified 90 \times .

system with a grating of 1800 grooves per mm, slit width of 50 μm , objective lens of 50 \times , and initial laser power of 20 mW. Up to 100 scans were accumulated to achieve a better signal-to-noise ratio. Raman spectra of the host sapphires were collected in the same orientation used for the inclusions by slightly moving the sample stage horizontally. Raman spectra of the zircon inclusions in both the unheated and heated sapphires were obtained by subtracting an appropriate percentage of the host sapphire spectrum (i.e., when Raman peaks from corundum disappeared entirely) from that collected directly from the inclusions.

In addition, to better evaluate the spectral features of the zircon inclusions, we analyzed two faceted free-standing zircons (one blue and one colorless) in several random directions. We also analyzed a euhedral purple zircon crystal that had well-developed prismatic morphology with the c-axis parallel, at 45 $^\circ$, and perpendicular to the laser polarization. The geographic sources of these single-crystal zircons are unknown.

RESULTS

Unheated Samples. In the 16 unheated sapphires, minor amounts of monazite and apatite were present, but zircon was the most common inclusion. Thirteen of the samples showed pink-purple coloration; the other three were colorless, blue, and greenish yellow. Abundant zircon inclusions were observed in the colorless and 11 of the pink samples.

Microscopic Observation. Typically, the unheated zircon inclusions were transparent with a slightly elongate crystal habit and well-developed {110} form, although many were slightly rounded. They ranged from less than 10 μm to about 100 μm in the longest dimension, though most were smaller than 50 μm . A few samples contained mostly individual inclusions (figure 2), while others displayed clusters (figure 3). The latter usually consisted of less than 10 zircon crystals and no other minerals; in two samples, they showed as many as 100 crystals. Generally, the inclusions were randomly distributed within the host sapphire, but three samples showed linear orientation to some extent. Even when viewed at up to 100 \times magnification, their interfaces with the host sapphire were almost always clear and transparent. The crystal faces of the zircons were flat or slightly rounded, and reflective. Some of the larger zircon crystals and clusters were accompanied by radial fractures in the surrounding corundum (figure 4); however, the depth of these fractures extending from the inclusion surface into the sapphire hosts was limited, with most no larger than the inclusion itself. Some were very subtle and could only be observed with carefully oriented lighting. Similar to the interface between the zircon inclusions and the host sapphire, these fractures were clean and smooth. No foreign material or apparent frosting was observed (again, see figure 4).

SEM-EDS Analysis. Seven pristine zircon inclusions in two unheated sapphires (nos. 75974 and



Figure 4. Radial fractures were often present around larger zircon inclusions. The depths of the fractures were limited, and most were close to the size of the inclusions and only rarely reached the surface of the host sapphire. Photomicrograph by W. Wang; magnified 112 \times .



Figure 5. This backscattered electron image shows a uniform zircon crystal that has a sharp planar boundary with the surrounding host sapphire. Due to its high content of the heavy element zirconium, the zircon inclusion appears much brighter than the surrounding host sapphire. Image width 70 μm .

75975) were chemically analyzed using SEM-EDS (representative data in table 2). BSE images of inclusions exposed at the surface showed uniform zircon crystals with sharp planar or slightly rounded boundaries (figure 5) and no evidence of decomposition; a few displayed growth zoning. Chemical analysis revealed that these inclusions were nearly

pure zircon (ZrSiO_4) with only minor amounts of HfO_2 (from less than the instrument detection limit up to ~ 2 wt.%).

Infrared Absorption Spectroscopy. The unheated host sapphires displayed few features in the mid-IR region other than a weak absorption at 3309 cm^{-1}

TABLE 2. Representative element concentrations (wt.% oxide) of zircon inclusions and of their reaction products after the heating experiments.

Sample no.	Heating temperature ($^{\circ}\text{C}$)	Phase	Na_2O	MgO	Al_2O_3	SiO_2	K_2O	CaO	TiO_2	FeO	ZrO_2	Ce_2O_3	HfO_2
75974	Unheated	Zircon	– ^a	–	–	32.6	–	–	–	–	65.8	–	1.6
		Zircon	–	–	–	32.4	–	–	–	–	65.7	–	1.9
		Zircon	–	–	–	32.1	–	–	–	–	66.4	–	1.5
75975	Unheated	Zircon	–	–	–	32.8	–	–	–	–	67.2	–	–
		Zircon	–	–	–	32.4	–	–	–	–	67.7	–	–
75967	1400	Zircon	–	–	–	32.9	–	–	–	–	67.1	–	–
		Baddeleyite	–	–	1.7	9.4	–	–	–	–	87.6	–	1.4
65458	1450	Zircon	–	–	–	33.0	–	–	–	–	67.0	–	–
		Baddeleyite	–	–	1.9	21.2	–	–	–	–	76.9	–	–
75968	1600	Zircon	–	–	–	34.1	–	–	–	–	62.8	–	3.2
		Baddeleyite	–	–	1.0	–	–	–	–	–	96.0	–	3.1
75969	1600	Baddeleyite	–	–	–	–	–	–	–	–	95.1	–	4.9
		Melt	–	4.5	21.8	71.4	0.9	–	–	–	2.1	–	–
56018	1680	Baddeleyite	–	–	2.7	–	–	–	–	–	97.7	–	–
		Melt	3.2	–	18.4	54.8	–	4.2	2.5	–	16.9	–	–
56020	1730	Baddeleyite	–	–	–	–	–	–	–	–	98.6	–	1.4
		Melt	–	–	73.7	26.3	–	–	–	–	–	–	–
56023	1780	Baddeleyite	–	–	3.2	–	–	1.4	–	–	95.4	–	–
		Melt	0.2	3.2	28.6	41.7	–	14.7	2.5	0.2	8.4	0.5	–
56024	1850	Baddeleyite	–	–	–	–	–	–	–	–	100.0	–	–
		Melt	–	–	29.3	66.4	–	–	–	2.0	4.6	–	–

^a – = not detected.

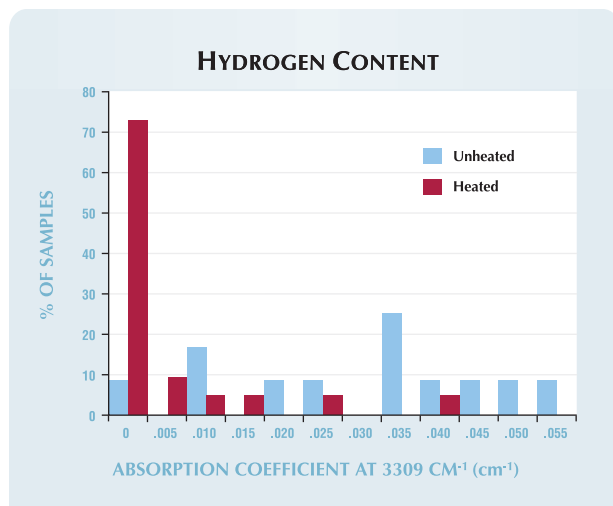


Figure 6. The hydrogen-related absorption coefficient at 3309 cm^{-1} was much stronger in the unheated sapphires from Madagascar than in the heated samples. Most of the latter, which were heated in an oxidizing environment, contained no structurally bonded hydrogen after treatment.

produced by structurally bonded hydrogen. All but one of the unheated sapphires showed the 3309 cm^{-1} absorption, with intensity of the absorption coefficient varying from ~ 0.010 to $\sim 0.055\text{ cm}^{-1}$ (figure 6). These data indicate that trace hydrogen is common in unheated Madagascar sapphires.

Raman Spectroscopy. Micro-Raman analysis produced some interesting information on the zircon inclusions. All displayed seven or eight peaks in the region of $1050\text{--}200\text{ cm}^{-1}$ (figure 7, top spectrum). These peaks were much broader and weaker in intensity than the characteristic Raman peaks of synthetic end-member zircon in the $1050\text{--}200\text{ cm}^{-1}$ region (again, see figure 7, bottom spectrum; G. Rossman, pers. comm., 2006; see also Nasdala et al., 2003). The peaks above 1020 cm^{-1} were also observed in the spectra from the blue and colorless free-standing zircons. Three peaks (ν_1 —symmetric stretching, ν_2 —symmetric bending, ν_3 —antisymmetric stretching [again, see figure 7]; Griffith, 1969; Syme et al., 1977) were relatively sharp with full width at half maximum (FWHM) of $6.7\text{--}11.2\text{ cm}^{-1}$, $13.6\text{--}18.4\text{ cm}^{-1}$, and $10.1\text{--}13.5\text{ cm}^{-1}$, respectively, at 514.5 nm laser excitation.

Most of the Raman peaks from the inclusions were shifted from the values of the two faceted free-standing zircon samples (figure 8). In particular, for the ν_3 mode, the Raman peaks in these free-standing zircons had a very limited range of variation ($1007.8\text{--}1008.4\text{ cm}^{-1}$). In the free-standing purple crys-

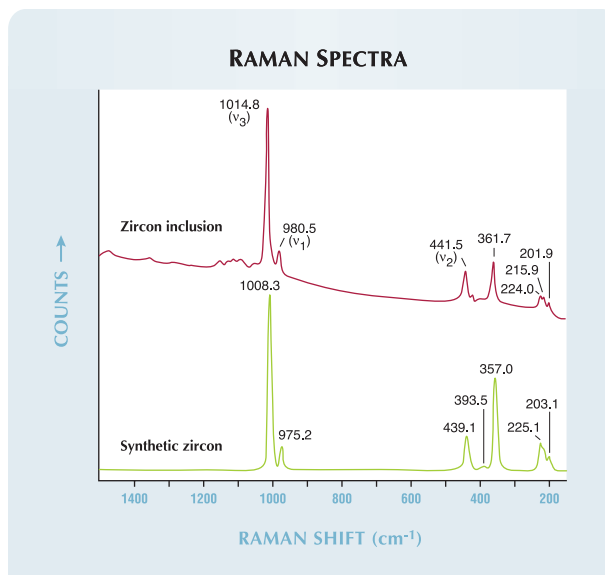
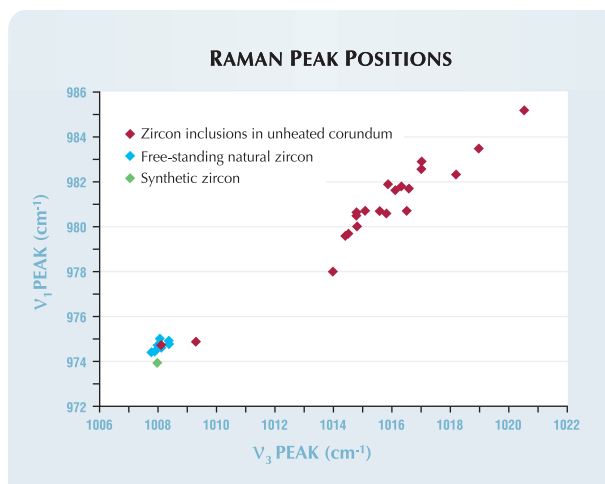


Figure 7. Strong Raman peaks overlying a relatively flat background were recorded in all analyzed zircon inclusions. Compared with synthetic end-member zircon (G. Rossman, pers. comm., 2006), a notable feature is the evident shifting of almost all Raman peaks.

tal tested in several orientations, we observed significant variations in peak intensities, but no shifting in peak positions. When the c-axis was parallel to the

Figure 8. Among the 23 analyzed inclusions in unheated sapphires, the Raman peaks of only two inclusions fell in positions similar to those of synthetic end-member zircon (G. Rossman, pers. comm., 2006) or unheated zircons analyzed in this study. All the other zircon inclusions exhibited much higher peak positions. In addition, a positive correlation was observed between peak positions. Similar positive relations were detected between other peaks (not shown).



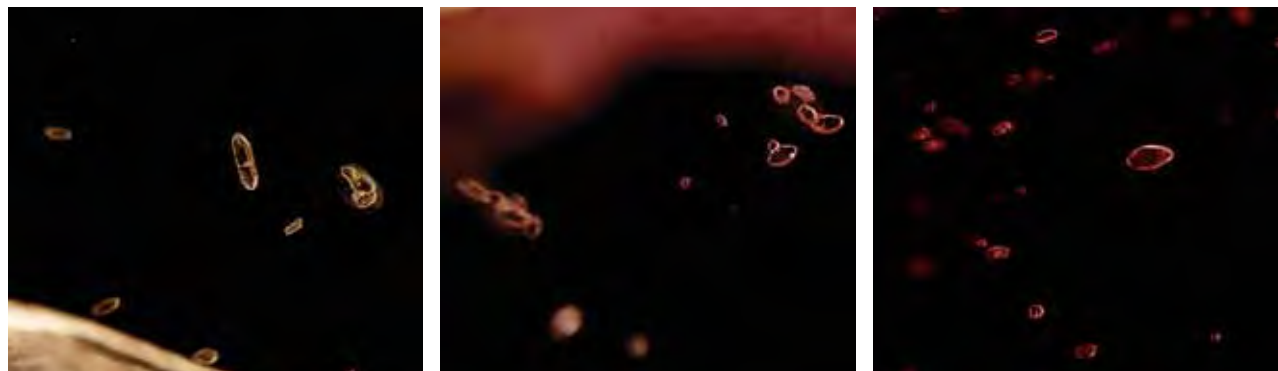


Figure 9. At or below 1500°C, the morphology of the zircon inclusions did not change noticeably (left, 1400°C [sample no. 75967]; center 1450°C [no. 65459]; right 1500°C [no. 65460]). However, in some zircons, portions of the interface between the inclusion and the host became slightly turbid or frosted, as did some fractures around the inclusions. Photomicrographs by W. Wang; magnified 100×.

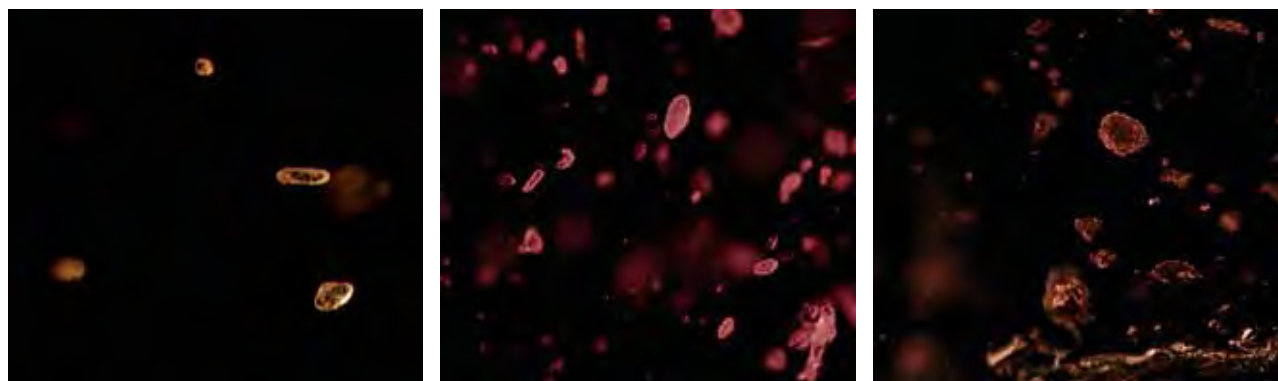
vibrational direction of the incident laser beam, the ν_1 and ν_3 peaks almost disappeared entirely. The strongest intensities of ν_1 and ν_3 were observed when the c-axis was 45° to the vibrational direction. The three major peaks showed very limited positional variations when measured at different orientations (ν_1 : 974.4–975.0 cm^{-1} ; ν_2 : 438.7–438.9 cm^{-1} ; ν_3 : 1007.8–1008.1 cm^{-1}). These values are similar to those from synthetic end-member zircon (again, see figure 7).

In contrast, of the 23 zircon inclusions in 12 unheated sapphires that were measured, only two fell within the positional ranges observed in the free-standing zircon samples. All the other inclusions yielded peaks that were shifted to much higher positions (e.g., ν_3 : 1014–1021 cm^{-1} ; again, see figure 8). The largest shift from ideal position was nearly 13 cm^{-1} . Similar peak shifting occurred for other peaks (ν_1 , ν_2 , and another major peak at ~360 cm^{-1}), and a clear positive correlation was observed among the

peaks (e.g., ν_1 vs. ν_3 in figure 8). Multiple inclusions within the same sapphire also showed large variations in peak position. For example, in sample no. 75975, ν_3 of one zircon occurred at 1008.1 cm^{-1} , but two other inclusions had positions ranging from 1015.6 to 1017.7 cm^{-1} . Similar large variations for the position of ν_3 were observed in sample no. 76732 (1009.3 cm^{-1} and 1014.8–1015.1 cm^{-1}). Five zircon inclusions were analyzed in sample no. 76726, but the position of ν_3 showed only a very limited range of variation (1014.4–1016.5 cm^{-1}).

Heated Samples. Visual Observation. Color changes were observed in these sapphires after heat treatment, with a deeper pink color in some stones and lighter pink in others. As noted earlier, we did not track systematic variations in color with temperature. The zircon inclusions displayed distinct changes in crystal morphology after heating to suffi-

Figure 10. As the temperature was increased to 1550°C (left [sample no. 65462]), the frosted/turbid regions became larger and more noticeable. At 1600°C (center [no. 56017]), the surfaces of nearly all the zircon inclusions became noticeably frosted, and only a few transparent regions remained. At 1680°C (right [no. 56018]), the zircon crystals lost their original outlines, resulting in irregular shapes. Photomicrographs by W. Wang; magnified 100×.



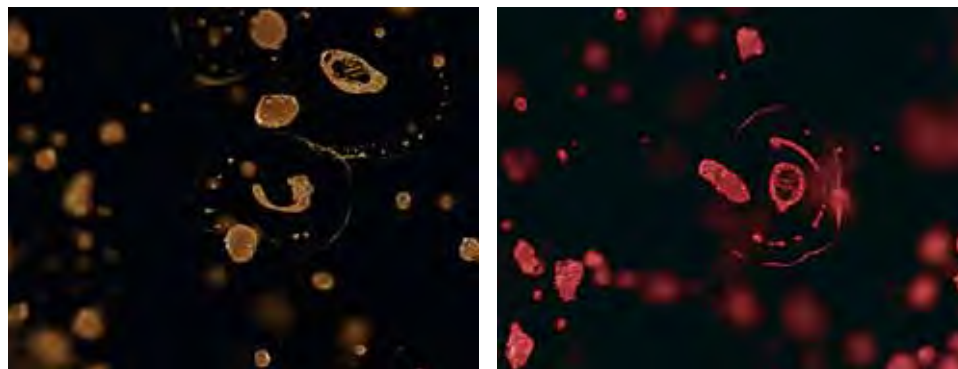


Figure 11. Melting and formation of discoid fractures began around 1730°C (left, heated for 12 hours [sample no. 75973]) and intensified as the temperature increased (right, 1780°C, 5 hours [no. 56022]). Photomicrographs by W. Wang; magnified 100×.

cient temperatures. Below 1550°C, the euhedral morphology generally remained unchanged (figure 9). Crystal faces and edges were clearly observable, and the only detectable variation occurred at the interface between the zircon inclusions and the host sapphire. At temperatures as low as 1400°C, portions of the interface between some zircons and the host sapphire became slightly turbid or frosted, though most of the body of the zircons remained clear and transparent. Some radiating fractures around inclusions also became frosted. Other zircon inclusions in the same sample, particularly smaller ones, showed virtually no visible changes. Heating at 1450°C and 1500°C did not intensify the degree of frosting of the inclusion boundaries, and many inclusions (close to two-thirds) remained as pristine as those in unheated sapphires.

When the temperature was increased to 1550°C, however, most of the zircon inclusions were noticeably affected, with the greater part of their surfaces frosted or turbid looking (figure 10, left). After heating at 1600°C, the zircon inclusions displayed even more distinct morphological variations (figure 10, center). While the overall outline remained fundamentally unchanged, the crystal faces and distinct interface with the host sapphire almost entirely disappeared. Most notably, the sur-

faces of nearly all the inclusions were strongly mottled and frosted. In only a few (~5%), did we observe isolated regions that were transparent and pristine-looking after heating at this temperature. When heated at 1680°C and above, the shapes of the inclusions became irregular, losing their euhedral outlines (figure 10, right). Development of melt aureoles, drip-like trails, and discoid fractures began at ~1730°C and intensified notably with increasing temperature up to the maximum of 1850°C (figures 11 and 12). These melt-filled fractures showed basically the same orientation within the sapphire host and were nearly parallel to each other. Dendritic quenched crystals of baddeleyite (see next two sections for phase identification) were rare (~5%) after heating at 1680°C but common (>50%) at 1730°C and above.

SEM-EDS Analysis. This is a powerful technique for detecting phase changes and their reaction products. Changes in some zircon inclusions occurred at temperatures as low as 1400°C. Subsolidus decomposition reactions (a chemical reaction in which one solid phase turns into two or more separate solid phases without any melting) dominated below 1550°C. At these temperatures, the reaction was usually limited to the outermost rims of the zircon inclusions and

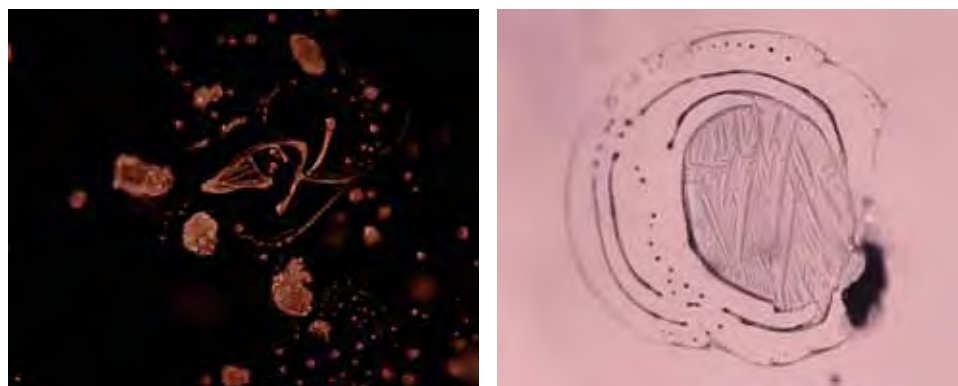


Figure 12. At 1850°C, melt aureoles, drip-like trails, and discoid fractures were common. The variation in color in these inclusions is caused by the different colors of the host sapphires. Photomicrographs by W. Wang; magnified 100× (left [sample no. 56024]) and 55× (right [no. 56025]).

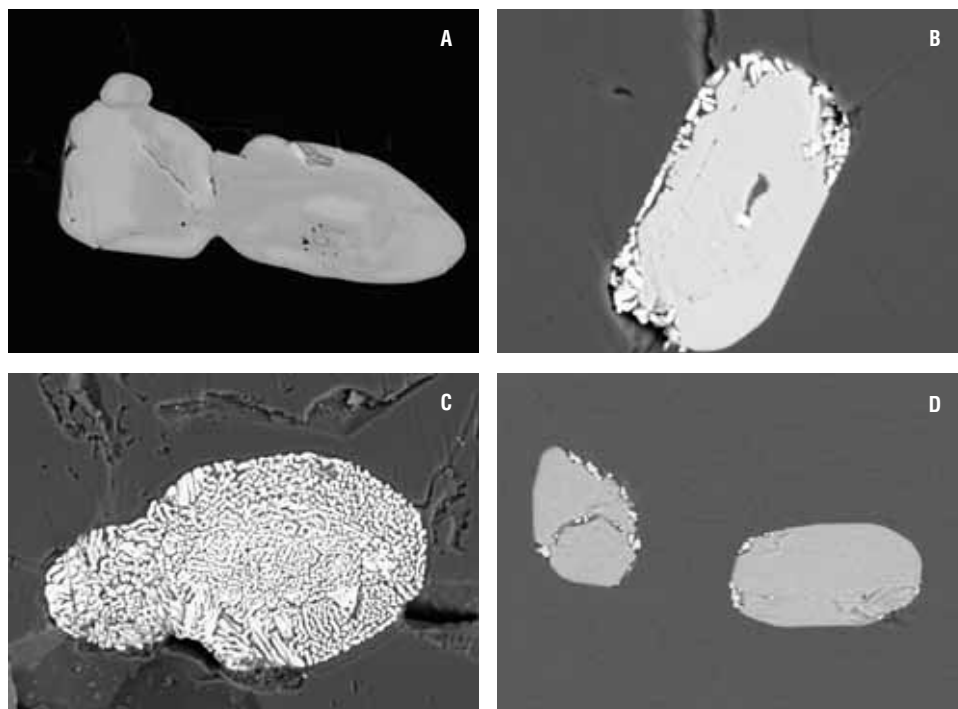


Figure 13. From 1400°C (A, B, C) to 1450°C (D), subsolidus decomposition reactions mainly occurred at the rims of some zircon inclusions, as seen in these back-scattered electron images. The very bright areas are euhedral grains of baddeleyite (ZrO_2), which are surrounded by a dark, irregular SiO_2 -rich phase containing up to 3 wt.% HfO_2 . One zircon inclusion decomposed entirely (C). BSE image widths 180 μm (A); 80 μm (B); 160 μm (C); 140 μm (D).

involved the formation of two phases with extremely high contrast in the BSE images (figure 13). One inclusion showed no detectable reaction; in addition, it displayed clear growth zonation caused by variations of HfO_2 content in different regions (figure 13A). However, another inclusion in this sample was altered entirely, with no zircon surviving (figure 13C). Instead, very bright euhedral grains of baddeleyite (ZrO_2) were surrounded by a dark, irregular SiO_2 -rich phase (refer to the Raman spectroscopy subsection below for phase identification and table 2 for chemical composition). The baddeleyite developed as small elongated euhedral crystals up to several micrometers in size. In contrast, the SiO_2 -rich phase occurred as an interstitial material phase among baddeleyite crystals. The baddeleyite contained up to 3 wt.% HfO_2 . Because of the very small grain sizes and strong

overlap with surrounding minerals, we could not accurately determine the chemistry of the SiO_2 -rich phase. Most of the interiors of individual zircon crystals remained unchanged. In general, the overall euhedral crystal outline of the inclusions was not disturbed. In a few cases, the reactions occurred internally but were limited in area.

The progression of these subsolidus decomposition reactions between 1400°C and 1550°C varied between samples and even between inclusions in the same sapphire. In sample nos. 75966 and 65458, which were heated to 1400°C and 1450°C, respectively, decomposition reactions were observed among a few isolated inclusions. Other zircons in the same sapphires showed no reaction at all (no. 75966), while one zircon inclusion in sample no. 75967 (heated to 1400°C) decomposed entirely (fig-

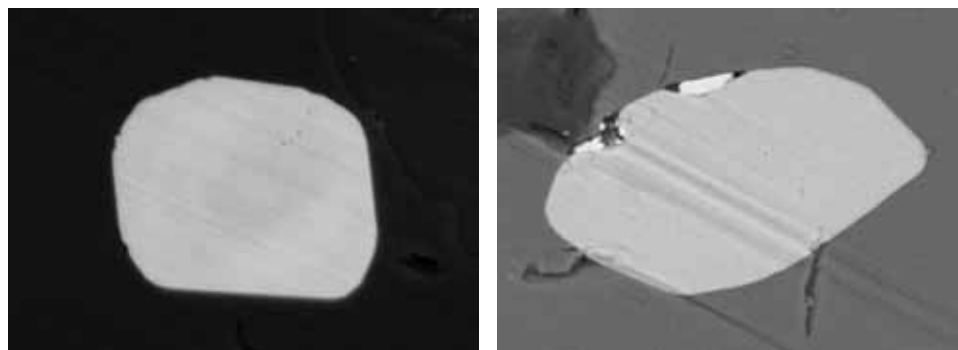


Figure 14. Some zircon inclusions heated to 1500–1550°C showed no observable changes (1500°C, left). Subsolidus reactions similar to those observed at 1400–1450°C (figure 13) were observed after heating at 1550°C (right). BSE image widths 20 μm .

Figure 15. When the zircon inclusions were heated to 1600°C, both subsolidus decomposition (left) and melting reactions (right) were observed. Heating for longer periods (25 hours, right) caused the formation of larger baddeleyite crystals, the brighter grains (compare to 5 hours, left). BSE image widths about 150 μm.



ure 13C). In contrast, none of the inclusions in sample nos. 65459 and 65461, which were heated to 1450°C and 1500°C, respectively, showed any observable changes (e.g., figure 14, left). A similar reaction to that occurring at 1400°C–1450°C was observed in one zircon inclusion after heating to 1550°C (no. 65463, figure 14, right).

After heating to 1600°C, both subsolidus decomposition and melting reactions were observed (figure 15). Sample no. 75968, which was heated for 25 hours, exhibited limited decomposition reactions along the rim of a zircon crystal, but the baddeleyite crystals that formed were larger (about 10 μm) than those seen after heating at lower temperatures and for shorter duration (2–3 μm; figure 15, left). Nevertheless, the euhedral morphology and outline of the original zircon were mostly preserved. Partial melting of a zircon inclusion occurred in sample no. 75969, which was also heated to 1600°C (figure 15, right). The melted inclusions consisted of baddeleyite crystals and Al₂O₃- and SiO₂-rich quenched melt. The original euhedral crystal outlines were indistinct.

Above 1680°C, partial melting occurred in nearly all the zircon inclusions (figure 16). In addition, the baddeleyite crystals within the Al₂O₃- and SiO₂-rich quenched glass matrix crystallized in a dendritic structure that was very different from the individual baddeleyite crystals that formed at lower temperatures. Reactions between the zircon inclusions and the host sapphire were intensified at temperatures at or above 1730°C, and the outlines of the original inclusions became difficult to discern (figure 17). Up to 5 wt.% HfO₂ was detected in baddeleyite in these melted inclusions. The melt (i.e., the quenched glass) was mainly composed of Al₂O₃ and SiO₂ with some ZrO₂ (up to 17 wt.%). The concentrations of Al₂O₃ and SiO₂ varied dramatically between different analysis locations. Average compositions of the melts are listed in table 2. Significant amounts of Na₂O, MgO, CaO, TiO₂, and/or K₂O were also detected in the melted portions of a few inclusions.

Infrared Absorption Spectroscopy. No absorption from either the zircon or the decomposition reaction products was detected by FTIR analysis after heating at any temperature. In addition, after heating in an oxidizing environment at high temperatures, most of the sapphire samples showed very little evidence of hydrogen. Of the 22 heated sapphires analyzed with FTIR, trace hydrogen was detected in only six. The intensity of the hydrogen absorption coefficient at 3309 cm⁻¹ varied from 0 to 0.040 cm⁻¹ (again, see figure 6). A very weak absorption at 3309 cm⁻¹ was detected in sample no. 56017 after heating at 1600°C for 5 hours, but in a similar sample (no. 75968) heated at the same temperature for 25 hours, no hydrogen-related absorption was present. Notably, our heating experiments in oxidizing conditions did not result in the complete removal of structurally bonded hydrous components.

Raman Spectroscopy. In each of the heated samples, two to four inclusions were randomly selected for analysis. For sapphires heated at 1400°C and 1450°C,

Figure 16. When heated above 1680°C, nearly all the zircon inclusions showed some degree of melting, in addition to subsolidus reactions. In this inclusion, the quenched baddeleyite had a dendritic structure. BSE image width 85 μm.



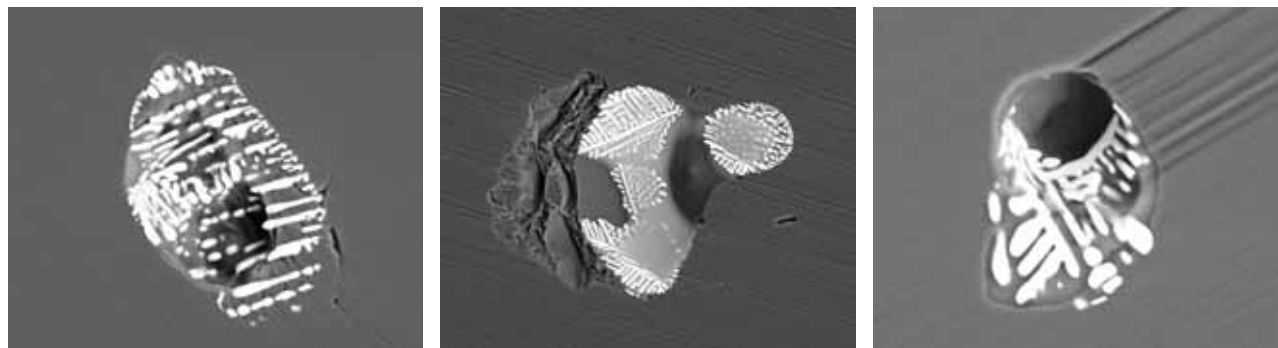


Figure 17. For temperatures at or above 1730°C, the outlines of the original zircon inclusions were diffused, and reactions between the inclusions and the host sapphire intensified (1730°C, left; 1780°C, center; 1850°C, right). Tiny dendritic-like quenched crystals of baddeleyite also formed, and the melt often penetrated into surrounding discoid fractures. BSE image widths 130 μm (left); 250 μm (center); 80 μm (right).

the inclusions displayed only the characteristic zircon Raman peaks, and no obvious differences from unheated zircon inclusions were observed. In samples heated to 1500°C and above, variations in Raman spectra were apparent. In the four inclusions analyzed in sample no. 65461 (1500°C for 5 hours), two inclusions showed at least seven additional emission peaks in the scattering region of 1300–1050 cm^{-1} , in addition to the dominant peaks from zircon when excited with a 514.5 nm laser (figure 18, top spectrum).

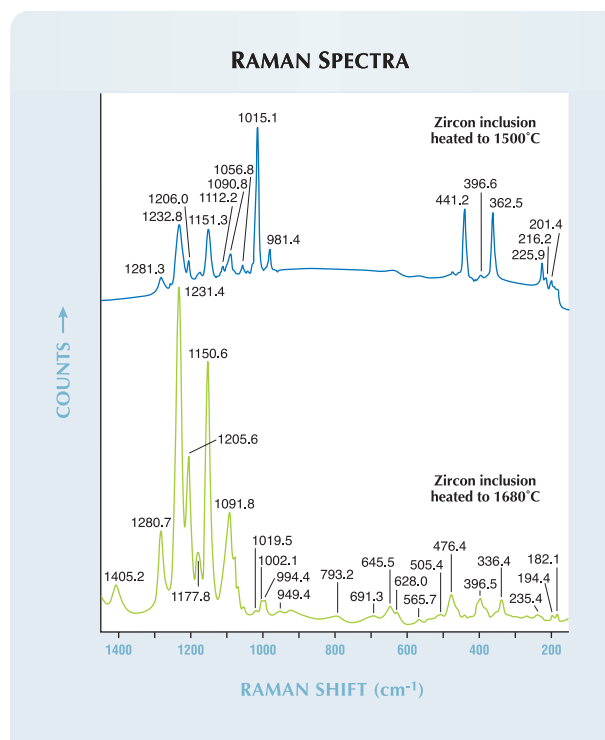
The characteristic zircon Raman peaks from most heated inclusions were shifted to higher wavenumbers ($\nu_3 = 1012\text{--}1021 \text{ cm}^{-1}$) compared to those observed for the natural free-standing single zircons, as was the case with the zircon inclusions in unheated sapphires. Raman peaks from zircon were the dominant features until melting occurred at $\sim 1600^\circ\text{C}$. However, the FWHMs of the Raman peaks in the heated inclusions were significantly lower than those measured in the unheated zircon inclusions. For example, the average ν_3 FWHM for zircons that remained intact after heating was 8.7 cm^{-1} (1400°C), 8.5 cm^{-1} (1450°C), 8.4 cm^{-1} (1500°C), 7.9 cm^{-1} (1550°C), and 8.5 cm^{-1} (1600°C). In contrast, the average ν_3 FWHM for unheated zircon inclusions was 11.5 cm^{-1} .

The seven additional Raman peaks observed at 1500°C in sample no. 65461 were present in all inclusions heated at 1600°C and above. A secondary laser with 488 nm excitation confirmed that these peaks were due to luminescence and not the Raman effect.

The zircon-specific Raman peaks disappeared entirely from inclusions that were heated above 1680°C, and were replaced by several weak Raman peaks below 1050 cm^{-1} (figure 18, bottom spectrum). Of the more than 15 peaks that were recorded (not all of which are apparent in figure 18), several (645.5, 476.4, 396.5, and 336.4 cm^{-1} , and a characteristic

doublet at 182.1 cm^{-1} and 194.4 cm^{-1}) were consistent with the Raman spectrum for baddeleyite (Stefanc et al., 1999; Fredericci and Morelli, 2000; McKeown et al., 2000), confirming its presence in the heated inclusions.

Figure 18. At least seven additional emission peaks in the 1300–1050 cm^{-1} scattering region due to luminescence were recorded for inclusions in a sample heated to 1500°C when 514.5 nm laser excitation was used (top). Most of these luminescence peaks were much stronger when the sample was heated at 1680°C or above. At wavenumbers less than 1020 cm^{-1} , there is a relatively weak spectrum for baddeleyite.



DISCUSSION

Raman Spectroscopy of Unheated Zircon Inclusions and Metamictization. Details of the Raman spectrum of zircon have been well known since the 1970s. The three main peaks at 1008, 974, and 439 cm^{-1} are related to internal SiO_4 vibration modes. It is generally agreed that the three other peaks at 225, 214, and 202 cm^{-1} are lattice vibrational modes involving interactions between SiO_4 tetrahedra and Zr atoms (Griffith, 1969; Syme et al., 1977).

As shown in figure 8, the Raman spectra from the zircon inclusions in unheated Madagascar sapphires were quite variable, particularly in the positions of the peaks. Shifting of peak ν_3 was as high as 13 cm^{-1} . The positions and relative intensities of Raman peaks are affected by many factors, including chemical composition, pressure, temperature, and crystallographic orientation. Analysis of the purple zircon crystal in multiple directions using 514.5 nm laser excitation demonstrated that relative peak intensity varied greatly with sample orientation. When the c-axis was parallel to the vibrational direction of the incident laser beam, the peaks ν_1 and ν_3 became very weak relative to other orientations, or they disappeared entirely. However, the peak positions showed virtually no change when the sample was in different orientations, as the largest shift was $<0.5 \text{ cm}^{-1}$. These observations indicate that differences in crystal orientation most likely were not responsible for the shifting of Raman peaks observed in zircon inclusions from Madagascar sapphires.

We also considered whether these large peak shifts could be explained by HfO_2 substitution, since HfO_2 is a common minor oxide in zircon inclusions in Madagascar sapphires. In a careful study of Raman peak positions in synthetic end-member zircon (ZrSiO_4) and hafnon (HfSiO_4), Nicola and Rutt (1974) found that both had very similar Raman spectra, but the ν_3 peak position in hafnon was about 10 cm^{-1} higher than that of zircon, and the ν_1 and ν_2 peaks were also shifted to higher positions (9–10 cm^{-1}). In contrast, the 356 cm^{-1} peak in zircon (ZrSiO_4) occurred at 350 cm^{-1} in hafnon (HfSiO_4). Based on previous research (Hoskin et al., 1996), 3–5 wt.% HfO_2 in zircon is insufficient to cause the observed peak shift.

Thus, we do not believe that the large peak shifts that we observed (6–13 cm^{-1} ; again, see figure 8) can be explained by either HfO_2 substitution or crystal orientation. Instead, the most likely scenario is that the zircon inclusions in Madagascar sapphires are

confined under relatively high pressures. It has been well documented that Raman peaks for many minerals shift to higher wavenumbers with increasing pressure. The relationship between pressure and peak position is nearly linear, as observed from mineral inclusions in natural diamonds (see, e.g., Liu et al., 1990; Izraeli et al., 1999; Sobolev et al., 2000). When a zircon crystal is originally trapped within a newly formed sapphire at moderate temperatures (250°C–1400°C; G. Rossman, pers. comm., 2003), its volume is the same as the space it occupies in the host sapphire. However, the coefficient of thermal expansion of zircon ($3.2\text{--}5.4 \times 10^{-6}/^\circ\text{C}$; Bayer, 1972) is lower than that of corundum ($7.6 \times 10^{-6}/^\circ\text{C}$; White and Roberta, 1983). Consequently, when the sapphire is brought to the earth's surface, where temperature and pressure are lower, differential expansion occurs between the inclusion and its host. The volume of the host sapphire and the original space the inclusion occupied decreases more than that of the zircon inclusion itself, placing the zircon under pressure and creating stress in the host sapphire surrounding the inclusion. Where the stress exceeds the tensile strength of sapphire, fractures develop (again, see figure 4). Similar features are common in natural diamonds with mineral inclusions. Knittle and Williams (1993) studied the Raman peak shifting of zircon under pressure at room temperature and found that the four major peaks (ν_1 , ν_2 , ν_3 , 357 cm^{-1}) shifted positively and linearly. Based on their experimental results, the largest shift of the ν_3 peak in our data (13 cm^{-1}) corresponds to 27 kbar of pressure. Similar pressures were calculated from the shifting of other peaks.

Natural zircons also usually contain measurable amounts of radioactive trace elements. Radioactive decay of Th and U can damage zircon's crystal lattice, a process referred to as *metamictization*, which causes expansion of the zircon; this expansion can create internal stress (e.g., Guo et al., 1996; Hughes, 1997). Radiation damage also causes the Raman peaks of zircon to become less intense, broader, and to shift to lower wavenumber positions (Nasdala et al., 1995, 2003).

Raman peaks of pristine, unheated zircons in Madagascar sapphires were mostly strong and sharp, overlying a nearly flat background and shifted to higher wavenumbers (figures 7 and 8) than in free-standing and synthetic zircons. The observed shift to higher wavenumbers likely is a reconciliation of the compressive and tensile stresses caused by the competing mechanisms of thermal expansion and metamictiza-

tion. Even so, distinct radiation-related features were observed in these spectra. Crystalline zircon is a much better Raman scatterer than metamict zircon. As a result, the Raman spectra of metamict zircons are still dominated by peaks of crystalline zircon even with relatively high levels of radiation damage (Nasdala et al., 2003). Nasdala et al. (1995) found that the FWHM of the ν_3 peak was a very good indicator for metamictization in zircon. In a well-crystallized zircon, the ν_3 FWHM is less than 5 cm^{-1} . Partially metamict zircons commonly show FWHM values of more than 10 cm^{-1} , and highly metamict, X-ray amorphous samples have values $\geq 30 \text{ cm}^{-1}$.

The FWHM values of ν_3 from unheated zircon inclusions in this study were in the range $10.1\text{--}13.5 \text{ cm}^{-1}$, with an average of 11.5 cm^{-1} . These relatively high values strongly indicate that the zircon inclusions in the unheated samples were partially metamict. This conclusion is supported by the significant decrease of ν_3 FWHM after heating experiments. Average FWHM values for sapphires heated to 1400°C were 8.7 cm^{-1} , 8.5 cm^{-1} at 1450°C , 8.4 cm^{-1} at 1500°C , 7.9 cm^{-1} at 1550°C , and 8.5 cm^{-1} at 1600°C . We interpret this observed decrease to gradual recovery and repair of the radiation-damaged crystal structure through annealing at high temperatures.

All of these observations indicate that the zircon inclusions in the Madagascar sapphires were metamict to some extent. Radiation damage and differential thermal expansion during transport of the sapphires to the earth's surface most likely generated the radial cracks surrounding the zircons. However, differences in the radioactive trace-element composition of individual inclusions would result in varying degrees of metamictization. Thus, significant variations in internal stresses for different inclusions in the same sapphire would be anticipated. Indeed, large variations in ν_3 positions between sample nos. 75975 (ν_3 positions for three zircon inclusions = 1017.7 , 1015.6 , and 1008.1 cm^{-1}) and 76732 (ν_3 = 1015.1 , 1014.8 , and 1009.3 cm^{-1}) are probably the result of some combination of metamictization and differential thermal expansion.

Reactions of Zircon Inclusions at High Temperatures. Zircon inclusions experience a number of reactions and changes as they are exposed to increasing temperature (figure 19). Our microscopic observations, SEM-EDS chemical analyses, and Raman spectroscopy revealed that decomposition of zircon

inclusions began at temperatures as low as 1400°C by the reaction: $\text{ZrSiO}_4 \text{ (solid)} \rightarrow \text{ZrO}_2 \text{ (solid)} + \text{SiO}_2 \text{ (solid)}$. This subsolidus reaction involved no melting up to 1550°C . It is evident that the decomposition reaction was mostly limited to the rims of some zircon inclusions and did not occur for all of them. In rare cases, this reaction could occur throughout a whole inclusion, and no zircon survived in these inclusions. The reaction occurred exclusively in the zircon crystals, and the host sapphire was not involved. As a result, the overall morphology of the inclusions remained basically unchanged. However, the formation of tiny baddeleyite crystals and SiO_2 -rich phases along the rims of some of the zircons significantly changed their reflective optical properties, giving the interfaces between the inclusions and host sapphire a frosty appearance (figures 9 and 10, left).

Both subsolidus and melting reactions were observed after heating at 1600°C . Decomposition reactions at this temperature (e.g., figure 15, left) were similar to those occurring at lower temperatures, except for the better crystallization of baddeleyite due to the higher temperature and longer periods of heating up to reach the target temperature. However, melting of zircon inclusions was observed in a few samples heated under these conditions (e.g., figure 15, right) following the reaction: $\text{ZrSiO}_4 \text{ (solid)} + \text{Al}_2\text{O}_3 \text{ (solid)} \rightarrow \text{ZrO}_2 \text{ (solid)} + \text{melt (liquid)}$. Above 1680°C , all the zircon inclusions showed evidence of melting. High concentrations of Al_2O_3 in the melt (again, see table 2) provided ample evidence that the host sapphire was involved in the reaction at the highest temperatures. Melting of both the zircon inclusion and dissolution of the surrounding sapphire destroyed the original euhedral outline of these inclusions, producing irregular shapes. Widespread formation of tiny dendritic quenched crystals of baddeleyite caused the inclusion surfaces to appear severely mottled and frosted. Rapid volume expansion of the inclusions during melting generated high internal stresses, and caused the formation of discoid fractures in the surrounding sapphire. Zircon inclusions heated to these high temperatures may be identified by the presence of melt penetrating into the discoid fractures (again, see figures 11 and 12).

Through subsolidus and melting reactions due to heating at various temperatures, new phases are introduced into the original zircon-corundum system. Just as the IR absorption spectra of sapphires with zircon inclusions before heating experiments

EFFECT OF TEMPERATURE ON ZIRCON INCLUSIONS IN MADAGASCAR SAPPHIRE

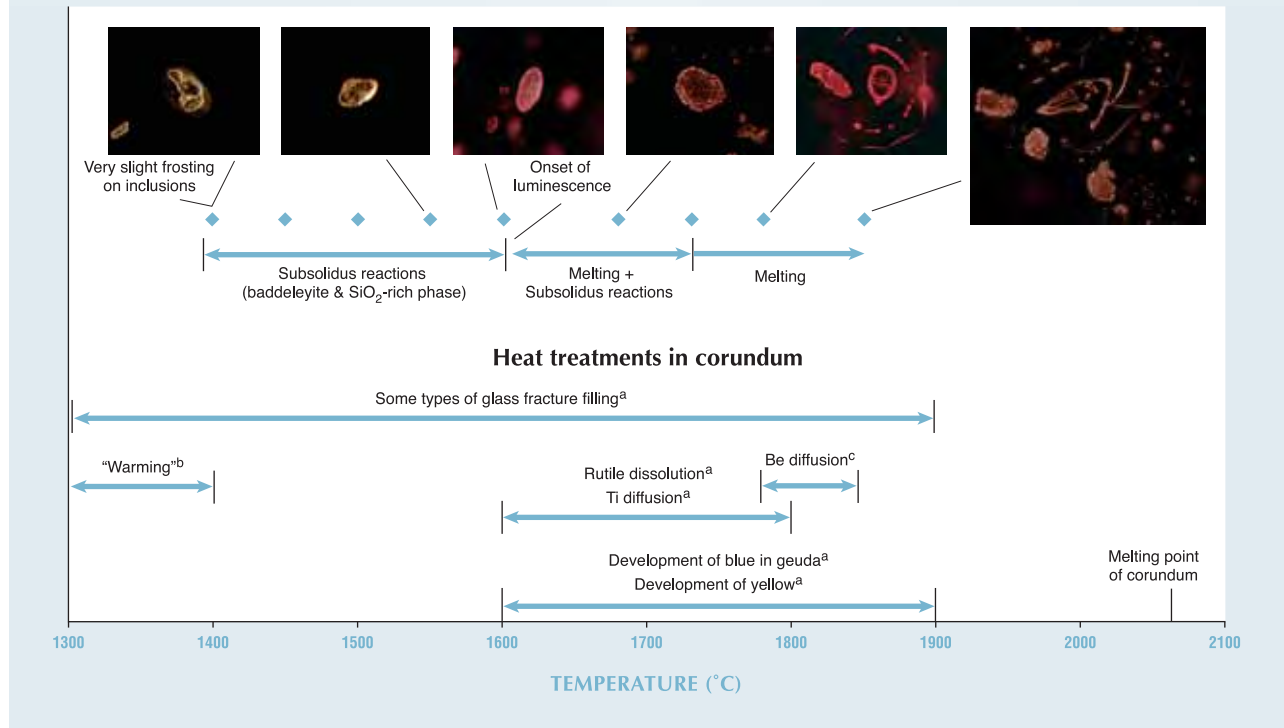


Figure 19. The morphology of zircon inclusions in the sapphires changed systematically as a function of heating temperature. Also shown are the general temperature ranges of common heat treatments. (References: ^aHughes, 1997; ^bMcClure et al., 2006; ^cEmmett et al., 2003.) Photomicrographs by W. Wang.

showed no zircon-related absorption, the IR absorption spectra of the heated samples did not show any features that could be attributed to reaction products. The main reason is that corundum has a strong absorption in the region below 1600 cm^{-1} , which masks any possible absorption in this region from reaction products. In addition, both the inclusions and the reaction products have a very limited volume compared to that of the host corundum, so the absorptions would be too weak to be detected even if they occurred above 1600 cm^{-1} . These observations indicate that IR absorption spectroscopy is not very sensitive in detecting the presence of minor amounts of zircon inclusions in corundum or its decomposition products after heating.

Lowered Melting Point of Zircon. Well-crystallized zircon is known to be stable up to 1690°C at ambient pressure (Nasdala et al., 2003). Above this temperature, it decomposes into the constituent oxides ZrO_2 and SiO_2 . Zircon inclusions in sapphire form a simple $\text{ZrSiO}_4\text{-Al}_2\text{O}_3$ system, the lowest melting temperature of which should be 1700°C–1800°C

(Budnikov and Litvakovskĭ, 1956). For the zircon inclusions in this study, both subsolidus and melting reactions started at much lower temperatures. The main possible causes for this discrepancy are radiation-related metamictization and the coexistence of other minerals mentioned below.

Internal structural damage from radiation could also affect the thermodynamic stability of zircon when heated. In an annealing study of radiation-damaged zircons (Zhang et al., 2000), it was found that heavily damaged samples tend to decompose into ZrO_2 and SiO_2 at high temperatures. In that study, tetragonal ZrO_2 was observed after annealing between 852°C and ~1327°C, while monoclinic ZrO_2 (baddeleyite) appeared above 1327°C. Such a decomposition temperature range is much lower than that for well-crystallized zircon. Zhang et al. (2000) also pointed out that ZrO_2 and SiO_2 from the decomposition could recrystallize to form new zircon around 1230°C.

All of these factors indicate that the final decomposition products of a zircon after heating would depend on the intensity of radiation damage, the annealing temperature, and the duration of heating.

This could explain the large variations in subsolidus decomposition for inclusions in individual sapphires, as well as the zircon decomposition observed at temperatures as low as 1400°C. There are two possible explanations for the pristine appearance of some zircon inclusions after the heating experiments: Either no decomposition occurred because they had experienced minimal radiation damage, or subsequent recrystallization occurred after decomposition. As seen in the Raman spectra, a few zircon inclusions showed the same peak positions as those of synthetic end-member zircon (figure 8), indicating that decomposition may not occur in all inclusions.

Although metamictization causes a dramatic decrease in the temperature at which subsolidus decomposition reactions begin, it is less likely to affect the melting temperature of this system. Melting of zircon inclusions in these Madagascar sapphires was first observed at 1600°C, more than 100°C lower than has been reported for a pure $\text{ZrSiO}_4\text{-Al}_2\text{O}_3$ system (Budinikov and Litvakovskĭ, 1956). Significant concentrations of MgO, CaO, K_2O , and TiO_2 were detected in the melted parts of a few inclusions (again, see table 2). Since all the samples were polished after heating to remove contamination, the most likely explanation is that these other minerals were originally present within or adjacent to the zircon inclusions. From the chemical composition of the melt, possible minerals include calcite, dolomite, magnesite, and/or feldspar.

Decomposition of zircon inclusions has also been reported in naturally heated corundum from Australian basalts (Guo et al., 1996). Similar to the studied sapphires, both partially reacted zircons and pristine inclusions were described in the same Australian corundum crystal. Guo et al. suggested that the presence of a SiO_2 phase with zircon inclusions would significantly decrease the melting point of the system. Unfortunately, extensive micro-Raman spectroscopic analysis of the unheated zircon inclusions failed to detect any signal from coexisting minerals. This is probably due to the sampling scale (μm) of Raman analysis and the uneven distribution of the coexisting minerals. In addition, small amounts of volatiles such as water and fluorine (undetectable with the spectroscopic and chemical techniques applied here), present as inclusions within or as a rim around the zircons, may also have a marked effect on decreasing the melting temperature of the $\text{ZrSiO}_4\text{-Al}_2\text{O}_3$ system.

Luminescence in the 542–552 nm Range. The presence of zircon decomposition reaction products was also detected through luminescence features in the $1300\text{--}1050\text{ cm}^{-1}$ (542–552 nm) range in the Raman spectra. Rankin and Edwards (2003) discovered at least seven emission peaks (514.5 nm laser excitation) in the $1300\text{--}1050\text{ cm}^{-1}$ region in zircon inclusions in extensively heated corundum crystals from Chimwadzulu Hill, Malawi. These peaks were thought to be due to luminescence from zircon decomposition reaction products, leading to speculation that they might be useful for correlation to high-temperature treatment of sapphire. Our study confirmed that these peaks were luminescent. In addition, we found that these peaks first appeared in two of the four analyzed zircon inclusions at 1500°C, and they were present in all of them after heating to >1600°C. The nature and source of the luminescence is unknown, but it is clearly not related to ZrSiO_4 , because all of the zircon disappeared entirely after heating to >1680°C.

Applications for Gem Identification. Visual evidence of modification or destruction of solid inclusions in sapphire and ruby are powerful clues for determining if a stone has been heated. Experimental results from this study can be used to determine not only the possibility of heat treatment of sapphires with zircon inclusions, but also an estimate of the temperature applied (again, see figure 19). When some zircon inclusions (but not all) display limited frosted regions, well-preserved euhedral shapes, and only the characteristic zircon peaks in the Raman spectra, then the heating temperature is very likely $\leq 1450^\circ\text{C}$. With similar features seen under magnification but the occasional occurrence of luminescence peaks in the 542–552 nm region, the heating temperature might have reached 1500°C–1550°C. Heat treatment at $\sim 1600^\circ\text{C}$ might be identified by frosting of most of the zircon inclusion surfaces with the overall outline of the crystal remaining virtually unchanged; zircon features in the Raman spectra may or may not be detected when a stone has been treated at this temperature. If the zircon inclusions appear irregular and formless, but there is no evidence of melt-filled discoid fractures, the heating temperature was very likely around 1680°C. Treatment at this temperature also results in quenched dendritic crystals, a baddeleyite Raman spectrum, and strong luminescence in the 542–552 nm region. The presence of melt-filled



Figure 20. Many colors of Be-diffused sapphires (here, 0.5–2.0 ct) have been seen in the marketplace. The morphology of inclusions can supply useful information in determining if a sapphire should be tested further for the presence of Be. Photo by Elizabeth Schrader.

discoïd fractures and halos with quenched dendritic crystals indicates that the heating temperature was $>1730^{\circ}\text{C}$.

Any estimates of heating temperature must be based on careful observation of multiple zircon inclusions in a ruby or sapphire host. It is particularly important to examine multiple inclusions with samples that were possibly heated at $<1550^{\circ}\text{C}$. Below this temperature, reactions involving zircon inclusions are very limited, and not all inclusions within a single stone will display the same features.

We feel this experiment could have particular application to the identification of Be diffusion in sapphires. Usually, trace-element chemical analysis (e.g., SIMS, LIBS, or LA-ICP-MS) is required to confirm if a stone is Be diffused. However, these instruments are expensive and not always available. Since treatment of Be diffusion in many cases requires a very high temperature (around 1800°C), the appearance of the zircon inclusions could be useful in estimating the heating temperature, assessing the need for trace-element analysis, and determining the color origin of sapphires and rubies.

CONCLUSIONS

Pristine zircon inclusions in Madagascar sapphires usually exhibit a euhedral crystal form and transparent interfaces with the host sapphire; occasionally, they have small sets of surrounding fractures.

Most of the inclusions are under relatively high confining pressures due to differential thermal expansion and radiation damage related to their geologic history. Other minerals may coexist with zircon to form composite inclusions. The decomposition reaction and melting temperatures of these inclusions are apparently lower than they would be for a pure, well-crystallized $\text{ZrSiO}_4\text{-Al}_2\text{O}_3$ system. Microscopic and spectroscopic documentation of the systematic modification or destruction of zircon inclusions as a function of temperature provides a useful tool for determining whether a zircon-bearing ruby or sapphire has been heated, and for estimating the heating temperature.

Similar experimental studies are needed for other common mineral inclusions in ruby and sapphire to evaluate a wider range of heat-treatment conditions and to better constrain the temperature estimates. While these results may apply for the heat treatment of sapphires with zircon inclusions from localities other than Madagascar, a slight variation in the resulting modification or destruction of zircon inclusions is likely because metamictization significantly contributes to lowering the temperature of decomposition in these samples. Rubies and sapphires, including those from Madagascar, have historically been treated at a wide variety of temperatures: from very high, as with Be diffusion (figure 20), to lower temperatures than those examined in this study. To extend the possible usefulness of observed variations in zircon inclusions, similar heating experiments at 800°C – 1400°C are ongoing.

ABOUT THE AUTHORS

Dr. Wang (wuyi.wang@gia.edu) is a research scientist at the GIA Laboratory, New York; Mr. Scarratt is director of Research at GIA Thailand, Bangkok; Dr. Emmett is a principal of Crystal Chemistry, Brush Prairie, Washington; Dr. Breeding is a research scientist at the GIA Laboratory, Carlsbad; Mr. Douthit is a principal of Crystal Chemistry, Los Altos, California.

ACKNOWLEDGMENTS

The authors are grateful to Matthew Hall, Shane McClure, Thomas Moses, Dr. Andy Hsi-Tien Shen, Dr. James Shigley, and Christopher Smith at the GIA Laboratory, and to Richard Hughes and John Koivula at the America Gem Trade Association Gemological Testing Center, for stimulating and helpful discussions. Dr. Chi Ma and Dr. George Rossman, of the California Institute of Technology, Pasadena, kindly provided assistance with the SEM-EDS analysis. Special thanks to Dr. George Rossman for the Raman spectrum of synthetic zircon.

REFERENCES

- Bayer G. (1972) Thermal expansion of ABO_4 compounds with zircon and scheelite structures. *Journal of the Less-Common Metals*, Vol. 26, pp. 255–262.
- Beesley C.R. (1982) The alchemy of blue sapphire. *Jewelers Circular Keystone*, Vol. 153, No. 8, pp. 102–103.
- Budinikov P.P., Litvakovskĭ A.A. (1956) [title unknown]. *Doklady Akademia Nauk S.S.S.R.*, Vol. 106, p. 268.
- Cozar J.S., de Vincente-Mingarro I. (1995) Alteración de las inclusiones de zircón, apatito y vidrio en el tratamiento térmico de rubíes y zafiros. *Boletín del Instituto Gemológico Español*. Vol. 36, pp. 47–54.
- Crowningshield R. (1966) Developments and highlights at GIA's lab in New York: Unusual items encountered. *Gems & Gemology*, Vol. 12, No. 3, p. 73.
- Emmett J.L., Douthit T.R. (1993) Heat treating the sapphires of Rock Creek, Montana. *Gems & Gemology*, Vol. 29, No. 4, pp. 250–272.
- Emmett J.L., Scarratt K., McClure S.F., Moses T., Douthit T.R., Hughes R., Novak S., Shigley J.E., Wang W., Bordelon O., Kane R.E. (2003) Beryllium diffusion of ruby and sapphire. *Gems & Gemology*, Vol. 39, No. 2, pp. 84–135.
- Fredericci C., Morelli M.R. (2000) Corrosion of AZS and AZ crucibles in contact with a blast-furnace slag-based glass. *Materials Research Bulletin*, Vol. 35, pp. 2503–2514.
- Griffith W.P. (1969) Raman studies on rock-forming minerals. Part I: Orthosilicates and cyclosilicates. *Journal of Chemical Society (A)*, Vol. 1969, pp. 1372–1377.
- Gübelin E.J. (1973) *Internal World of Gemstones*. ABC Verlag, Zurich.
- Gübelin E.J., Koivula J.I. (1986) *Photoatlas of Inclusions in Gemstones*. ABC Edition, Zurich.
- Guo J.F., O'Reilly S.Y., Griffin W.L. (1996) Zircon inclusions in corundum megacrysts: I. Trace element geochemistry and clues to the origin of corundum megacrysts in alkali basalts. *Geochimica et Cosmochimica Acta*, Vol. 60, No. 13, pp. 2347–2363.
- Hoskin P.W.O., Rodgers K.A. (1996) Raman spectral shift in the isomorphous series $(Zr_{1-x}Hf_x)SiO_4$. *European Journal of Solid State Inorganic Chemistry*, Vol. 33, pp. 1111–1121.
- Hughes R.W. (1997) *Ruby & Sapphire*. RWH Publishing, Boulder, Colorado.
- Izraeli E.S., Harris J.W., Navon O. (1999) Raman barometry of diamond formation. *Earth and Planetary Science Letters*, Vol. 73, No. 3, pp. 351–360.
- Knittle E., Williams Q. (1993) High-pressure Raman spectroscopy of $ZrSiO_4$: Observation of the zircon to scheelite transition at 300K. *American Mineralogist*, Vol. 78, No. 1, pp. 245–252.
- Liu L.G., Mernagh T.P., Jaques A.L. (1990) A mineralogical Raman-spectroscopy study on eclogitic garnet inclusions in diamond from Argyle. *Contributions to Mineralogy and Petrology*, Vol. 105, No. 2, pp. 156–161.
- McKeown D.A., Muller I.S., Buechele A.C., Pegg I.L., Kendziora C.A. (2000) Structural characterization of high-zirconia borosilicate glasses using Raman spectroscopy. *Journal of Non-Crystalline Solids*, Vol. 262, pp. 126–134.
- McClure S.F., Smith C.P., Wang W., Hall M. (2006) Identification and durability of lead glass-filled rubies. *Gems & Gemology*, Vol. 42, No. 1, pp. 22–34.
- Nasdala L., Wolf D., Irmner G. (1995) The degree of metamictization in zircon: A Raman spectroscopic study. *European Journal of Mineralogy*, Vol. 7, No. 3, pp. 471–478.
- Nasdala L., Pidgeon R.T., Wolf D. (1996) Heterogeneous metamictization of zircon on a microscale. *Geochimica et Cosmochimica Acta*, Vol. 60, pp. 1091–1097.
- Nasdala L., Zhang M., Kempe U., Panczer G., Gaft M., Andrut M., Plotze M. (2003) Spectroscopic methods applied to zircon. In J.M. Hanchar and P.W.O. Hoskin, Eds., *Reviews in Mineralogy and Geochemistry*, Vol. 53, Mineralogical Society of America, Washington DC, pp. 427–467.
- Nicola J.H., Rutt H.N. (1974) A comparative study of zircon ($ZrSiO_4$) and hafnon ($HfSiO_4$) Raman spectra. *Journal of Physics C: Solid State Physics*, Vol. 7, pp. 1381–1386.
- Rankin A.H. (2002) Natural and heat-treated corundum from Chimwadzulu Hill, Malawi: Genetic significance of zircon clusters and diaspore-bearing inclusions. *Journal of Gemmology*, Vol. 28, No. 2, pp. 65–75.
- Rankin A.H., Edwards W. (2003) Some effects of extreme heat treatment on zircon inclusions in corundum. *Journal of Gemmology*, Vol. 28, No. 5, pp. 257–264.
- Roberts R.B. (1975) Absolute dilatometry using a polarization interferometer. *Journal of Physics E*, Vol. 8, pp. 600–602.
- Scarratt K. (1983) Heat treated sapphires. *Retail Jeweller*, Vol. 22, No. 543, pp. 16–17.
- Schwieger R. (1990) Diagnostic features and heat treatment of Kashmir sapphires. *Gems & Gemology*, Vol. 26, No. 4, pp. 267–280.
- Sobolev N.V., Fursenko B.A., Goryainov S.V., Shu J.F., Hemley R.J., Mao H.K., Boyd F.R. (2000) Fossilized high pressure from the earth's deep interior: The coesite-in-diamond barometer. *Proceedings of the National Academy of Sciences of the United States of America*, Vol. 97, No. 22, pp. 11875–11879.
- Stefanc I.I., Music S., Stefanic G., Gajovic A. (1999) Thermal behavior of ZrO_2 precursors obtained by sol-gel processing. *Journal of Molecular Structure*, Vol. 480–481, pp. 621–625.
- Syme R.W.G., Lockwood D.J., Kerr J. (1977) Raman spectrum of synthetic zircon ($ZrSiO_4$) and thorite ($ThSiO_4$). *Journal of Physics C: Solid State Physics*, Vol. 10, pp. 1335–1348.
- White G.K., Roberts R.B. (1983) Thermal expansion of reference materials: Tungsten and $\alpha-Al_2O_3$. *High Temperatures-High Pressures*, Vol. 15, pp. 321–328.
- Zhang M., Salje E.K.H., Capitani G.C., Leroux H., Clark A.M., Schlüter J., Ewing R.C. (2000) Annealing of α -decay damage in zircon: A Raman spectroscopic study. *Journal of Physics: Condensed Matter*, Vol. 12, pp. 3131–3148.

FACETING TRANSPARENT RHODONITE FROM BROKEN HILL, NEW SOUTH WALES, AUSTRALIA

Paul W. Millsted

Transparent rhodonite is considered one of the most difficult of all gems to facet because of its perfect cleavage and brittle, uneven fracture. This article describes a technique for successfully faceting gem rhodonite that was developed through experiments on eight crystals from the North mine at Broken Hill, New South Wales. This was accomplished through a systematic structural, crystallographic, and optical analysis and the use of a nonconventional faceting approach—the “greasy lap” technique. This method uses a mixture of petroleum jelly and diamond grit to charge a non-embedded lap, allowing the diamond grit to “roll free” during the lapping process.

Named from the Greek *rose* or *rhodos*, in allusion to its characteristic pink color (Jasche, 1819; Gaines et al., 1997), gem rhodonite commonly occurs as opaque or at best translucent material that is cut in cabochon form or as tablets (Koivula et al., 1994). Transparent, faceted gems (see, e.g., figure 1) are extremely rare and are sourced primarily from crystals found at Broken Hill, New South Wales, Australia, and Honshu, Japan (Bank et al., 1974; Gaines et al., 1997), with some facet-quality material recently reported from Minas Gerais, Brazil (Quinn and Laurs, 2004). However, the primary sulfide ore at Broken Hill has unquestionably been the richest source of gem rhodonite crystals in the world (see, e.g., figure 2; for more information on

the geology and history of rhodonite mining at Broken Hill, see Millsted et al., 2005).

Rhodonite has moderate hardness ($5\frac{1}{2}$ – $6\frac{1}{2}$), and the familiar massive (microcrystalline) ornamental material is quite tough. A large percentage of massive rhodonite is found in sedimentary geologic environments, and this likely contributes to recorded differences in its texture and properties. In contrast, transparent gem rhodonite, such as from the metamorphic Broken Hill deposit, occurs in granular textured ore. Unlike the ornamental material, the transparent variety is very brittle and has gained a reputation as one of the most difficult gems to facet (Arem, 1977).

The largest faceted rhodonite ever recorded from Broken Hill—currently on display at the Royal Ontario Museum in Toronto—weighs 10.91 ct and resembles a red spinel in color and clarity (see figure 2 in Millsted et al., 2005). Another stone, a 4.89 ct emerald cut, is part of the U.S. National Gem Collection at the Smithsonian Institution (figure 3, left; Post, 1997), while the Australian Museum recently acquired a 2.24 ct modified step cut (figure 3, right), also from Broken Hill (G. Webb, pers. comm., 2005). A 4.5 ct faceted gem rhodonite from Broken Hill was recorded by Arem (1977).

It must be recognized, however, that for every successfully cut rhodonite there have undoubtedly been numerous catastrophic failures, which has limited the economic value of the rough. It is the

See end of article for About the Author and Acknowledgments.
GEMS & GEMOLOGY, Vol. 42, No. 2, pp. 151–158.
© 2006 Gemological Institute of America



Figure 1. Rhodonite is one of the most difficult gem materials to facet. However, with proper techniques, attractive faceted stones can be created. The 0.86 ct Barion cut rhodonite shown here, which was faceted as part of this article, is mounted with a 1.0 ct yellow sapphire in a palladium–white gold alloy. Photo by Ben Klimpsch.

author's intent with this article to offer a technique for successfully faceting gem rhodonite and thereby enhancing its value to the industry.

CRYSTALLOGRAPHIC AND OPTICAL PROPERTIES

The successful fashioning of gem rhodonite requires an understanding of some basic crystallographic, optical, and structural features of the material. By way of comparison, in diamond, which has a Mohs hardness of 10, each carbon atom is linked to four neighboring C atoms in a face-centered cubic unit cell. The close three-dimensional covalent linking (which completes the outer electron shell of each atom) is very strong, and this is manifested in diamond's great hardness. Though perfect, its cleavage is quite difficult.

Rhodonite (MnSiO_3), by contrast, is characterized by chains of SiO_3 that are arranged parallel to the c-axis, but bound together very weakly. The perfect, easy, splintery cleavages and the Mohs hardness of $5\frac{1}{2}$ – $6\frac{1}{2}$ are expressions of this chain structure (Gaines et al., 1997). It is the extremely brittle nature of the cleavage planes—perfect along $\{1\bar{1}0\}$ and $\{110\}$, which are 92.5° to one other, and good along $\{001\}$ (figure 4)—and the conchoidal-to-uneven fracture that make transparent rhodonite so difficult to facet.

The highly prized intense pinkish to brownish red color of Broken Hill rhodonite incorporates three major directions of light vibration (again, see figure 4) within the crystal lattice, which are referred to as X, Y, and Z (or α , β , and γ):

X = the axis of greatest ease of vibration. Light vibrating perpendicular to X travels with maximum velocity; yellowish red pleochroic color.

Z = the axis of least ease of vibration. Light vibrating perpendicular to Z travels with minimum velocity; pale yellowish red pleochroic color.

Y = the intermediate axis, at right angles to the plane of X and Z. Light travels at a velocity between X and Z; pinkish red pleochroic color.

Figure 2. These two transparent rhodonite crystals (70.50 and 51.52 ct) are representative of the finest material found at Broken Hill. Clean, well-formed crystals such as these are considered most suitable for faceting. Courtesy of George Stacey; photo by P. Millsted.



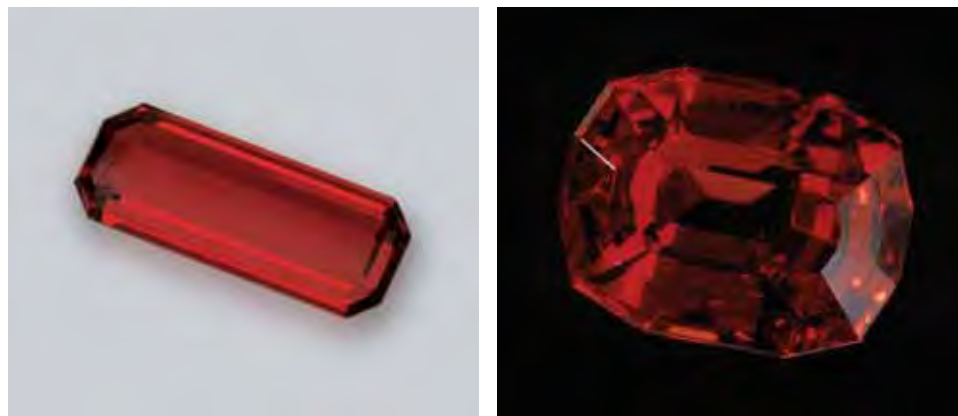


Figure 3. Though very rare, fine examples of faceted rhodonite do exist. The 4.89 ct emerald cut on the left is part of the U.S. National Gem Collection at the Smithsonian Institution in Washington D.C. The 2.24 ct modified step cut on the right is currently on display at the Australian Museum in Sydney. Photos by Chip Clark, Smithsonian Institution, left; Stuart Humphreys, Australian Museum, right.

The pleochroism in rhodonite is generally weak. The brown color component commonly seen in material from Broken Hill results from Fe impurities in the rhodonite. The optic axis angle ($2V$) for gem rhodonite from Broken Hill has been measured at 70° or 74° (Bank et al., 1973a,b); this produces a biaxial-positive optic sign. These values fall within the accepted range of 61° – 87° (Gaines et al., 1997).

While Brown and Bracewell (1993) make reference to the problems associated with the cleavage and fracture in rhodonite from Broken Hill, no systematic evaluation of its potential as a faceted stone has been elaborated to date.

MATERIALS AND METHODS

Eight transparent rhodonite crystals (1.15–5.28 ct) with minimal well-developed visible cleavage were used. All displayed a rich blend of pinkish red to yellowish brownish red. The intensity and variation of the color in each crystal was dependent on orientation (again, see figure 4). All of the rough was doped with the direction of the widest crystal face c (001) as the table orientation, taking advantage of the pinkish red absorption direction (Y). The prominent m {110} cleavage plane projected an acute plane downward from the c face, while the M {1 $\bar{1}$ 0} cleavage plane is projected at 92.5° to m {110}, as illustrated in figure 4. The crystals were initially doped with Titon epoxy, a procedure recommended for most gems. It is not advisable to use a hot-wax dopping technique on a mineral as brittle and sensitive as gem rhodonite.

The first three stones were fashioned using conventional faceting techniques, employing copper laps with embedded diamond grit and water as a lubricant. Stones 1 and 2 were cut by Robert Hunt and stone 3 by Scott Langford. When conventional faceting proved unsuccessful, the approach referred

to here as the “greasy lap” technique was adopted. This method was developed in 1985 by Ralph Westen as an alternative to conventional diamond-embedded laps, which use water as a lubricant. Generally, this method has proved successful to minimize scratching and cleaving in a variety of gem minerals (Westen, 1996).

The greasy lap technique uses as little as a match-head-sized bead of petroleum jelly mixed with diamond grit to charge a non-embedded lap. This is a stable mixture: The diamond grit does not sink or separate from the petroleum jelly as it would with a less viscous oil. It is uniformly smeared across the lap surface using light finger pressure. The fundamental attribute of the technique is the use of a “water-free” diamond paste. The success of the technique lies in its ability to reduce easy cleavage and the development of fractures, since the diamond grit “rolls free” during the lapping process.

Four stages of lapping are generally required with the greasy lap technique: (1) a preforming stage on a copper lap using 240-grit ($53.5 \mu\text{m}$) diamond, (2) a 1,200-grit ($15 \mu\text{m}$) diamond prepolishing stage using a copper lap, (3) a 3,000-grit ($6 \mu\text{m}$) diamond prepolishing stage using a copper lap, and (4) a polishing stage on type metal (a mixture of 92% lead, 5% tin, and 3% antimony) using 100,000-grit ($0.25 \mu\text{m}$) diamond. Any lap may be used in the greasy lap technique; however, with continuous use over time, the diamond grit will eventually become embedded in the lap material through crystallization of the metal component.

This technique was developed and used by Ralph Westen when he faceted stones 4 and 5. It was then adopted by Donna Naissen when she faceted stones 6, 7, and 8.

A scanning electron microscope (SEM) image was taken of stone 4 after it cleaved during faceting. The imaging was carried out at 15 kV and 1 nA.

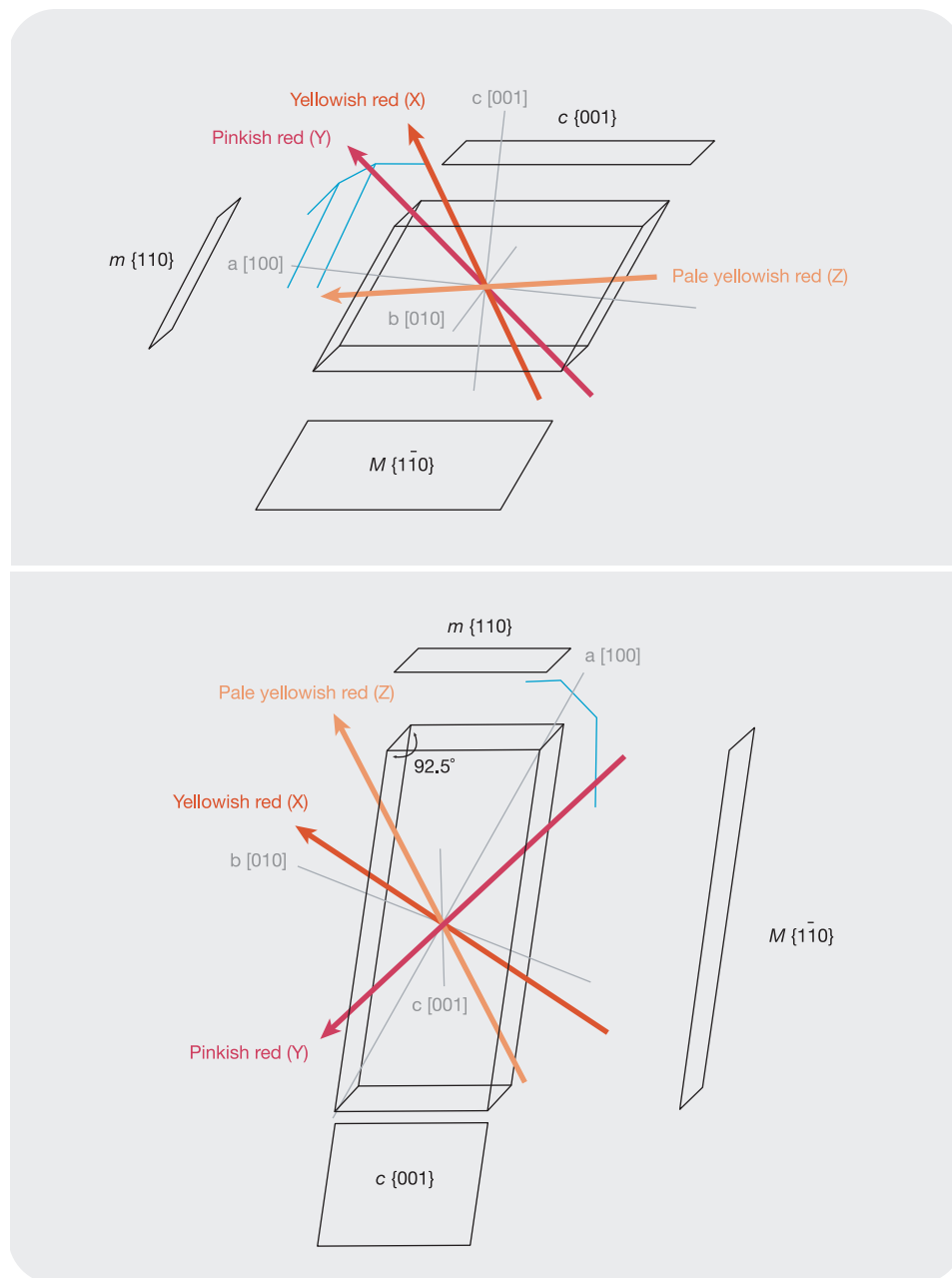


Figure 4. Crystallographic axes $a [100]$, $b [010]$, $c [001]$; light vibration directions X , Y , Z ; and cleavage planes $M \{1\bar{1}0\}$, $m \{110\}$, $c \{001\}$ of rhodonite are shown from two perspectives in these drawings (interpreted and compiled from Diehl and Berdesinski, 1970; Bank et al., 1973a, b, 1974; Gaines et al., 1997). When faceting rhodonite, the c -axis should be placed perpendicular to the table facet to take advantage of the pinkish red absorption direction. The blue lines represent the crystal faces of rhodonite and serve as a guide to dopping the stone for faceting.

RESULTS AND DISCUSSION

The crystals were initially examined through a binocular microscope and then with a 10 \times loupe until the cleavage planes $m \{110\}$ and $M \{1\bar{1}0\}$ were identified (again, see figure 4). For reasons of orientation (which relate to optimum color and stone shape), typically the longest dimension of the rough crystal should be parallel to the M cleavage plane, and the shortest dimension should be parallel to the m cleavage plane. Cleavage fragments are generally regarded as unsuitable for faceting.

As noted above, the cutting of crystal 1 was

begun by Mr. Hunt using a conventional faceting technique. After the pavilion and crown facets were almost completed, the stone suddenly cleaved in half along the M plane (figure 5). The crown was unrecoverable.

Mr. Hunt's cutting of crystal 2 appeared successful until the stone developed a major structural dislocation along a natural uneven internal fracture, as shown in figure 6. As Mr. Hunt cut the crown facets, cleaving became problematic. After several attempts, he stopped work on the stone.

The polish on both stones was good; however,



Figure 5. The first rhodonite crystal (2.50 ct) cleaved along the M plane during faceting. Note the outline of the pavilion facets, which were almost completed. The crown was unrecoverable. Photo by P. Millsted.

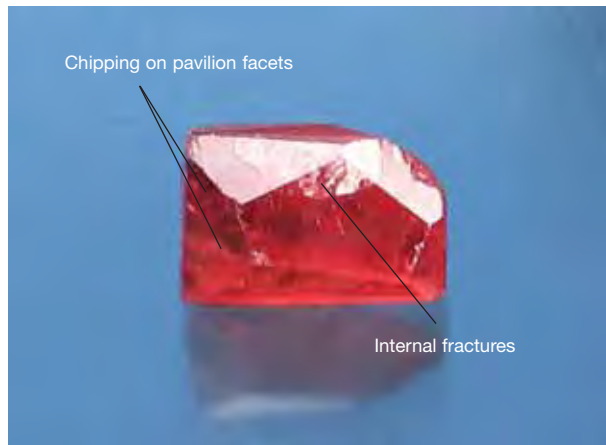


Figure 6. The stone produced from the second rhodonite crystal (3.00 ct) suffered structural splintering along internal fractures, in addition to minor chipping on the pavilion facets. Photo by P. Millsted.

none of the facets met very well due to repeated attempts to recut some of them. Severe chipping also occurred. These problems were likely due to the embedded diamonds in the conventional laps tearing at the brittle structure of the crystal, particularly the cleavage planes.

Again using conventional faceting techniques, Mr. Langford attempted to cut crystal 3. He met with relative success (figure 7, left), but significant chipping was observed on some of the pavilion facets (figure 7, right). In addition, the girdle was thicker than average (1 mm), which may have reduced further chipping, fracturing, and cleaving at the crown/pavilion interface. The final polish was good. A freeform shape was used to minimize the loss of material during the faceting process. The finished stone also contained two large inclusions, of galena and spessartine, seen at the bottom of figure 7 (left).

After this initial trial, Mr. Westen concluded that

the fundamental limitations of gem rhodonite (the brittle structure, perfect cleavage, and a profound conchoidal-to-uneven fracture) required a new approach, the greasy lap technique. Stone 4 was then cut by Mr. Westen using this method, but he ran into difficulty when he cut the facets that were approximately parallel to the *m* cleavage plane first instead of last. After he cut the 45° corners across the *m* plane, internal stresses were released along the plane, resulting in a delayed cleaving. This relationship is illustrated by the SEM image in figure 8, which shows the critical intersection point of the 45° facets, with the facet approximately parallel to the *m* cleavage plane. A view of the *m* cleavage plane intersecting the table of the faceted rhodonite is also shown, along with the faint surface intersection of the *M* cleavage plane. Although this stone suffered structural failure, the final polish and facet meet were excellent. To obtain consistent and reproducible results, it therefore appears critical that the

Figure 7. This freeform 3.96 ct rhodonite was successfully cut using conventional faceting techniques (left). However, it still suffered chipping on the pavilion facets, and the girdle was unusually thick (right). Photo by P. Millsted.



facets approximately parallel to the m cleavage plane direction be cut last.

Mr. Westen revised his technique accordingly and successfully faceted stone 5, a transparent 0.86 ct Barion cut (figure 9), a significant turning point in the study. The stone was cut with the c face as the table orientation. Subsequent to the completion of stone 5, Ms. Naissen faceted three more stones using the greasy lap technique (again, see figure 9). The largest of these was a 3.72 ct emerald cut. Although the stones were relatively clean, they did show some small eye-visible fractures and inclusions. The rich pinkish to brownish red color and dispersive characteristics of gem rhodonite were successfully displayed in all of the stones faceted. In stone 5, however, dispersion was noticeably enhanced by the style of cut. Stone 5 was subsequently mounted in a palladium–white gold alloy setting designed by jeweler Ben Klimpsch (again, see figure 1). A yellow sapphire was incorporated into the piece to compliment the yellowish red pleochroic color of the rhodonite. During the setting procedure of any stone, even diamond, there is some risk of damage; with faceted rhodonite, this risk certainly is considerable. Mr. Klimpsch mounted the stone with a modified bezel technique (using great care and minimal pressure) combined with strategically placed resin mounts.

The prerequisites and stages for the successful

faceting of gem rhodonite, using the greasy lap technique, were determined to be as follows:

The cutting angles are culet 42° , crown 40° . The pavilion must be cut first and the crown second.

The pavilion:

- The longitudinal sections parallel to cleavage plane M must be cut first.
- The 45° corner facets (across the m cleavage plane) are cut next.
- The facets that are approximately parallel to the m cleavage plane are cut last.

The crown:

- The table facet parallel to c must be cut first.
- The 45° corner facets (across the m cleavage plane) are cut next.
- The facets that are approximately parallel to the m cleavage plane are cut last.

Characteristically, for all of the cutters, the pressure applied to the lap was “normal” and without variation. Overriding the lap (applying too much pressure) is wasteful and results in undercutting (incomplete polishing of a facet).

Although the original crystals chosen were predominantly transparent, the presence of mineral

Figure 8. This SEM image of the fourth rhodonite sample (left) shows the intersection of the cleavage plane m with facets of the crown and pavilion. The stone cleaved after the 45° crown facets were cut across the m cleavage direction (indicated as the critical intersection point). On the right is an SEM view of the m cleavage intersecting the crown of the faceted rhodonite. Note also the faint surface intersection of the M cleavage. SEM images by P. Millsted.

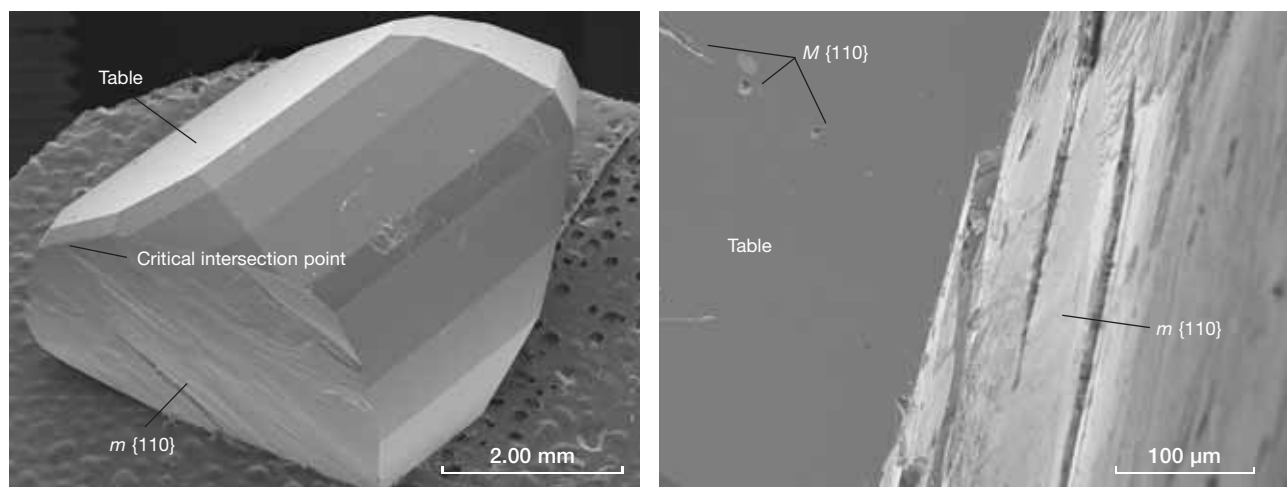




Figure 9. Despite the inherent difficulties, transparent gem rhodonite can be successfully faceted with proper techniques. Shown here are the five stones that were faceted as part of this study. Clockwise from left, the four largest rhodonites weigh 3.72, 3.96, 2.09, and 1.00 ct, respectively. The center stone (0.86 ct) was later set in the neck piece in figure 1. Photo by P. Millsted.

inclusions (Millsted et al., 2005), fractures, and cleavages is characteristic of this mineral. As is done with emerald and similar gem materials that are often heavily fractured, (see, e.g., Webster, 1995), it may be worthwhile to clarity enhance some gem rhodonites, provided that such is properly disclosed.

A recent review (Quinn and Laurs, 2004) suggested that cutting the newly discovered Brazilian gem rhodonite also poses a challenge, although the pendant illustrated in that report showed that faceted gem rhodonite could be successfully mounted and set in jewelry. However, it is still advised that this be done with considerable caution.

CONCLUSION

The results of these trials provide a means to successfully facet transparent rhodonite in a variety of sizes and styles (again, see figure 9). Current recorded weights of faceted rhodonite vary from 0.15 to 10.91 ct. The minimum requirements to successfully facet a rhodonite from Broken Hill are that the rough be transparent with little development of visible cleavage planes. In more difficult cases, a thicker girdle may be used. With the proper use of the greasy lap technique, the effect of inclusions can be minimized, although careful consideration must be given to rhodonite's structural and crystallographic properties.

ABOUT THE AUTHOR

Mr. Millsted (paulmillsted@hotmail.com) is a visiting researcher at Geoscience Australia, Canberra, Australian Capital Territory (ACT).

ACKNOWLEDGMENTS


The author thanks the following for their contributions: Ralph Westen and Donna Naissen of the Australian Faceters Guild and ACT Lapidary and Mineral Club, Canberra, for their perseverance and testing of this faceting technique; Robert Hunt of Goulburn, New South Wales, and Scott Langford of Adelaide, South Australia, for their participation in the initial experimental trials; Robert Preston, a miner at Broken Hill, for sharing knowledge on the source of the rhodonite specimens employed in this research; John Odwyer, a collector in Broken Hill, for supplying the rough crystal for the 1 ct stone; Ben Klimpsch of

J.E.K. Manufacturing Jewelers, Canberra, for the design and manufacture of the setting for the 0.86 ct Barion cut rhodonite; Arthur Main of the Gemmological Association of Australia, Canberra, for his support with the manuscript and gemological testing; Peter Blythe of the Mineshaft, Canberra, for furnishing the yellow sapphire for the setting; Mr. George Stacey, a collector in Canberra, for kindly loaning the rhodonite crystals in figure 2; Dr. Frank Brink of the SEM unit in the Research School of Biological Sciences, Australian National University, Canberra, for providing access to SEM facilities and advice on the technique; Dr. Wolf Mayer of the Department of Earth and Marine Sciences, Australian National University, Canberra, for his interpretation of the German references; and Gayle Webb of the Australian Museum, Sydney, and Jeffrey Post of the Smithsonian Institution, Washington, D.C., for providing images of their faceted rhodonites.

REFERENCES

- Arem J.E. (1977) *Color Encyclopedia of Gemstones*. Van Nostrand Reinhold Co., New York.
- Bank H., Berdesinski W., Diehl R. (1973a) Durchsichtiger Rhodonit aus Broken Hill/Australien. *Zeitschrift der Deutschen Gemmologischen Gesellschaft*, Vol. 22, No. 3, pp. 101–103.
- Bank H., Berdesinski W., Diehl R. (1973b) Durchsichtiger rötlicher Pyroxmangit aus Broken Hill/Australien und die Möglichkeiten seiner Unterscheidung von Rhodonit. *Zeitschrift der Deutschen Gemmologischen Gesellschaft*, Vol. 22, No. 3, pp. 104–110.
- Bank H., Berdesinski W., Ottermann J., Schmetzer K. (1974) Transparent red iron rich rhodonite from Australia. *Zeitschrift der Deutschen Gemmologischen Gesellschaft*, Vol. 23, No. 3, pp. 180–188.
- Brown G., Bracewell H. (1993) Rhodonite from Upper Coomera–SE Queensland. *Australian Gemmologist*, Vol. 18, No. 6, pp. 197–199.
- Diehl R., Berdesinski W. (1970) Twinning in pyroxmangite from the North mine in Broken Hill, New South Wales, Australia. *Neues Jahrbuch für Mineralogie Monatshefte*, Vol. 1970, No. 8, 348–362.
- Gaines R.V., Skinner H.C.W., Foord E.E., Mason B., Rosenzweig A., King V.T. (1997) *Dana's New Mineralogy*. John Wiley & Sons, New York, pp. 1326–1328.
- Koivula J. I., Kammerling R.C., Fritsch E., Eds. (1994) Gem News: Yukon rhodonite. *Gems & Gemology*, Vol. 30, No. 3, p. 196.
- Millsted P.W., Mernagh T.P., Otieno-Alego V., Creagh D.C. (2005) Inclusions in transparent gem rhodonite from Broken Hill, New South Wales, Australia. *Gems & Gemology*, Vol. 41, No. 3, pp. 246–254.
- Post J.E. (1997) *The National Gem Collection*. Harry N. Abrams, New York.
- Quinn E.P., Laurs B.M. (2004) Gem News International: Rhodonite of facet and cabochon quality from Brazil. *Gems & Gemology*, Vol. 40, No. 3, pp. 260–261.
- Webster R. (1995) *Gems: Their Sources, Description, and Identification*, 5th ed. Revised by P.G. Read, Butterworth-Heinemann, Oxford, U.K.
- Westen R. (1996) In the beginning. *Facet Talk*, September, p. 91.

NOW AVAILABLE!



GEMS & GEMOLOGY
IN REVIEW


COLORED DIAMONDS

The best of *Gems & Gemology* on the subject of colored diamonds
in one comprehensive research volume

This volume of *GEMS & GEMOLOGY IN REVIEW* presents a selection of articles and notes that have appeared in the journal since its inception in 1934. Some of the material is from issues long out of print. That means you won't find this information collected anywhere else but here!

- 340 pages of award-winning articles and beautiful, detailed color photography
- More than 70 years of cutting-edge research on the characterization and grading of colored diamonds
- Editorial commentary by colored diamond color-grading expert John King, technical director of the GIA Laboratory
- Insights on the past, present, and future of colored diamonds—in the marketplace and the laboratory
- The *GIA Colored Diamond Color Reference Charts* booklet explains and illustrates GIA fancy diamond color grades and descriptions for the most common diamond colors

To order your copy today
visit **GEMS & GEMOLOGY** at
www.gia.edu
or call
800-421-7250, ext. 7142
(outside the U.S.:
760-603-4000, ext. 7142)



This soft-cover 2-book set (complete with an attractive slipcase) is now available for \$59.95 (plus shipping and handling). Additional copies of the *GIA Colored Diamond Color Reference Charts* booklet can be purchased separately for \$19.95 (plus shipping and handling).

Thank You Donors

GIA appreciates gifts to its permanent collection, as well as gemstones, library materials, and other non-cash assets to be used in GIA's educational and research activities. These contributions help GIA further its public service mission while offering donors philanthropic benefits. We extend sincere thanks to all 2005 contributors.

CIRCLE OF HONOR

\$100,000 AND HIGHER, CUMULATIVE

The Aaron Group
Dr. Suman Agrawal
Almaza Jewelers
(Ziad H. Noshie)
American Pearl Company
Amsterdam Sauer
Aurafin Oro America
Banks International Gemology, Inc.
(Daniel and Bo Banks)
The Bell Group/Rio Grande
Allan Caplan
Chatham Created Gems, Inc.
(Thomas H. Chatham)
PierLuigi Dalla Rovere
The DeBeers Group
Dallas R. Hales
Dr. Gary R. and Barbara E. Hansen
J.O. Crystal Company, Inc.
(Judith Osmer)
JewelAmerica, Inc.
(Zvi and Rachel Wertheimer)
Kazanjian Bros., Inc.
KCB Natural Pearls
(K. C. Bell)
William F. and Jeanne H. Larson
Stephen Lentz
Sophie Leu
Marshall and Janella Martin
Roz & Gene Meieran
Nancy B & Company
Kurt Nassau, Ph.D.
John and Laura Ramsey
R. Ed Romack
Art Sexauer
Ambaji Shinde
S.H. Silver Company
(Stephen and Eileen Silver)
Dr. Geoffrey A. Smith
D. Swarovski & Co.
Shades of the Earth
(Laura and Wayne Thompson)
Touraine Family Trust
United States Pearl Co.
(James and Venetia Peach)
Robert H. Vanderkay
Vicenza Fair

2005 DONORS

\$50,000 to \$99,999

Debbie and Mark Ebert
Ted and Corky Grussing
Mona Lee Nesseth, G.G.

\$10,000 to \$49,999

Cos Altobelli
Dudley Blauwet
George Brooks
Teresa A. DeCrescenzo
Mr. and Mrs. Robert J. Flude, III
Fortunoff Fine Jewelry &
Silverware, Inc.
Sandra Manin Frias
The Gemesis Corporation
Gorenstein Family
Robert Grant
H. Stern Jewelers, Brazil
James Y. Hung, M.D.
Jewelmer

Korite International
Pascal Lacroix
Leslie Weinberg Designs
Dimitri K. Mantheakis
Pala International, Inc.
Michael J. Quinn, A.J.P.
Edward and Jane Rosenzweig
Muriel Roston
SAFDICO USA, INC.
Sant Enterprises Co., Ltd.
Sekikazu
Joanne Stacher, G.G.
Star Ring, Inc.
Joseph W. Tenhagen

\$5,000 to \$9,999

Thomas P. Gübelin
Chris and Karen Johnston
Terry Ledford
Tom Munsteiner
Gerald Stockton
World Sapphire

\$2,500 to \$4,999

Cecilia J. Annunziata
Armatris Fine Design
(Mary T. Armatris)
W. Ballreich
Maria Lucia Barbosa
Rose Carvalho
Maria José Cavalcanti
Linda Ching
Cathrine Clarke
Gloria Corbetta

Carmen D'Lamonica

Heinz Dreier
William Farias
Ferjenni
Syed Iftikhar Hussain
JCK Magazine
Robert E. Kane
Ketterman's Jewelers
Gail Brett Levine, G.G.
Linda Potichke Jewelry Designs
(Linda Potichke)
Robert F. Officer
Perry Jewelers
(Edward N. Perry)
Douglas Rountree
Thomas M. Schneider
Son T. Ta
Brenda Vidal
Christopher Wolfsberg
Tommy Wu
Yael Sonia

\$1,000 to \$2,499

Angeles Girl Scout Council
Antonio Bernardo Herrmann
Capalion Enterprise
Marya Dabrowski
Denoir
Bialice Duarte
Fire Mountain Gems
(Chris and Stuart Freedman)
FR Hueb
Si and Ann Frazier
Farooq Hashmi
Jewelry by Gail, Inc.
Bernardo Krengiel
Kenneth Win Kyi
Liliane Lima
Hussain Rezayee
Laurenice Singulani
Mark H. Smith
Prof. James P. Syvitski
Bia Vasconcellos
Vianna, Brazil
George A. Williams, Ph.D.

\$500 to \$999

John Bailey
Tom Cushman
G. Scott Davies
Mary Johnson and Mark Parisi
J. & S.S. DeYoung, Inc.
(Joseph H. Samuel, Jr.)
Pillar & Stone International, LLC
Murray Schulman

Julia P. Solodova, G.G.
Johann Viljoen
YAYO

Under \$500

Jeffery Lee Bergman
B.G. & J. Co., Ltd.
Jim Clanin
Fai Dee Gems Co. Ltd.
Fossheim Steinsenter
Gems TV
Aura M. Godoy, G.G.
Rainer Schultz Guttler
Christina Harrington
Nancy K. Hays
Hrand Djvahirdjian SA
Jan David Design Jewelers
Lalita R. Jaswal
K & K International
Dr. A. J. Kissin, G.G.
Hannes Kleynhans
Brendan Laurs
Little Big Stone
Kishmish Lodha
Lynn's Jewelry
Marle's Gemstone Service
Jim Marquardt
DeAnna Lynn McDaniel
Seung-Hae Moon
Raymond Naftule
National Jewellery Quality
Supervision Inspection Center of
China
Thomas W. Overton
Renato and Adriana Pagano
Dr. Jayshree Panjekar
C. D. Parsons/Dee Parsons
Jenny Peterson
J. Dennis Petimezas
Preciosa, a.s.
Radiance International
Anne Lajee Reynolds
Karen Schwab
Lea Seelig
The Shipley Family
Tibetan Sunstone Mine™
Thom S. Underwood
Unique Pawn Brokers—San Diego
Vasconcelos Minerals—Brazil
Stuart and Donna Wilensky
Richard and Joan Wilson
David E. Wright
Victor E. Zagorsky

If you are interested in making a donation and receiving tax benefit information, please contact Patricia Syvrud at (800) 421-7250, ext. 4432. From outside the U.S., call (760) 603-4432, fax (760) 603-4199. Or e-mail patricia.syvrud@gia.edu

EDITORS

Thomas M. Moses and Shane F. McClure
GIA Laboratory

CONTRIBUTING EDITORS

G. Robert Crowningshield
GIA Laboratory, East Coast
Cheryl Y. Wentzell
GIA Laboratory, West Coast

BONE Pendant

Animal bone may be one of the oldest jewelry materials in human society. Today, cow bone is most often seen, but camel bone is sometimes

Figure 1. This large pendant proved to be made from dyed yellow bovine bone. Most bone jewelry is made from cow, sheep, or camel bone, since these are durable enough to wear yet soft enough to work with primitive tools.



used in Asia. In Africa, cattle are a symbol of wealth, and thus cow bone beads and jewelry, especially large pieces, represent wealth and prosperity. Bone has also been used as a substitute for ivory. However, though the two may be similar in appearance, there are many differences.

The large pendant in figure 1 (33.90 × 15.05 × 10.25 mm) was submitted to the East Coast laboratory for identification. With magnification, it showed parallel banded structures in some areas and irregular structures in others (figure 2). This was quite distinct from the “engine-turned” appearance of polished ivory. It also showed yellow dye concentrations; it is a common practice to stain bone to make it appear older than it actually is. The patterns of these dye concentrations were apparent in the pendant’s moderate and very weak yellow

fluorescence to long- and short-wave ultraviolet (UV) radiation, respectively. The spot R.I. was 1.56 (within the typical range for organic gem materials). We could not determine the specific gravity of the pendant because of the mounting, though this would have been a good test to distinguish between bone and ivory (ivory’s S.G. is 1.7–2.0, while bone has a specific gravity of about 2.3).

The Raman spectrum of the pendant (figure 3) matched that of a bovine (e.g., cow, buffalo, or bison) bone reference spectrum, so we concluded that this pendant was fashioned from stained bovine bone, probably cow bone. (Additional spectral data for this sample are available in the *Gems & Gemology* Data Depository at www.gia.edu/gemsandgemology.)

*Paul Johnson, Kyaw Soe Moe,
and Carol Pearce*

Figure 2. With magnification, the bone pendant showed a parallel banded structure in some areas (left) and irregular structures elsewhere (right). Note the dye concentrations in some of the cracks and fissures. Magnified 40×.



DIAMOND

With Circular Brown or Green Radiation Stains

Green and brown “stains” are occasionally seen on both rough and faceted diamonds. These stains are believed to be the result of natural irradiation, with the brown color resulting when the green stains are subsequently exposed to heat. Although such stains are an important gemological feature, little is known about their physical properties. Recently, the East Coast laboratory examined two unusual natural diamonds, one with brown stains and the other with green stains (figure 4). However, unlike previously seen radiation stains, which usually show irregular outlines, all of these stains displayed nearly perfect circular shapes and each was centered on a clearly visible dark spot (figure 5).

In the first diamond, a 1.47 ct rectangular blocked stone, extensive brown stains were present in the culet region. This stone would have shown a light yellow color without these brown stains. We observed brown

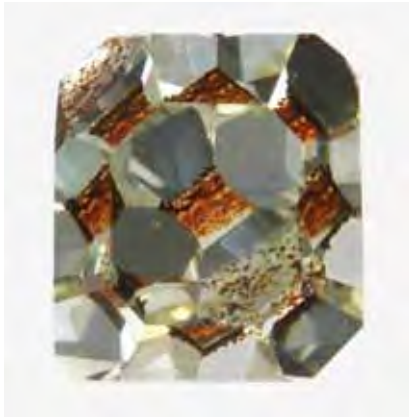


Figure 4. Unusual radiation stains were observed in these two diamonds. Extensive brown stains were present in the culet region (and are reflected in the face-up view) of the 1.47 ct rectangular blocked diamond on the left, whereas a few green stains were seen in the girdle region of the 1.60 ct Fancy Vivid green-blue diamond on the right.

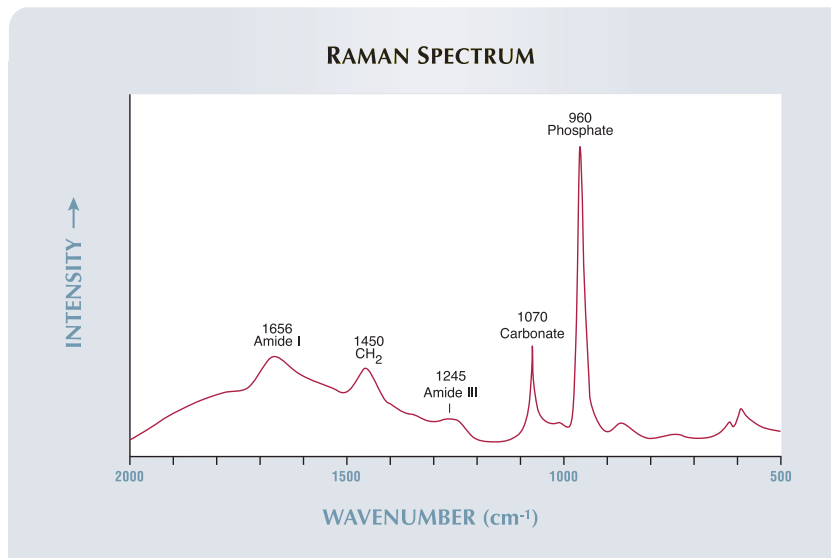
stains on areas that represented the pristine natural surface as well as on the slightly polished facets (again, see figure 5). For the most part, the brown circles were uniform in size, with diameters of about 35 μm . All the stains had a dark center spot when viewed with diffused light. Overlap among the circles was common, and

the color in some intersecting regions was dark brown. When viewed with fiber-optic illumination, the dark centers showed very bright reflections, indicating that they were actually micro-fractures.

In the other diamond, a 1.60 ct square shape, we observed green and yellowish green stains with a similar appearance on naturals in the girdle region, though with a much lower density as most appeared to have been polished off (figure 6). This stone was color graded Fancy Vivid green-blue. These features were somewhat different from those observed in the first diamond, in that very fine, well-developed etch channels began at the centers of the green circles; however, the diameters of the stains on the two stones were very similar.

Both diamonds were type Ia with very high concentrations of nitrogen. Raman spectra were collected from

Figure 3. The Raman spectrum (with peaks from phosphate, carbonate [B-type], proteins [amide I and III], and CH_2 bending) proves that the pendant in figure 1 was made from bovine bone.



Editor's note: The initials at the end of each item identify the editor(s) or contributing editor(s) who provided that item. Full names are given for other GIA Laboratory contributors.

GEMS & GEMOLOGY, Vol. 42, No. 2, pp. 160–168
© 2006 Gemological Institute of America

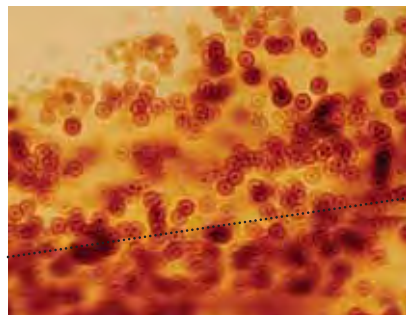


Figure 5. The numerous brown stains on the 1.47 ct diamond show a nearly perfect circular shape. The region above the dotted line is slightly polished, while the region below the line is unpolished. Image width is about 1 mm.

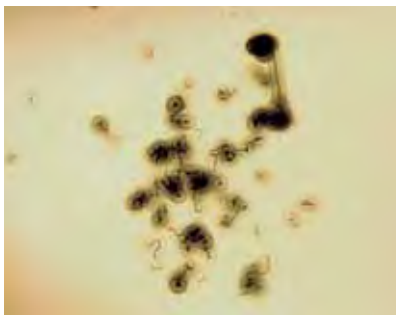
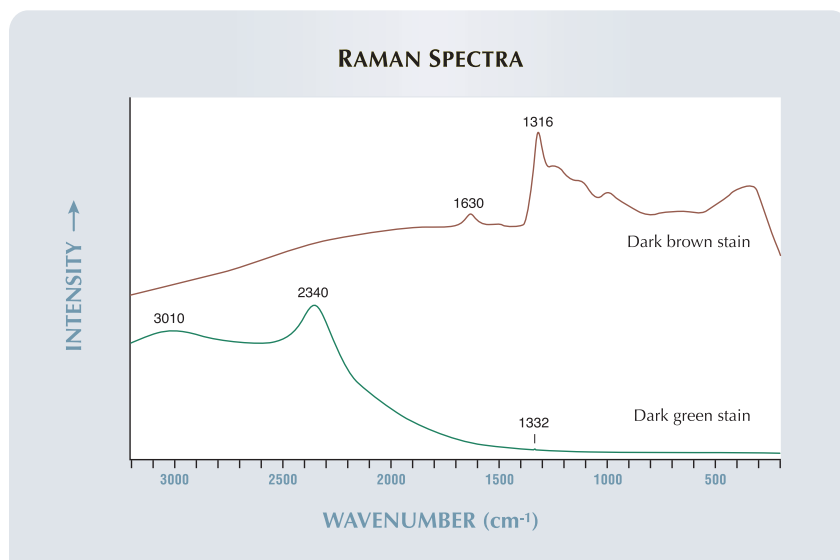


Figure 6. Circular green stains similar to those shown in figure 5 were observed in the 1.60 ct Fancy Vivid green-blue diamond, though in this case thin, well-developed etch channels appear to begin at the dark centers. Image width is about 1 mm.

several dark brown stains (four analyses) and dark green stains (seven analyses) using micro-Raman spectroscopy with 633 nm laser excitation (figure 7). The brown stains showed strong, broad bands centered at 1630 cm^{-1} and 1316 cm^{-1} . The 1630 cm^{-1} band likely has been observed previously in irradiated diamond (A. M. Zaitsev, *Optical*

Properties of Diamond: A Data Handbook, Springer-Verlag, Berlin, 2001, p. 114). The peak at 1316 cm^{-1} may signify low-quality diamond. Nanocrystalline diamond grown by chemical vapor deposition methods, diamond powders, and neutron-irradiated diamond all can show a shift to lower wavenumbers from the standard

Figure 7. Raman spectra of the dark brown (upper spectrum) and dark green (lower spectrum) stains showed little evidence of diamond. These results indicate that the material in the area of the stains is probably a mixture of various forms of carbon.



Raman peak for diamond, at 1332 cm^{-1} (see, e.g., Zaitsev, 2001, pp. 93–94). The region of crystal distortion was limited, though, as areas close to the stains showed a very strong peak at 1332 cm^{-1} .

Raman analysis of the green stains showed strong, broad bands centered at approximately 3010 cm^{-1} and 2340 cm^{-1} , while only a very weak diamond peak at 1332 cm^{-1} was detected. The spectrum of the surrounding green-blue diamond (~100 μm away), collected under the same conditions, showed a much stronger peak at 1332 cm^{-1} , while broad bands around 3010 cm^{-1} and 2340 cm^{-1} were also observed but with much weaker intensities. These results indicated that the stained areas did not possess a pure diamond structure; instead, they were probably a mixture of various forms of carbon. Under the short-wave UV radiation of the DiamondView, the brown and green stains were inert and appeared dark, while the surrounding diamond displayed strong blue fluorescence. This observation is consistent with the conclusion that these stains represented areas of the diamond that were severely damaged by radiation.

Wuyi Wang, Chin Cheung Cheung, and Thomas Gelb

With Clarity Affected by Intense Graining

The clarity grade of a faceted diamond is usually determined by the presence of inclusions, fractures, clouds, or etch channels. However, in the East Coast laboratory, we recently examined an unusual diamond with a clarity grade that was determined by intense internal graining.

The 8.01 ct rectangular modified brilliant cut ($11.86 \times 11.00 \times 6.97\text{ mm}$) in figure 8 was color graded Fancy Light blue. Infrared absorption spectroscopy showed a weak absorption at 2803 cm^{-1} , which confirmed that it was type IIb. Under the microscope, this stone appeared very



Figure 8. The clarity grade (VS₁) of this 8.01 ct Fancy Light blue diamond is mainly due to its strong internal graining.

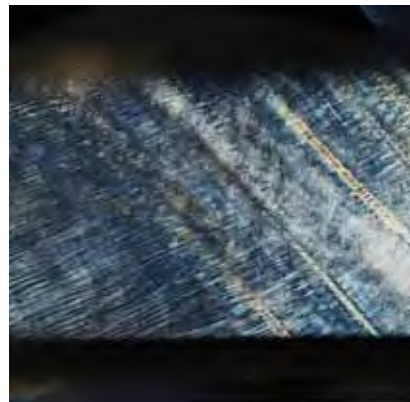
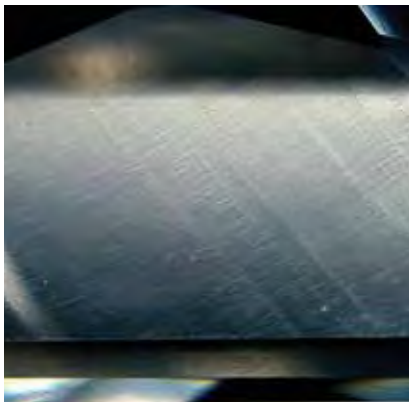


Figure 9. Intense graining can be seen throughout the blue diamond in figure 8 (left). It is dominated by several broad and near-parallel lines oriented in one direction. Graining was also observed perpendicular to this direction, but it was less intense. Birefringence imaging with crossed polarizers displayed a pattern similar to the graining (right). Magnified 22 \times .

clean, with no inclusions or fractures observed. However, intense graining was present throughout the entire diamond (figure 9, left), resulting in a clarity grade of VS₁. The graining was dominated in one direction by several broad and near-parallel lines. Graining perpendicular to this direction was also observed, but it was less pronounced. When the diamond was examined between crossed polarizers, it displayed a pattern comparable to that of the graining (figure 9, right), indicating that the graining was a result of distortion of the diamond lattice. Intense lattice distortion will divert light as it passes through a diamond, causing a hazy or translucent appearance as well as anomalous birefringence.

The intense internal graining may have contributed to other unusual features of this diamond. When exposed to short-wave UV radiation, it displayed weak-to-moderate orange fluorescence and a weak orange phosphorescence that lasted over 10 seconds. Of those natural IIb diamonds that show observable fluorescence and phosphorescence to short-wave UV, most show yellow fluorescence and phosphorescence, but of much weaker intensity than what was observed in this stone. Internal graining can have several causes (e.g., plastic deformation, uneven distribution

of impurities, or inclusions); however, the widespread distribution of linear graining in this diamond is most likely caused by plastic deformation.

TMM and Wuyi Wang

Coated Pink Diamonds

Natural diamonds with a strongly saturated pink hue are rare, but a number of treatment techniques have been developed to induce or enhance a pink color in natural and synthetic diamonds. These methods include irradiation and subsequent annealing (e.g., Summer 1995 Lab Notes, p. 121), high pressure/high temperature annealing (e.g., Fall 2001

Lab Notes, pp. 215–216), and coating (D. J. F. Evans et al., “Coated pink diamond: A cautionary tale,” Spring 2005 *Gems & Gemology*, pp. 36–41).

Recently, three intensely colored pink diamonds (0.70–1.05 ct) were submitted to the East Coast laboratory for identification. The colors were pink, orangy pink, and purple-pink (figure 10). When observed with magnification and regular diffused light, the pink coloration seemed evenly distributed, particularly when the diamonds were viewed face up. However, when the stones were immersed in methylene iodide, we saw distinct pink color concentrations at the facet junctions. With reflected diffused light, an iridescent film-like coat-

Figure 10. The intense pink color of these three diamonds (0.70–1.05 ct) proved to be the result of a surface coating.



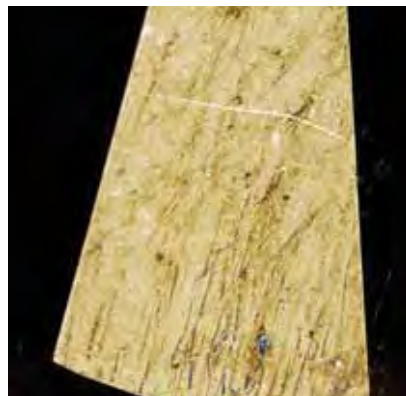


Figure 11. An iridescent film was observed on the pavilion facets of all three diamonds when viewed with reflected diffused light. In addition, colorless spots and lines were seen on all the coated facets. Magnified 60 \times .

ing—seen as interference colors on the surface—was easily visible on the pavilion facets of all three stones (figure 11). In addition, we noted random

colorless spots and lines on all the coated facets. Careful examination of all three diamonds confirmed that the coating was restricted to the pavilion; no coating was present on the table or crown facets.

Infrared absorption spectroscopy showed that the emerald-cut stone (far left in figure 10) was type IIa, while the other two stones were type IaAB with low-to-high concentrations of nitrogen. In the UV-visible spectra of all three stones (figure 12), a broad absorption band was centered at \sim 530 nm, similar to the \sim 550 nm absorption band seen in most naturally colored pink diamonds. However, the peak at \sim 390 nm, which always appears with the 550 nm band in natural pink diamonds, was *not* present. These spectroscopic features supported the visual observation that the pink color resulted from a coating treatment rather than lattice defects, as would be the case with natural pink diamonds. As a cautionary note, it is possible to get a

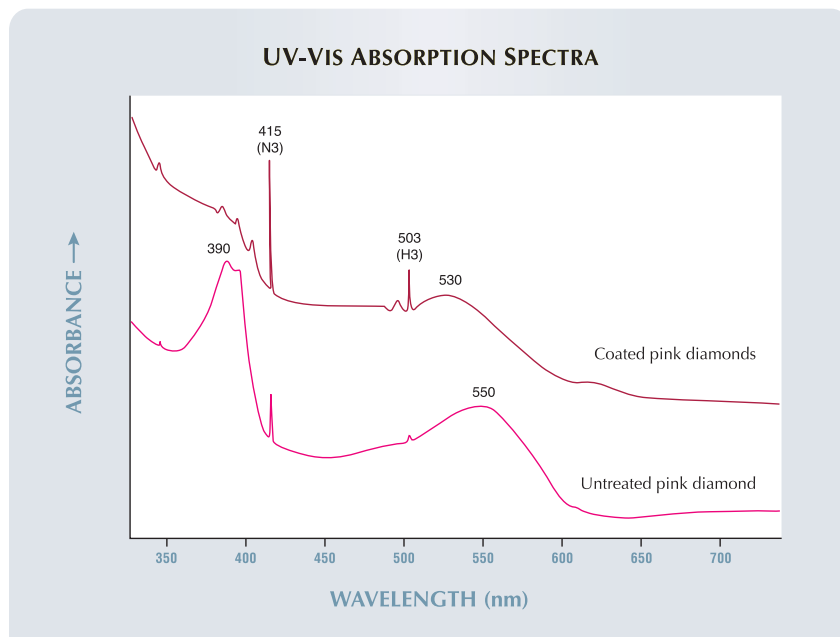
good pink color appearance by coating diamonds that have a slight brown hue; some brown diamonds have broad absorption bands at \sim 550 and 390 nm, in which case the spectra of the coated stones will appear more “natural looking.”

Identification of diamonds treated in this fashion is usually straightforward (see, e.g., E. Miles, “Diamond coating techniques and methods of detection,” Winter 1963–64 *Gems & Gemology*, pp. 355–364). Nevertheless, over the years, coated diamonds have occasionally been submitted to the laboratory for identification or grading. For example, a 10.88 ct “pink” emerald-cut diamond switched with a 9.58 ct Fancy pink prior to an April 1983 Sotheby’s auction was identified in the GIA Laboratory as having been coated with nail polish (Summer 1983 Lab Notes, pp. 112–113). Using a thin blue film to coat diamonds with a slight yellow coloration can substantially improve their apparent color grade (Winter 2003 Lab Notes, pp. 315–316). Although we did not try to identify the nature of the coatings on these three diamonds, Evans et al. (2005) performed elemental analysis on the coating of the pink diamond they studied. They suggested it might be calcium fluoride doped with gold. Since sophisticated film-coating techniques have long been used in the optical industry, we suspect that applying such a thin film over the pavilion facets of loose diamonds can be easily achieved in large quantities. We do know that a number of coated pink diamonds have entered the marketplace recently.

As we have noted previously, it is GIA policy not to issue grading reports for diamonds treated with foreign materials (e.g., coating, fracture filling), since these treatments are not permanent. Accordingly, these three stones were returned to the client with an identification report only.

Wuyi Wang, Thomas Gelb, and
Surjit Dillon

Figure 12. A broad absorption band centered at \sim 530 nm, similar to the \sim 550 nm absorption band in most naturally colored pink diamonds, was observed in the UV-visible spectrum of the coated pink diamonds (here, type IaAB). However, the peak at \sim 390 nm, which is typical of natural pink diamonds, was not present.



Diamond with Unusual Etch Channel

Etch channels, which are common in natural diamonds (both types I and II), appear in various shapes: from narrow hollow triangles and lines, to irregular worm-like features. These channels usually have rhombic-shaped openings at the surface.

The East Coast laboratory recently examined a 2.33 ct J-color round brilliant with a very unusual etch channel in the pavilion that resembled a palm tree or hydra (figure 13). The diameter of the channel decreased gradually with depth; six branches had developed before the etching process terminated.

Infrared absorption spectroscopy revealed that the diamond was type IaA, with a very high concentration of nitrogen and moderately high hydrogen. To investigate if the etch channel followed the diamond's growth zoning, we examined the stone with the DiamondView, which uses high-energy short-wave UV radiation to indicate diamond growth patterns. The fluorescence image of this diamond (figure 14) displayed a complex zonation, with each zone representing a specific growth stage. The difference in configuration of the lattice defects was well reflected in the variations in fluorescence color and intensity, and from this it was clear that the etch channel had developed within a single growth zone.

Although the mechanisms of etch-channel formation are still in debate (see, e.g., T. Lu et al., "Observation of etch channels in several natural diamonds," *Diamond and Related Materials*, Vol. 10, 2001, pp. 68–75), our examination of this diamond confirmed that the etch channels follow localized lattice defects. It also indicated that the penetration direction of an etch channel may change within the same growth zone, and the etching process could be stopped as it meets other growth zones.

*Alina Nemirovskaya
and Wuyi Wang*



Figure 13. Resembling a palm tree, this unusual etch channel was discovered in a 2.33 ct round brilliant diamond. Magnified 80 \times .

Diamond with Sapphire Inclusions

Diamonds often contain interesting suites of inclusions. Because of the quantity of diamonds that come through the lab, we occasionally see mineral inclusions that are very rare.

Such was the case with a 1.03 ct D-color SI₂ diamond we received (figure 15), which revealed several relatively large included blue crystals when examined with magnification. Few mineral inclusions in diamond are blue, so this immediately sparked our interest. Fortunately, some of these inclusions reached the surface of the stone, so we were able to determine their identity with Raman analysis. To our surprise, the crystals were sapphire. The largest crystal (figure 16) measured approximately 0.6 \times 0.6 \times 0.2 mm.

Corundum inclusions in diamond are extremely rare. We located only three reports of ruby crystals trapped in diamonds (H. O. A. Meyer and E. Gübelin, "Ruby in diamond," Fall 1981 *Gems & Gemology*, pp. 153–156; G. Watt et al., "A high-chromium corundum (ruby) inclusion in diamond from the São Luiz alluvial mine, Brazil," *Mineralogical Maga-*



Figure 14. DiamondView fluorescence imaging revealed that the etch channel formed within a specific growth zone, indicating that its development was probably controlled by localized lattice defects.

zine, Vol. 58, 1994, pp. 490–493; M. T. Hutchison et al., "Corundum inclusions in diamonds: Discriminatory criteria and a corundum compositional database," *Extended Abstracts*, 8th International Kimberlite Conference, Victoria, British Columbia, June 22–27, 2003, pp. 1–5), while just a single occurrence of blue sapphire (0.3 mm in diameter) has been documented (Hutchison et al., 2003). Of these,

Figure 15. This 1.03 ct diamond contained several large blue crystals that proved to be sapphire.



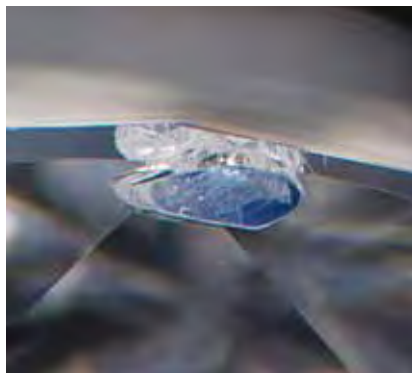
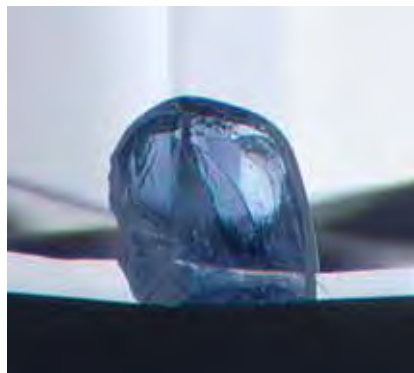


Figure 16. The largest blue crystal, $0.6 \times 0.6 \times 0.2$ mm, had a mostly rounded shape (left, as seen through the pavilion). It reached the surface of the crown (right), enabling Raman analysis that showed it to be sapphire. Magnified 40 \times .

only one (a ruby; Meyer and Gübelin, 1981) occurred in a gem diamond, and both the diamond (0.06 ct) and the inclusion (<0.4 mm) were very small. To the best of our knowledge, the blue sapphire inclusions described here are the first of their kind to be found in a gem diamond and represent the largest corundum inclusions reported in diamond to date.

The occurrence of syngenetic sapphire inclusions provides insight into the environment in which the host diamond crystallized. Corundum is widely reported to occur as an accessory mineral in several types of aluminum-rich, diamond-bearing eclogite xenoliths found in kimberlites. This association suggests that the diamond was most likely eclogitic and formed in a part of the earth's crust that was deeply subducted into the mantle. In previous reports of corundum in diamond (e.g., Hutchison et al., 2003), additional mineral inclusions suggested a crystallization depth of 700–800 km in the transition zone or lower mantle.

SFM and Christopher M. Breeding

IMITATION MELO "PEARLS"

Recently, the West Coast laboratory received two unusual spherical objects for identification (figure 17). The client had purchased them in

Vietnam as rare, nonnacreous Melo "pearls," which are produced by the *Melo* genus of mollusk and are notable for their orange color and interesting flame structure. Although these items had some visual similarities to Melo "pearls," they proved to be a very different product.

The first item was a translucent, banded, orange-to-white sphere that measured $27.75\text{--}28.05 \times 27.15$ mm. The second was a translucent, banded, light orange-yellow to orange ovoid that measured $27.40\text{--}27.65 \times 24.65$ mm. Both had a prominent banded structure. The sphere had a coarse flame structure oriented per-

pendicular to the banding (figure 18), but it was difficult to distinguish any flame structure on the ovoid. Although no dye was removed by swabbing with acetone, low-power magnification revealed numerous fractures and some cavities, both with orange dye concentrations (again, see figure 18). There were also wheel and polishing marks on the surfaces of the samples, which indicated that they had been fashioned. Fluorescence was moderate to long-wave UV radiation and weak to short-wave UV, and was a combination of chalky orange and yellow; the uneven fluorescence patterns appeared banded, with either spots or swirls.

Spot R.I.'s gave a birefringence blink for both samples, with values of 1.50–1.67 for the sphere and 1.52–1.67 for the ovoid. The S.G. values were 2.84 and 2.86, respectively. No absorption bands were visible in the desk-model spectroscope.

Coincidentally, we had recently completed the identification of a true Melo "pearl" submitted by Evan Caplan of Omi Gems, Los Angeles (figure 19). Although some of the properties (such as R.I.) overlapped with the two other samples, there were distinct differences. When examined with magnification, the $26.60 \times 25.60 \times 25.50$ mm (129.81 ct) Melo "pearl" also presented a very

Figure 17. This sphere and ovoid (158.69 and 142.43 ct, respectively) were submitted for identification as possible Melo "pearls." They proved to be dyed shell, as evidenced by the prominent banded structure.





Figure 18. A close-up image of the sphere in figure 17 reveals a coarse flame structure oriented perpendicular to the banded shell structure, and the presence of dye concentrations in fractures and cavities.

coarse flame structure, but the surface was slightly dimpled, especially at the bases of these flame structures, and there was no banding. It had a porcelaneous luster that is also characteristic of conch “pearls.” (The same high luster was not seen in the samples in figure 17.)

Its UV fluorescence was distinctly different from that of the other two samples as well. When exposed to long-wave UV radiation, the Melo “pearl” fluoresced a very weak brown that was mottled with weak-to-strong chalky greenish yellow spots; it was generally inert to short-wave UV, but also showed weak chalky greenish yellow spots. (For a more detailed discussion of the gemological properties of Melo “pearls,” please refer to K. Scarratt, “‘Orange pearls’ from the *Melo volutes* [marine gastropods],” in D. J. Content, Ed., *The Pearl and the Dragon: A Study of Vietnamese Pearls and a History of the Oriental Pearl Trade*, Houlton, Maine, 1999, pp. 79–108.)

Given the differences between the two samples and natural Melo “pearls” with regard to structure, the presence of dye, the UV fluorescence, and evidence of fashioning, it was obvious that the two samples were dyed imitations; the R.I. and banded structure indicated shell material. Ken Scarratt, of GIA Research in Bangkok,



Figure 19. The true nature of the imitations appears obvious when their structure is compared to that of this genuine Melo “pearl” (see also figure 28 on p. 310 of the Winter 2000 issue of G&G).

reports that he has seen a number of such imitations and that they are being produced in Vietnam and Myanmar. Some are fashioned from actual *Melo* shells (i.e., those that are particularly thick in the whorl), whereas others are manufactured from the shell of *Tridacna gigas* (the giant clam), which is also being used as a source of bead nuclei. However, we must reiterate that *Tridacna* is protected by a CITES agreement, and its importation is restricted (see the erratum in Winter 2004 Gem News International, p. 357).

CYW

MOONSTONE Imitations

Moonstone, typically an orthoclase feldspar that displays the phenomenon of adularescence, is a popular and comparatively inexpensive gemstone. Despite its affordability, we do occasionally see moonstone imitations. We have even seen instances where a piece bears an amazing resemblance to moonstone, even though it clearly was never intended to imitate the feldspar.

The 3.92 ct cushion shape in figure 20 was submitted to the West Coast lab for identification. When viewed face up, it had a slightly yellow bodycolor and what appeared to be blue adularescence; it looked very similar to albite moonstone from a relatively new find in Tanzania (see figure 20, right, and Spring 2005 Gem News International, pp. 60–61).

However, microscopic examination easily established that the cushion shape was not a genuine moonstone. An obvious separation plane parallel to the girdle identified the stone as assembled (figure 21). Refractive index readings taken from the top and bottom of the stone were 1.54–1.55, which showed those portions to be quartz. The source of the blue “adularescence” was a thin, transparent, foil-like material placed in the separation plane (figure 22).

Figure 20. While visually very similar, these two stones are not the same material. The 3.92 ct cushion shape on the left is actually a quartz triplet, while the stone on the right is an albitic moonstone from Tanzania.





Figure 21. When the triplet in figure 20 is viewed through the crown, the separation layer along the girdle can be seen to be the cause of the blue “adularescence” in this assembled stone. Note the scratches in the color layer. Magnified 10x.

Figure 23. Though it bears a strong resemblance to moonstone, the stone in this ring actually is a very translucent colorless jadeite.

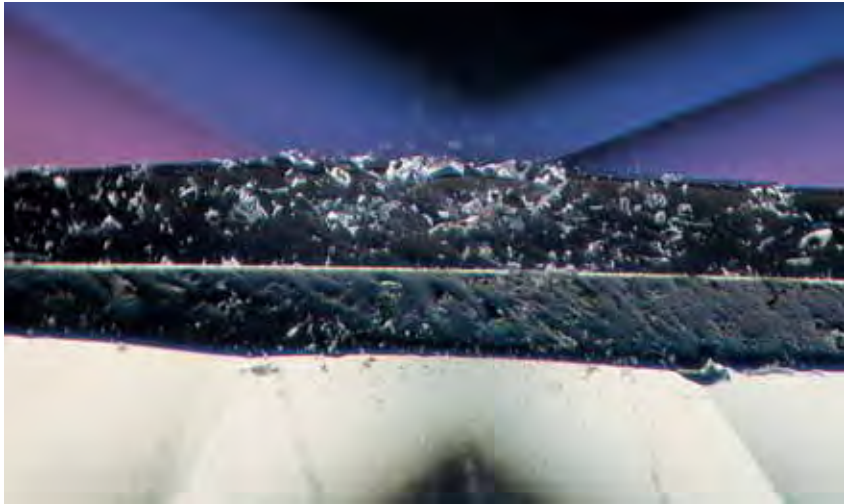


Figure 22. The central layer of the triplet is easily seen along the girdle. It is extremely thin compared to that of most triplets. Magnified 37x.

When this phenomenon was observed through the crown, it created a very good imitation of moonstone. If this assemblage was bezel set in a ring, it could easily pass as a moonstone to the unaided eye.

An “accidental” imitation of moonstone, set in a very nice piece of jewelry (figure 23), came into the West Coast lab several years ago. The oval cabochon was highly translucent, colorless, and appeared to have a white adularescence. However, the stone gave a spot R.I. reading of 1.66, and microscopic examination revealed a fine-grained, somewhat fibrous structure that was typical of jadeite. With close examination, it was evident that the setting was of a construction commonly used with fine jadeite: a closed-back white metal mounting in which the back plate is highly polished on the side facing the stone. With semitransparent to very translucent jadeite, this polished backing reflects light back through

the stone, often giving the appearance of an internal luminescence. In this case, it gave the jadeite its apparent adularescence.

Though the effect of the reflector was clearly intentional, we refer to this example as an “accidental” imitation because it was certainly not intended to imitate moonstone. An exceptionally translucent jadeite such as this one is highly prized and has a value many times that of moonstone. Since this first encounter, we have seen a few similar examples come through the lab.

SFM

PHOTO CREDITS

Jessica Arditi—1, 4, and 8; Kyaw Soe Moe—2; Wuyi Wang—5, 6, 9, 11, 13, and 14; Elizabeth Schrader—10; Robison McMurtry—15; Shane F. McClure—16, 21, and 22; C. D. Mengason—17–20; Maha Calderon—23.

For regular updates from the world of **GEMS & GEMOLOGY**, visit our website at:

www.gia.edu/gemsandgemology



EDITOR

Brendan M. Laurs (blairs@gia.edu)

CONTRIBUTING EDITORS

Emmanuel Fritsch, *IMN, University of Nantes, France* (fritsch@cnrs-imm.fr)

Henry A. Hänni, *SSEF, Basel, Switzerland* (gemlab@ssef.ch)

Franck Notari, *GIA GemTechLab, Geneva, Switzerland* (franck.notari@gia.edu)

Kenneth V. G. Scarratt, *GIA Research, Bangkok, Thailand* (ken.scarratt@gia.edu)

COLORED STONES AND ORGANIC MATERIALS

Alaskan amber. Few may think of Alaska as a source of amber, but the Inuit people have long collected this organic gem from northern beach gravels between Harrison Bay and Smith Bay on the Arctic Ocean. In *Gemstones of North America* (D. Van Nostrand Co., Princeton, NJ, 1959), J. Sinkankas noted that locals refer to the amber as *auma*, which translates as "live coal."

In 1943, an American soldier stationed in Alaska found a 117.8 g chunk of amber (figure 1) while strolling along the coast. Subsequent visits to the area yielded other smaller amber pieces, woolly mammoth teeth, and ivory

Figure 1. This Alaskan amber specimen (117.8 g; 78 × 59 × 36 mm) contains an unusually wide variety of trapped insects, some easily visible without magnification. Photo by R. Weldon.



tusk fragments. The amber in figure 1 was eventually acquired by Barry Schenck of M. M. Schenck Jeweler Inc., Chattanooga, Tennessee, who recently loaned it to GIA for examination. Mr. Schenck has counted more than 30 insects trapped inside the piece, as well as other organic materials, including an apparent seedpod. GIA subsequently purchased the piece (Collection no. 35840).

Most of the insects were eye-visible, though others were best seen with magnification (up to 40×). Prominent were a mosquito, spiders, beetles, gnats, ants, and possibly a bee (see, e.g., figure 2). Other inclusions consisted of gas bubbles and debris that was probably associated with the trees from which the amber formed. The specimen also contained a network of fissures that are undoubtedly due to the stress from numerous freeze-thaw cycles that the fossil endured over time.

Sinkankas (1959) noted that white cedar forests once covered vast swaths of the northern hemisphere, including Asia and Alaska. As resins oozed from the trees, they trapped a variety of insects. These exudations hardened over time, and the fossil resins were incorporated into sedimentary deposits. Geologic upheavals and erosion exposed these deposits, and in some cases the amber

Editor's note: The initials at the end of each item identify the editor or contributing editor who provided it. Full names and affiliations are given for other contributors.

Interested contributors should send information and illustrations to Brendan Laurs at blairs@gia.edu (e-mail), 760-603-4595 (fax), or GIA, The Robert Mouawad Campus, 5345 Armada Drive, Carlsbad, CA 92008. Original photos will be returned after consideration or publication.

GEMS & GEMOLOGY, Vol. 42, No. 2, pp. 169–188
© 2006 Gemological Institute of America



Figure 2. Viewed with 10× magnification, details of the Alaskan amber become evident: A mosquito, spider, and possibly a bee are permanent neighbors, entombed together with hundreds of gas bubbles. Photomicrograph by R. Weldon.

was loosened and tumbled by rivers or washed out to sea. Because amber floats in saltwater, it was carried by currents and deposited in a random fashion along Alaska's coast.

Robert Weldon (rweldon@gia.edu)
GIA, Carlsbad

Update on iridescent andradite from Mexico. During the past few years, additional production of iridescent andradite has come from the previously known mining area for this material that is located about 150–200 km southeast of Hermosillo, Sonora, Mexico. After two years of test marketing the garnet in Tucson, and a number of trips to the mine to purchase rough, Pala International (Fallbrook, California) and JOEB Enterprises helped reactivate the mine in January 2006.

The andradite crystals commonly consist of two distinct layers: an opaque dark brown core that is overgrown

by a layer of transparent greenish yellow material that shows the iridescence. Since the layer exhibiting the phenomenon tends to be very thin (i.e., less than 1–2 mm), pieces of rough are carefully polished to help bring out their colors. The polished material exhibits a range of spectral colors from orange to blue; a few stones also are chatoyant, and some show four-rayed stars. The color display is quite dramatic in daylight or with strong incandescent illumination; some of the initial material from this locality has even been mistaken for black opal (see Fall 1987 Gem News, pp. 173–174). The visual appearance of the material recently recovered is consistent with observations reported for earlier production in the Summer 1988 Gem News section (pp. 120–121). E. J. Gübelin and J. I. Koivula attributed the color display to interference colors, and referred to their lamellar appearance as “kaleidoscopic stripes” (*PhotoAtlas of Inclusions in Gemstones, Vol. 2*, Opinio Publishers, Basel, Switzerland, 2005, pp. 482–484).

The garnets are mined from a skarn deposit (figure 3). In 2003, local miners using only picks and shovels recovered enough material to bring two parcels to the U.S. The initial parcel consisted of about 20 small crystals ranging from 5 to 10 mm in diameter. The miners were encouraged to polish as much of the production as possible for the 2004 Tucson gem show, and they subsequently produced approximately 100 polished crystal fragments and cabochons. Marketed as Rainbow garnet, interest in higher-quality material especially (e.g., figure 4) has been strong among designers and collectors.

John McLean, Pala International's mine foreman, subsequently worked with the local mine owners to introduce more effective mining methods through the use of explosives and a compressor to operate a pneumatic jackham-

Figure 3. The iridescent andradite is mined from a skarn deposit, as shown in this boulder. The iridescent garnet is cut from the greenish yellow material, which here has been mostly removed, leaving the underlying brown garnets. Photo by E. Boehm.



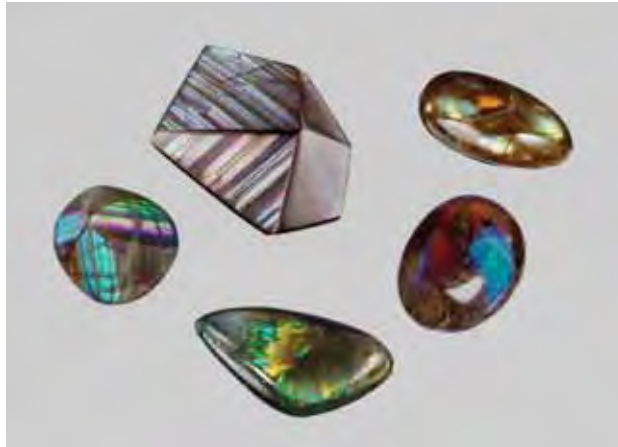


Figure 4. These cabochons and polished crystal fragments of Rainbow garnet (2.38–6.23 ct) are representative of recent production from the previously known mining area in Sonora, Mexico. Courtesy of Pala International © JOEB Enterprises; composite photo by C. D. Mengason.

mer. By the beginning of April 2006, they had achieved production of approximately 50 kg of material consisting of small crystals with areas of cutting quality. Today, several lapidaries are experimenting with polishing, cutting, and carving the material. Because the iridescence is restricted to such a thin overgrowth, they must exercise extreme caution to avoid cutting through it and exposing the dark underlying garnet. Nevertheless, sizable carvings have been produced from some of the crystal clusters (figure 5). Most of the rough, however, has a finished yield of less than 10%, which is lower than the yield from most transparent gem rough (usually about 20%). As of June 2006, approximately 70 finished gems had been produced, in sizes ranging from just under 2 ct to more than 20 ct.

Edward Boehm (joebgem@aol.com)
JOEB Enterprises, Solana Beach, California

Two unusual star emeralds. The Gem Testing Laboratory, Jaipur, India, recently examined two fine bright green emeralds that showed asterism (5.40 and 11.37 ct; figure 6). Both displayed a weak (though distinct) six-rayed star, with the strongest ray aligned parallel to the length of the stone.

The gemological properties were consistent with natural emerald: A spot R.I. was measured at around 1.59, the hydrostatic S.G. was 2.73, and both specimens exhibited the strong chromium absorption spectrum characteristic for emeralds when they were examined with a desk-model spectroscope.

Observation of both cabochons with magnification and strong fiber-optic lighting revealed minute iridescent inclusions in abundance (figure 7). At higher magnification, these inclusions appeared to be hexagonal and triangular discs or platelets; some were elongated as well, similar to knife-shaped rutile silk in corundum (see, e.g., K.



Figure 5. At 25.89 ct, this free-form carving is the largest fashioned Rainbow garnet known to this contributor. Carved by Bud Standley (Oceanside, California) and courtesy of Pala International; photo by Wimon Manrotkul.

Schmetzer et al., “Asterism in beryl, aquamarine and emerald—an update,” *Journal of Gemmology*, Vol. 29, No. 2, 2004, pp. 65–71). In transmitted light, the inclusions appeared gray, varying from translucent to opaque (figure 8), whereas they appeared weakly birefringent in cross-polarized illumination.

When the stones were viewed in immersion (using bromoform), the inclusions were seen to form cloudy planes that were mainly oriented perpendicular to the

Figure 6. These emeralds (5.40 and 11.37 ct) show asterism as well as an attractive green color. Photo by G. Choudhary.



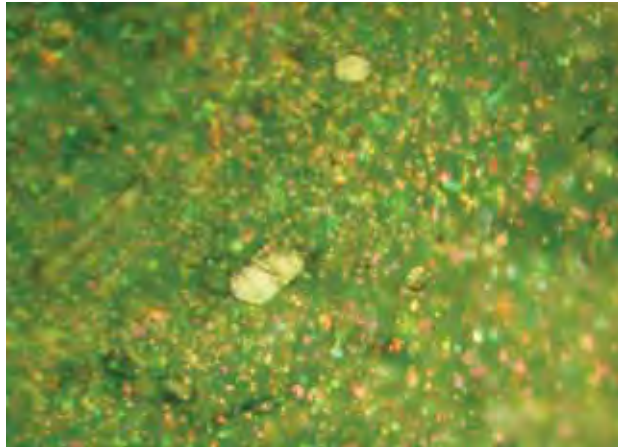


Figure 7. Magnification of the star emeralds in figure 6 revealed iridescent hexagonal and triangular platelets that are mainly concentrated in planes perpendicular to the c-axis. Although not visible in this image, some of the inclusions were elongated. Photomicrograph by G. Choudhary; magnified 50 \times .

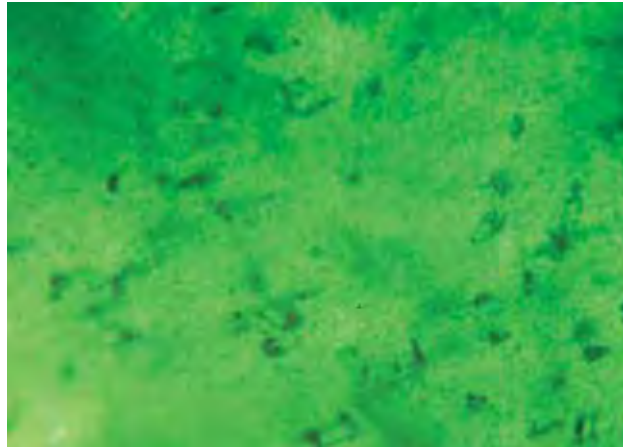


Figure 8. When the star emeralds were immersed in bromoform and viewed with transmitted light, the inclusions in figure 7 appeared gray, with diaphaneity varying from translucent to opaque. Photomicrograph by G. Choudhary; magnified 50 \times .

c-axis. These orientations are similar to those seen in star corundum. The maximum concentration of inclusions occurred at the center of both stones, causing the central area of the star to appear brightest when the stones were viewed with reflected light. Careful examination showed that the inclusions within the planes were roughly aligned (figure 9); up to three directions of alignment could be seen that intersected at approximately 60°. This, combined with the elongate habit of some of

Figure 9. In this view looking down the c-axis of one of the star emeralds, two directions of inclusion alignment (oriented at approximately 60°) can be seen. A third direction of alignment was also present in the samples; combined with the elongate habit of some of the inclusions, it was apparently responsible for the asterism. Photomicrograph by G. Choudhary; in immersion with transmitted light, magnified 35 \times .



the inclusions, is apparently responsible for the asterism seen in these emeralds.

Both stones also contained a number of long, tube-like, two-phase inclusions parallel to the c-axis (figure 10). Other inclusions present were colorless rhombohedrons and rounded colorless crystals.

The source of these stones is not known, but star emeralds have been reported from Brazil (Nova Era and Santa Terezinha) and Madagascar (Mananjary area; see K. Schmetzer et al., 2004, and references therein). Although star emerald is unusual, the bright green color of these emeralds makes them even rarer.

Gagan Choudhary (gtljpr_jpr@sancharnet.in)
Gem Testing Laboratory, Jaipur, India

Figure 10. Long, tube-like, two-phase inclusions were oriented parallel to the c-axis in the star emeralds. Photomicrograph by G. Choudhary; magnified 40 \times .

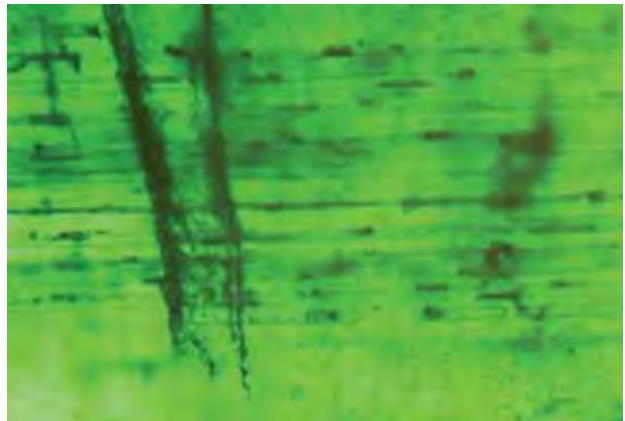




Figure 11. This 9.50 ct euclase from the Chivor emerald mine in Colombia is notable for its size and intense greenish blue color. Photo by C. D. Mengason.

Faceted blue euclase from Colombia. The Spring 2003 Lab Notes section (p. 42) reported on an attractive crystal specimen of greenish blue euclase from Pauna, Boyacá District, Colombia (also see erratum, Spring 2004 *Gems & Gemology*, p. 65). Another source of blue euclase in Colombia is the famous Chivor emerald mine, also located in the Boyacá District, approximately 110 km southeast of Pauna. Most of the euclase has been produced sporadically from a small area of this mine (i.e., the San Francisco tunnel). The site is located about 8 km from the nearest town and can only be reached by a four-wheel-drive vehicle or a helicopter. The euclase was initially found in the 1980s, when a large amount of emeralds were produced from Chivor. The miners did not give much importance to the euclase because they lacked knowledge of the material and were focused on the important emerald production at that time.

Recently, some fine gem-quality crystals of blue euclase have been appearing in the Colombian market, and the faceted gems are sometimes seen in parcels of cut

emeralds offered in Bogotá. The cut euclase is light-to-medium greenish blue, and the stones typically weigh less than 2 ct. By contrast, the 9.50 ct Chivor euclase in figure 11 is notable for its size and intense greenish blue color; the rough was reportedly mined in 2005.

The 9.50 ct euclase was loaned to the GIA Laboratory for examination, and the following gemological properties were recorded by Shane F. McClure: Color—greenish blue; pleochroism—near colorless, light purple, and blue-green; R.I.—1.650–1.670; biaxial optic figure; hydrostatic S.G.—3.10; fluorescence—inert to long- and short-wave UV radiation; and no spectrum was observed with the desk-model spectroscope. Examination with a gemological microscope revealed a large cleavage plane, inclusions of tiny transparent colorless crystals, and strong angular graining and associated color zoning.

In addition to Colombia, gem-quality euclase is known from Brazil and Zimbabwe (Summer 1993 Lab Notes, pp. 125–126). Nevertheless, euclase remains a rare stone. Unless a productive source is discovered in the future, the supply of this material will likely remain limited to a few sporadic gems destined for museums and private collectors.

Daniel A. Sauer
(danielsauer@amsterdamsauer.com)
Amsterdam Sauer, Rio de Janeiro

BML

Color-change fluorite. Fluorite shows a remarkable diversity of color, crystal morphology, and optical properties—specifically, the UV fluorescence from which its name derives—that make it one of the most fascinating minerals. Fluorite is known to occur in almost every hue, and often exhibits distinct and beautiful color banding/zoning. Some fluorite shows a distinct color change. Such was the case with a 10.00 ct triangular modified brilliant that these contributors noticed in the local market. The stone appeared medium blue in daylight-equivalent fluorescent light and in indirect sunlight, but it changed to a medium purple in incandescent light (figure 12).

Figure 12. This 10.00 ct fluorite exhibits a distinct color change from blue in day or fluorescent light to purple in incandescent light. Photos by N. Sturman.



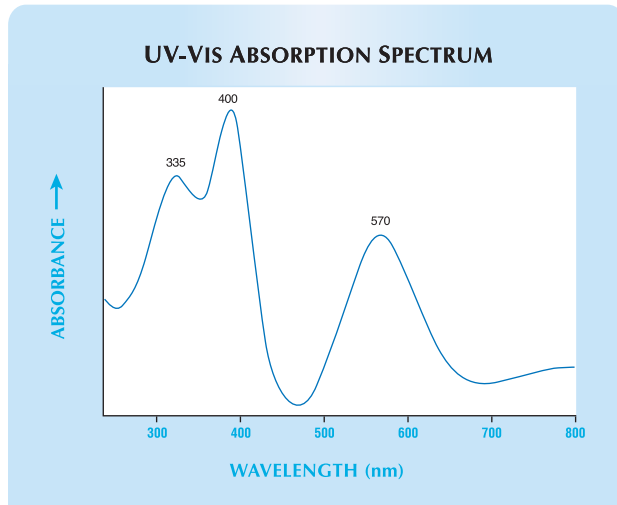


Figure 13. The UV-Vis absorption spectrum of the color-change fluorite shows absorption bands centered at ~400 and ~570 nm. The transmission windows in the blue-green and red regions, and a local absorption maximum in the yellow region, are consistent with that of other true color-change stones.

The R.I. (1.430) and hydrostatic S.G. (3.18) were consistent with fluorite, including an irradiated color-change fluorite reported in the Summer 2002 Gem News International section (p. 186). Magnification revealed prominent wavy color banding that was related to fine planar zones of minute pinpoint inclusions. Damage to one point of the stone (again, see figure 12) revealed the distinct cleavage present in fluorite, as did some minor surface-reaching cleavage fractures.

With a handheld spectroscope, the fluorite showed an

Figure 14. These cut stones (2.06 and 5.52 ct) and crystal (14 g) of herderite are from northern Pakistan. Courtesy of Farooq Hashmi; photo by C. D. Mengason.



absorption band in the yellow-orange area of the spectrum and some absorption in the violet region. This could be seen more clearly in the UV-Vis spectrum (figure 13), with absorption bands centered at ~400 and ~570 nm. Consistent with other true color-change stones, the spectrum showed transmission windows in the blue-green and red regions and a local absorption maximum in the yellow region. As expected given the spectral features, the fluorite appeared very strong red through the Chelsea color filter. Although fluorite commonly fluoresces to UV radiation, this sample was inert, as was the irradiated color-change fluorite in the Summer 2002 GNI entry. However, the inert behavior of the present color-change fluorite does not necessarily indicate that it has been irradiated, since fluorite does not always show fluorescence.

The Summer 2002 GNI entry mentioned that no fade testing was performed on the irradiated color-change fluorite described. Similarly, we did not perform fade testing on the present fluorite. Although fade testing could reveal the presence of unstable color centers that were created by exposure to radiation, it could not confirm whether this exposure occurred naturally or artificially.

Nick Sturman (nick@commerce.gov.bh)
and Abeer Al-Alawi
Gem & Pearl Testing Laboratory
Manama, Kingdom of Bahrain

Herderite from Pakistan. Herderite—hydroxyl-herderite [$\text{CaBePO}_4(\text{F},\text{OH})$] has been known from granitic pegmatites in Pakistan's Northern Areas for several years. Well-formed crystal specimens of herderite from this region are sought after by mineral collectors, but the material is rarely transparent enough to be faceted. In June 2006, Farooq Hashmi (Intimate Gems, Jamaica, New York) loaned GIA some rough and cut examples of "lime" green herderite that he obtained during the past two years in the mineral market of Peshawar, Pakistan. The material was represented as coming from the Shigar Valley, as well as from the more general localities of Skardu and Gilgit, which are common gem and mineral trading areas in northern Pakistan. The most likely source of the gem herderite is the Kandahar mine, Baha, Braldu Valley (about 35 km north of Skardu), according to Dudley Blauwet (Dudley Blauwet Gems, Louisville, Colorado), who has extensive experience traveling to the gem and mineral localities of northern Pakistan. Mr. Blauwet also indicated that he recently obtained cuttable herderite from two additional locations in the Shigar Valley area: near Chhappu in the Braldu Valley, and at a new mine near Doko in the Basha Valley.

The two faceted herderites (2.06 and 5.52 ct; figure 14) were characterized by one of us (EPQ) for this report; the properties of the smaller stone are listed first, as appropriate: color—light green and medium-light green; pleochroism—both stones showed weak-to-moderate green and yellowish green (a third color was not observed); diaphaneity—transparent; R.I.—1.587–1.616 and

1.586–1.616; birefringence—0.029 and 0.030; hydrostatic S.G.—3.02 and 3.04; Chelsea filter reaction—none; fluorescence—weak-to-moderate blue and moderate-to-strong blue to long-wave UV radiation, weak violet and moderate violet to short-wave UV radiation; and a weak 585 nm absorption feature was observed with the desk-model spectroscope for both stones. Microscopic examination of both samples revealed moderate-to-strong doubling and numerous partially healed fractures with negative crystals, some of which contained both a liquid and a gas. EDXRF spectroscopy of the larger stone showed major amounts of Ca, P, and Sr, and minor Cr, Mn, Y, and Pb. The instrument cannot detect Be or F.

The properties of these Pakistani samples are comparable to those previously reported for herderite (e.g., Spring 2004 Lab Notes, pp. 61–62), although their refractive indices were somewhat higher. Based on the work of P. B. Leavens et al. ("Compositional and refractive index variations of the herderite-hydroxyl-herderite series," *American Mineralogist*, Vol. 63, No. 9–10, 1978, pp. 913–917), the R.I. values of the Pakistani herderite indicate that the composition is near the midpoint between the OH- and F-dominant end-members. Such a composition was also inferred from an R.I. value ($n_b = 1.610$) of a herderite from the Shigar Valley area by A. H. Kazmi et al. ("Gem pegmatites of the Shingus-Dusso area, Gilgit, Pakistan," *Mineralogical Record*, Vol. 16, No. 5, 1985, pp. 393–411). Although we have referred to the material as *herderite* in this entry for simplicity, the correct mineralogical designation is herderite-hydroxyl-herderite.

BML

Elizabeth P. Quinn
GIA GemTechLab, Geneva, Switzerland

Jeremejevite from Myanmar and Sri Lanka. Jeremejevite is a rare gem that is mainly known from Namibia (Cape Cross and the Erongo Mountains) and the Pamir Mountains of Tajikistan (see K. Scarratt et al., "Jeremejevite: A gemological update," Fall 2001 *Gems & Gemology*, pp. 206–211; Fall 2002 GNI, pp. 264–265). More recently, a near-colorless 7.88 ct jeremejevite was documented from an additional locality, Madagascar (Winter 2004 GNI, pp. 340–341). With only a few sources of this rare gem known for many years, it is surprising that two more localities for gem-quality jeremejevite have just been reported: Myanmar (Burma) and Sri Lanka (figure 15).

The Burmese jeremejevite was recently documented by H. Kyi and K. Thu ("A new deposit of jeremejevite from the Mogok Stone Tract, Myanmar," *Australian Gemmologist*, Vol. 22, No. 9, 2006, pp. 402–405), who pictured a 4.35 ct light yellow faceted stone and indicated that gemmy crystals can reach 4.0×1.3 cm. They reported that the jeremejevite ranges from colorless to light yellow and was mined from alluvial deposits and associated pegmatite



Figure 15. These jeremejevites are from Sri Lanka (left, 5.26 ct) and Myanmar (right, 1.34 ct). Courtesy of Dudley Blauwet; photo by C. D. Mengason.

dikes. Their samples came from a pegmatite on Loi-Sau mountain, which is located 19 km northeast of Mogok, near Pan-tara village; some pink tourmaline and quartz crystals were also produced from this mine (K. Thu, pers. comm., 2006). According to Bill Larson (Pala International, Fallbrook, California), who regularly travels to Myanmar, most of the jeremejevite was produced 1–2½ years ago. Well-formed crystals have been found, with terminations that show varying development of pyramidal and basal forms (figure 16).

Figure 16. Jeremejevite crystals from Myanmar are prismatic and commonly of gem quality. The crystal on the left is 21.6×5.4 mm. Courtesy of Bill Larson; photo by Wimon Manorotkul.



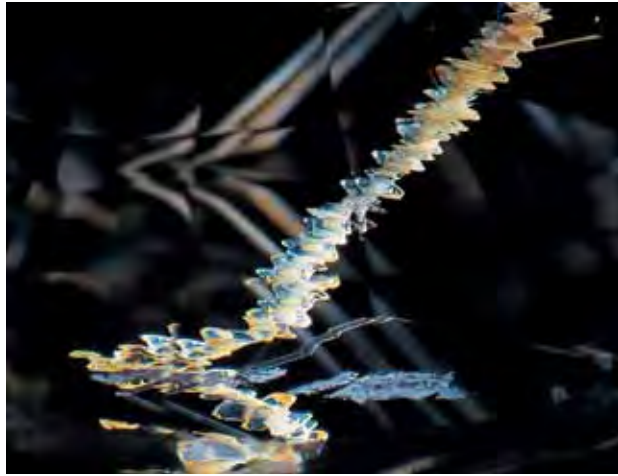


Figure 17. The Sri Lankan jeremejevite contained a conspicuous inclusion formed by angular platelets that ranged from white to yellow to orange. This feature might have been created by a series of negative crystals that were epigenetically iron-stained. Photomicrograph by Shane F. McClure; magnified 15 \times .

In late 2005, Dudley Blauwet loaned a 1.34 ct Burmese jeremejevite to GIA for examination (again, see figure 15). The following properties were determined by one of us (EAF): color—light yellowish orange; R.I.—1.643–1.650; birefringence—0.007; hydrostatic S.G.—3.29; and fluorescence—inert to long-wave and weak yellow to short-wave UV radiation. No absorption features were observed with the desk-model spectroscope. Microscopic examination revealed angular growth lines, growth tubes, and two-phase inclusions. The R.I. values of this stone fell within a slightly narrower range (yielding a lower birefringence) than was reported for Burmese jeremejevite by Kyi and Thu (2006; $n_e = 1.640$ and $n_o = 1.653$).

Sri Lankan jeremejevite was brought to our attention by Mr. Blauwet in September 2005. He obtained a piece of rough that was reportedly from the Ratnapura area, and it was subsequently faceted into a 5.26 ct colorless gem with an interesting inclusion centered beneath the table (again, see figure 15). Mr. Blauwet's supplier in Sri Lanka indicated that several small pieces of colorless jeremejevite have been found sporadically in the same area over the past few years. Examination of the 5.26 ct jeremejevite by one of us (EAF) yielded the following properties: color—colorless; R.I.—1.640–1.649; birefringence—0.009; hydrostatic S.G.—3.29; and fluorescence—inert to long- and short-wave UV radiation. Again, no absorption features were observed with the desk-model spectroscope. Microscopic examination showed that the inclusion under the table consisted of a linear arrangement of angular platelets that ranged from white to yellow to orange (figure 17). Primary fluid inclusions of similar shape have been seen in jeremejevite crystals previously by J. I. Koivula (pers. comm., 2005); he suggested that those in the Sri Lankan stone

are probably drained negative crystals that have been epigenetically iron-stained. No other inclusions were observed in this stone. Mr. Blauwet recently informed us about another colorless jeremejevite that was found in the Ratnapura area in May 2006, which is expected to yield a cut stone weighing ~2 ct.

BML

Eric A. Fritz

GIA Laboratory, Carlsbad

Pink opal from Monte Rosa, Peru. Peru is an important producer of a few lapidary materials, especially chrysocolla and blue and pink opal from the Acari mine near Nazca (460 km south of Lima), as well as "gem silica" (chrysocolla-stained chalcedony) from the Lily mine near Pisco (J. Hyršl, "Gemstones of Peru," *Journal of Gemmology*, Vol. 27, No. 6, 2001, pp. 328–334), 150 km south of Lima. Pink opal is a mixture of opal with palygorskite, and the color is caused by organic compounds called quinones (E. Fritsch et al., "Relationship between nanostructure and optical absorption in fibrous pink opals from Mexico and Peru," *European Journal of Mineralogy*, Vol. 16, 2004, pp. 743–752). Pink and blue opals probably form in volcanic lake environments.

Pink opal from the Acari mine is typically of mediocre quality, and only rarely has it been found in homogeneously colored pieces large enough to be polished into gems. Much better quality material (e.g., figure 18) was found in 2002 at Monte Rosa, about 5 km east of Ica and 250 km southeast of Lima. At present, about 60 people are using primitive methods to mine the deposit via tunnels that reach almost 100 m underground. The saturated pink opal forms veins up to 30 cm thick. The veins sometimes contain very soft, felt-like aggregates of white

Figure 18. This specimen of pink opal (9 cm long) was mined at a relatively new locality in Peru, known as Monte Rosa. Photo by J. Hyršl.



palygorskite. Also typical in the opal are cavities, sometimes with a sparkling surface caused by an overgrowth of drusy quartz crystals (figure 19). Some specimens of the pink opal are covered by a layer of milky white opal. However, the youngest phase of deposition identified was a crust of botryoidal colorless hyalite opal, up to 7 mm thick, which commonly fluoresced green to short-wave UV radiation. So far, blue Cu-bearing opal has not been found at Monte Rosa.

Gemological properties were collected on five cabochons and two pieces of polished rough pink opal that were obtained from a local dealer who regularly visits Monte Rosa: R.I.—1.475, hydrostatic S.G.—2.18–2.25, Mohs hardness—6, and fluorescence—inert to short-wave UV radiation and weak pinkish white to long-wave UV. These properties are identical to those reported for the Acari material (Hyršl, 2001). Powder X-ray diffraction analysis confirmed that this material is a mixture of opal, palygorskite, and minor chalcedony.

The Monte Rosa opal is available in large quantities (tonnes) from several dealers in Lima and at international gem shows. The relatively large size of the veins allows the material to be carved into large objects; an attractive fish carving measuring 60 cm in diameter was seen by this contributor in Lima. The mine owners plan to develop a large open pit, which will help guarantee a steady production of this attractive material in the future.

Jaroslav Hyršl (hyrsl@kuryr.cz)
Kolin, Czech Republic

Figure 19. Drusy quartz crystals have overgrown the pink opal within a cavity in this 7-cm-long sample from Monte Rosa, Peru. Note also the surrounding layers of milky white opal and the thin crust of botryoidal colorless hyalite opal on the top of this sample, which represents the last stage of deposition in the vein. Photo by J. Hyršl.



Figure 20. Prehnite from Australia is being mined by a new venture, and the higher-quality material is being polished into cabochons and faceted stones in colors ranging from yellowish green to yellow. The cabochons shown here weigh 9.52–45.80 ct, and the faceted stones are 1.55 and 7.19 ct. Gift of Robert Sielecki–Ausrox/Crystal Universe; GIA Collection nos. 32980–32984. Photo by C. D. Mengason.

Update on prehnite from Australia. The Spring 2001 Gem News International section (pp. 71–72) reported on attractive gem-quality prehnite from Wave Hill, Northern Territories. At the 2006 TGMS show in Tucson, Arizona, some new samples of prehnite from this deposit (e.g., figure 20) were shown to this contributor by Robert Sielecki (Ausrox/Crystal Universe, Port Melbourne, Victoria, Australia). Mr. Sielecki reported that in early 2005, his company began exploring an area of Wave Hill that had been prospected for 30 years by Gerald Pauley, who became interested in collaborating on developing the prospect. The deposit is located near the small township of Kalkarindji on the edge of the Tanami Desert, approximately 885 km (550 miles) by road south of Darwin. Mr. Sielecki stated that this area is underlain by ancient (early Cambrian) flood basalts of the Antrim Plateau Volcanics, and there are several minerals produced in addition to prehnite: scolecite, calcite, amethyst, smoky quartz, and agates.

So far the prehnite has only been surface collected as part of a bulk-sampling program being conducted to assess the viability of the deposit for commercial production. A program of pitting and trenching will commence shortly, and full-scale mining is planned for late 2006, depending on the onset of the rainy season (which will limit access to the area). Preliminary results suggest that approximately 3% of the prehnite is of sufficient gem grade for polishing cabochons or faceted stones, with 95% of this yellowish green and the remainder yellow. While to date mostly small faceted stones have been cut from the weathered surface material, Mr. Sielecki expects to recover larger and more transparent rough once mining begins. The lower-quality prehnite is being fashioned into



Figure 21. The largest cabochon in figure 20 contains a conspicuous radiating internal feature that is attributed to the fibrous structure of the prehnite. Photo by C. D. Mengason.

beads, carvings, and objects for the metaphysical market. Mr. Sielecki has trademarked the yellowish green prehnite as "SunJade" and the yellow material as "Golden SunJade." In addition, an unusual green-to-yellow variety of prehnite, which contains radial white patterns resembling flowers, will be marketed as "Flower SunJade." He indicated that the fibrous nature of the prehnite also produces chatoyancy or adularescence in some cabochons. The largest cabochon with adularescence that has been cut so far weighed 61 ct.

Mr. Sielecki donated three cabochons and two faceted stones of the Australian prehnite to GIA for examination (again, see figure 20). Since the gemological properties of this material were already reported in the Spring 2001 GNI entry, these samples were not characterized for this report. One of these samples contained the radial pattern mentioned above (figure 21). Raman analysis of the white radial inclusions by GIA research scientist Dr. Mike Breeding showed no difference from the surrounding prehnite. This indicated that the inclusions are structural features related to the fibrous nature of the material, rather than a foreign mineral.

BML

Prehnite from Mali. In 1994, gem-quality garnets were discovered in western Mali in the "Zone of Sangafé," about 130 km east of Kayes and 100 km south of the border with Mauritania (M. L. Johnson et al., "Gem-quality grossular-andradite: A new garnet from Mali," Fall 1995 *Gems & Gemology*, pp. 152–166). Initial mining of alluvial deposits progressed into bedrock, and the mines were soon exhausted. More than 13 tonnes of garnet were recovered before most operations ceased. However, the Kayes region continues to support small-scale mining for garnet as well as epidote, chalcedony, vesuvianite, and prehnite. In December 2005, two of these contributors (RHC and DP) traveled to this region and observed mining for prehnite and associated minerals at several localities

near the villages of Bendoukou and Diakon. The most active locality was Djouga (N14°36'08.2", W10°14'57.1"), located about 5 km north of Bendoukou village.

Several types of minerals were available in the market in Mali's capital, Bamako, but prehnite and garnet were dominant. We saw >1-m-high piles of rough "apple" green prehnite, although some of the material was weathered and discolored by iron stains. The cobbled prehnite is commonly shipped in 120 kg bags to lapidary factories (mostly for beads) in Asia. The prehnite consisted of crusts, balls, and intergrown clusters of spheres or hemispheres that reached up to 5 cm in diameter but were typically 2–3 cm (see, e.g., figure 22). Most of the prehnite was oiled to improve its appearance.

The prehnite is mined from a rather small area centered around Bendoukou village. The deposits are associated with localized diabase intrusions in the vast sedimentary Taoudeni Basin lying north of the Niger and Senegal Rivers. The mineral occurrences are hosted within a Neoproterozoic (800–600 million years old) sequence of sandstones and calcareous rock, which overlay flat-lying, aeolian sandstones. The prehnite, epidote, garnet, and vesuvianite mineralization is hosted by brecciated calcisilicate rocks adjacent to the diabase intrusions.

Figure 22. Prehnite balls joined with black epidote crystals create striking mineral specimens, such as this one from the Kayes region of Mali (5.1 cm tall). Photo © Jeff Scovil; Laura Delano collection.



Over the past three years, prehnite mining has become an important part of the economy of Bendoukou. The mines—actually, individual shafts—are worked by rudimentary methods (figure 23) and the material is hand-sorted on-site. We observed 50–75 independent miners during the trip, but the workforce fluctuates according to agricultural priorities; it grows to several hundred at the end of the dry season. There were about 120 shafts within a 200 × 100 m area, reaching a maximum depth of about 24 m. They were dug randomly until prehnite-bearing rock was located, and then tunnels radiated outward from the shaft. The production included crusts of translucent gray-green, blue-green, and yellow-green prehnite up to a maximum of 10 cm thick, although most are 2–5 cm thick. Many of these crusts have flat undersides and had grown on what may have been anhydrite crystals that subsequently dissolved. Also found in this area were balls and intergrown spherical clusters of prehnite, sometimes intergrown with stout, black, prismatic epidote crystals up to about 5 cm long (again, see figure 22).

Another area near Bendoukou, called Baga (N14°30'34.2", W10°15'54.9"), produced prehnite crusts that varied in color from gray to grayish green. Specimens weighing at least 100 kg were produced at this deposit, but prehnite mining has ceased because of the poor color. Baga is also the source of some very fine epidote specimens, with crystals up to about 10 cm, as well as abundant small, rhombic dodecahedral yellow-brown garnets, some associated with epidote.

Four polished samples of prehnite from unknown localities in Mali were donated to GIA by Dudley Blauwet, and were characterized by one of us (EPQ). The samples consisted of three oval modified brilliants and one cabochon (figure 24), and they yielded the following gemological properties: color—light-to-medium grayish green and yellow; diaphaneity—transparent to semitransparent; R.I.— $n_{\alpha}=1.617$ – 1.619 and $n_{\gamma}=1.643$ – 1.645 from the faceted stones; birefringence—0.026; hydrostatic S.G.—2.92–2.93; Chelsea filter reaction—very weak red reaction from the three green stones and no reaction from the yellow sample; and fluorescence—inert to both long- and short-wave UV radiation. No absorption was observed with the desk-model spectroscope. These properties are comparable to those reported for prehnite by R. Webster (*Gems*, 5th ed., rev. by P. Read, Butterworth-Heinemann, Oxford, 1994, p. 361). Microscopic examination of the four samples revealed a wavy fibrous aggregate structure that sometimes showed a radiating pattern, “fingerprints,” hazy clouds, and reflective thin films. The yellow prehnite had some weak, irregular color zoning.

Rock H. Currier (rockcurrier@cs.com)
 Jewel Tunnel Imports
 Baldwin Park, California
 Demetrius Pohl
 Sanú Resources Ltd., Los Angeles
 Elizabeth P. Quinn



Figure 23. Djouga is the most active mining area for prehnite in Mali. Simple hand methods are used to follow the prehnite veins underground for up to 24 m. Photo by R. H. Currier.

Natural sapphire with unusual inclusions. A 3.56 ct blue cushion-shaped mixed cut (figure 25) was tested and certified at the Gem Testing Laboratory, Jaipur, India. Refractive indices of 1.760–1.770 and a hydrostatic S.G. value of 3.99 confirmed the stone as corundum.

With magnification, the sample displayed some unusual inclusion patterns. Long, parallel needle-like inclusions with some curved bends (figure 26, left) were present, along with long, slightly wavy fiber- or needle-like

Figure 24. Although prehnite from Mali is typically sold to bead manufacturers, a small amount of the production is polished into cabochons and faceted stones (here, 17.91 ct and 1.62–2.19 ct, respectively). Gift of Dudley Blauwet; GIA Collection nos. 32974–32977. Photo by Maha Calderon.

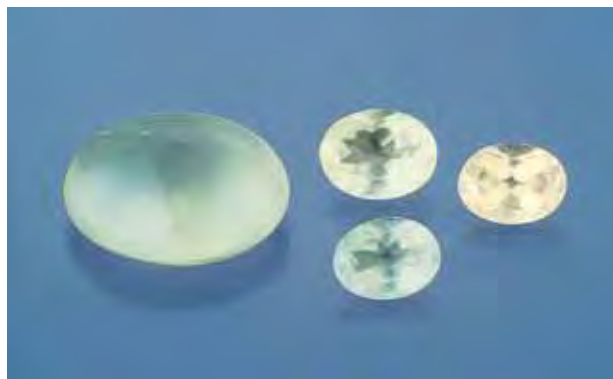




Figure 25. Magnification revealed some unusual inclusions in this 3.56 ct sapphire. Photo by G. Choudhary.

structures (figure 26, right). The visual appearance of both was similar to etch channels seen in stones such as scapolite (Summer 2004 GNI, pp. 172–173) or diamond. Additionally, the stone contained a reddish brown to white inclusion, with a hexagonal cross-section, that resembled a hockey stick (figure 27). Its appearance varied from sugary to wavy to cloudy; in some areas, it gave the impression of a hollow tube filled with foreign material.

When viewed at higher magnification using a fiber-optic light, the sapphire displayed three directions of platelets and short needles that were oriented at approximately 60° to one another (figure 28), which indicated natural origin. The overall undamaged inclusion pattern indicated that the sapphire had not been subjected to high-temperature heat treatment.

Gagan Choudhary (gtljpr_jp1@sancharnet.in)
and Meenu Brijesh Vyas
Gem Testing Laboratory, Jaipur, India

Sillimanite from India resembling moonstone. In mid-2005, these contributors received an interesting sillimanite (figure 29) that showed an unusual blue-white sheen when strongly illuminated in certain orientations. The stone was donated to GIA by Scott Davies (American-Thai Trading, Bangkok), after he noticed its optical behavior in

a large parcel of transparent faceted sillimanites he had obtained in mid-2004 in Jaipur, India.

The 6.65 ct oval modified brilliant displayed a weak-to-moderate blue-white sheen that was similar in appearance to the billowy adularescence displayed by some moonstones. The following properties were obtained by one of us (EPQ): color—light gray; diaphaneity—transparent; R.I.—1.661–1.680; birefringence—0.019; hydrostatic S.G.—3.26; no Chelsea filter reaction; and inert to both long- and short-wave UV radiation. No absorption features were observed with a desk-model spectroscope. The properties of this stone are generally consistent with those listed for sillimanite (fibrolite) by R. Webster (*Gems*, 5th ed., revised by P. Read, Butterworth-Heinemann, Oxford, England, 1994, p. 337). Microscopic examination revealed that the stone contained two-phase inclusions and numerous fine, parallel, whitish needles.

Moonstone's billowy sheen (known as adularescence) is caused when light is scattered off very thin alternating lamellae of albite and orthoclase feldspars. The exact cause of the bluish sheen displayed by this sillimanite is not yet fully understood and would require further research. It appears to be due to a combination of the scattering of light off submicroscopic particles (responsible for the bluish color of the sheen) and the reflection of light from the numerous fine needles throughout the stone (causing the sheen to be strongest in two directions; figure 30). If the stone had been cut *en cabochon*, we believe it would have shown chatoyancy.

Elizabeth P. Quinn (equinn@gia.edu) and BML

Sphene from Afghanistan. The Spring 2006 GNI section (pp. 68–69) reported on some “golden” orange sphene from Pakistan that has been mined for the past two years. We were surprised, therefore, when we recently encountered another source of this uncommon gem from the same general region: Badakhshan, Afghanistan. This material was brought to our attention by Scott Davies and Dudley Blauwet, who both reported that it first appeared in late 2005 in the gem market of Peshawar, Pakistan. Mr. Blauwet

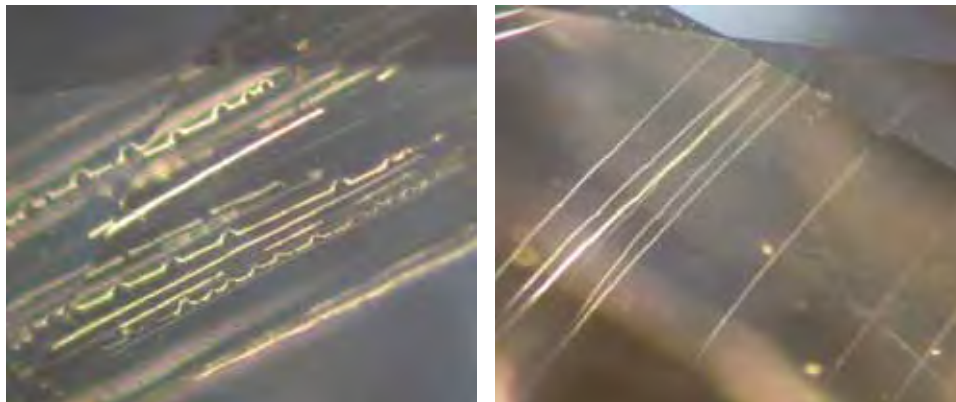


Figure 26. Needle-like inclusions with curved bends (left) and slightly wavy needle-like inclusions (right) in the 3.56 ct sapphire are possibly etch channels. Photo-micrographs by G. Choudhary; magnified 25×.

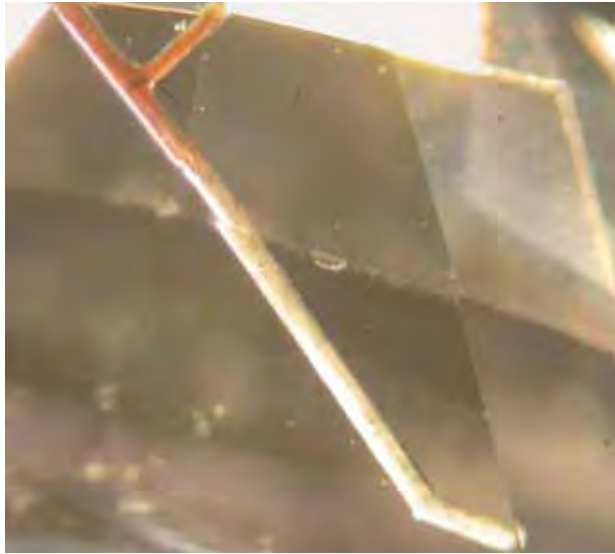


Figure 27. This inclusion in the 3.56 ct sapphire, which resembles a hockey stick, appears to be a hollow tube that is filled with foreign material. Photomicrograph by G. Choudhary; magnified 30 \times .

learned that the sphene is mined near the village of “Fargon Meeru” (Farghāmīrū), which is four hours by jeep down the Kokcha Valley from the lapis lazuli mines and four hours by jeep up from the capital of Badakhshan, Faizābād (Feyzābād).

During a visit to Peshawar in early 2006, Mr. Davies was shown approximately 20 kg of rough material (considerably more than was available at that time from deposits in Pakistan). Unlike the Pakistani material, which varies from yellow to orange-brown (with rare greenish hues), the

Figure 29. When viewed with strong lighting in certain directions, this 6.65 ct sillimanite showed a weak-to-moderate blue-white sheen that is reminiscent of the adularescence displayed by some moonstones. Gift of G. Scott Davies; GIA Collection no. 32498. Photo by C. D. Mengason.



Figure 28. Higher magnification reveals fine needles and platelets in the sapphire, which are oriented in three directions at approximately 60° to one another. They show that the sapphire has not undergone high-temperature heat treatment. Also visible is a portion of the “hockey stick” inclusion in figure 27. Photomicrograph by G. Choudhary; magnified 70 \times .

color of the Afghan sphene he examined fell into a narrower range of light-to-medium greenish yellow to brownish yellow (and, rarely, reddish orange). In addition, while the Pakistani sphene was typically seen as broken crystal fragments, the Afghan rough consisted of smaller but more complete crystals, with some showing glassy surfaces. He reported that most of the stones he has cut from 1.2 kg of selected rough weighed 1–2 ct, with a few in the 3–5 ct range, and only six clean gems were over 5 ct. The largest clean stone he has cut weighed 8.36 ct.

Mr. Davies indicated that sizeable clean gems are difficult to produce for two reasons: the abundance of inclusions and the twin plane that is typical of sphene. Fractures are common in the sphene, and it must be

Figure 30. As seen here through the pavilion of the sillimanite in figure 29, the blue-white sheen shows linear concentrations that correlate to the orientation of parallel needle inclusions. Photomicrograph by James E. Shigley; magnified 20 \times .





Figure 31. These brownish yellow to brownish greenish yellow sphenes from Afghanistan (1.28–1.95 ct) show the narrow range of color that is typically seen in material from this locality. Gift of G. Scott Davies; GIA Collection nos. 32908–32912. Photo by Candice Grobon.

faceted so that the twin plane does not intersect the crown or it will be easily seen. The twin plane does not appear to be a source of weakness; his cutters have not reported any breakage along it. Positioning the twin plane below the girdle restricts the cutter's options for orienting the rough, and therefore reduces the size of the cut gems and decreases the overall yield. For example, Mr. Blauwert reported that he was able to facet only about 70 carats of clean 4–5 mm round brilliants from 450 grams of rough. The bright yellow color and dispersion shown by these stones gave a resemblance to yellow diamond.

Mr. Davies donated five faceted samples (1.28–1.95 ct; figure 31) of the Afghan sphenes to GIA, and gemological properties were collected by one of us (EPQ): color—brownish yellow to greenish yellow; trichroism—medium yellow, yellow-brown, and yellow-green; diaphaneity—transparent; dispersion—strong with predominantly red and green flashes; R.I.—above the limits of a standard refractometer; hydrostatic S.G.—3.53–3.54; Chelsea filter—weak pink; and fluorescence—inert to both long- and short-wave UV radiation. All of the sphenes displayed a 580 nm doublet along with a 510 nm line when viewed with a handheld spectroscope. These properties are comparable to those reported for sphenes by R. Webster (*Gems*, 5th ed., revised by P. Read, Butterworth-Heinemann, Oxford, England, 1994, pp. 375–376). Microscopic examination of the five samples revealed strong doubling, straight and/or angular transparent growth lines, partially healed fractures with two-phase negative crystals containing a liquid and a doubly refractive crystal (in all but one stone), one or more twin planes (in three samples), and a few small crystals (in two of the stones).

EDXRF spectroscopy of three of the samples indicated Si, Ca, and Ti, as expected, along with varying amounts of Al, Fe, Nb, Zr, and Nd with some Y. Interestingly, these sphenes showed a subtle shift in their colors when viewed

under different light sources. In both incandescent light and natural daylight, three of the stones appeared brownish yellow and the other two were greenish yellow. But when they were viewed with a 5500 K non-daylight-equivalent fluorescent light, we observed that the three brownish yellow sphenes shifted to brownish greenish yellow and the two greenish yellow sphenes changed to yellow-green. This shift in color could be due to the interaction between the rare-earth elements in the sphenes and the emission bands of the fluorescent light.

We previously reported on a material (manufactured glass) that exhibited a “color change” also believed to be caused by the interaction of rare-earth elements and certain fluorescent light sources (see Winter 2005 GNI, pp. 364–365). To fully understand this type of “color change,” however, more research would be needed.

Elizabeth P Quinn and BML

Uvite-dravite tourmaline from Morogoro, Tanzania. At the 2006 Tucson gem shows, Menahem Sevdernish of Advanced Quality A.C.C. Ltd., Ramat Gan, Israel, showed one of us (BML) some new tourmalines from Morogoro, Tanzania, that were available in a range of “earth tone” colors. The rough was recovered from alluvial deposits in January 2005, as waterworn pebbles weighing 0.1–5 grams. Most of the rough material (95%) that Mr. Sevdernish obtained weighed up to one gram. Larger pieces have been recovered, but most were too dark (only about one-third of the 2+ gram material was suitable for faceting). He estimated that an average of about 5–10 kg per month of fine facetable material was being produced. The faceted tourmalines typically range from 0.25 to 3 ct, although stones as large as 15 ct have been cut.

Six faceted stones (0.93–9.05 ct; figure 32), representing the range of color of this tourmaline, were loaned to GIA by Mr. Sevdernish, and one of us (EPQ) recorded the following properties: color—brownish orange, brown-yellow, orangy yellow, brownish yellowish green, and yellowish green, with one stone appearing bicolored in yellow-green and reddish brown due to its cut revealing strong pleochroism face-up; pleochroism—moderate to strong in brown-yellow, brown-orange, yellow-brown, or reddish brown, and yellowish green to green; diaphaneity—transparent; R.I.— $n_o=1.641-1.643$, $n_e=1.622-1.623$; birefringence—0.019–0.021; hydrostatic S.G.—3.05–3.07; Chelsea filter reaction—none to medium red; fluorescence—inert to long-wave UV radiation and weak-to-strong chalky greenish yellow to short-wave UV (again, see figure 32). The properties of this stone are generally consistent with those listed for tourmaline by R. Webster (*Gems*, 5th ed., revised by P. Read, Butterworth-Heinemann, Oxford, England, 1994, pp. 168–169); this reference also mentions the short-wave UV fluorescence in tourmaline of this color range from Tanzania. Microscopic examination revealed moderate doubling, straight and angular transparent growth lines, pinpoints and small clouds in two stones occurring

in linear stringers oriented near-parallel to the c-axis and also in three directions at $\pm 28^\circ$ from the c-axis (perpendicular to the three pyramid faces), and a small semitransparent crystal in one stone.

The six samples were chemically analyzed by electron microprobe at the University of Oklahoma, Norman. Energy-dispersive X-ray analysis showed that the tourmalines are Ti-bearing solid solutions between the end members uvite and alkali-deficient dravite. Alkali-deficient (or alkali-free) dravite is an aluminum-rich theoretical end-member in which Al^{3+} is accommodated in the normally divalent Y site by removal of cations from the X (alkali) site (G. Werding and W. Schreyer, "Alkali-free tourmaline in the system $\text{MgO-Al}_2\text{O}_3\text{-B}_2\text{O}_3\text{-SiO}_2\text{-H}_2\text{O}$," *Geochimica et Cosmochimica Acta*, Vol. 48, 1984, pp. 1331–1344). Two of the samples were dominated by the alkali-deficient dravite component, three were dominated by uvite, and one of them was transitional between the end members (slightly uvite-dominant). The Ti concentrations ($\sim 0.5\text{--}1.1$ wt.% TiO_2) were higher in the alkali-deficient dravite

Figure 32. Tourmaline has recently been recovered from the Morogoro region of Tanzania in a range of "earth tone" colors (top, 0.93–9.05 ct). Chemical analysis of these samples revealed that they are uvite-dravite tourmalines. The stones display weak-to-strong chalky greenish yellow fluorescence when exposed to short-wave UV radiation (bottom). Courtesy of Advanced Quality A.C.C. Ltd.; photos by Candice Grobon (top) and Franck Notari (bottom).

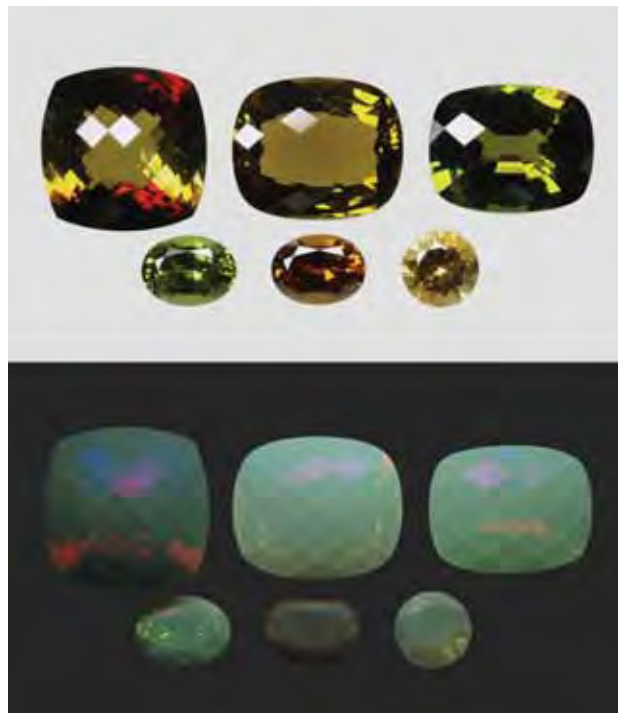


Figure 33. This faceted stone (3.70 ct) and cabochon (14.97 ct) of triploidite were cut from a portion of the rough sample, which was obtained at a local mineral market in Guilin, China. Courtesy of John Lucking; photo © Jeff Scovil.

samples. No Fe or other cations were found at the detectable concentration of $\sim 0.3\text{--}0.5$ wt.% on an oxide basis. The chemical analyses of these samples indicate that gemologists would best refer to them as tourmalines in the uvite-dravite series.

Elizabeth P. Quinn and BML

Triploidite from China. In August 2004, mineral collector John Lucking (Phoenix, Arizona) purchased a reddish orange mineral while visiting a local stone market in Guilin, China. The dealer represented the material as rhodochrosite, but the color, luster, cleavage, and hardness suggested a different mineral. Mr. Lucking was unable to obtain reliable information on the source of the mineral, but based on the associated minerals and other material that he saw for sale, he believes that it came from the tin-polymetallic sulfide deposits near Dachang, Guangxi, China. After returning to the U.S., he asked Mark Kaufman (Kaufman Enterprises, San Diego, California) to cut a cabochon and a faceted stone from this material (figure 33).

In March 2005, Mr. Lucking submitted samples to researchers at the Department of Geosciences of the University of Arizona, Tucson. Single-crystal X-ray diffraction (XRD) and chemical analysis obtained by two of these contributors (MJO and RTD) identified the mineral as triploidite, which has an idealized formula of $\text{Mn}_2(\text{PO}_4)(\text{OH})$ and a Mohs hardness of $4\frac{1}{2}\text{--}5$. Powder XRD data and Raman spectra for the sample are available on the Internet at <http://ruff.geo.arizona.edu/ruff> (search for R050186, and click the icon under "Options"). The results for both electron-microprobe analysis and a crystal structure refinement yielded an empirical formula of $(\text{Mn}_{1.70}\text{Mg}_{0.15}\text{Fe}_{0.06}^{3+}\text{Fe}_{0.05}^{2+}\text{Ca}_{0.04})(\text{P}_{0.97}\text{Fe}_{0.03}^{3+})\text{O}_4(\text{OH}_{0.67}\text{F}_{0.33})$. The triploidite occurred with quartz (identified by Raman spectroscopy), pyrite (identified by XRD), and sphalerite (identified by XRD), which is consistent with an origin from a hydrothermal mineral deposit.

In March 2006, Mr. Lucking loaned the faceted stone and the cabochon (3.70 and 14.97 ct, respectively) to GIA, and donated some fragments of the triploidite. The following gemological properties were collected by one of us (EAF) on the polished samples: color—reddish orange, with very weak pleochroism in reddish orange and yellowish orange; diaphaneity—transparent (faceted stone) and translucent (cabochon); R.I.—1.660–1.679 (faceted stone) and a spot reading of 1.66 (cabochon); birefringence 0.019; hydrostatic S.G.—3.83 and 3.80; and fluorescence—inert to long- and short-wave UV radiation. A cutoff at 420 nm and an absorption band at 530–550 nm were seen in both samples with the desk-model spectroscope. Microscopic examination revealed numerous two-phase (liquid-gas) inclusions and fractures.

The R.I. values are lower than those reported for triploidite in mineralogy textbooks (e.g., 1.723–1.730 for a sample with a Mn/Fe ratio of 3.3:1; C. Palache et al., *The System of Mineralogy, Volume 2*, John Wiley & Sons, New York, 1966, pp. 853–855). However, lower R.I. values are expected for triploidite Mn end-member compositions (Palache et al., 1966), and this is consistent with the much higher Mn/Fe ratio of the gem-quality triploidite reported here. The S.G. of triploidite is typically reported as 3.70, which is considerably lower than the values recorded in the present study. Nevertheless, the density calculated from the crystal structure refinement was 3.82 g/cm³, which is quite similar to the S.G. values that were measured hydrostatically.

UV-Vis-NIR spectra of the two samples showed features similar to those noted in the desk-model spectroscope (e.g., figure 34): A strong absorption at 400–420 nm (actually a doublet) and a broad peak at approximately

Figure 34. This UV-Vis-NIR spectrum of the faceted triploidite shows a strong absorption at 400–420 nm and a broad peak at approximately 520–560 nm, as well as a series of absorption features in the UV region below 370 nm.

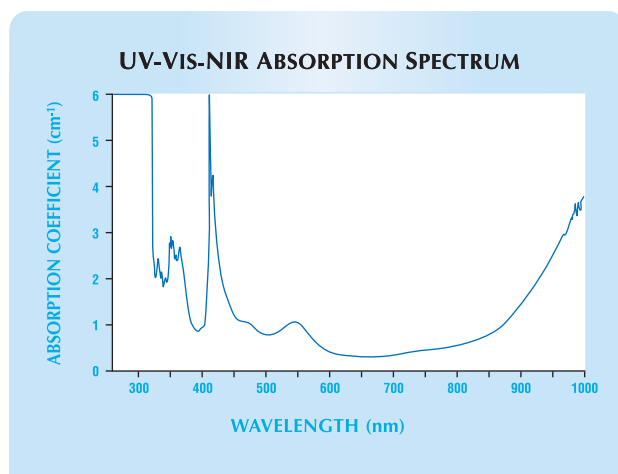


Figure 35. Laghman, Afghanistan is reportedly the source of these vāyrynenites (0.09–0.17 ct). Courtesy of Farooq Hashmi; photo by C. D. Mengason.

520–560 nm. A series of absorption features were also recorded in the UV region below 370 nm.

To our knowledge, this is the first report of gem-quality triploidite.

BML

Eric A. Fritz

Marcus J. Origlieri and Robert T. Downs
Department of Geosciences
University of Arizona, Tucson

Vāyrynenite from Afghanistan. The Spring 2006 Gem News International section (p. 75) documented a faceted vāyrynenite from Pakistan, which had properties comparable to a vāyrynenite from an unspecified locality that was described in the Summer 1994 Lab Notes section (p. 121). Since it is such a rare mineral, we were quite surprised when we received three more faceted vāyrynenites in May 2006, this time from a different locality. The stones were supplied by Farooq Hashmi, who obtained the rough from Afghan suppliers in Peshawar, Pakistan; they reported that the material came from granitic pegmatites in Laghman Province, Afghanistan, but they did not know the identity of the mineral. Over the course of the past two years, Mr. Hashmi saw a few parcels of this material in Peshawar, with a total weight of up to 20 grams, but only small pieces of gem rough were available. He noticed that the Afghan vāyrynenite was more pink and less orange than the Pakistani material.

Gemological properties of the three faceted stones (0.09–0.17 ct; figure 35) were collected by one of us (EAF): color—orangy pink, with orange and pink pleochroism; R.I.— $n_{\alpha}=1.640$ – 1.642 and $n_{\gamma}=1.668$ – 1.770 ; birefringence—0.028; hydrostatic S.G.—3.20–3.25; Chelsea filter reaction—none; and fluorescence—inert to both long- and short-wave UV radiation. An absorption line at 413 nm, and weak bands at 435, 465, 505, and 565 nm, were visible with the desk-model spectroscope in the two larger stones. With magnification, all three stones had numerous fractures and chips, and the largest vāyrynenite also contained a “fingerprint.” EDXRF spectroscopy recorded the expected Mn and P, as well as minor amounts of Fe.

The n_{γ} and birefringence values of the Afghan vāyrynenite were somewhat higher than those reported in the two *Gems & Gemology* entries referenced above, but they are

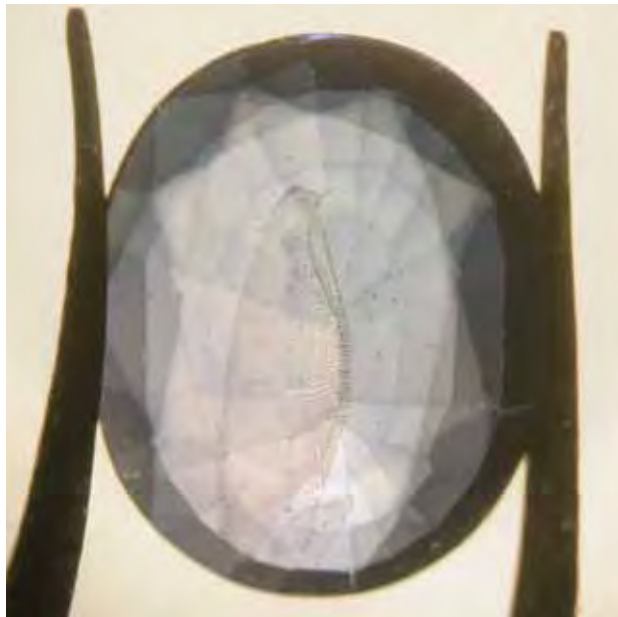


Figure 36. This 2.95 ct pale blue gem was identified as a flame-fusion synthetic sapphire treated by a diffusion process. Photo by G. Choudhary.

still consistent with the values given for väyrynenite in mineralogy textbooks. The absorption in the blue-green to green region of the spectrum (i.e., at 500–570 nm) was somewhat different from the absorption features reported previously. While the Pakistani väyrynenite was also described as orangy pink, slightly more pink color was seen in these Afghan stones, which is consistent with Mr. Hashmi's observations.

BML and Eric A. Fritz

Figure 37. When viewed with immersion, the blue color in the 2.95 ct synthetic sapphire is concentrated along facet junctions, which is an indication of diffusion treatment. Also note the large surface-reaching fingerprint inclusion. Photomicrograph by C. Golecha.



SYNTHETICS AND SIMULANTS

Diffusion-treated synthetic sapphire. Recently, a 2.95 ct transparent blue oval mixed cut (figure 36) was submitted for identification to the Gem Testing Laboratory, Jaipur, India. Initial testing produced values of R.I.—1.763–1.772; birefringence—0.009; uniaxial negative optic sign; and hydrostatic S.G.—3.99. These were consistent with either natural or synthetic sapphire.

When exposed to short-wave UV radiation, the specimen showed a strong patchy chalky blue fluorescence following the crown facets. The pavilion was inert, although a weak internal glow was observed through the pavilion that is commonly associated with synthetic material. There was no reaction to long-wave UV. Such an overall result could indicate the presence of an assembled stone. However, no other features were detected (such as a separation plane) that might indicate a composite material.

With magnification and immersion of the stone in bromoform, a slightly wavy "fingerprint" inclusion was observed that was oriented almost parallel to the optic axis (figure 37). On careful examination at higher magnification, this fingerprint appeared to be made up of opaque, dark, nonreflective flux-like particles arranged in linear and square-shaped patterns (figure 38). A similar but smaller fingerprint was seen inclined to the first; both reached the surface of the stone. No other inclusions were visible.

Further examination with diffuse illumination confirmed the source of the blue color. The patchy, shallow coloration and its confinement to the facet junctions

Figure 38. This fingerprint inclusion in the synthetic sapphire consists of unusual square-shaped arrangements of flux particles. The linear trails are somewhat similar to rows of mineral inclusions in natural stones. The flux was apparently trapped in surface-reaching fractures during the diffusion treatment. Photomicrograph by C. Golecha; magnified 35x.

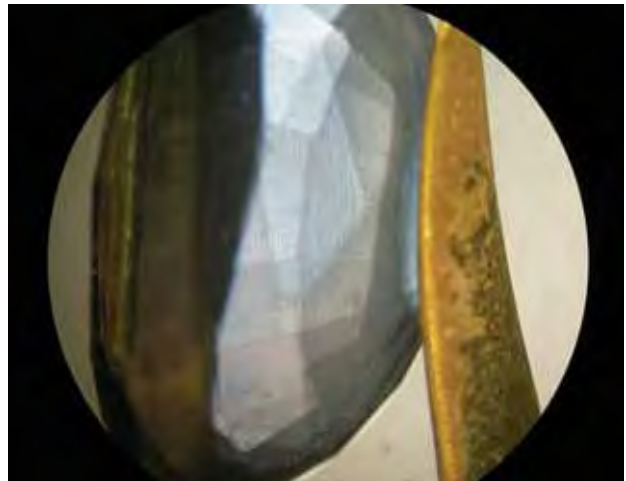




Figure 39. Plato lines are seen when the synthetic sapphire is viewed between crossed polarizers in the optic-axis direction while immersed in bromoform. This feature is strongly indicative of Verneuil synthetic sapphires. Photomicrograph by G. Choudhary; magnified 40 \times .

indicated that the specimen owed its color to a diffusion process (again, see figure 37). No curved color banding or angular color zoning was present, which would have been expected if the color was inherent to the sapphire, synthetic or natural. Since the use of flux is common with high-temperature heat treatment (which is typically required for diffusion treatment), we concluded that a pre-existing fracture may have trapped flux during the diffusion process. However, the square-shaped patterns of the flux particles were highly unusual.

The specimen, still immersed in bromoform, was then examined between crossed polarizers. When viewed down the optic axis, distinct Plato lines were observed (figure 39), which are highly indicative of a Verneuil synthetic origin (see Spring 1999 Gem News, pp. 58–59; S. Elen and E. Fritsch, "The separation of natural from synthetic colorless sapphire," Spring 1999 *Gems & Gemology*, pp.

30–41). This feature consisted of two sets of lines (with one set being more prominent than the other) that formed a crisscross pattern in certain portions of the specimen. Plato lines have traditionally been seen only in pale-colored flame-fusion synthetic sapphires, and this is consistent with this sample since the blue color was a result of the surface diffusion treatment of a pale starting material.

Synthetic materials with natural-appearing features are encountered from time to time (see, e.g., Spring 1991 Lab Notes, p. 45; K. Schmetzer and F. J. Schupp, "Flux-induced fingerprint pattern in synthetic ruby: An update," Spring 1994 *Gems & Gemology*, pp. 33–38; Fall 1996 Lab Notes, pp. 211–212; Fall 2003 Gem News International, pp. 239–240). However, this is the first time we have seen flux inclusions trapped in a square-shaped arrangement. The cause of such an unusual inclusion pattern, as well as the unusual fluorescence characteristics, is unclear. Any suggestions or comments that might help explain these features are welcome.

With other standard gemological properties being similar, magnification is the key to separating natural from synthetic gemstones. However, the several reports of misleading natural-appearing features in synthetic materials reinforce the importance of careful examination.

Acknowledgment: The author is grateful to Gagan Choudhary, assistant director of the Gem Testing Laboratory, Jaipur, for his helpful discussions.

Chaman Golecha (chaman_golecha@yahoo.com)
Gem Testing Laboratory, Jaipur, India

TREATMENTS

Lead glass-filled ruby bead necklace. Gem trade fairs provide an excellent opportunity to screen gem materials currently in the market. During the recent BaselWorld

Figure 40. All of the ruby rondelles in this necklace (13–23 mm in diameter) proved to be lead-glass filled. Photo by H. A. Hänni, © SSEF Swiss Gemmological Institute.





Figure 41. With magnification, numerous gas bubbles are apparent in the glassy substance filling fractures, twin planes, and cavities in this ruby bead. Photomicrograph by H. A. Hänni, © SSEF Swiss Gemmological Institute; magnified 15x.



Figure 42. This ruby bead contains filled fractures and twin planes, as well as cavities with multiple gas bubbles. Photomicrograph by H. A. Hänni, © SSEF Swiss Gemmological Institute; magnified 30x.

fair, the SSEF Swiss Gemmological Institute received a ruby necklace for an identification report. The necklace consisted of 41 translucent “raspberry” red rondelles with a total weight of 290 grams (figure 40). A microscopic inspection revealed the presence of undamaged inclusions such as rutile and negative crystals, indicating that the beads had not been subjected to high-temperature heat treatment.

However, further examination with the microscope showed evidence of glass filling, such as faint bluish flashes and gas bubbles throughout the beads. In addition, many fractures, twin planes, and cavities were filled with a glassy substance (figure 41). Some of the cavities even contained more than one gas bubble,

Figure 43. These semitranslucent ruby crystals from an East African source are typical of the material used for lead-glass filling. Photo by H. A. Hänni, © SSEF Swiss Gemmological Institute.



another sign that the beads were glass filled (figure 42). The presence of the undamaged natural inclusions was not surprising, since modern fissure treatment in rubies can be done with lead-bearing glass at lower temperatures than are commonly used with the traditional borax process. Although the yellowish color in the larger cavities that is characteristic of lead-glass filling was not evident, analysis of the rondelles with EDXRF spectroscopy did reveal the presence of Pb in addition to the expected Al, Cr, Fe, and Ga.

While in Kenya recently, this contributor had the opportunity to see large amounts of rough Tanzanian corundum that was intended for lead-glass treatment in Thailand (figure 43). The tabular crystals were closer to pink sapphire than ruby, but filling of porous material usually causes an increased saturation of the color.

HAH

ANNOUNCEMENTS

AGTA Spectrum Awards competition. The 2007 AGTA Spectrum Awards will recognize outstanding colored gemstone and cultured pearl jewelry designs from North America, as well as achievements in the lapidary arts. Winning entries will be displayed and award recipients honored at the 2007 AGTA GemFairs in Tucson and Las Vegas. The entry deadline is September 22; the competition will be held in New York City during October. For entry forms and more information, visit www.agta.org or call 800-972-1162.

NAJA conference scholarship. The National Association of Jewelry Appraisers is offering a scholarship for gemology students who are interested in exploring a career in gem and jewelry appraising. Open to GIA, FGA, FGAA, FGG, and FCGmA students, the scholarship covers the conference fee for NAJA's 27th Annual Winter Educational Conference January 29–30, 2007, in Tucson. Applications

are available at www.najaappraisers.com or by fax to 718-997-9057. The submission deadline is November 1, 2006, and the selection will be announced December 1.

Conferences

Gems at IAGOD. The 12th Quadrennial International Association on the Genesis of Ore Deposits symposium will be held on August 21–24, 2006, in Moscow, Russia. The program will include symposia titled “Genesis of Gem Deposits” and “Genesis of Diamonds.” A field trip to diamond placer deposits of the Central Ural Mountains will take place on August 25–31. Visit www.iagod.sgm.ru or e-mail iagod@sgm.ru.

Goldschmidt 2006. 16th Annual V.M. Goldschmidt Conference will take place August 27–September 1 in Melbourne, Australia. This important geochemistry conference will feature a session titled “The deepest lithosphere and beyond: Diamonds and related research, a session in honour of Jeff Harris.” Visit www.goldschmidt2006.org or e-mail goldschmidt2006@tourhosts.com.au.

Diamond 2006. The 17th European Conference on Diamond, Diamond-like Materials, Carbon Nanotubes, and Nitrides will be held September 3–8 in Estoril, Portugal. Presentations on the growth, processing, and characterization of diamond will be given at this meeting. Visit www.diamond-conference.elsevier.com or e-mail Nina Woods at n.woods@elsevier.com.

Santa Fe Symposium changes venue in 2006. The 20th annual Santa Fe Symposium on jewelry manufacturing technology will be held in Nashville, Tennessee, on September 10–13. Visit www.santafesymposium.org.

Minerals, Magmas and Megastructures. Diamonds will be among the topics included at the 2006 Geological Society Ferman Meeting, titled *Minerals, Magmas and Megastructures*, which will be held at the Natural History Museum in London on September 13–15, 2006. Visit www.geolsoc.org.uk/fermor2006.

Clasp: A Convergence of Jewelers. This new conference aimed at small manufacturers, metalsmiths, jewelry designers, and bench jewelers will be held September 15–17 in Nashville, Tennessee. The educational program will cover all aspects of the art, methodology, and business of jewelry making, from design to marketing. Visit <http://secure.lenos.com/lenos/riogrande/clasp>.

Hong Kong Jewellery & Watch Fair. Held at the AsiaWorld-Expo (September 18–23, 2006) and the Hong Kong Convention & Exhibition Centre (September 19–23), this show will also host GIA GemFest Asia (on pearls) on Thursday, September 21. RSVP to giahk@netvigator.net, or call +852-2303-0075 in Hong Kong. A num-

ber of educational seminars are also planned. For more information visit www.jewellerynetasia.com/exhibitions.

Gem and Mineral Conference in China. The 1st International Minerals & Gem Crystal Conference and Exhibition will be held October 9–10 in Beijing. The program includes educational seminars on gem and mineral localities, collecting, and marketing in China, and optional visits to gem mines in Hunan Province. Visit www.aaamineral.com/Minerals/conference/conference_details.asp.

Exhibits

Upcoming GIA Museum Exhibits. Beginning August 27, 2006, in conjunction with the 4th International Gemological Symposium, the GIA Museum in Carlsbad will present “Celebrating Excellence in Gems & Jewelry,” an exhibit featuring mineral specimens, finished gems, jewelry, and jeweled objects that are superlative examples of their type or have special provenance or historic significance. This exhibit will remain open until November 30, 2006.

During the International Gemological Symposium, there will be additional exhibit areas open throughout the Institute, including a display of important and historic diamond replicas from Graff; photos by noted photographers Harold & Erica Van Pelt, Tino Hammid, and Robert Weldon; and gems and jewelry from the GIA Collection; these will remain on view until March 2007.

King Tut Returns. “Tutankhamun and the Golden Age of the Pharaohs,” an exhibition of more than 130 artifacts from the tomb of King Tut and other royal tombs in Egypt's Valley of the Kings, are on display at the Field Museum in Chicago through January 1, 2007. Among the items included are a gem-studded gold diadem and a jeweled pectoral ornament. Only a few of the artifacts in this exhibit were part of the famed 1977 exhibition, and many have never traveled outside Egypt. Visit www.kingtut.org.

ERRATA

1. The biography for Dr. Wuyi Wang in the Spring 2006 Most Valuable Article Award section (p. 3) should have read, “Wuyi Wang is a research scientist for GIA Research and Identification in New York. He holds a Ph.D. in geology from the University of Tsukuba in Japan, and has considerable experience in studying diamond geochemistry.” *Gems & Gemology* regrets the error.
2. In the Spring 2006 article by S. F. McClure et al., “Identification and durability of lead glass-filled rubies,” the carat weight given in figure 5 on p. 26 was in error. The correct weight of the stone is 2.31 ct, as stated on p. 33. We thank Brent Malgarin, Elegant Gems Ltd., Spokane, Washington, for bringing this to our attention.

EDITORS

Susan B. Johnson
Jana E. Miyahira-Smith
Stuart Overlin

The Heartless Stone: A Journey through the World of Diamonds, Deceit and Desire

By Tom Zoellner, 294 pp., publ. by St. Martin's Press, New York, 2006. US\$24.95

The mystique and value of diamonds is a double-edged sword, inspiring the passions that help fuel an industry with \$65 billion in worldwide sales while engendering a great number of myths and not-so-noble emotions. Like several other mainstream books about diamonds, *The Heartless Stone* offers a pastiche of history, myth, assumption, fact, and misinformation into an engagingly written stew. The book describes diamond mining in Canada, Brazil, Angola, and Russia; provides an overview of "The Cartel" (the De Beers Diamond Trading Company); and examines diamond cutting in India as well as consumer markets of the U.S. and Japan. Unfortunately, much of this information is inaccurate.

Typical of how information is presented in this book is the first chapter, in which the author juxtaposes his own ill-fated engagement and the diamond that sealed it with the history of the Central African Republic (CAR). He recounts the sociopolitical troubles of the CAR from its French colonial past through the reign of Emperor Bokassa in the 1970s and '80s, in the process maintaining that the republic is part of the "conflict diamonds" trade. Zoellner's choice of the CAR as an example is odd, given that the country, while governed badly, has not experienced widespread conflict or civil war. Nor has it ever been named by the United Nations, Kimberley Process, or any

nongovernmental organization as a source of conflict diamonds—its economy, for the most part, is sustained by foreign aid.

Even more problematic is his statement that conflict diamonds comprise 14% of the stones in the market. In reality, at the peak of the Angolan and Sierra Leone civil wars, conflict diamonds represented between 4% and 5% of all diamonds in the market. *Illicitly traded* diamonds, those smuggled or under declared to avoid taxes, made up an estimated 14% before the 2003 Kimberley Process forced accountability.

In the chapter on the U.S. diamond market, titled "The Big Nothing," the author states that the markup on diamond engagement rings and other diamond jewelry "is nothing short of outrageous," adding that the term *keystone* was developed "several years ago" as a euphemism to disguise this fact. Of course, *keystone* has been in use for many decades, and retail jewelry profit margins are in fact in line with those of similar consumer products such as apparel and sporting goods. Mall jewelers, Zoellner says, "have the power to foist some of the worst deals onto the consumer thanks to their mammoth volumes," failing to note that those same jewelers typically pay 5–6% assessments on gross sales as part of their mall lease agreements. Zoellner does discuss the impact of the Internet but fails to note how deeply it has cut into the margins on diamond solitaires.

The chapter on India, "The Stone Mills," asserts on page 213 that children constitute 10% of the workforce in the country's diamond industry, citing a 1997 statement from the

International Confederation of Free Trade Unions—which at the time represented the Belgian diamond workers' unions in bargaining for benefits in the face of Indian competition. Four pages later, however, Zoellner credits the same source for a statement that "20% of India's [diamond] workers were underage." In reality, an independent survey of India's diamond labor force conducted by Ferguson Associates in 2003 found that less than 3% of India's diamond workers were under 15 years old, and many of these were apprentices of family-run businesses. The author also fails to point out that the great majority of India's diamond workers earn wages well above the national average, and that in recent years Surat has made a dramatic transformation from one of the most poverty-stricken cities in India to a center of budding prosperity (as a recent visit by this reviewer attests).

Old myths long established as apocryphal, such as the "Belgian" (Asscher was Dutch) who cleaved the Cullinan diamond fainting after he struck the first blow (there is no evidence this occurred), are presented as fact. At the same time, newer myths, such as De Beers crushing the attempt to develop the Crater of Diamonds deposit in Arkansas into a viable mine, are given new life. On the latter, Zoellner spends pages

**This book is available for purchase through the GIA Bookstore, 5345 Armada Drive, Carlsbad, CA 92008. Telephone: 800-421-8161; outside the U.S. 760-603-4200. Fax: 760-603-4266. E-mail: myorder@gia.edu*

discussing the alleged potential of the "kimberlite" (actually lamproite) deposits at Murfreesboro despite extensive bulk sampling performed in the late 1990s by the state of Arkansas (which he dismisses as a few "core samples") that clearly established the deposit as uneconomic (about 1.1 ct/100 tonne at \$12.30/ct; see D. P. Dunne, "Diamond economics of the Prairie Creek lamproite, Murfreesboro, AR, USA," *Ore Geology Reviews*, Vol. 22, No. 3-4, 2003, pp. 251-262).

No one disputes that conflict diamonds remain an issue today: Even at less than 1% they are too numerous. And certainly not every diamond worker in India finds prosperity and not every consumer in the U.S. gets a great deal on a diamond. But these facts must be considered against the whole picture, which was not offered here. The tragedy of this book is that, like his literary predecessors Edward Jay Epstein, Matthew Hart, and Janine Roberts, Zoellner possesses the skill and drive to produce a work that could have lasting value, but instead chose to perpetuate misinformation.

RUSSELL SHOR

*Gemological Institute of America
Carlsbad, California*

Making the Most of Your Flex-shaft

By Karen Christians, 96 pp., illus., publ. by MJSA/AJM Press and the Ganoksin Project, Providence, RI, 2006. US\$34.95

As Karen Christians states in her new book, one of the first power tools a new jeweler should purchase is a flex-shaft. This lightweight device's electric motor powers a flexible shaft that drives an assortment of rotational tools such as burrs and drills, or oscillating tools such as hammers. *Making the Most of Your Flex-shaft* is a clearly written, easy-to-understand guide to this important jewelry manufacturing tool.

Christians takes the time to carefully show how the electric motor of the flex-shaft works, right down to internal views and schematics. Explaining torque vs. rpm or the relationship between volts and ohms can be difficult, but she succeeds in using analogies to make it easy for the reader to understand the inner workings of the machine. She also gives a brief history lesson on the inventors of the flex-shaft and chuck key (the tool used to tighten and loosen attachments on the handpiece).

Christians then explains why different models of the flex-shaft may fit different uses more or less effectively. Using this book as a guide, jewelers looking to purchase a flex-shaft will be able to choose a unit whose motor size will best suit their needs.

Of course, the flex-shaft itself is only half the equation, the other being the tool that is attached to it. There are innumerable varieties of tools that can be used for operations such as cutting, grinding, texturing, and polishing, and each can be made from a range of different materials. Depending on the type of metal being worked or the speed being used, the right tool may be made from high-speed steel, from carbide, or from another material. Christians uses a handy chart to categorize the different operations a user may need to perform, and recommends the specific tool or variety of tools that is best for each. This can be of tremendous value to a beginner and can prevent the purchase of costly tools that will never be used. The category of polishing tools itself is so large that it has its own chart to explain all the different varieties a jeweler may need.

In addition to the basics of the flex-shaft and its uses, there is some very helpful information on various add-on tools that are available, such as tools to assist in the stone setting process, wax carving jigs, and drill press attachments. This information on items that are clamped on or attached to the hand pieces is of value to the intermediate-level jeweler as well, and shows the flexibility of this tool platform.

Possibly the most important section of the book covers the maintenance that these fairly simple machines require. The flex-shaft is a relatively expensive purchase for a beginning jeweler, and good maintenance will greatly extend its operating life. Christians is very specific on the required lubrication and cleaning, and even the changing of the motor brushes, to ensure optimal performance.

Finally, a few choice tips and tricks on using the flex-shaft in unusual ways that even a seasoned jeweler may find useful are added near the end of the book.

Overall, this is a very useful and easy-to-understand text covering the operation and maintenance of one of the most frequently used tools in the jeweler's arsenal. I would recommend it for beginning- to intermediate-level jewelers.

MARK MAXWELL

*JA Certified Master Bench Jeweler
Gemological Institute of America
Carlsbad, California*

Charming: The Magic of Charm Jewelry

*By Deborah Alun-Jones and John Ayton, 112 pp., illus., publ. by Thames & Hudson Inc., New York, 2005. US\$19.95**

Judging from the attention they have received in the fashion media, charm bracelets have once again become *de rigueur* for the stylish woman. Yet for as long as there has been personal adornment, charms have been worn. Because charm jewelry often commemorates important events in the wearer's life or represents personal beliefs, charms tend to have high sentimental value.

This book offers a lovely look at charms, their history, and the reasons they are worn. Heavily illustrated with photographs of wonderful charms and women wearing charm jewelry, it is broken into six chapters: Magical Talismans, Spiritual Devotion, Just for Luck, Love Tokens,

Style and Sensibility, and Milestones and Celebrations. Especially engaging are the brief anecdotes describing pieces worn by famous people, such as the charm bracelet of crosses given to the Duchess of Windsor by the Duke of Windsor.

As a collector of charms, I greatly enjoyed this book. Attractive and interesting, it held my attention until the very end. It's the perfect addition to the library of anyone who appreciates charm jewelry.

JANA E. MIYAHIRA-SMITH
Gemological Institute of America
Carlsbad, California

Bedazzled: 5,000 Years of Jewelry

*By Sabine Albersmeier for The Walters Art Museum, 64 pp., illus., publ. by D. Giles Ltd., London, 2005. US\$9.95**

Each summer, travelers descend on European towns in search of the small museums that guidebooks call "little gems." This slim volume captures the glint of a stateside gem, The Walters Art Museum of Baltimore, a city better known for crab cakes than classicism.

Assistant curator of ancient art Sabine Albersmeier presents 50 key items from the Walters' collection dating from the 2nd millennium BC to the early 20th century. These works were once part of the private collection of Henry Walters, son of railroad magnate and art collector William T. Walters. At his death in 1931, the younger Walters bequeathed to the city and citizens of Baltimore an entire jewelry collection culled from World's Fairs, expositions, and antiquarians around the globe.

Highlights include two lavish gemstone-encrusted gold bracelets dating to the first century BC, which exemplify ancient Greek embellishments of inlay, cloisonné, and beading. Spain's 6th century Visigoth past is dramatized by two gemstone and glass *fibulae*, the ornamental pins used to fasten medieval garments.

Elaborate crucifixes and rings from the Renaissance are well represented by clean photography and color details.

The collection's later works include a stunning piece Walters acquired from René Lalique at the 1904 Louisiana Purchase Exposition—a *plique-à-jour* enamel, glass, gold, and blue sapphire pansy brooch. Another floral masterpiece, a gold-stemmed Tiffany corsage ornament with Montana sapphires and demantoid garnets, won the grand prize at the famed 1900 Paris *Exposition Universelle*. The Walters' treasures are complemented by loans from the Zucker family ring collection, which include an interlocking ruby-and-diamond gimmel ring from 1631.

A whirlwind summary of Western jewelry traditions and a compact glossary expand the 7" x 7" (about 18 x 18 cm) catalogue's accessibility to audiences beyond devotees of antiquity, history, and jewelry making.

Albersmeier is organizing curator for the traveling exhibit, which is scheduled to visit Nashville's Frist Center for the Visual Arts from September 2006 to January 2007 and the John and Mable Ringling Museum of Art in Sarasota, Florida, from February to May 2007.

MATILDE PARENTE
Libertine
Indian Wells, California

Modernist Jewelry, 1930–1960: The Wearable Art Movement

By Marbeth Schon, 227 pp., illus., publ. by Schiffer Publishing Ltd., Atglen, PA, 2004. US\$69.95

Modernist jewelry came at a crossroads of "isms"—Constructivism, Primitivism, Modernism, Surrealism, Cubism, Expressionism, Dadaism—each contributing to the overall artistic sensibilities. The pioneering modernist designers developed their voices at a time when the art movement was prevalent, giving rise to a panoply of seemingly divergent aesthetics.

This book examines the work of 175 of the most important American modernist jewelry artists.

As with nearly every jewelry movement, some of the resulting works may appear crude or elemental. Indeed, one common theme during the modernist period was a lack of embellishment, as artists preferred the materials left in their original state as much as possible. Gemstones, wood, and other natural materials were roughly tumbled and cut into bold shapes. Often the metal was allowed to show the "imperfections" of hammering, texturing, and natural patination, while the necessary functional parts of jewelry—findings, pins, etc.—were integrated into the overall design.

Many of the biographical sketches in *Modernist Jewelry* give a true sense of the artists' struggles and creativity, though others are much briefer, in some cases because little information exists. For instance, the two gorgeous photos of Madeline Turner's earrings and enamel work are accompanied by a mere two-sentence bio. For the modernist Arthur King, there are his maker's marks and photos of a ring and a cuff bracelet, yet no biography.

This book is especially interesting when the iconic jewelry of the artist appears with the bio. The maker's marks are not shown as line drawings but as crisp images of the actual stampings, though only 73 hallmarks are presented. Also of benefit are photos of the artists that visually connect the creator with the final product. "Prices"—or values, if you will—are used sparingly and appropriately as a range to reflect such variables as condition, rarity, and geography.

Between 1930 and 1960, these modernist designers, jewelers, and metalsmiths laid the groundwork for the next two decades of metal work and wearable art jewelry, giving artistic sustenance to the generations of respected artists who have followed.

GAIL BRETT LEVINE
National Association of Jewelry
Appraisers
Rego Park, New York

'06

gemological
ABSTRACTS

EDITORS

Brendan M. Laurs
Thomas W. Overton
 GIA, Carlsbad

REVIEW BOARD

Christopher M. Breeding
 GIA Laboratory, Carlsbad

Jo Ellen Cole
 Vista, California

Eric A. Fritz
 GIA Laboratory, Carlsbad

R. A. Howie
 Royal Holloway, University of London

Alethea Inns
 GIA Laboratory, Carlsbad

Hyejin Jang-Green
 GIA Laboratory, New York

Paul Johnson
 GIA Laboratory, New York

David M. Kondo
 GIA Laboratory, New York

Taijin Lu
 GIA Research, Carlsbad

Wendi M. Mayerson
 GIA Laboratory, New York

Kyaw Soe Moe
 GIA Laboratory, New York

Keith A. Mychaluk
 Calgary, Alberta, Canada

James E. Shigley
 GIA Research, Carlsbad

Boris M. Shmakin
 Russian Academy of Sciences, Irkutsk, Russia

Russell Shor
 GIA, Carlsbad

Rolf Tatje
 Duisburg University, Germany

Sharon Wakefield
 Northwest Gem Lab, Boise, Idaho

COLORED STONES AND
ORGANIC MATERIALS

Beryl and its color varieties. A. Falster et al., Eds., *extraLapis* English, No. 7, 2005.

This is an English translation of *extraLapis* No. 23, *Aquamarine & Co.* (2002), which has been updated with some new information. It begins with a summary of beryl-group mineralogy and crystallography that includes details on some of the more obscure minerals of the beryl group (i.e., pezzot-taite, bazzite, and stoppaniite). Emerald is given only passing mention, as it was addressed in a previous *extraLapis* volume, *Emeralds of the World* (see Fall 2002 *Gems & Gemology*, p. 284). Reviews of all major localities follow, and recent information on new finds in Canada and Finland is provided.

Some of the more interesting locality reviews include a detailed analysis of China's future potential as a source of gem beryl, a review of beryl mining in southern California, and a discussion of the "mysterious golden water of Tajikistan" (heliodor reportedly from this locality is thought by the author to be irradiated goshenite from elsewhere).

The issue concludes with a brief review of gem beryl pricing and a history of the discovery, mining, and industrial uses of beryllium. Like all *extraLapis* publications, this one is well illustrated with high-quality gem and mineral photographs as well as detailed maps and line drawings. TWO

Les corindons à changement de couleur [Color-changing corundum]. L. Massi (laurent.massi@cnr-immn.fr), *Revue de Gemmologie a.f.g.*, No. 152, 2005, pp. 16–19 [in French with English abstract].

By examining natural and synthetic samples of color-change

This section is designed to provide as complete a record as practical of the recent literature on gems and gemology. Articles are selected for abstracting solely at the discretion of the section editors and their reviewers, and space limitations may require that we include only those articles that we feel will be of greatest interest to our readership.

Requests for reprints of articles abstracted must be addressed to the author or publisher of the original material.

The reviewer of each article is identified by his or her initials at the end of each abstract. Guest reviewers are identified by their full names. Opinions expressed in an abstract belong to the abstracter and in no way reflect the position of Gems & Gemology or GIA.

© 2006 Gemological Institute of America

corundum with UV-visible spectroscopy, the author describes four different types of color change, based on trace-element content. Type 1, which changes from blue (daylight) to purple (incandescent and fluorescent light), contains chromium, iron, and titanium. Type 2, which changes from green (daylight) to orange (incandescent/fluorescent), contains only iron and titanium. The color change in type 3 sapphires, which involves green and red (daylight color is different from that seen with incandescent light, which is different from the color in fluorescent light), is due to vanadium. Type 4, which shows bluish green (daylight) and reddish violet (incandescent/fluorescent), contains chromium, iron, and nickel.

Almost all natural color-change corundum belongs to type 1, although type 2 is also found in natural corundum. Type 3 can be seen in corundum of various origins. Verneuil synthetics show either type 1 or type 3. Type 4 occurs in hydrothermal synthetics.

A natural sapphire from Myanmar studied by the author showed purple, bluish green, and orangy yellow colors. This sapphire also contained nickel, which is unusual in natural corundum. RT

Gem corals: Classification and spectroscopic features. V. Rolandi, A. Brajkovic [anna.brajkovic@unimib.it], I. Adamo, R. Bocchio, and M. Landonio, *Australian Gemmologist*, Vol. 22, No. 3, 2005, pp. 285–297.

Several gem corals of the classes *Hydrozoa* and *Anthozoa* of the phylum *Cnidaria* were analyzed by FTIR and Raman spectroscopy. Such spectroscopic characterization has proved useful for determining the main features of the mineral phases (calcite or aragonite) and of the organic contents in each sample. Chromophore complexes belonging to the carotenoid family were detected. Coral zoology is also discussed. RAH

Identification of an imitation of pearl by FTIR, EDXRF and SEM. T. L. Tan, T. S. Tay, S. K. Khairoman, and Y. C. Low, *Journal of Gemmology*, Vol. 29, No. 5/6, 2005, pp. 316–324.

In recent years, there has been an increase in the quality and number of imitation pearls in the marketplace. Many imitation pearls now show strong iridescence and thus are not easily distinguished by visual observation. This article reports on an investigation showing that EDXRF and FTIR spectroscopy, in combination with scanning electron microscopy (SEM), can lead to reliable identification of both imitation and cultured pearls. Reactions to UV radiation were also studied. The objects tested in this investigation were five natural-color freshwater cultured pearls, four dyed freshwater cultured pearls, four imitation pearls, one bead representative of those commonly used in cultured pearls, and one bead used for imitation pearls.

EDXRF spectroscopy showed that both the naturally colored and dyed cultured pearls, as well as the bead used for pearl culturing, contained C, O, and Ca, the compo-

nents of calcium carbonate (CaCO_3). The EDXRF spectra of the imitation pearls showed only C and O, with peaks consistent with the presence of polymers. No Ca was present. EDXRF data for the imitation pearl bead showed the presence of O, Si, Al, and Na, with peaks indicating glass.

FTIR data for the naturally colored and dyed freshwater cultured pearls, as well as the cultured pearl bead, showed typical absorption peaks for CaCO_3 . The FTIR data for the imitation pearls and bead were very different and easily distinguished from that of the cultured pearls. Spectra for the imitation pearls revealed polymeric material but no CaCO_3 peaks. The imitation bead was opaque to infrared below 2500 cm^{-1} and showed a broad band centered at 3510 cm^{-1} , which indicated that it was made from a different material than the imitation pearl coating.

The SEM results also identified obvious differences between the cultured and imitation pearls. Both the naturally colored and dyed cultured pearls showed layered, contoured, flake-like patterns consistent with crystalline layers of CaCO_3 . In contrast, the pearl imitations showed small cubic particles, all of approximately the same size, randomly distributed over the whole surface. The dense suspension of these polymeric cubes created the iridescent effect that mimicked the iridescence of nacre. WMM

Identification of seawater cultured pearls with dyed nucleus. L. Li and M. Yang, *Journal of Gems and Gemmology*, Vol. 7, No. 2, 2005, pp. 7–8 [in Chinese with English abstract].

Recently, saltwater cultured pearls with unusual colors have been seen in the Chinese market. These products were developed in 2002 by a company in Guangxi using dyed nuclei and other techniques. In this article, the authors, including one of China's top pearl researchers (LL), report their preliminary results for the identification of these saltwater cultured pearls.

Three loose cultured pearls ("rosy red," orange, and bluish gray), one bluish gray pearl earring, and one "rosy" red pearl earring were collected for the investigation, and their undyed counterparts were used for comparison. To collect Raman spectra from the nuclei, the nacre was partially peeled off to expose the dyed surfaces. Microscopic observation was also performed.

It was found that clear, parallel color bands from the dyed nucleus could be seen with strong transmitted light. The colored nuclei and colorless nacre layers could also be seen through the drill holes. The "rosy" red and bluish gray samples showed weak bluish white fluorescence to UV radiation. Raman spectra of the cultured pearl surfaces were the same, regardless of whether the nuclei were dyed or untreated. However, Raman spectra of the actual dyed nuclei (even when taken through the drill hole) displayed a strongly fluorescent background and several weak peaks in the $1600\text{--}1400\text{ cm}^{-1}$ range that are related to the dye materials.

The identification of these saltwater cultured pearls with dyed nuclei can be made using both traditional and advanced gemological techniques. TL

The study of phosphorus in seawater cultured pearls using FTIR. L. Wang, P. Zhou, Y. Liu, and Y. Tang, *Spectroscopy and Spectral Analysis*, Vol. 25, No. 6, 2005, pp. 866–869 [in Chinese with English abstract].

The luster of saltwater cultured pearls is proportional to their phosphorus content. However, due to P's low concentration, it is unclear where and in what state this element exists. In this article, the authors report their investigations of structural variations in saltwater cultured pearls using high-resolution FTIR spectroscopy, powder X-ray diffraction (XRD) analysis, and differential thermal analysis (DTA) techniques.

Cultured pearls of similar color and size were divided by luster into several groups of 50. The nacre layers were collected and crushed into powder; the powdered samples were further subdivided into several groups that were heated to 160°C for varying durations (2 hours, 4 hours, etc.). Analyses by FTIR, XRD, and DTA were conducted before and after heating.

Several new IR absorption peaks (1083, 1049, 630, and 600 cm⁻¹) were seen in the heated samples. These peaks were not related to carbonates, and their intensities increased with heating time. XRD results showed two new diffraction peaks in the heated samples. Analysis of the FTIR and XRD results suggested that the P may be present in a hydroxyl apatite compound (called *pahuite* in the abstract) in the pearls. TL

Study on relationship between luster and surface structure of pearl. L. Cao, S. Guo, and L. Shi, *Journal of Gems and Gemmology*, Vol. 7, No. 3, 2005, pp. 23–25 [in Chinese with English abstract].

The relationship between surface features and luster in pearls has been extensively investigated since the 1950s. Good luster generally results from uniform surface structures; however, investigators are still trying to confirm this relationship. In this article, the authors investigate the surface features of Chinese cultured pearls.

Pink freshwater cultured pearls from Jiangsu and Zhejiang Provinces and white saltwater cultured pearls from Guangdong Province were observed with polarized microscopy and scanning electron microscopy. The samples were divided into three groups (poor, fair, and good) based on their luster.

There was a clear relationship between luster and surface features. SEM images showed spots, voids, and foreign materials on the surface of the freshwater cultured pearls with poor luster; in addition, the aragonite crystals in the nacre were not distributed uniformly and had an average size of about 4 μm. Samples with good luster had aragonite crystals of about 3 μm that were uniformly

arranged in a layered structure. The freshwater cultured pearls with fair luster had characteristics that were intermediate to those described above. There was a similar relationship between luster and surface structure in the saltwater cultured pearls; however, the size of the aragonite crystals was about 2.5 μm for samples showing good luster.

The authors suggest that voids between the aragonite crystals in the cultured pearls showing poor luster could be filled to enhance their luster. TL

DIAMONDS

Diamond formation in metal-carbonate interactions. J. Siebert [julien.siebert@lmcp.jussieu.fr], F. Guyot, and V. Malavergne, *Earth and Planetary Science Letters*, Vol. 229, No. 3–4, 2005, pp. 205–216.

While the earth's inner core could contain the metal-carbon alloy Fe₃C, the carbon within the mantle is predominantly composed of carbonates (and diamond). Thus, a better understanding of carbon alloy and carbonate chemistry would aid the understanding of diamond formation within a young Earth. Reduced silicon alloyed with iron metal reacts chemically with FeCO₃ (siderite) at pressures of 10–25 GPa and temperatures of 1700–1800°C according to: $2\text{FeCO}_3 + 3\text{Si}_{(\text{in metal})} = 2\text{Fe}_{(\text{in metal})} + 3\text{SiO}_{2(\text{stishovite})} + 2\text{C}_{(\text{diamond})}$. The only source of C for diamond formation was the carbonate phase. Prior research and modeling suggested carbonate-containing fluids, not metals, were the likely carbon source for diamond.

Thermodynamic modeling of this reaction suggests that under mantle conditions, no Si-bearing metal can coexist with carbonates. Therefore, a high concentration of silicon would encourage diamond formation by reaction with the carbonates under the kinetically favorable conditions of high temperature and pressure. RAH

Kalimantan diamond: Morphology, surface features and some spectroscopic approaches. T. T. Sun [fegemlab@singnet.com.sg], P. Wathanakul, W. Atichat, L. H. Moh, L. K. Kem, and R. Hermanto, *Australian Gemmologist*, Vol. 22, No. 5, 2005, pp. 186–195.

Alluvial diamonds are found around the Landak River in western Kalimantan (the Indonesian portion of Borneo), in the Linhaisai minette in the headwaters of the Barito River in central Kalimantan, and in the Banjarmasin-Martapura area of southeastern Kalimantan. Mining activities date back to 600 AD; fine blue, pink, and canary yellow diamonds have been reported.

A 2002 visit to the Banjarmasin-Martapura area, which produces about 200 carats per month, is described. After a general outline of the mining and trading activities, the authors report the characteristics of 14 rough gem-quality diamonds that ranged from 0.03 to 1.82 ct and were colorless to yellow and brown. The diamonds

showed variable crystal habits (octahedron, tetrahedron, dodecahedron, and macle), and surface features consisted of percussion scars and common black and brown radioactivity stains. They showed predominantly blue and green (and minor yellow) cathodoluminescence. Inclusions identified by Raman spectroscopy consisted of diamond, zircon, perovskite, and diopside. FTIR spectra showed that both type IaA and type IaB diamonds were present. RAH

Kimberlites of Zimbabwe: Abundance and composition.

A. D. Khar'kiv, E. F. Roman'ko, and B. M. Zubarev, *Russian Geology and Geophysics*, Vol. 46, No. 3, 2005, pp. 318–327.

The authors provide data on several unusual kimberlite pipes in Zimbabwe, at Chingwisi and River Ranch in the south and Quest in the north. The Chingwisi pipe is capped with a hard calcium carbonate horizon known as *calcrete*; it formed within the upper few meters of the pipe and has a much different mineral composition (>90% carbonates) than the underlying unaltered kimberlite. This suggests that such an outcrop of kimberlite could go unrecognized. However, indicator-mineral collection revealed many of the usual kimberlite pathfinders, including pyrope, picroilmenite, Cr-spinel, and clinopyroxene. Detailed chemical analysis of these indicators led the authors to conclude that the Chingwisi pipe has the potential to host diamonds and is mineralogically similar to pipes in the Sakha area of Russia.

The two Quest pipes yielded unique indicator-mineral chemistry. Although both are diamondiferous, only one G10 (high Cr) subcalcic garnet grain was collected, whereas abundant Na-bearing pyrope-almandine garnets were found (up to 40% of the indicators). This unique garnet signature was apparently used by Reunion Mining of Australia to search for more kimberlites in the region. The authors believe the garnets were derived from upper-mantle eclogites that were incorporated into the kimberlite magma. Only generic information is provided for the River Ranch pipe, which hosts Zimbabwe's single active diamond mine.

Although Zimbabwe has a large Archean-aged craton (where Clifford's Rule, simplified, suggests diamond-bearing kimberlites may be found), all the diamondiferous pipes studied by the authors are located *outside* of this craton. Thus, the data and conclusions made by the authors will allow scientists and explorers to modify their theories on diamond formation and emplacement. KAM

Mineral inclusions in diamonds from the Panda kimberlite, Slave Province, Canada. R. Tappert [rtappert@ualberta.ca], T. Stachel, J. W. Harris, N. Shimizu, and G. P. Brey, *European Journal of Mineralogy*, Vol. 17, No. 3, 2005, pp. 423–440.

The mineral inclusions in 90 diamonds from the Panda kimberlite (Ekati mine, Northwest Territories, Canada)

were chemically analyzed using electron microprobe and secondary ion mass spectrometry techniques, and nitrogen aggregation characteristics of the host diamonds were measured by IR spectroscopy. The Panda diamonds are derived principally from peridotitic sources (85%), with a minor content of eclogitic diamonds (10%). Ferropericlasite-bearing diamonds (5%) contain combinations of this mineral with olivine, with Mg-Al spinel + olivine, or with a pure silica phase. The chemical characteristics of these inclusions indicate a lithospheric origin from ferropericlasite-bearing dunites; however, ferropericlasite coexisting with CaSiO₃ (probably originally Ca-perovskite) is regarded as evidence for a lower-mantle origin.

Major-element compositions indicate that the peridotitic diamonds formed in a moderately depleted environment. Inclusion geothermobarometry indicates formation of the peridotitic diamonds in the temperature range 1100–1250°C, following a geothermal gradient of 40–42 mW/m². The nitrogen contents in Panda diamonds vary strongly from below detection (<10 ppm) to 2700 atomic ppm. Taking the early Achaeon Re-Os isochron date for sulfide inclusions in Panda diamonds at face value, the low aggregation states of undeformed diamonds may indicate mantle residence at relatively low temperatures (<1100°C); if this is the case, diamond formation beneath the central Slave Province may be restricted to short-lived and localized thermal events. An apparent increase in geothermal gradient with depth in the lithospheric mantle beneath the central Slave Province during the time of kimberlite eruptions (Upper Cretaceous to Eocene) may reflect transient heating of the deep lithosphere during melt infiltration. RAH

GEM LOCALITIES

Basalt petrology, zircon ages and sapphire genesis from Dak Nong, southern Vietnam. V. Garnier [virginie_garnier@inrs-ete.quebec.ca], D. Ohnenstetter, G. Giuliani, A. E. Fallick, T. Phan Trong, V. Hoàng Quang, L. Pham Van, and D. Schwarz, *Mineralogical Magazine*, Vol. 69, No. 1, 2005, pp. 21–38.

Sapphire deposits associated with basalt can be found throughout the world. Blue, green, yellow, and colorless sapphires are recovered from the Dak Nong mining district in Dak Lak Province, southern Vietnam. The mining targets are Quaternary and Upper Pleistocene eluvial and alluvial placers derived from the several-hundred-meters-thick basalt flows. The 23,000 km² basalt field is made up of a tholeiitic suite without any xenocrysts and an alkaline suite with mantle and lower-crustal xenocrysts. The sapphire xenocrysts contain Fe (0.43–1.26 wt.%), Cr (33–1582 ppm), Ti (35–1080 ppm), Ga (149–308 ppm), and V (28–438 ppm), and are poor in Zn and Mg. Their oxygen isotope ($\delta^{18}\text{O}$) composition ranges from 6.0 to 6.9‰, which

is not in equilibrium with the basalt values of 5.0–5.7‰. The chemical composition and O-isotope data from the analyzed sapphires, along with the presence of mantle xenoliths, suggest that the sapphires crystallized deep within the earth and not from the erupting basalt. The $\delta^{18}\text{O}$ data of the corundum show that the crystals were formed in a magma chamber at the crust-mantle boundary and that the magma was contaminated by crustal material. The U-Pb dating of zircons recovered from the sapphire-bearing placers indicates that there were two eruptive events occurring at roughly 6.5 and 1 million years ago. The dates for these basaltic eruptive episodes are in agreement with published data on other regional sapphire-bearing basalt fields. *EAF*

Characteristics of cathodoluminescence spectra of jadeite jades from Burma. X. Yuan, L. Qi, and S. Zhang, *Journal of Gems and Gemmology*, Vol. 7, No. 2, 2005, pp. 9–13 [in Chinese with English abstract].

Different types of jadeite jade display different characteristic cathodoluminescence (CL) spectra depending on their composition (e.g., the presence of color-causing impurities such as Cr^{3+} , Fe^{3+} , and Mn^{3+}). In this article, the authors investigated 97 jadeite samples of varying colors using a specially developed CL spectroscopy.

The BY-1 cathodoluminescence spectroscopy features an interconnected UV-Vis spectrophotometer (Ocean Optics USB-2000) and a digital camera. The jadeite samples were divided into five groups by color (white, purple, green, yellow-brown, and grayish green). Standard gemological properties and IR spectra of all samples were obtained before testing with the BY-1 instrument.

The CL colors and the corresponding spectral peaks varied depending on the jadeite color. White jadeite displayed dark blue, light purple, or greenish yellow CL, with peaks at either 370 or 554 nm. Pinkish purple and purple jadeite showed bright purplish red to reddish purple CL, with peaks located at 370 nm (dominant) and 680 nm (subordinate). Bluish purple jadeite displayed bluish purple CL; the peaks were at 370 nm (subordinate) and 508 nm (dominant). Light green to green jadeite showed bright green to yellowish green CL, with peaks at 554 and 760 nm, while dark green jadeite usually displayed dark red CL and peaks at 693 nm (subordinate) and 760 nm (dominant).

Differences in CL features between natural and treated jadeites were also seen, such as the presence of polymer in B-jade. *TL*

Exfiltrative mineralization in the Bukantau ore district (Central Kyzyl Kum region, Uzbekistan). V. G. Pechenkin [pechenkin@urangeo.ru] and I. G. Pechenkin, *Lithology and Mineral Resources*, Vol. 40, No. 5, 2005, pp. 462–471.

The discovery of uranium deposits in the central Kyzyl Kum region of Uzbekistan led researchers to study the ore-bearing potential of young sedimentary sequences. Uplift

roughly 1.6 million years ago exposed Paleozoic basinal structures along rejuvenated faults. This movement allowed for the interaction of various ascending fluids with surface-related processes. The edges of the uplifted blocks were marked by the formation of erosional windows that served as discharge centers for ore-bearing solutions. The formation of manganese ore bodies and gem deposits occurred near these windows at different geochemical barriers. As portions of the Paleozoic fault blocks were uplifted, they underwent extensive fracturing and decompaction. Then, as metalliferous fluids derived from the sedimentary cover layers moved toward the erosional windows, they encountered a newly formed oxygenated barrier which caused the precipitation of manganese oxides. When this same fluid was drawn into the decompacted basement structures, turquoise was deposited on fault surfaces at the reductive (sulfide) geochemical barrier. Thus, turquoise and manganese deposits are vertically separated in cross section although they were formed from the same ore-bearing solutions during a single geologic process. Throughout the section, opal was deposited on fault surfaces within zones of the most intense fracturing and folding. The slightly basic surface fluids had a relatively high Si solubility, so when the fluid encountered deeper acidic fluids the amorphous silica precipitated. Only the most recent tectonically active areas in the north-central portions of the district contain the complete sequence of turquoise, opal, and manganese oxides. *EAF*

Gemstone resources of China. C. M. Ou Yang [cmouyang@hkgemlab.com.hk], *Australian Gemmologist*, Vol. 22, No. 4, 2005, pp. 349–359.

The occurrence of gemstones in China is reviewed after brief notes on the geology of this large area. Two diamond-bearing kimberlite pipes in the Wafangdian district of Liaoning Province are yielding 80,000–90,000 carats/year (30–40% gem quality); 12 kimberlite pipes in Mengyin, Shandong Province, produce 50,000 carats/year (10–15% gem quality). Alluvial deposits in Hunan Province yield 20,000–30,000 carats/year (60–65% gem quality, but of small size). Chinese sapphire deposits are found mainly in alkaline basalts and derived alluvium, and are widely distributed over 20 provinces. Ruby (mostly cabochon quality) is found in impure marbles in Yunnan Province. Emeralds are associated with Precambrian pegmatites and greisen in the Wenshan district of southeastern Yunnan Province. Both transparent and chatoyant aquamarine is found mainly in the Altai pegmatite area of Xinjiang Province. Details are also given for gem-quality tourmaline, citrine, and amethyst, mainly from the Altai Mountains; gem-quality pyrope from Cenozoic alkali basalts of eastern China; and peridot from Tertiary alkaline basalts in Zhangjiangkou County, Hebei Province, and in Jiaohe County, Jilin Province. Occurrences of nephrite and bowenite (antigorite serpentine) are also described. *RAH*

The Italian island of Elba: A mineralogical jewel in the Tuscan archipelago. F. Pezzotta, *extraLapis English*, No. 8, 2005.

Like the other issues in this series, this volume is an English translation of previously published work from *extraLapis* (in this case, No. 20, *Ensel Elba Die Urlaubsinsel der Mineralogie*, 2002), updated with some new information.

The work begins with a review of the island's mineralogical history. Elba was a source of copper and iron in antiquity. Scientists began studying Elba's mineralogy during the 18th century, and European mineral collectors were soon drawn to the island's many diverse localities. More than 170 minerals have been identified on Elba (it is the type locality for nine of these), and specimens from Elba form an important part of many notable mineral collections. The island is particularly known for specimens of hematite, pyrite, spessartite, and of course, elbaite tourmaline.

A short summary of Elba's geology follows. The volume then reviews in detail all of Elba's major gem and mineral localities, including classic ones such as the Monte Capanne pegmatites and the historic ore deposits, as well as some lesser-known sites. Capsule spotlights of noted collectors are provided, as are high-quality photographs of important specimens.

Also included are sections on visiting Elba for collecting trips, suggestions for prospecting certain localities, a brief review of Elba's snakes (some of which are venomous), and a concluding commentary that offers a tourmaline-related explanation for an element of the Greek myth of Jason and the Argonauts. TWO

Jazidas minerais: Ametistas [Mineral deposits: Amethysts]. *Diamond News*, Vol. 6, No. 20, 2005, pp. 35–40 [in Portuguese].

This article gives a comprehensive description of amethyst deposits in Brazil's Rio Grande do Sul State. Amethyst and other quartz varieties formed at approximately 50°C within lava deposits covering large areas of this state about 130 million years ago. Amethyst is recovered via open-pit and underground mining, and at present there are 374 mining operations in eight municipalities of Rio Grande do Sul, more than half of which are in Ametista do Sul. Geodes of 200–300 kg are common, and they can attain sizes up to 3,000 kg and 3 m³. Some of the amethyst is heat treated at 450–475°C to produce citrine. Amethyst production in 2000 was 235 tonnes per month; 80% is exported, mainly to the U.S., Japan, and Germany, with 97% of the material exported as rough. Geodes must yield at least 25% cuttable crystals to be worth processing for facet rough, which is approximately 2% of the overall weight of the geode and about 0.5% yield after cutting. Amethyst and citrine represent 12.5% of Brazil's entire export of gem rough and 10.6% of cut gems. The article explains the classification criteria for the geodes and cut stones, and is illustrated

with a geologic map of Rio Grande do Sul and photos of mines and samples. RT

Musgravites from Sri Lanka. K. Schmetzer [schmetzerkarl@hotmail.com], L. Kiefert, H.-J. Bernhardt, and M. Burford, *Neues Jahrbuch für Mineralogie, Abhandlungen*, Vol. 181, No. 3, 2005, pp. 265–270.

This article presents the physical and chemical properties of four faceted musgravites (BeMg₂Al₆O₁₂) that are most probably from Sri Lanka; this represents the first data for this rare species originating from the numerous secondary deposits of this island. The musgravites were identified by Raman spectroscopy and electron-microprobe analysis. Their refractive indices and densities were determined and related to the contents of transition metals, especially Fe and Zn. Mineral and multiphase inclusions indicate the formation of these samples in different geologic environments. A musgravite crystal containing spinel exsolution lamellae was possibly formed in high-grade metamorphic rocks, whereas two samples with graphite and magnesite inclusions may have originated in magnesian skarns. RAH

"Paraíba-Tourmaline" aus Quintos de Baixo, Rio Grande do Norte, Brasilien. C. C. Milisenda, *Gemmologie: Zeitschrift der Deutschen Gemmologischen Gesellschaft*, Vol. 54, No. 2–3, 2005, pp. 73–84 [in German with English abstract].

Paraíba tourmalines were first produced from pegmatites at São José da Batalha near Salgadinho, Paraíba State, Brazil. Today they are also found in the Quintos de Baixo and Boqueirão mines near Parelhas in the neighboring state of Rio Grande do Norte. At all three mines, the pegmatites intruded quartzites of the Ecuador Formation.

The author describes the Quintos de Baixo mine, which began as a beryl mine in 1976. Mechanized underground mining for tourmaline started in 1996. Tourmaline is hand-picked and mostly occurs as crystal fragments averaging approximately 10 g. They are blue, green, bluish green, and red-violet, as well as color-zoned. The largest cut stone to date is "turquoise" blue and weighs 15 ct.

Microprobe analyses of 12 samples showed elbaite composition, with copper and manganese as the most important trace elements (CuO: 0.32–1.96 wt.%; MnO: 0.11–2.53 wt.%). Microscopic examination showed inclusions typical for tourmaline. The author points out that, like tourmaline from other locations, these stones can be color enhanced by gentle heating to approximately 600°C. RT

The pegmatitic gem deposits of Molo (Momeik) and Sakhangyi (Mogok). H. Kyi [macgems@baganmail.net.mm], T. Themelis, and K. Thu, *Australian Gemmologist*, Vol. 23, No. 7, 2005, pp. 303–309.

Molo, about 51 km northeast of Momeik in Myanmar's

Shan State, is a new source of rare gems and minerals, including phenakite, petalite, hambergite, Cs-rich morganite, and pollucite. Botryoidal-type tourmalines of various colors, aquamarine, topaz, and lepidolite also occur. All of these minerals are recovered from alluvial deposits and pegmatitic dikes that intrude the peridotite country rock.

The pegmatite at Sakhan-gyi is about 16 km west of Mogok in the Mandalay Division, and is a source of aquamarine, goshenite, topaz, and quartz. The pegmatite is about 15 million years old and intruded the Kabaing granite (20–16 Ma). Brief details on these pegmatites and their minerals are presented. *RAH*

Rubellite and other gemstones from Momeik township, northern Shan State, Myanmar. T. Hlaing and A. K. Win, *Australian Gemmologist*, Vol. 22, No. 5, 2005, pp. 215–218.

Colored tourmalines occur as euhedral gem-quality crystals, mushroom-shaped aggregates, and botryoidal masses in pegmatites near Molo village. Associated minerals with gem potential are aquamarine, trapiche morganite (characterized by the presence of a fixed six-rayed star), and hambergite; other associated minerals are quartz, orthoclase, lepidolite, and petalite. The tourmalines range from black schorl to green and pink fibrous tourmalines. The pink fibrous tourmalines have $n_c = 1.630$, $n_o = 1.650$, S.G. = 2.84–3.06, and are Mn-bearing (average 6.58 wt.% MnO). Hambergite forms as colorless prismatic crystals with $n_\alpha = 1.557$, $n_\gamma = 1.630$, S.G. = 2.33, and hardness = 7½. *RAH*

Trapiche of Myanmar. K. K. Win, *Australian Gemmologist*, Vol. 22, No. 7, 2005, pp. 269–270.

Myanmar is the source of a range of gems that display a distinctive spoke-like star, often referred to as a *trapiche*. Representative examples are illustrated, including sapphire, ruby, green tourmaline, aquamarine, morganite, and quartz. Three origins are suggested for the several types of trapiche gems: color-inducing trace elements, inclusions of other minerals, or intergrowths of the same mineral of different color or orientation. *RAH*

INSTRUMENTS AND TECHNIQUES

Complementary use of PIXE-alpha and XRF portable systems for the non-destructive and in situ characterization of gemstones in museums. L. Pappalardo [lighea@lns.infn.it], A. G. Karydas, N. Kotzamani, G. Pappalardo, F. P. Romano, and Ch. Zarkadas, *Nuclear Instruments and Methods in Physics Research B*, Vol. 239, 2005, pp. 114–121.

The authors used a combination of two portable, custom-built chemical analysis systems to examine three red gemstones set in Hellenistic (4th century BC to 1st century AD) gold jewelry at the Benaki Museum in Athens,

Greece. The instruments consisted of a PIXE-alpha particle spectrometer with a ^{210}Po source for analyzing light elements (Na to Zn), and an XRF spectrometer with a Rh-anode X-ray tube source for detecting heavier trace elements (Cr and Y). Overall sensitivities were in the 0.2–0.3 wt.% range for each element. Both systems were calibrated against known standards, and the two types of analyses were combined to get overall chemical compositions of the red gems.

The gems were found to be garnets. Two had compositions consistent with almandine from an unknown deposit in India, while the third was an Fe- and Ca-bearing pyrope consistent with a Sri Lankan origin. *Abstracter's note:* The captions "SiK" and "AlK" appear to have been reversed in figure 6 of the article.

Mary L. Johnson

Practical application for measuring gemstone dispersion on the refractometer. T. Linton, *Australian Gemmologist*, Vol. 22, No. 4, 2005, pp. 330–344.

The low-dispersion barium glass hemicylinder refractometer prism of the Eickhorst SR/XS refractometer allows measurement of refractive index in deep blue light (below 500 nm). A summary is given of two relevant papers that were previously published. The combination of these measuring techniques and extrapolation of a wavelength dispersion curve using Sellmeier's linear conversion permits extrapolation of refractive indices at the B (686.7 nm) and G (430.7 nm) Fraunhofer lines. Previous B-to-G lists of the dispersion of gemstones are inaccurate and provide conflicting data. A new list of values is presented for the dispersion of 217 gem materials, measured at the C-F (656.3–486.1 nm) interval. Measurement of dispersion with the gemologist's refractometer produces apparent dispersion, but with the use of a technique for subtracting apparent dispersion from the sum of true + apparent dispersion, this value can be converted to true dispersion. *RAH*

Probing diamonds with ions. B. J. Griffin [bjg@cmm.uwa.edu.au] and R. Stern, *Rough Diamond Review*, No. 8, 2005, pp. 42–44.

A new analytical technique called nanoSIMS holds some promise for diamond research. This higher-resolution version of SIMS (secondary ion mass spectrometry) can provide scientists with chemical information on the nanometer level, allowing them to better study internal diamond growth structures.

The basic principle of SIMS is to "sputter" a sample with a beam of ions, and as this primary beam is very finely controlled, it can scan across a sample surface. Charged particles (secondary ions) emitted from the sample are collected by a mass spectrometer, which can detect concentrations of elements down to the ppb (parts per billion) range. NanoSIMS uses oxygen and cesium ion beams at resolutions of up to 100 and 25 nm, respectively. Although minimally destructive, it can ablate successive nanometer

layers of material from sample surfaces, providing depth profiles of elements. The ability of nanoSIMS to provide high-resolution, high-sensitivity chemical data in three spatial dimensions makes this technique quite promising, especially with respect to diamonds.

NanoSIMS analysis of nitrogen in diamond is shown to be well correlated to cathodoluminescence data. Both techniques indicate zoning where nitrogen content differs from one region to another. NanoSIMS may be particularly useful for exploring the chemical and isotopic compositions of these growth structures due to its high resolution, and it reveals finer details than CL imagery. It is hoped that quantifying chemical data on the nanometer level will lead to insights into source classification, thereby allowing individual diamonds to be traced back to their point of geologic origin.

DMK

Quantitative trace-element analysis of diamond by laser ablation inductively coupled plasma mass spectrometry. S. Rege [srege@els.mq.edu.au], S. Jackson, W. L. Griffin, R. M. Davies, N. J. Pearson, and S. Y. O'Reilly, *Journal of Analytical Atomic Spectrometry*, Vol. 20, No. 7, 2005, pp. 601–611.

LA-ICP-MS was used to quantitatively measure 41 trace elements in two fibrous diamonds from Botswana's Jwaneng mine that were previously analyzed by instrumental neutron activation analysis (INAA) and particle-induced X-ray emission (PIXE). A range of instrumental conditions showed that a 266 nm UV laser at 10 Hz provided the best sensitivity, and that synthetic oil and a doped cellulose were the most suitable external standards. Typical detection limits were 5–20 ppb for the rare-earth elements and <500 ppb for the transition elements; Na and Fe had higher detection limits (2–3 ppm). Detailed analytical results are presented. The trace-element patterns obtained by this technique may be used for the characterization of diamonds in genetic studies. RAH

Use of IR-spectroscopy and diffraction to discriminate between natural, synthetic and treated turquoise, and its imitations. A. Pavese [alessandro.pavese@unimi.it], L. Prospero, and M. Dapiaggi, *Australian Gemmologist*, Vol. 24, No. 4, 2005, pp. 366–371.

An overview is given on the use of IR spectroscopy, combined in some cases with X-ray diffraction, for determining the nature of turquoise, whether natural, synthetic, treated, or imitation. A total of 94 samples (32 natural, 12 synthetic, 16 treated, and 34 imitations) were analyzed by IR spectroscopy in reflectance mode; some treated turquoise specimens were also examined in transmission mode. Differences in the spectra between natural, treated, and synthetic turquoise were observed. X-ray diffraction was used to resolve ambiguities in identifying some turquoise imitations, and was particularly useful in the precise identification of their constituent phases. RAH

Use and misuse of optical mineralogy constants in gemmology. D. B. Sturman [darkos@rom.on.ca], *Australian Gemmologist*, Vol. 22, No. 2, 2005, pp. 234–243.

Dangers inherent in the direct transfer of optical data and concepts from mineralogy to gemology are highlighted; these can give rise to confusion and misunderstandings. In particular, the dispersion coefficient is not a reliable indicator of "fire" in faceted gemstones. The author suggests that faceted diamonds show strong "fire" not because of the large dispersion of diamond, but because of other factors not yet well understood. Refractive index plays an equally important role. Factors contributing to doubling are described, and diagrams are presented for the estimation of the doubling effect in gemstones. RAH

X-ray luminescence, a valuable test in pearl identification. H. A. Hänni [gemlab@ssef.ch], L. Kiefert, and P. Giese, *Journal of Gemmology*, Vol. 29, No. 5/6, 2005, pp. 325–329.

The majority of the world's natural pearls come from salt-water oysters. Today, increasing numbers of beadless freshwater cultured pearls are entering the market. Traces of manganese (Mn) found in the nacre of freshwater cultured pearls and the shells of the mollusks that produce them cause them to luminesce to X-rays. In contrast, the nacre of saltwater-borne samples is inert to X-rays. By use of a sensitive camera, this visible luminescence can be recorded and displayed on a monitor.

A difficulty in using this technique as a means of separation arises because Japanese Akoya cultured pearls and South Sea cultured pearls (both from saltwater) use freshwater bead nuclei, which contain Mn and luminesce to X-rays. The thick nacre common to South Sea cultured pearls obscures the luminescence of the bead nucleus, so it is typically not seen on exposure to X-rays. However, the thinner nacre on Akoya cultured pearls allows the luminescence from the freshwater beads to shine through. Another concern is the presence of dye or natural pigment in the nacre, which may inhibit the luminescence reaction. Therefore, this article suggests that X-ray luminescence only be used as an additional test (after X-radiography) to help separate natural saltwater pearls from beadless freshwater cultured pearls. WMM

JEWELRY HISTORY

The history of the Ekaterinburg faceting factory. N. Moukhina, *Platinum*, Vol. 1, No. 16, 2005, pp. 62–65 [in Russian].

The Ekaterinburg stone cutting factory was established in 1726, only three years after the founding of the city, which later became the center of the Urals mining and metallurgy industries. Initially, the factory made marble facades for buildings in St. Petersburg. In the mid-18th century, however, it began specializing in faceting gems

and carving decorative stones (e.g., jasper, agate, rhodonite, and quartzite). The craftsmen excelled in "Russian mosaic"—constructing images from small pieces of malachite and jasper. The factory also operated a school for cutting, polishing, faceting, engraving, and making mosaics, and the best pupils were sent to St. Petersburg for additional training.

Most of the artifacts produced in Ekaterinburg were items used to decorate the palaces of the emperors and other nobility. The loveliest materials were made of grayish green Kalkan jasper and serpentine. The article includes photographs of the factory's museum of engraving and jewelry art pieces, such as vases, plates, architectural details, and stone stamps. Notable among these is a mosaic map of France that received the Grand Prize at the 1900 Paris Exhibition. This map was presented to France and exhibited in the Louvre for many years. *BMS*

Ural gemmas. T. Parnyuk, *Platinum*, Vol. 1, No. 16, 2005, pp. 46–49 [in Russian].

Many gem carvings were produced by the Ekaterinburg stone cutting factory between 1796 and 1847, but only at the end of the 20th century was this unique art restored. A special feature of these works is the wide spectrum of materials used: jasper, chalcedony, and agate, among others. Examples of articles made by I. Golubev, I. Nasibulin, G. Ponomarev, and A. Zhukov are described; some are shown in photographs. There are faces of well-known writers and women, fantastic bird figures, landscapes, flower symbols, and folk-tale subjects. The skill of the engravers is apparent through their use of the texture, color, and translucent properties of the stones. Artifacts of Ural masters are very popular at Russian and international expositions. *BMS*

PRECIOUS METALS

Giving gold jewelry and coins as gifts: The interplay of utilitarianism and symbolism. B. Ertimur and O. Sandikei, *Advances in Consumer Research*, Vol. 32, 2005, pp. 322–327.

Turkey is the world's fifth largest market for gold jewelry, and gold jewelry and coins serve a number of cultural functions. They are important for gifts that mark certain rites of passage, as well as a form of women's empowerment and safeguard against misfortune. This article contains interviews with Turkish consumers discussing the reasons they purchased gold coins and jewelry. The authors conclude that gold is a preferred gift for many reasons: investment, adornment, tradition, confidence that it will be well-received, and a statement of a bond between giver and receiver. *RS*

Gold—The emotional metal. J. Cross [jessica@virtualmetals.co.uk], *Applied Earth Science*, Vol. 114, 2005, pp. B101–107.

Gold differs from other commodities in that the vast majority of the metal mined over the centuries remains available in the form of existing bars, coins, and jewelry, and it attracts investors who have an emotional belief in it, beyond economic fundamentals. In addition, gold serves as an unofficial currency in unstable areas.

This article examines how these factors affect three major components of the gold market: official sales, adornment jewelry, and investment. In the first component, governments hold gold as a hedge even though it earns no interest or return. Nevertheless, in 1999 nations of the European Union agreed to sell portions of their official holdings on an orderly basis (approximately 2,000 tonnes from a total of ~16,000 tonnes during 1999–2004). In the jewelry sector, gold adornment items continue to be important in the Middle East and India. In the West, however, it goes through different periods of fashion. In the U.S., yellow gold is losing market share to other consumer items, and in the United Kingdom, it has been equated with crass popular culture. There are difficulties with the investment market as well, because there are no easy ways to invest directly in the metal. *RS*

SYNTHETICS AND SIMULANTS

Characteristics of large-sized ruby crystal grown by temperature gradient technique. C. Song [soocii@mail.siom.ac.cn], Y. Hang, C. Xia, J. Xu, and G. Zhou, *Optical Materials*, Vol. 27, No. 4, 2005, pp. 699–703.

This article describes the use of the temperature gradient technique (TGT) to grow a large ruby crystal. The initial experiment produced a 75 × 45 mm boule. The bulk of the as-grown crystal, 60 × 30 mm, was of good quality with minimal inclusions, showed only Cr³⁺ (no Cr²⁺ or Cr⁴⁺ byproducts), and displayed a high degree of crystalline symmetry.

Based on their previous work and the current study, the authors believe the inclusions are gas bubbles and foreign impurities. Concluding remarks suggest that larger, higher-purity crystals can be achieved with the TGT process by implementing meticulous procedures for preparing the ingredient powders (Al₂O₃ and Cr₂O₃) and improved control of the thermal field during crystal growth. *SW*

Growth of large high-quality type-IIa diamond crystals. X.-C. Wang, H.-A. Ma, C.-Y. Zang, Y. Tian, S.-S. Li, and X.-P. Jia [xjia@mail.jlu.edu.cn], *Chinese Physics Letters*, Vol. 22, No. 7, 2005, pp. 1800–1802.

Colorless high-quality type IIa synthetic diamond crystals up to 4 mm in size have been grown by the temperature-gradient technique at pressures of 5.5 GPa and temperatures of 1200–1300°C. The solvent metal is an Fe-Co-Ni alloy. Ti is added to the solvent metal to reduce the N content in the synthetic diamond, and Cu is added to inhibit

the formation of titanium carbide inclusions. Growth rates are about 1.1–1.6 mg/h. Within the growth chamber, a modified ring-shaped carbon source is used, with the opening in the ring positioned directly above the growing crystal. With this configuration, titanium carbide particles that form in the molten alloy during a growth run are able to float upward and away from the growing crystal, and are thereby less likely to become entrapped within the synthetic diamond as dark metallic inclusions. *JES*

Synthesizing single-crystal diamond by repetition of high rate homoepitaxial growth by microwave plasma CVD. Y. Mokuno [mokuno-y@aist.go.jp], A. Chayahara, Y. Soda, Y. Horino, and N. Fujimori, *Diamond & Related Materials*, Vol. 14, No. 11/12, 2005, pp. 1743–1746.

Many promising technological applications have prompted ongoing research into optimizing the size, quality, and growth rate of single-crystal synthetic diamond produced by the chemical vapor deposition (CVD) method. In this article, three developments are summarized. Use of an “enclosed” substrate holder resulted in the growth of tabular synthetic diamond crystals with smooth and flat surfaces. With this apparatus, a 4.65 ct, 1-cm-thick (~5 × 5 × 10 mm) single-crystal synthetic diamond was produced by 24 repetitive stages of crystallization over a total growth time of about 150 hours. Some crystals grown in this way were then polished with six cube faces. Further repetitive growth stages on several of these faces resulted in a three-dimensional enlargement of the synthetic diamond. *JES*

TREATMENTS

Beryllium-treatment. A. Peretti, D. Günther, and A.-L. Graber, *Contributions to Gemology*, No. 4, 2005.

The fourth installment of *Contributions to Gemology* compiles previously published research on Be diffusion treatment of corundum from the first two issues, with updates and corrections, and adds new photomicrographs of corundum inclusions.

In the first section, using a variety of advanced methods (SEM, EDXRF, LA-ICP-MS, CL), as well as gemological and spectroscopic testing, the authors examine a wide variety of natural, synthetic, untreated, and treated (before and after) corundum. Although the originally published (2002) version of this report attributed the induced color changes to “internal movement of color centers,” the corrections in this edition clearly establish the role of Be diffusion.

In the second section, the authors use LA-ICP-MS chemical analyses to further examine the mechanisms of the color changes induced by Be diffusion. In contrast to other published reports, they correlate the formation of orange color centers to the Ti/(Mg+Be) ratio; the presence of Si was not found to be related. Orange color was

induced when Ti/(Mg+Be) > 1. The role of other trace elements in the formation of color centers was limited or nonexistent.

The new material in the third section of this issue consists of several pages of high-quality inclusion photomicrographs (untreated and treated corundum) with explanatory captions. *TWO*

High-temperature annealing of optical centers in type-I diamond. A. T. Collins [alan.collins@kcl.ac.uk], A. Connor, C.-H. Ly, A. Shareef, and P. M. Spear, *Journal of Applied Physics*, Vol. 97, 2005, pp. 083517-1–083517-10.

The widespread availability of commercial high pressure, high temperature (HPHT) services for changing the color of brown gem diamonds to colorless or other fancy colors has led to the need for a better understanding of the optical defect changes that occur during annealing. Several type Ia natural diamonds and type Ib synthetic diamonds were irradiated with neutrons or 2 MeV electrons, annealed at 800°C, then subsequently either annealed at 1000°C–1750°C and ambient pressure or subjected to HPHT conditions (2300°C, 5 GPa). One type IaA and one type IaB natural diamond, both electron irradiated, were annealed at 33–50°C intervals from 800°C–1600°C to study changes in the H1b and H1c centers. For reference, one natural type Ia brown diamond was annealed at 1600°C–1750°C and several others were subjected to HPHT conditions. FTIR and Vis-NIR absorption spectra (room temperature and 77 K) and cathodoluminescence (77 K) measurements were collected before and after each heating step.

Annealing of type IaA and IaB irradiated diamonds to 1600°C revealed that the H4 defect was destroyed by conversion to H3, confirming that H3 is more stable than H4 and explaining the absence of H4 in most natural diamonds that have undergone long-term annealing in the earth. In addition, carefully controlled interval heating defined the temperature-dependent sequence of creation and destruction of the 594 nm, H1b, H1c, H2, H3, and H4 centers. Annealing of irradiated type Ib synthetic diamonds revealed the creation of both H3 and, surprisingly, N3 centers, as well as the increased development of Ni-N complexes. Annealing of the reference natural brown diamonds resulted in the complete removal of H4 defects and the 491 nm CL line related to plastic deformation, as well as the development of H3 and H2 centers. The ease with which the 491 nm line was annealed out and its distinct presence in natural brown diamonds suggests that plastic deformation occurred very late in their history, most likely during eruption to the surface. Finally, the data indicate that H2 and H3 centers are destroyed by HPHT treatment of dislocation-free diamonds, but their intensities are dramatically increased during HPHT annealing of natural brown diamonds (with abundant dislocations). This suggests a dynamic, competitive process where the final diamond color depends on a combination

of annealing temperature, duration, and the defects present in the diamond before treatment. CMB

Scale determination of wax and macromolecule polymer-filled jadeite jade. L. Qi, X. Yuan, G. Peng, and G. Yang, *Journal of Gems and Gemmology*, Vol. 7, No. 3, 2005, pp. 1–6 [in Chinese with English abstract].

Jadeite can be enhanced by a variety of processes, such as pure bleaching, corrosion by alkalis/acids, waxing, and polymer filling. Treated jadeite can be identified by microscopic observation and FTIR spectroscopy. However, the relationships among these enhancement processes are unclear, and there has been no detailed investigation of the quantity of wax- and polymer-filling materials in treated jadeite.

Enhancement experiments were mainly performed by one author (GY) at Xiangfa Jade Ltd Co., Foshan, China. A solution of oxalic acid and H₂O₂ with diluted HCl was used at 115°C for the pure bleaching treatment, followed by waxing. In the polymer filling treatment, samples were first placed in a solution of H₃PO₄ and H₂O₂ or HNO₃ and H₂O₂, followed by a NaOH solution to precipitate solid particles into the voids created by the corrosion process, and finally were subjected to polymer filling. Various treated jadeite samples were cut into ~1 cm³ pieces and dried at 210°C for 5 hours before FTIR spectra were obtained.

In the bleached and waxed samples, the intensity of the C-H stretching bands at 2919 and 2850 cm⁻¹ increased with immersion time in the wax. A group of characteristic polymer-related bands in the 3100–2800 cm⁻¹ range (3053, 2967, 2929, and 2874 cm⁻¹) were detected, and slight differences were noted in the fine structures of these bands in other samples reportedly treated by different factories. The absorption of CH₂ and CH₃ related to the amount of wax and polymer in the jadeite, was correlated to two parameters involving the 2919 and 2851 cm⁻¹ bands. TL

MISCELLANEOUS

Diamonds, foreign aid and the uncertain prospects for post-conflict reconstruction in Sierra Leone. J. A. Grant. *The Round Table*, Vol. 94, No. 381, 2005, pp. 443–457.

In the 1990s, Sierra Leone was racked by a gruesome civil war, which local diamond production played a role in sustaining. Since 2002, with the assistance of international aid organizations, the United Nations, and various governments, the country has been trying to rebuild its shattered economy and infrastructure. Sierra Leone's two chief revenue sources are agricultural products and diamonds.

The country has made significant progress in regaining a degree of control over its production of diamonds from alluvial fields in the interior. Official production rose from \$1.2 million in 1999 to \$126.7 million in 2004. One reason for this dramatic increase is the Kimberley

Process, which requires certification for rough diamonds indicating that they were mined and sold legitimately. However, some industry analysts believe that the majority of Sierra Leone diamonds continue to be exported illegally to avoid the 3% export duty. In addition, entrenched corruption and limited law enforcement resources continue to hinder attempts to regain full control of the country's diamonds and other resources. RS

Economic feasibility of small-scale black-lipped pearl oyster (*Pinctada margaritifera*) pearl farming in the South Pacific. Q. S. W. Fong, S. Ellis, and M. Haws, *Aquaculture Economics & Management*, Vol. 9, 2005, pp. 347–368.

This article offers a detailed economic analysis of the costs involved in starting and operating a black pearl farm in the South Pacific. A number of island nations in that region have little private industry and remain heavily dependent on aid from foreign governments and development agencies. The authors analyzed the start-up costs—labor, equipment, seeding, land-lease, etc.—factoring in issues such as anticipated oyster mortality and percentage of rejected cultured pearls, to develop an economic model for cultured pearl production over a 20-year period.

The authors project that an initial investment of about \$200,000 would be needed to establish a farm with 25,000 oysters in seed. Because of the time required for the pearl culturing, there would be no income for three years against yearly operating costs ranging from \$160,000 to \$236,000. Years four and five would bring income equaling 40% of expenses, while the operation would turn a small profit (\$44,000) in year six. Profits would begin in earnest in year seven, where returns of \$143,000 would be realized against revenues of \$437,000. These figures, however, are highly dependent on fluctuations in the market price for black cultured pearls (a 1% decrease in price would cause a 5% decrease in profits). In addition, a small farming operation would find it difficult to compete against large, established producers unless a number of farms created cooperatives to realize economies of scale. RS

Finer points of cutting. D. Knoote [dean.knoote@argylediamond.com.au], *Rough Diamond Review*, No. 8, 2005, pp. 27–28.

This article reviews developments in the history of diamond bruting. Bruting began in the mid-16th century by rubbing the edge of one diamond against another to round the corners and form the face-up shape. Machine-driven bruting was introduced in the 19th century and is still used today.

The bruting process is similar to lathing except the diamond sharp (cutting edge) is clamped to a long holder. By tucking the shaft under the arm and clasping the end holding the sharp, a bruter leverages the stick about a cradle block, and can exercise accurate control of the tool while sensing a feel for the cutting.

Manual bruting requires years of experience. The apprentice bruter first learns to center a diamond, which is critical to maximizing diamond yield. One of the most important skills is being able to shape the rough fast enough to maintain productivity but slowly enough to avoid bearding. Preserving weight versus improving clarity and geometry are also important considerations. Highly skilled and experienced bruters have an advantage over automatic systems, which are not yet as sensitive to subtleties in the process.

Automated bruting was developed in the 1980s. These bench-top machines work by grinding two contra-rotating diamonds against each other. Automated bruting takes longer than manual bruting (~2 hours vs. 15–30 minutes), but this is offset by an operator being able to monitor five or more operations at once. The process also creates very parallel girdles that are particularly suitable for the holders used with automatic polishing machines.

Laser bruting has the advantage of being able to create virtually any shape in about 30–40 minutes; multiple stones can be loaded into special cartridges for unattended operation. When coupled with a computerized scanning and imaging system, laser bruting machines can create shapes with perfect symmetry. One drawback is that once a cutting path is started, the cut is committed, unlike manual bruting where the bruter can monitor and adjust the process.

With the advent of these technologies, the number of manual bruters has declined rapidly. The author predicts that they will soon become redundant, as have manual kerfers. *HJ-G*

The history and prehistory of pearling in the Persian Gulf.

R. Carter [racbahr@hotmail.com], *Journal of the Economic and Social History of the Orient*, Vol. 48, No. 2, 2005, pp. 139–209.

The author examines pearling activities in this ancient area from three points of view: (1) written accounts about pearls and pearl harvesting in the Persian Gulf, (2) pearls and related archeological artifacts found at various sites in the region, and (3) indirect archeological evidence of possible pearling activities.

On the first point, the author found that the earliest explicit reference to pearling dates from the 4th and 3rd centuries BC in what is now Abu Dhabi and Bahrain. Pearling had become an established enterprise by the time of Alexander the Great. Centuries later, Pliny noted that pearls were the most highly prized valuable in Roman society and praised those from the Persian Gulf. By the 15th century AD, pearling had become “quite a large industry,” with Bahrain as the primary center. Records of the Dutch East India Company from 1724 estimate that Bahrain pearlery extracted one million pearls annually. The industry continued to grow through the 19th century, with the vast majority of the trade going to India.

On the second point, archeologists discovered pearls

in Late Stone Age (6th and 5th millennia BC) settlements in what is now Kuwait. Most of the pearls were irregularly shaped, and some were incorporated into ornaments. The author argues that these came from deliberate pearl fishing, though this issue is apparently in dispute.

On the third point, the author reviews shifts in human population throughout the area that parallel the development of the pearling industry.

By the beginning of the 20th century, pearling was the primary industry of the region, providing the foundation of wealth for many of today’s ruling families. The majority of pearls still went to India. Starting in the 1920s, demand for Persian Gulf pearls declined dramatically with the availability of Japanese cultured pearls. The closure of Kuwait’s pearl oyster market in 2000 ended 7,000 years of pearling in the region. *RS*

Pathology of pearl oyster mortality. M. Hirano, Y. Sugi-shita, S. M. A. Mobin, K. Kanai, and K. Yoshikoshi (ykazuma@net.nagasaki-u.a.c.jp), *Journal of Aquatic Animal Health*, Vol. 17, No. 4, 2005, pp. 323–337.

Cultured pearl farming of the *Pinctada fucata martensii* oyster has been marked by mass mortality events in some western Japanese farms. First seen in the Kagoshima prefecture in 1993 and progressively identified in the Oita and Ehime prefectures, mass mortality of these cultured oysters was prominent throughout western Japan by 1997. This article presents the results of a case study of healthy and affected oysters.

Based on a single strain of test oysters, mortality events were examined at several farms. Accompanied by water temperature data and growth and mortality rates, most of the information was derived from examinations of affected oysters using optical microscopy and transmission electron microscopy. A histopathological examination of these oysters was comprised of dissection, dehydration, and stabilization of specimens, followed by slicing them thinly. After drying, the structure of the tissue was examined by pathologists using microscopy.

The pathologists found that the tissue of diseased oysters was characterized by blebbing and cell necrosis, spreading from the digestive organ to other regions. No viral, bacterial, mycotic, or parasitic organisms were detected. This is in contrast to earlier suggestions that their mortality was due to an infectious disease. Mass mortality events were demonstrated to be regular annual events, with very similar patterns between farms. Water temperature was found to be only an indirect factor in mass mortality events: It altered the timing and sometimes the severity of the outbreaks, but it is not suspected to be the cause. One suspected environmental factor is the presence of neighboring fish farms, which are known to cause water pollution and deoxygenation resulting from decaying fish waste. This study speculates that at least some farms were probably influenced by organic pollution from these fish farms. *DMK*

A COLORED DIAMONDS CHRONOLOGY

August 2006 marks the release of the second book in the GEMS & GEMOLOGY IN REVIEW series, on colored diamonds. This 340-page volume, edited by GIA Laboratory technical director John M. King, contains more than 100 articles and other reports on historic colored diamonds, characterization of colored diamonds, and color grading, which span 70-plus years of GEMS & GEMOLOGY issues. A special feature is the 20-page booklet of color reference charts, which provides examples of GIA fancy-color grades for yellow, blue, orange, pink, and green diamonds. Some of these charts are updated versions of those previously seen in G&G, whereas others have never been published before.

Following are some of the highlights in the history of colored diamonds in the marketplace, the public eye, and the gemological laboratory.

1631–1668: Intrepid French gem dealer Jean-Baptiste Tavernier makes six voyages to India. In 1642, it is widely believed, he acquires a 112.5 ct diamond crystal that becomes known as the Tavernier Blue. Following its theft from the French Treasury in 1792, the Tavernier Blue is recut and eventually yields the 45.52 ct Hope diamond.

1726: A London merchant writes a letter offering the Dresden Green diamond to Friedrich Augustus, ruler of Saxony, for 30,000 pounds sterling—the first known documentation of this historic stone.

Circa 1878: The Tiffany diamond, perhaps the most famous of all yellow diamonds, is recovered from the Kimberley mine in South Africa. The 287 ct piece of rough is subsequently fashioned into a 128.54 ct square antique modified brilliant.

1903: South Africa's Premier mine (renamed the Cullinan in 2003) is discovered. In addition to producing large colorless diamonds, the mine becomes known as a source of superb blue diamonds.

Mid-1950s: The GIA Gem Trade Laboratory begins issuing color grading and origin-of-color reports for colored diamonds.

1958: Harry Winston donates the Hope diamond to the Smithsonian Institution in Washington, D.C., where it is now seen by some four million museum visitors each year.

Mid-1970s: Stanley Doppelt and Louis Glick's Starburst cut and Henry Grossbard's radiant cut are introduced. These experimental cuts are found to intensify the face-up color of yellow diamonds, which leads to a revolution in fancy-color diamond cutting. No longer are colored diamonds exclusively manufactured in the same shapes, cutting styles, and proportions as their colorless and near-colorless counterparts.

August 1979: The first diamond crystals are found in the area now

known as the Argyle mine in Western Australia, which soon becomes the world's largest volume producer of diamonds. The production includes brown stones that are creatively marketed as "cognac" and "champagne" diamonds, as well as a small but consistent supply of very rare pink diamonds.

April 28, 1987: At Christie's in New York, a 0.95 ct Fancy purplish red diamond known as the Hancock Red sells for \$880,000. At \$926,000 per carat, it still holds the record per-carat price for any gem sold at auction.

November 1988: Two gemologists from the GIA Gem Trade Laboratory visit the Green Vaults in East Germany to conduct the first complete gemological examination of the 41 ct Dresden Green, one of the few green diamonds whose bodycolor is known to be of natural origin.

December 12, 1988: The unmounted Hope diamond is graded by the GIA Gem Trade Laboratory, the first time it has ever been graded by a widely recognized system. The historic diamond receives a color grade of Fancy Dark grayish blue and a VS₁ clarity grade.

Early 1995: GIA formally introduces modifications to its colored diamond color grading system, which include two additional fancy-grade terms, Fancy Deep and Fancy Vivid. The system and its enhancements were first described in the Winter 1994 issue of *Gems & Gemology*. In 1996, the color of the Hope diamond is updated to Fancy Deep grayish blue.

June 27–September 15, 2003: The "Splendor of Diamonds" exhibit appears at the Smithsonian Institution. The display features one colorless diamond and six spectacular colored diamonds, including: the 101.29 ct Fancy Vivid yellow Allnatt, the 59.60 ct Fancy Vivid pink Steinmetz Pink, and the 27.64 ct Fancy Vivid blue Heart of Eternity.

Available now: To order *Gems & Gemology in Review: Colored Diamonds*, visit www.gia.edu/gemsandgemology or call toll-free 800-421-7250, ext. 7142. Outside the

U.S. and Canada, call 760-603-4000, ext. 7142, or e-mail gandg@gia.edu. **Price:** \$59.95 plus shipping and handling.

